Combined endogenous MR biomarkers to assess tumor oxygenation and response to radiation therapy

CAO PHAM Thanh Trang

Thesis presented in fulfillment of the requirements for the degree of « Docteur en Sciences Biomédicales et Pharmaceutiques »

Promotor: Prof. Bénédicte F. Jordan
Co-promotor: Prof. Bernard Gallez

October 2018

ACKNOWLEDGEMENTS

Mon travail de recherche ne pourra loin d'être avancé et abouti sans les soutiens et les aides précieux que vous m'avez apportés durant mon doctorat.

Je tiens tout d'abord à remercier ma promotrice, le professeur Bénédicte Jordan, qui m'a donné l'opportunité de réaliser cette thèse et m'a accueillie en REMA. Je te remercie également pour tes conseils, tes écoutes, ta compréhension, ta patience et aussi pour ta confiance. C'est grâce à ton encadrement, ta disponibilité, tes regards critiques que j'ai pu évoluer positivement au sein du laboratoire.

Puis, également un grand merci à mon co-promoteur, le professeur Bernard Gallez. Je vous remercie d'avoir passé du temps avec moi à discuter des résultats, et d'avoir me donné des bons conseils afin de m'aider à éclaircir mes idées. Vos expériences ont été des repères importants pour clarifier mes réflexions.

Merci à vous, le professeur Olivier Feron, d'avoir accepté d'être le président du comité de thèse ainsi que pour vos conseils avisés et constructifs.

Je tiens également remercier le professeur Thierry Duprez et le professeur Vincent Grégoire de m'avoir donné des commentaires très constructifs et vos points de vue clinique.

Merci au professeur Carine Michiels pour votre relecture minutieuse du manuscrit de thèse.

Merci professeur Laurent Lemaire d'avoir accepté de participer au jury de ma thèse et pour vos suggestions pertinentes.

I would like to thank Professor Uwe Himmereilch for accepting to be part of my PhD committee. Thank you for reading my thesis, and for your useful advices to improve my thesis.

Je remercie tous les membres du laboratoire REMA : Merci à An, pour ton soutien, les conversations scientifiques, tes conseils bienveillants et ton amitié. Merci Florence de m'avoir introduit à des manipulations d'IRM au début de ma thèse. Merci Céline Desmet pour tes aides et ta gentillesse. Merci Stefania pour ton humour et des bons moments que nous avons partagés ensemble. Merci Lionel de ta gentillesse et de tes aides. Merci Nicolas pour tes aides durant les manips d'IRM et pour ton programme d'analyse des données qui m'a aidé à économiser beaucoup de temps. Merci Philippe de m'avoir aidé

dans les analyses statistiques. Merci aussi à Donatienne, Pierre, Céline Schoonjans, Florian, Samantha pour vos gentillesses et l'ambiance agréable dans notre bureau.

Je remercie Télévie et l'UCL d'avoir financé mon projet.

En fin, je remercie ma famille, mes parents, mon mari pour votre soutien, vos supports et encouragements.

Un grand merci à vous tous !!!

TABLE OF CONTENTS

ABBREVIATIONS

ΔB_0	macroscopic field inhomogeneities
AIAs	angiogenesis inhibiting agents
ARCON	accelerated radiotherapy with carbogen and nicotinamide
ASL	arterial spin labelling
ASTRO	American Society of Therapeutic Radiation Oncology
ATP	adenosine triphosphate
bFGF	basic fibroblast growth factor
BOLD-MRI	blood oxygen level-dependent magnetic resonance imaging
BVf	blood volume fraction
CA IX	carbonic anhydrase IX
CB	carbogen
CBP/p300	CREB-binding protein/ E1A-binding protein p300
CT	computed tomography
Cu-ATSM	Cu(II)-diacetyl-bis(N 4-methylthiosemicarbazone)
DANHACA	Danish head and neck cancer
DCE-MRI	dynamic contrast-enhanced magnetic resonance imaging
dHb	deoxyhemoglobin
DMF50	dose-modifying factor 50
DPBC	dose painting by numbers
DPBN	dose painting by contours
DW-MRI	diffusion weighed magnetic resonance imaging
EGFR	epidermal growth factor receptor
EPO	erythropoietin
EPR	electron paramagnetic resonance
EPRI	electron paramagnetic resonance imaging
FAZA	fluoroazomycinarabinofuranoside
FETA	fluoroetanidazole
FETNIM	fluoroerythronitroimidazole
FIH	factor inhibiting HIF-1
FMISO	fluoromisonidazole
FOV	field of view
FREDOM	fluorocarbon relaxometry using echo planar imaging for dynamic oxygen mapping
GLUT1	glucose transporter 1
GRE-MRI	gradient echo magnetic resonance imaging
GSH	Glutathione
H&NC	head and neck cancer
HBO	hyperbaric oxygen
HbO_2	oxyhemoglobin
HER2/neu	human epidermal growth factor receptor 2

HIFs	hypoxia-inducible factors
HRE	HIF-responsive element
HSF	hypoxic-specific factor
HSV5	hypoxic subvolume with pO_2 less than 5 mmHg
HX4	flortanidazole
IAZA	iodoazomycin arabinoside
IAZG	iodoazomycin galactoside
IHC	immunohistochemistry
IMRT	intensity-modulated radiation therapy
ITPP	*myo*-inositol tripyrophosphate
k^{trans}	volume transfer constant of Gd-DTPA
MAPK	mitogen activated protein kinase
MOBILE	mapping of oxygen by imaging lipid relaxation enhancement
M-PTX	paclitaxel-loaded micelles
MR	magnetic resonance
MRI	magnetic resonance imaging
MTD	maximum tolerated dose
NF-kB	nuclear factor kappa-light-chain-enhancer of activated B cells
NMR	nuclear magnetic resonance
NO	nitric oxide
NSAIDs	nonsteroidal anti-inflammatory drugs
OCR	oxygen consumption rate
ODC	oxygen dissociation curve
OE-MRI	oxygen-enhanced magnetic resonance imaging
OPN	osteopontin
PDH	prolyl hydroxylase-domain protein
PET	positron emission tomography
PFCs	perfluorocarbons
PIBT	pre-irradiation gas breathing time
PIMO	pimonidazole
PSA	prostate-specific antigen
PTX	paclitaxel
ROS	reactive oxygen species
RT	radiation therapy
SCCHN	squamous cell carcinoma of the head and neck
SDF-1	stromal cell-derived factor-1
SO_2	absolute blood oxygen saturation
SPECT	single photon emission computed tomography
STAT3	signal transducer and activator of transcription 3
SUV	standardized uptake value
T/B	tumor-to-blood uptake ratio
TCD50	tumor control dose 50
TCP	tumor control probability

TOLD	tissue oxygen level dependent
VDAs	vascular disrupting agents
VEGF	vascular endothelial growth factor
VHLp	Von Hippel-Lindau suppressor protein
VTAs	vascular targeting agents

FOREWORD

Hypoxia or lack of oxygen is the common feature of most solid tumors. The hypoxic environment is associated with the reduced efficacy of cancer treatments, especially radiation therapy. Although modification of tumor hypoxia improves the outcome of radiation therapy, screening for the presence of hypoxia has not been the entry criterion prior to hypoxia modification trials. To bridge the gap between the occurrence of tumor hypoxia and the routine clinical practice, there is an important need to have a method to robustly map tumor oxygenation for patient stratification and treatment adaptation.

Among the methods that have been developed to measure hypoxia, oxygen sensitive MRI endogenous contrast biomarkers, including R_1 and R_2*, appear to be a relevant approach for this purpose. Since there is a lack of study comparing R_1 and R_2* in response to oxygen modifiers, the aim of this thesis is to address the value of R_1 and R_2* to assess tumor oxygenation and response to radiation therapy using different oxygen modifiers.

The introduction first presents an overview of hypoxia, the causes, consequences and characteristics of hypoxia. The next part introduces different approaches that have been developed to assess tumor hypoxia along with their advantages, drawbacks and their characteristics such as sample volumes (macroscopic or microscopic); time intervals of sampling; compartment sampled; invasiveness; resolution; sensitivity; and repeatability. The third part discusses about treatment strategies to overcome hypoxia in radiation therapy. Then, the role of imaging on tumor hypoxia identification is addressed. The predictive value of radiation therapy outcome of different methods to measure tumor oxygenation is highlighted in the last part of introduction.

The aims of thesis are described in the second section.

The results section is divided in two parts corresponding to two major axes of the thesis. The first part addresses the validation of MRI biomarkers using a hyperoxic challenge (i.e. carbogen) to improve tumor pO_2, with two associated publications. The first article assesses the sensitivity of MRI biomarkers to the change in tumor oxygenation and validates these MRI parameters as predictive markers of response to the outcome of radiation therapy. The second article focuses on the combined MRI biomarkers predictivity of the basal tumor oxygenation and of the response to carbogen breathing. This article also discusses the importance of the analysis of heterogeneity and applies the voxel-wise analysis of the combined R_1 and R_2* to predict different tumor hypoxic fractions. In the second part, a third publication shows the application of MRI biomarkers to assess changes in tumor oxygenation induced by an allosteric effector of hemoglobin, ITPP.

The final section summarizes the principal findings of the thesis and discusses about important issues arising from the thesis as well as suggests possible future perspectives.

INTRODUCTION

1. TUMOR HYPOXIA

1.1. Introduction

Hypoxia or oxygen deprivation occurs when oxygen delivery to the tissue is not enough for oxygen consumption of the tissue. Hypoxia compromises the function of cells and is commonly observed in solid tumors.

1.2. Causes

The transport of oxygen to tissue is guaranteed by hemoglobin. In normal tissue, the oxygen delivery is supported by an intact, structured vascular system. Oxygen is then released by hemoglobin and consumed by cells. Oxygen status in normal tissue is regulated by an appropriate balance between oxygen supply and OCR of cells. However, in tumor tissue, the oxygen supply cannot fulfill the high oxygen demand of tumor cells that contributes to the arising of hypoxia. Figure 1 summarizes the main causes of hypoxia.

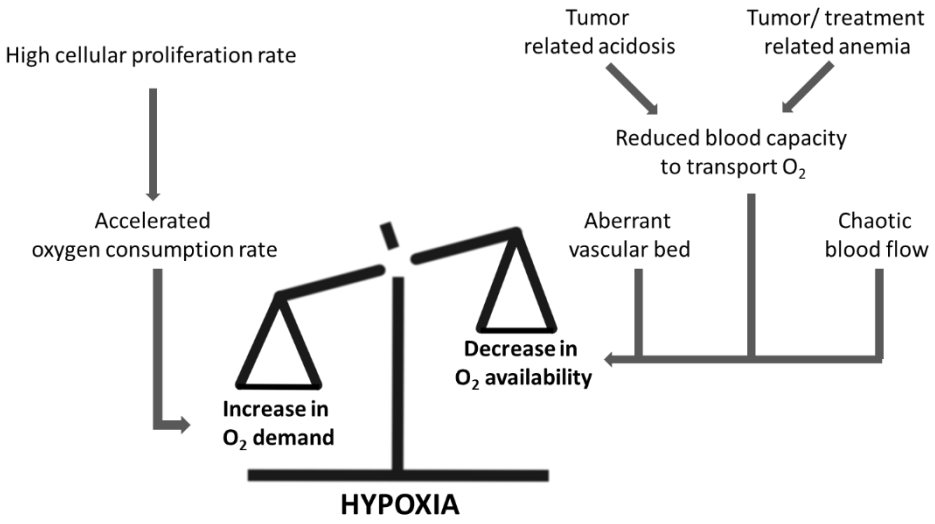

Figure 1: Causes of tumor hypoxia. Adapted from [1]

On the one hand, tumor cells have a high metabolic activity. Moeller et al. have reported that the OCR of tumor could rise up to five-fold comparing to normal tissue because of the rapid and uncontrolled proliferation of tumor cells [2].

On the other hand, multiple factors could contribute to the decrease in the oxygen supply to tumor. Tumor vasculature is often immature, leaky, tortuous, elongated with excessive branching which results in a chaotic organization and a lack of regulation in response to metabolic demand. This leads to the structural deficiencies and aberrant functionality of tumor microvessel, e.g. increase in the geometry resistance to blood flow as well as in the transcapillary and vascular permeability, which impairs the oxygen distribution to tumor. Besides, tumor- or therapy-related anemia decreases the oxygen transport capacity of blood, thus enhancing tumor hypoxia [3]. Tumors also have a lower pH than normal tissue. The reasons are two folds. First, the tumor cells are highly metabolically active which increase the production of H^+ [4]. On one hand, the enhanced glycolysis in anaerobic tumor areas results an increase in lactate production and renders the tumor more acidic. On other hand, the hydration of CO_2 in the aerobic tumor areas also produces H^+ ions. Second, the chaotic architecture of tumor vasculature hinders the drainage of H^+ thus leads to an accumulation of H^+ in tumor microenvironment [4]. Hence, tumor related acidosis reduces the binding capacity of hemoglobin to oxygen according to Bohr Effect thus reduces the blood capacity to transport oxygen.

1.3. Classifications

One remarkable feature of hypoxia is that the level of hypoxia fluctuates over time. Traditionally, hypoxia is classified in two main forms: chronic and acute (Figure 2).

Thomlinson and Gray first reported chronic hypoxia in lung carcinoma [6]. Other names of chronic hypoxia such as continuous hypoxia, diffusion-limited hypoxia, sustained hypoxia, long-term hypoxia depict characteristics of this type of hypoxia. Chronic hypoxia can last from a few hours to many days and is assumed to be caused by a gradually decrease in oxygen diffusion from the perfused blood vessel into the surrounding tissue. As the diffusion distance increases, the oxygen gradient rapidly tapers off because of the high oxygen extraction rate of tumor cells within a functionally impaired vascular network.

Brown first mentioned the existence of acute hypoxia in 1979 [7]. Later on, in 1986, Chaplin et al. experimentally evidenced this type of hypoxia [8]. Acute hypoxia is also called transient hypoxia, short-term hypoxia, perfusion-limited hypoxia, cyclic hypoxia, fluctuating hypoxia and intermittent hypoxia. The time frame of acute hypoxia is assumed to be relatively shorter than chronic hypoxia, which lasts from minutes to hours. Contrary to chronic hypoxia, acute hypoxia occurs more intermittently and does not depend on the distance from blood vessel. This form of hypoxia is believed to be the result of temporary, local disturbances in perfusion.

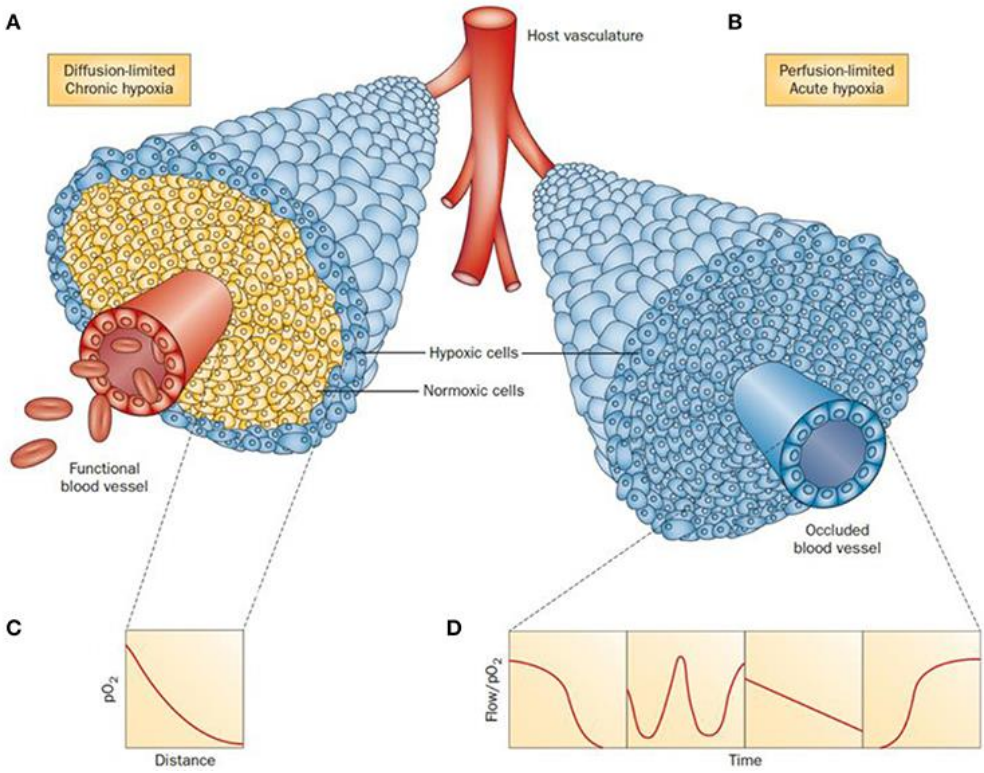

Figure 2: Illustration of diffusion-limited chronic hypoxic cells (A) and perfusion-limited acute hypoxic cells (B) growing as a cord around blood vessels. As the diffusion distance increases, the oxygen gradient decreases (C) in chronic hypoxic conditions (A). Representative flows of pO_2 over time in the occluded regions are shown for comparison (D) in acute hypoxic conditions (B). Reprinted from [5].

However, this traditional way of classification is oversimplified and overlooks the pathogenesis involved. Thus, the group of Vaupel proposed a refined classification based on pathogenesis of hypoxia as follows [9, 10].

Chronic hypoxia is divided in three subtypes: (1) Diffusion-limited hypoxia, referring to the increase in oxygen diffusion distances is linked to low vascular density that enlarges diffusion distances or to elongated, tortuous vessels. This subtype of hypoxia decreases longitudinal intravascular oxygen gradient. (2) Hypoxemic hypoxia is caused by either a reduction in total hemoglobin (e.g. tumor-associated or therapy-induced anemia) or by

a decrease in blood capacity to transport O_2 (e.g. Hb blocked by carbon monoxide in heavy smokers). (3) Hypoxia that arises from compromised perfusion of microvessels (e.g. intratumor thrombosis).

Acute hypoxia is divided into two subtypes: (1) Hypoxia can raise from temporary flow stop in microvessels, that results in a complete or heavily reduction in perfusion. The cause could be the development of vessel obstruction (from fibrin or blood cells or tumor) or vascular remodeling. (2) Transient hypoxemia that reduces temporary oxygen content in microvessels. This subtype of hypoxia could occur when there is a fluctuation in red blood cell fluxes or in plasma flow in tumor microvessels.

Perfusion-related parameters such as nutrient supply, waste removal or delivery of drugs vary depending on the causative mechanisms of hypoxia as resumed in Table 1. The refinement of classification of the different types of hypoxia may contribute to the understanding of the impact of acute and chronic hypoxia on treatment strategies.

Table 1: Associated consequences according to causative mechanism of types/ subtypes of hypoxia (adapted from [9, 10])

Type of hypoxia	**Causes of hypoxia**	**Perfusion**	**Nutrient supply, waste removal, delivery of drugs**
Chronic hypoxia	Diffusion limitation	Maintained	Reduced/ abolished dependent on diffusion distance
	Hypoxemia	Maintained	Maintained
	Compromised perfusion of microvessels	Reduced/ abolished dependent on blood pressure	Reduced/ abolished dependent on blood pressure
Acute hypoxia	Flow stop	Abolished	Abolished
	Transient hypoxemia	Maintained	Maintained

Baudelet et al. have successfully monitored the acute and chronic hypoxia via the combined T_2*-weighted gradient echo (GRE) MRI and dynamic contrast-enhanced (DCE) MRI in a fibrosarcoma mouse model [11]. Authors observed two categories of T_2* fluctuations during 1h sampling period. The true fluctuations were characterized by the sequential signal increase and decrease and the frequency of fluctuation ranged from 3 min to 1 hour per cycle. The fluctuations were associated with functional vessels tumor regions. The other category of signal fluctuation was characterized by a profound drop in signal intensity without signal recovery. This type of signal was associated with tumor regions that were impacted by vessel functional impairment.

1.4. Consequences

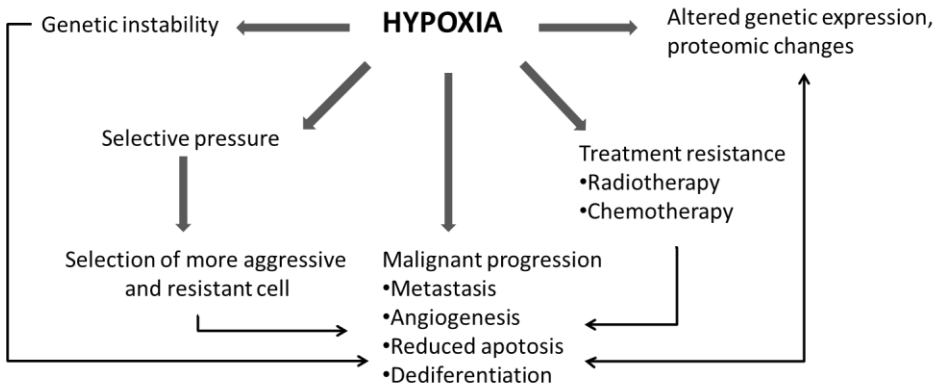

Figure 3: Consequences of hypoxia (adapted from [1])

A reduction in partial oxygen pressure below a critical value results in the death of both cancer cells and normal cells. However, cancer cells have the intrinsic ability to adjust the cell physiology and biochemistry in order to survive and even proliferate in the hostile environment. Hypoxia is known to induce important proteomic and genomic changes in cells. Experimental and clinical evidences reported a possible relation between tumor hypoxia and the promotion of metastasis, selection of malignant cellular phenotype, angiogenesis, apoptosis, induction of genetic instability, increase in tumor resistance to treatments [1, 12].

1.4.1. HIF-1α and molecular mechanism of hypoxia

Hypoxia-inducible factors (HIFs) signaling is a key mediator of tumor response to hypoxia. HIFs predominantly regulate the proteomic and genomic transforms of cells, which lead to alteration in multiple biological processes such as angiogenesis, cell proliferation and survival, glucose metabolism, pH regulation, and apoptosis [13, 14]. Among the family of heterodimeric transcription factors HIFs that are up-regulated in hypoxic condition, HIF-1 acts as a master regulator of oxygen homeostasis. HIF-1 orchestrates genes that increase O_2 delivery or helps cells to survive under the deprivation of O_2. HIF-1 consists of two subunits: HIF-1β, the aryl hydrocarbon receptor nuclear translocator, and HIF-1α, the subunit sensitive to oxygen concentration.

Figure 4 depicts the protein stability of HIF-1α under different conditions of oxygenation.

The expression of HIF-1α is oxygen-dependent. Under normoxic condition, the HIF-1α is rapidly degraded. The hydroxylation of HIF-1α by the prolyl hydroxylase-domain protein (PDH) allows the binding with Von Hippel-Lindau suppressor protein (VHLp). The complex is subsequently ubiquitynated and labeled for degradation by 26S proteasome. HIF-1α can also be hydroxylated by a factor inhibiting HIF-1 (FIH), a hydroxylase with a different oxygen sensitivity level than PDH.

Under hypoxic conditions, oxygen is not enough to warrant the activity of PDH or FIH. As a result, HIF-1α does not undergo the proteasome degradation and accumulates in the cells. HIF-1α interacts with CREB-binding protein/ E1A-binding protein p300 (CBP/p300, the essential coactivator of HIF) then heterodimerizes with HIF-1β. The heterodimer binds to the HIF-responsive element (HRE) in the promoter regions of hypoxia-regulated genes resulting an upregulation of its target genes.

Erythropoietin (EPO) was the first gene discovered to be under HIF regulation [16]. Besides erythropoietin, another well-characterized HIF-regulated gene is VEGF (vascular endothelial growth factor), which is involved in the regulation of endothelial cell proliferation and blood vessel formation in both normal cells and cancer cells. Hypoxia also promotes the undifferentiated cell state in stem cells through interaction with the Notch signaling pathway. The Notch intracellular domain interacts with HIF-1α, leading to recruitment of HIF-1α to Notch responsive promoters and to activation of Notch downstream genes [17]. HIF-1α and VEGF, a direct transcriptional target of HIF-1α, have also been shown to up-regulate Delta 4, a ligand for the Notch receptor, which is important for physiological and pathological angiogenesis [18]. HIF-1α is also known to regulate tumor pH via carbonic anhydrase IX (CA-IX), glucose metabolism via glucose transporter 1 (GLUT-1), cell proliferation, cell survival via nuclear factor kappa-light-chain-enhancer of activated B cells (NF-kB), and apoptosis via signal transducer and activator of transcription 3 (STAT3, p53). Many of the known oncogenic signaling pathways overlap with hypoxia-induced pathways, and a recent review placed HIF at the center of the major oncogene and tumor-suppressor gene pathways [19].

Clinical and experimental evidences supported HIF-1 as one molecule responsible for hypoxia-related tumor aggressiveness and for resistance to therapy. Indeed, numerous studies found a direct correlation between HIF-1α and cancer progression, invasiveness, resistance to therapy and poor patient outcome [13, 20, 21]. However, it should be noted that HIF-1α can also be stabilized in an oxygen-independent process (e.g some signaling pathways such as prostaglandin E2 receptor, receptor tyrosine kinase, mitogen-activated protein kinase MAPK) [22].

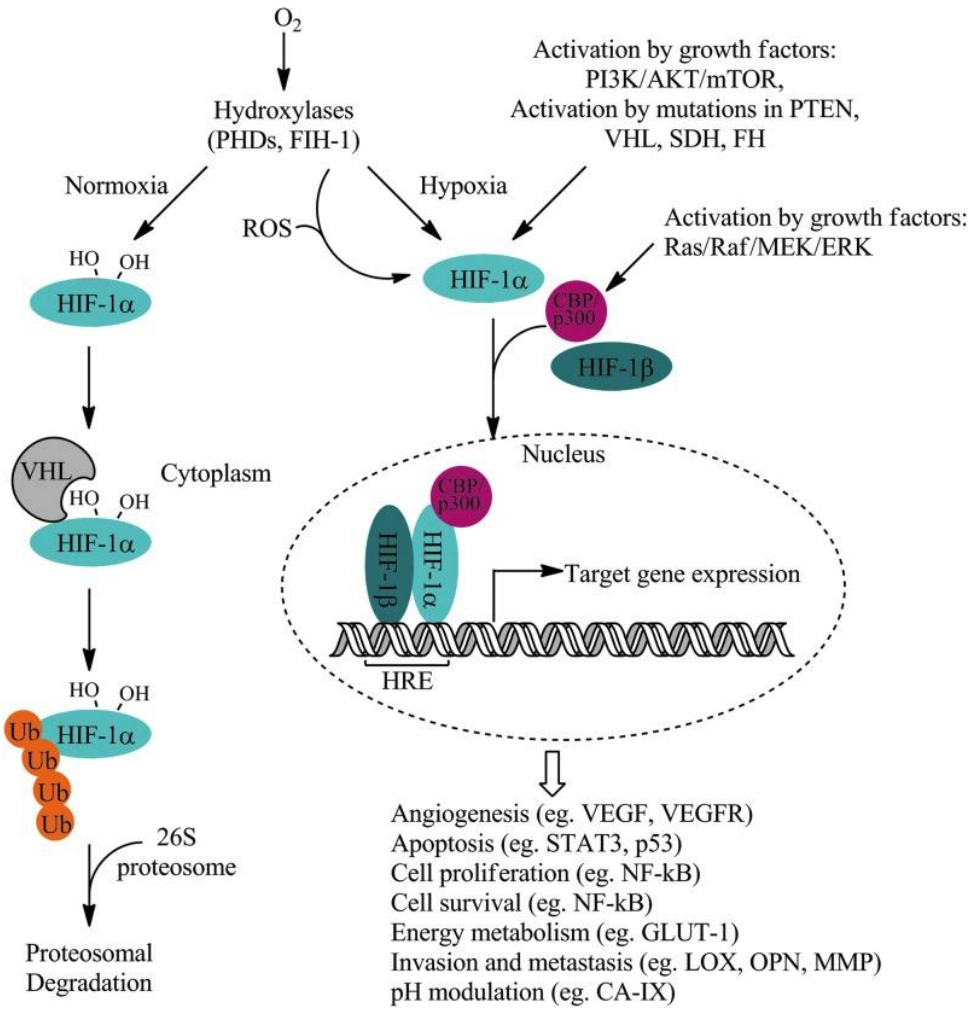

Figure 4: Regulation of HIF-1α protein stability under different oxygenation conditions (reprinted from [15]).

1.4.2. Resistance to cancer therapy

Tumor hypoxia impairs the outcome of radiotherapy, of chemotherapy and even of surgery, the three actual mainstays of cancer treatment.

Tumor hypoxia increases the resistance to chemotherapy

Hypoxia-induced chemoresistance of cancer cells is multifactorial. (1) Hypoxia impedes the effectiveness of drug delivery. Tumor vasculature is tortuous, disorganized with structural deficiencies and aberrant functionalities. Under hypoxic condition, angiogenic factors such as VEGF are up-regulated in order to increase the oxygen and nutrition supply to the tumor. However, the newly formed microvessels fail to address the metabolic demand and create a vicious loop that further worsens the hypoxic condition. As a consequence, the delivery of chemotherapy becomes more irregular and may be insufficient under hypoxia. (2) Hypoxia induces the cell cycle arrest (quiescence) which reduces the growth rate and the proliferation of tumor cells [23, 24]. The quiescent and undifferentiated state would protect cancer cells from external stress. Thus, quiescent cells are not sensitive to conventional chemotherapy drugs which mainly target the rapidly proliferation characteristic of cancer. (3) Hypoxia inhibits apoptosis and senescence of cancer cells. Deprivation of oxygen induces apoptosis in normal cells and in neoplastic cells mainly via the p53 pathway. However, tumor cells are able to escape the cell death programming by acquiring mutations in genes regulating apoptosis. Additionally, the hypoxic condition creates a selective force for cells that lost the apoptotic potential [25]. (4) Hypoxia may interfere with cell uptake of conventional chemotherapeutic agents via the alteration of tumor pH [26]. Indeed, the low extracellular pH increases the uptake of weakly acidic drugs (e.g. cyclophosphamide and cisplatin) but slows down the uptake of weakly basic drug (e.g. doxorubicin and vinblastine) [26]. Besides, hypoxia can also be associated with the expression of drug efflux pump such as P-glycoprotein [27]. (5) Finally, lack of oxygen impedes the generation of free radicals required for the cytotoxic effect of some chemotherapeutic agents [28].

Tumor hypoxia increases the resistance to radiotherapy

The response of cancer cells to radiotherapy depends on the nature of radiation, the state of cell cycle and especially the level of oxygenation. (1) Different types of radiations including gamma, X-ray, neutron radiation, or alpha and beta particles, possess different linear transfer energy levels that affect the penetration and damage induced by the radiation. (2) The sensitivity of cells to radiation depends on its cell cycle phase. Indeed, the level of radiosensitivity increases from “the end of S phase” to “G1 phase” to “G2/M phase” [29]. Thus, the most radiosensitive cells are in a fast proliferation phase whereas the most radioresistant cells are in a quiescent, low-proliferating state which is more likely be found in hypoxic niche of tumor. (3) Besides, oxygenation plays a key role in the response of cell to radiotherapy since the highly reactive free radical R• produced after the absorption of radiation energy is most likely responsible for the biological damage (usually DNA) [30]. The widely accepted mechanism is the oxygen-fixation hypothesis (Figure 5). Free radical R• can be produced either directly in the target molecule (usually DNA) or indirectly via the production of OH• consecutive to hydrolysis of molecules that can diffuse far enough to reach DNA and form R• in DNA. These unstable R• molecules have different fate depending on the presence of oxygen. The R•

free radicals rapidly react with the oxygen available to produce RO_2• and then undergo further reactions to yield the stable ROOH which leads to irreversible DNA damage. Without oxygen, or in the presence of reducing species, R• has a longer half-life and can react with H^+ leading to the restitution of the original form. Thus, hypoxic cells are about three times more radioresistant than normoxic cells [31].

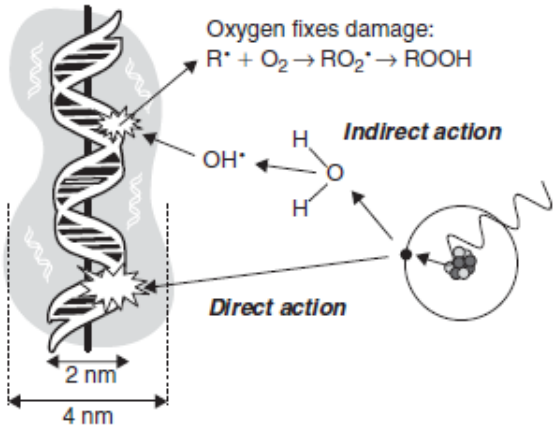

Figure 5: The oxygen fixation hypothesis. Reprinted from [30]

The mutations acquired during hypoxia also contribute to the radioresistance of cancer cells. Hypoxia creates a niche that protect malignant cells against irradiation. Indeed, hypoxic cells with reduced apoptotic potential are still able to proliferate and the DNA damage from radiation is reduced under this condition. Moreover, the expression of proteins controlled by HIF-1, e.g. VEGF and basic fibroblast growth factor (bFGF) were reported to enhance the radioresistance of cells [32, 33].

Tumor hypoxia reduces the outcome of surgery

Hypoxia has been found to be responsible for poorer surgical outcome. Clinical evidence in advanced cancers of the uterine cervix treated with primary surgery showed a significantly better overall and disease-free survival probabilities in patients with normoxic tumors (pO_2 > 10 mmHg) compared to those with hypoxic tumors (pO_2 < 10 mmHg) [34]. The treatment failure in hypoxic tumors was mainly due to locoregional recurrence with and without the development distant metastases [34]. Although the reason has not fully understood, authors believed that the recurrence of

hypoxic tumors might be linked to hypoxic pressure that selected aggressive phenotype and favoured the development of metastatic disease. Studies have suggested the mechanism of the acquisition of metastatic phenotype as a stepwise selection process driven by hypoxia [35]. The expression of proteins regulated under hypoxic condition supports the formation of distant metastasis via the enhancement of tumor cell motility and invasion, intravasation, extravasation, and metastatic colonization [36]. The deterioration of tumor vasculature due to pericytes detachment from the basement membrane and the overexpression of VEGF result in leaky vasculature and high vessel permeability, which promote both intravasation and extravasation of tumor cells and cancer stem cells. In addition, both chemokine stromal cell-derived factor-1 (SDF-1) and its receptor CXCR4 have been reported to be hypoxia-inducible. Evidences suggested that the SDF-1/CXCR4 axis could involve in tumor progression and the development of distant metastases [37].

1.5. Characteristics of tumor hypoxia

1.5.1. Tumor hypoxia classification

Normoxia: Each peripheral tissue exhibits a distinct normal oxygenation level. According to the data from a meta-analysis of Vaupel et al [38], the median oxygen levels from normal tissue range from 26 to 52 mmHg. Individual tissues maintain their optimal median oxygen levels by homeostasis, which implies that oxygen sensitivities of cells are determined by their origins.

Physiological hypoxia: A slight drop in oxygen level triggers tissue-response to maintain a sufficient oxygen level (e.g. vasodilation, increasing blood flow, and/or temporary stabilization of HIF). As a result, the tissue oxygenation rapidly returns to normoxia. Mckoewn defined this oxygen level as “physiological hypoxia” [39]. This homeostasis mechanism that is able to regulate oxygenation may be activated at different oxygenation levels in different tissues.

Pathological Hypoxia: Below “physiological hypoxia” is hypoxia or “pathological hypoxia” as suggest by Mckoewn [39] where the homeostatic mechanisms cannot respond effectively to reverse the situation. In tumors, hypoxia level variations depend not only on the tumor localization but also on the surrounding microenvironment. Indeed, tumor vasculature is generally recognized to be chaotic, unstructured with blind ends and prone to collapse leaky vessels. Hence, it is understandable this type of vasculature is unable to fulfil the fast growing oxygen demand of tumor regardless evidence that HIF-1 is up-regulated most of the time [40]. Despite the fact that angiogenesis is often enhanced in tumors, numerous studies have shown that the average oxygen level of tumors is significantly lower than the oxygenation of the corresponding normal tissue, ranging from 2 to 32 mmHg with a majority falling below 10 mmHg [38].

It is widely accepted that under an adequate oxygen supply, the oxygen consumption rate (OCR) and the production of adenosine triphosphate (ATP) in tumors are usually comparable to the ones found in the corresponding normal tissues [41]. Under hypoxic conditions, tumor oxygenation drops below a critical value causing a progressive fall of OCR and ATP production rate. Consequently, the prolonged exposure to hypoxia creates a selection pressure that kills the putative hypoxic sensitive cells and leaves hypoxia tolerant cells. These surviving cells are reported to be stress resistant and more malignant [41]. The term “Janus face” describes well the characteristic of tumor hypoxia. On the one hand, hypoxia can exert antiproliferative effects: restraint proliferation, promotion differentiation, and induction apoptosis and necrosis [42]. On the other hand, as a result of a Darwinian process, tumor cells acquire new mutations that changes the gene expression, confers a more aggressive phenotype, and promotes local and distant spread in order to adapt to hypoxic stress [42].

It is difficult to determine the precise threshold of hypoxia but it is assumed that hypoxia begins when the oxygen level falls below 1% (7 mmHg) and may well be significantly lower [41]. Lack of oxygenation below 7 mmHg stimulates angiogenesis via upregulation of growth factors (such as vascular endothelial growth factor, platelet-derived growth factor-B, transforming growth factor β, insulin-like growth factor-2, and epidermal growth factor) and switch-off of angiogenesis inhibitors (i.e., angiostatin, endostatin, 16 kDa protactin, leukemia inhibitory factor) [43]. HIF-1s and especially HIF-1α is the master transcriptional factor that regulates the expression of genes involved in the adaptation process (tumor progression and aggressiveness) [44].

Severe oxygen depletion below 0.1% or 0.7 mmHg will impair molecular mechanism such as gene amplification, apoptotic potential, OCR, oxidation status of cytochromes, inducing genomic and epigenomic instabilities and increased selection pressure [45]. In order to survive in the hostile and nutrient-deprived microenvironment, the Darwinian process on cancer cells results in the selection of highly aggressive and therapy resistant phenotype that further enhances hypoxia and leads to a vicious circle.

It should be noted that the fraction of cells with malignant phenotype is minor in quantity (perhaps < 5 %) and hypoxia selection pressure may favour the survival of this small cell population which can determine the fate of patient outcome [43].

To summarize, a single hypoxic threshold for a general application does not exist. Moreover, it should be kept in mind that there is also no sharp threshold between hypoxia and normoxia for any functional parameter.

1.5.2. Heterogeneity of hypoxia

Tumor oxygenation is heterogenous both between and within tumors. Intratumoral hypoxia is characterized by temporal and 3D-spatial variations, which could be seen as

the “4D heterogeneity” of hypoxia. The presence of hypoxia is shown to be independent on tumor stage or histological type [45].

The spatial variations are characterized by the degree of hypoxia (level and severity), the topographical distribution (center vs. periphery of tumor), the extension of hypoxic area, number of hypoxic subvolumes (single vs. multiple) [45].

As a matter of fact, tumor oxygenation is usually communicated as a median value, which ignores the heterogeneity within individual tumor. The gradient of oxygen diffused to cancer cells changes longitudinally and axially, that depends strongly on the functionality of local blood vessels. The longitudinal O_2 diffusion gradient decreases along the blood vessel from the arterial to the venous end. The radial O_2 diffusion gradient relies on the proximity of local blood vessels and decreases from microvessels to surrounding cell layers. Indeed, the cellular proliferation pushes cells away from the capillaries resulting in a progressively decrease in oxygen delivery. The diffusive distance ranging from 70 to 200 µm [6, 46, 47, 48] around the perfused blood vessel creates the “cord” of actively growing cells. The two factors determining the slope of these gradients are the O_2 availability (capacity to transport O_2 of the blood x flow rate) and O_2 extraction rate (OCR, O_2 diffusivity and the cell packing density) [49]. Considering the radial O_2 gradient, the more oxygen the cells require, the smaller the tumor “cords” will be. Outside the tumor cord, the hypoxia tolerance of cells determines their survival in hypoxic region. These cells remain viable under the quiescent state. The more tolerant cells will remain quiescent longer resulting in the extension of hypoxic region over the cord and a deeper degree of hypoxia.

In case of acute hypoxia, the oxygen supply is abolished or strongly reduced either by the spontaneous fluctuations of red blood cell fluxes that cause temporary drop of intravascular hematocrit or by physical obstructions that cause transient flow stops or critically reduced perfusion [10]. Consequently, the temporal disruption of microvessels function leads to the development of hypoxia in regions where the affected microvessels are responsible for O_2 supply.

Nevertheless, tumor oxygenation not only depends on the O_2 diffusion gradients as described above but also on numerous pathophysiological features e.g. O_2 shunt diffusion, the abnormality of tumor vasculature. Hence, no singular “typical” O_2 diffusion distance but a broad distribution (continuum) of O_2 diffusion distances is usually observed in malignant tumor. Of note, hypoxic region could be at a micron scale and present a steep pO_2 gradient between well-oxygenated and hypoxic subvolume (up to 60 mmHg/mm) [49]. This fact has a significant clinical implication e.g. for dose painting to precisely target the hypoxic region in order to effectively eradicate the tumor. However, we are still unable to assess this subregional heterogeneity with the currently available techniques due to the averaging problem of an insufficient spatial resolution.

One fallacy, which is widely accepted, claims that malignant tumor is usually hypoxic and necrotic in the center and better oxygenated in the periphery. The concept may be true for some human tumors (e.g. glioblastoma) but could not apply for all cases. Clinical evidences in numerous tumor types proved at microscopic scale that hypoxic subregions are distributed all over the viable tumor mass [50, 51].

2. ASSESEMENT OF TUMOR OXYGENATION

Acknowledging the highly complexity of tumor oxygenation, we do not expect any measurement method that is able to cover the full extent of spatial and temporal heterogeneity of tumor hypoxia. If there were a method that could completely resolve the complexity of tumor hypoxia, it would not be a useful tool but a burden of an overwhelming data far more than needed to solve the investigated problem. Methods currently available for oxygenation measurement differ in several ways. They can measure tumor oxygenation directly (e.g. pO_2) or indirectly (e.g. hemoglobin saturation, perfusion, endogenous markers). Other characteristics have to be taken into account such as sample volumes (macroscopic or microscopic); time intervals of sampling; compartment sampled (intravascular, interstitial, or intracellular); invasiveness; resolution; sensitivity; and repeatability. A well comprehension of how these factors change in each technique can help the interpretation of the data. Besides, the combination of multiple techniques increases the precision and robustness of the measurement since each technique reflects different facets of tumor oxygenation.

The assessment of tumor oxygenation may have profound clinical implications in at least three scenarios: (1) to provide an early prediction about the prognostic of the disease; (2) to improve the treatment outcome by identification of patients who could benefit from oxygen modification agents; (3) to select an adaptive treatment regime in patients whose tumor is resistant to radio- or chemotherapy.

In this part, different techniques along with their intrinsic parameters are reviewed to highlight their value on the outcome of cancer treatment.

2.1. Direct oxygen mesurements

2.1.1. Oxygen Probes

a. Polarographic electrodes – Eppendorf histograph

Back to 1960s, tumor oxygenation was measured directly by the homemade glass electrodes. The method involved the insertion of electrode into the tissue. The negative voltage between cathode and anode reduced oxygen at the surface of cathode, which generated a current that is proportional to the local pO_2. These cumbersome, fragile polarographic electrodes only allowed a few measurements at a depth of 3-4 mm [52].

The commercialization of Eppendorf histograph marked a revolution in the measurement of oxygenation. Two outstanding improvements were made: (1) the oxygen sensor was protected inside a metal needle resulting in a more robust electrode; (2) multiple measurements in sub-millimeter steps could generated along the electrode thanks to a stepping motor attached to the electrode. The measurement provided extracellular pO_2 histogram of a tissue volume about 50–100 cells located around the probe [53]. The method was then widely applied in clinical investigation on numerous tumor types and yielded up to 70 research articles between 1988 and 2005 [38]. These studies came up to a conclusion that hypoxia may determine the patient prognosis and influence the outcome of therapy. Evidences have been reported in head and neck cancer (H&NC) [54, 55], cervix [56, 57], soft tissue sarcomas [58], and prostate [59]. Interestingly, a study in cervix found that primary tumors of patients with metastases were less oxygenated than those of patients without metastases [60].

Although Eppendorf electrode is considered safe without adverse effects [38] and is widely cited as the "gold standard" for hypoxia determination [61], nowadays it is no longer commercially available. The invasiveness is the major inconvenience of Eppendorf electrode, which impedes repeated measurements on the same site. Besides, the technique is operator-dependent and demands a technically skilled user. The probe is also unable to map tumor hypoxia heterogeneity thus hinders therapy planning. Furthermore, the tumor location should be easily accessible to employ the technique. Importantly, the probe does not distinguish between viable and necrotic tissue that may lead to an overestimation of hypoxic fraction. Likewise, the Eppendorf electrode cannot access the temporal fluctuation in tumor oxygenation since it consumes oxygen for each measurement, thus differentiation between acute and chronic hypoxia is impossible. It should also be kept in mind that the technique was never predictive for treatment outcome at the individual level. One of the first clinical studies in head-and-neck [62] clearly demonstrated this. Thirty-five patients were stratified in two subgroup based on the oxygenation/ hypoxia status using Eppendorf electrode for irradiation. Despite the significant difference in local tumor control after radiation therapy (RT) between two groups, 40% of the patients did not fall within the correct category, meaning that some hypoxic patients were controlled by irradiation while some non-hypoxic patients failed to respond to irradiation.

b. Fibre optic probe/ Fluorescence quenching

Another approach to measure tumor oxygenation is the fibre optic probes with the commercialized brand name OxyLite™ [63]. The technique measures the quenching time of a fluorophore by oxygen, which is inversely proportional to oxygen tension at the tip of the probe where the fluorophore is located. As the technique does not consume oxygen, the major advantage of the fibre optic probes is the ability to perform continuous measurement, thus allowing the assessment of the temporal heterogeneity in tumor pO_2 as well as the effect of hypoxia modification therapies. The method is however sensitive

to temperature, thus an attached thermocouple to the probes is needed for temperature correction. Moreover, the probe only reports on an average pO_2 of a volume that is several hundred times larger than the tip of the electrode, where the fluorophore is located. Consequently, pO_2 heterogeneity cannot be assessed by this approach. Nonetheless, the method still encounters drawbacks similar to Eppendorf electrode such as invasiveness, operator-dependence, and accessibility of tumor. Hitherto, fibre optic probes have not been applied in the clinical setting.

c. Phosphorescence tomography

The method involves the infusion of water-soluble phosphor probes into the vasculature [64]. A pulse of light excites the phosphorescent probes to emit their own light from which the decay rate is proportional to the local oxygen concentration. The technique is independent of probe concentration since O_2 concentration relies on the lifetime of the emission light but not on signal intensity. Phosphorescence tomography also has a high temporal resolution. It takes only a few seconds or less for a measurement, thus real-time measurement of tumor oxygenation is possible. The method may aid therapy planning thanks to the possibility to construct a map of the tumor oxygenation as well as to repeat the measurements. However, the penetration of the excitation pulse determines the sample volume. Therefore, the application of the technique depends on tumor location. Importantly, the administration of external probe to the vasculature system results in the oxygen measurement from blood vessel but not from tissue. These features limit the application of the method to map tumor oxygenation only in preclinical animal models [65, 66] but not yet in patients.

2.1.2. Magnetic Resonance Oximetry

a. ^{19}F-MRI

Perfluorocarbons (PFCs) are used as probes for ^{19}F-NMR spectroscopy and imaging to quantify tissue oxygenation at the pixel level [67]. The highly hydrophobic PFCs have a better O_2 solubility than water. The principle of the method lays on the interaction of PFC with dissolved O_2. The change of the ^{19}F spin-lattice relaxation rate at a given temperature is proportional to the O_2 concentration [68]. Hence, the technique provides a non-invasive and quantitative mapping of tissue oxygenation when temperature is tightly controlled [69].

PFCs show some features that facilitate the *in vivo* applications including high sensitivity to changes in pO_2, high reproducibility even at low pO_2, and low toxicity [70]. The sensitivity of the method can reach 1 – 3 mmHg in hypoxic region [71]. The pO_2 assessed by ^{19}F-MRI has been compared with more traditional techniques such as Eppendorf electrode [72], immunohistochemistry [71], and near-infrared spectroscopy [73]. Both the ^{19}F echo planar imaging approach and the Eppendorf histograph showed similar oxygen tension distributions in experimental tumors and determined that larger

tumors were significantly less oxygenated than smaller tumors [72]. ^{19}F-MRI also successfully characterized the hypoxic status of two Dunning prostate R3327 rat tumor sublines that was confirmed by immunohistochemistry [71]. Significant correlations were found between the variations in vascular HbO_2 concentration (reported by near-infrared spectroscopy) and the change in tumor pO_2 (reported by ^{19}F-MRI) in rat breast 13762NF tumors with respect to hyperoxic gas breathing [73].

The FREDOM procedure (fluorocarbon relaxometry using echo planar imaging for dynamic oxygen mapping) using fast ^{19}F-MRI technique allows a dynamic mapping of tumor pO_2 as well as monitoring the tumor pO_2 change in response to hyperoxic challenge [74, 75]. Monitoring pO_2 by FREDOM evidenced a successful elevation of tumor pO_2 during irradiation correlating with delayed tumor development [76]. Jordan et al. further used a snapshot inversion recovery pulse sequence to reduce the acquisition time up to 1.5 min allowing the identification of spontaneous oxygen fluctuation [75, 77].

There are three protocols to administer PFCs. The first one involves the systematic introduction of PFCs emulsion via intravenous injection. This approach allows the measurement of the vascular oxygenation, the tissue uptake and sequestration of the compound. However, most of PFCs are sequestrated in the reticuloendothelial system including liver, spleen, and bone marrow leading to the risk of hepatomegaly [78] and reducing the signal in tumor. Moreover, the delivery of PFCs depends on the vasculature, thus PFCs are preferentially sequestered in well-perfused areas instead of hypoxic poor- perfused area. The second protocol is the intratumoral injection of pure PFCs to resolve the problem. The echo planar imaging FREDOM method (fluorocarbon relaxometry using echo planar imaging for dynamic oxygen mapping) relies on this second protocole to map the pO_2. The procedure involves the multi-injection of hexafluorobenzene directly into the tumor in a fan pattern using of a fine needle (32 G) to ensure distribution of hexafluorobenzene throughout a plane across the tumor [79]. However, intratumoral injection limits its potential clinical application because of the tumor accessibility issue. Both protocols allow repeated measurements within a certain period. For a long follow-up, a repeated administration is needed because of the clearance of PFCs over time. The third protocol employs the encapsulation of the PFCs in an oxygen-free diffusible material that does not require the re-injection of PFCs for a stable pO_2 readout. Yet, the protocol requires surgery for probe implantation. In addition, the oxygenation reported is locally at the site of implantation and the spatial information is lost. Limitations of these protocols make ^{19}F-MRI using PFCs suitable for research in pre-clinical application but not yet in clinical setting.

b. Electron paramagnetic resonance EPR

The principle of EPR relies on the capacity to detect the electron spin of paramagnetic unpaired electron species. Although molecular oxygen is paramagnetic, the direct detection of oxygen is impossible since the EPR spectra of dissolved oxygen in tissue

are too broaden to be detectable. Hence, an indirect method including the introduction of a paramagnetic probe is required to assess the tissue oxygenation. The principle is based on the paramagnetic properties of oxygen that makes the molecule an efficient relaxer for other paramagnetic probes. The interaction with oxygen modifies the resonance characteristics of the probes and thus its EPR spectrum of which the enhancement of relaxation rates is proportional with the oxygen concentration [12]. The most common method to measure oxygenation relies on the broadening of the principal hyperfine line, which is related to T_2 of EPR spin probe. The measurement of the linewidth of the EPR spectrum provides a non-invasively real-time monitoring of tissue oxygenation. An ideal EPR probe should have a single and narrow resonance line, a linewidth that is proportional to pO_2, no toxicity and a good metabolic stability. Interestingly, the natural presence of endogenous paramagnetic material is minor and undetectable *in vivo*. Consequently, by introducing an external paragmagnetic probe, the sensitivity of EPR is higher than that of nuclear magnetic resonance NMR (about 700 times greater [12]) thanks to the absence of a background signal. Of note, the EPR technology operates at higher frequencies and lower fields than NMR because the gyromagnetic ratio of an unpaired electron is much larger than that of a proton. The high frequency decreases the sample size thickness that can be analyzed because of the non-resonance absorption of the electromagnetic radiation by water in the sample, e.g. the depth of measurement is less than 1 mm at 9.5 GHz and increases up to 1 cm at 1 GHz. For *in vivo* application, the low operating frequency (200 MHz to 1.5 GHz [12]) extents the sensitive deepness of the sample. Another feature of EPR that should be kept in mind is the short relaxation times of paramagnetic species (nanosecond) comparing to that of NMR protons (millisecond) [80]. Consequently, the EPR spectra are obtained via continuous wave experiments, which means the sample is irradiated constantly and the resonant response is recorded by sweeping the applied magnetic field [81]. Thus, the acquisition time of EPR is longer than that of NMR. Recently, Yasui et al. have developed the pulsed technique (like for NMR) for *in vivo* EPR application to reduce the acquisition time [82].

Nowadays, two classes of probes are used for *in vivo* studies, the soluble probes for EPR imaging (EPRI) and the insoluble probes for EPR spectroscopy.

EPRI provides a spatial quantification of tissue pO_2 but the soluble probes are less sensitive to changes in oxygenation than insoluble particle probe [12]. The repeated measurements are possible in EPRI but re-introduction of probe is required for longtime follow-up. Lately, the development of the instrument for the co-registration of EPRI and MRI allowed an integration of anatomical information and pO_2 distribution [82 - 85]. The coil operates at low frequency (300 MHz) at which both the detection of EPRI probe (OX63, a paramagnetic oxygen-sensitive triaryl methyl radical) and MRI acquisitions are feasible. The co-registration has been applied to monitor the changes in tumor oxygenation following a hyperoxic challenge [82, 85] or the effects of radiation [86].

Compared to the soluble probes, the insoluble particles are unable to provide the spatial distribution of pO_2 but are more sensitive to changes in pO_2 (less than 0.2 mmHg [22]) and once being implanted, the particles remain at the sites indefinitely allowing repeated measurements over time. Thanks to these advantages, EPR spectroscopy oximetry is widely used to monitor the changes in tumor oxygenation e.g. the effect of hypoxia targeted co-treatment on pO_2 as well as on outcome of cancer therapy [87 - 93].

The application of the EPR technique in human remains limited, with only two clinical systems being available worldwide. The first clinical trials using EPR oximetry involved OxyChip - an oxygen-sensing paramagnetic crystal LiNc-BuO encapsulated in a biocompatible polymer matrix [94]. The implantation of the chips allows repeated measurements in tumor tissues located within 20 mm from skin surface. The oximetry measurement using India Ink were performed on patients with melanoma, basal cell, soft tissue sarcoma, and lymphoma tumors during radiation and chemotherapy [95]. The current limitations to further implement EPR in the clinical setting are due to the availability of instrumentation but also to the limitation of sample thickness, limiting its applications to accessible tumors/tissues.

2.2. Indirect oxygen measurements - Exogenous markers

Different exogenous probes have the ability to specifically accumulate in hypoxic cells. Hypoxia is then indirectly measured via different techniques that are able to detect these markers.

2.2.1. 2-nitroimidazole markers

The most known exogenous markers are 2-nitroimidazole-based markers, which are characterized by an NO_2 group attached to the imidazole ring (Figure 6). The markers diffuse passively into the cells. Under hypoxic condition, the stable NO_2 moiety can undergo 6 successive electrons reductions to give rise to the NH_2 moiety that is also unreactive. Of note, one of the intermediate forms is highly reactive and can bind to any cellular macromolecule that traps the markers within the cell [96]. The reduction only takes place under the activity of active enzymes, thus nitroimidazole uptake is specific to viable hypoxic cells but not necrotic. With the presence of O_2, the markers rapidly re-oxidize into the stable form. The unreactive species are gradually washed out from the cell, leaving only the bound molecules, which will be detected afterwards. The 2-nitroimidazole-based markers are widely detected with immunohistochemistry (IHC), positron emission tomography (PET) or single photon emission computed tomography (SPECT).

It should be noted that the distribution 2-nitroimidazole-based markers relies on the tumor vasculature system. The chaotic, disorganized structure of tumor vessels may hinder the accessibility of markers to hypoxic regions where the blood supply is usually reduced. Consequently, a paradoxical situation may occur where the nitroimidazole

uptake in severe hypoxic regions is weakened because of the limited drug delivery in these regions.

The effectiveness of nitroimidazole markers relies on the specificity of markers to accumulate into hypoxic areas. Two useful factors can be used to predict the relative quality of a nitroimidazole marker, including the hypoxic-specific factor (HSF) and the oxygen dependency. HSF is the ratio between the binding marker within the cells incubated under severe hypoxic conditions and that of cells incubated at 21% O_2. An ideal value of HSF ranges from 30 -100. The oxygen dependency is the cellular oxygen concentration at which the bound markers is at 50% of its maximum rate. An oxygen dependency of 0.3% to 0.5% oxygen in the equilibrium gas phase is optimal [97].

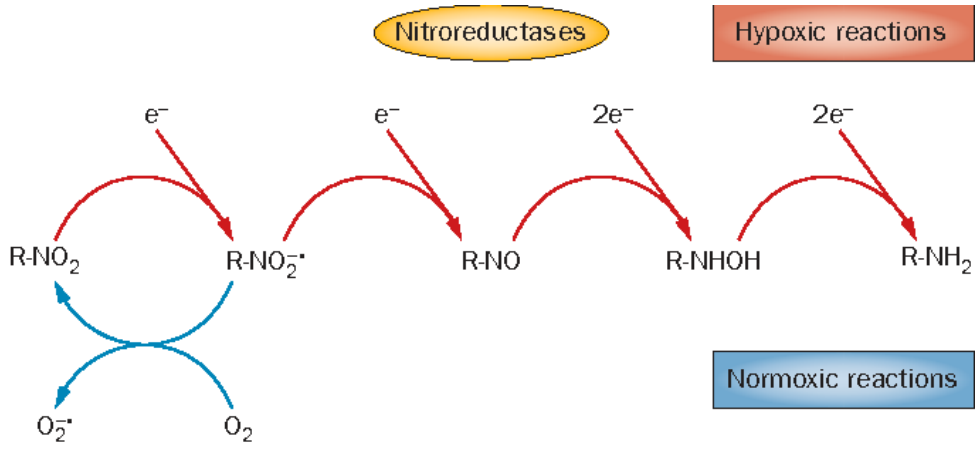

Figure 6: Mechanism of nitroimidazoles (R-NO_2) reduction. Under hypoxic condition (red arrow), NO_2 group can reduce to NH_2 group. These two groups are inactive but one of the intermediate products is highly active that can bind to macromolecules within cells. Under normoxic condition (blue arrows), the reduction is reversible with the presence of O_2. (adapted from [96])

a. Immunohistochemistry (IHC)

Two IHC 2-nitroimidazole-based markers are approved for clinical applications: pimonidazole PIMO and EF5 [98, 99]. Both markers are administered to patients intravenously prior to biopsy or surgery (several hours for PIMO and 24-48h for EF5). Hypoxia is assessed by estimation of stained cells fraction. The detection of compound

adducts relies on the specific binding of antibodies to antigens (EF5 or PIMO) in biological tissues. The antigen-antibody binding can be visualized thanks to the tagged fluorophore to antibody. Strong linear correlations have been found between PIMO accumulation and pO_2 *in vivo* [100].

The main advantage of IHC is that the approach provides the most precise spatial information of tumor microenvironment compared to other methods. However, the trade-off is its invasiveness. To perform the measurement, biopsy or surgical is required to examine the tumor tissue. Thus, repetitive measurements to evaluate the dynamic change of hypoxia are difficult. In addition, the sampling size is limited in certain regions of the tumor resulting the loss of the spatial heterogeneity information of the whole tumor. Consequently, one IHC image is only the snapshot of the tumor oxygenation at a giving moment.

b. Radiolabeled hypoxia markers

The detection of radiolabeled markers depends on the decay half-life of the labelled radioisotopes and the pharmacology of the markers. Hence, an ideal radiolabeled marker should rapidly and homogenously distribute to all tissues. To have a good signal, markers should remain in the tissue long enough to accomplish the bioreductive process. Besides, the unreactive markers should be cleared from the cells fast enough to decrease the background signal. For the patient's convenience, the imaging should be done within a short-time frame depending on the half-life of the radionuclide. [22]

PET tracers

PET techniques involve the detection of tracers labelled with positron-emitting radioactive isotopes. The isotope undergoes the positron decay. The positron emitted (e+) interacts with an electron (e-) leading to the annihilation of both particles, which induces a pair of photons with opposite directions that are detected by a PET scanner.

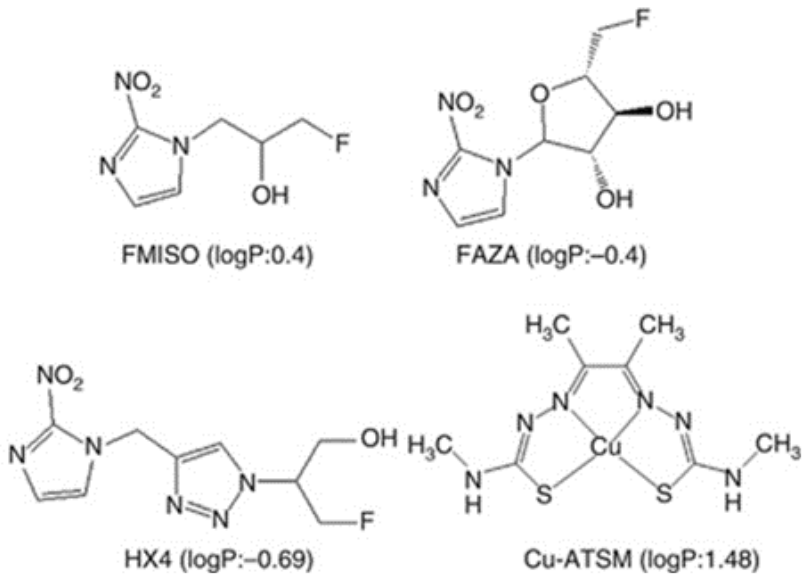

Figure 7: Structures and logP-values of PET hypoxia radiotracers (logP > 0: lipophilic molecule, logP < 0: hydrophilic molecule). Adapted from [101]

^{18}F-fluoromisonidazole. ^{18}F-FMISO is the first hypoxia-tracer developed for PET and also the most extensively studied hypoxia PET tracer in clinical studies [101]. The tracer is lipophilic (logP = 0.4) which ensures a good penetration and diffusion to cells. Evidences have proved that the intracellular binding of FMISO requires an oxygen level less than 10 mmHg and can rise up to 28 times higher than in normoxic conditions [102]. However, the high lipophilicity could also be the reason of the FMISO intense background since the excretion of the tracer is as low as 3 % of the total administration dose [103]. Consequently, a tissue showing a tumor to blood ratio of more than 1.2 after minimum 2 h post-injection is generally considered to be hypoxic. Studies on gliomas, head and neck, breast, lung and renal cancer patients showed that the FMISO retention is specific for hypoxic regions [104]. However, results in sarcomas are variable, the accumulation of FMISO in rectal cancer was non-specific, and no FMISO uptake was observed in pancreatic tumors [101]. Previously, the accumulation of FMISO was found to be significantly correlated with pO_2 (fraction pO_2 < 2.5 mmHg or < 5 mmHg), as assessed by Eppendorf polarographic method [104, 105] in H&NC patients. However, recently, in an extensive study by Mortensen et al. in the same cancer type, the authors showed a lack of correlation between FMISO retention and Eppendorf measurements using virtual voxel model [106], a method that treated the information of PET and

Eppendorf histogram on the same site. Although having a high hypoxic selectivity and being widely studied, FMISO failed to be accepted in clinical routine due to its slow clearance kinetics limiting image contrast.

To overcome the limitation of FMISO, other tracers have been developed which are more hydrophilic than FMISO, including fluoroetanidazole (FETA), fluoroerythronitroimidazole (FETNIM), fluoroazomycinarabinofuranoside (FAZA) and HX4. Among them, FAZA and HX4 are currently in clinical evaluation [107, 108].

^{18}F-fluoroazomycinarabinofuranoside. The hydrophilicity of ^{18}F-FAZA (logP = -0.4) improves the clearance from blood and normal tissues resulting in a higher signal-to-noise ratio compared to ^{18}F-FMISO. In preclinical studies, ^{18}F-FAZA uptake correlated with tumor pO_2 reflecting that this tracer was able to quantify tumor hypoxia [110, 111]. In clinical studies, ^{18}F-FAZA has been successfully used to image hypoxia in gliomas, lymphomas, lung, head and neck, cervical and rectal tumors, with better results than ^{18}F-FMISO thanks to an improvement in hypoxic/ normoxic contrast and an earlier acquisition time point [101]. The report of the DAHANCA 24 trial on H&NC patients involving the ^{18}F-FAZA image before and after treatment (including primary radiotherapy, nimorazole, and concomitant cisplatin) showed that the tracer uptake was a non-invasive prognostic marker of treatment outcome [112].

^{18}F-flortanidazole. ^{18}F-HX4 is the most hydrophilic PET tracer (logP = -0.69) possessing a good water solubility and faster background clearance, resulting in improved pharmacokinetic and clearance properties as compared with ^{18}F-FMISO [101]. Although ^{18}F-HX4 has the potential for shorter acquisition times than ^{18}F-FMISO [113], later scan times (2–4 h post injection) can increase the hypoxic-to-normoxic contrast [114] with the trade-off of the reduced radioactivity and noisier data.

It should be noted that the cells must be hypoxic for significant time periods to be detected by the nitroimidazole-based hypoxia PET markers [96]. In other words, diffusion-limited chronic hypoxia is more likely be detected than acute hypoxia resulting from transient fluctuations in blood flow.

Alternatively, nitroimidazole is also labelled with ^{124}I, which has a longer haft-life than ^{18}F. For example, two ^{124}I labelled nitroimidazole: [^{124}I]-iodoazomycin arabinoside (^{124}I-AZA) and [^{124}I]-iodoazomycin galactoside (^{124}I-AZG) allow to delay scans up to 24 and 48 h post-injection, respectively [52]. The long scan delay is expected to increase the normoxia/hypoxia contrast by maximizing the clearance of unbound tracers from blood and tissue. However, the results did not show any improvement in image contrast with a poor counting statistic [115, 116].

SPECT tracers

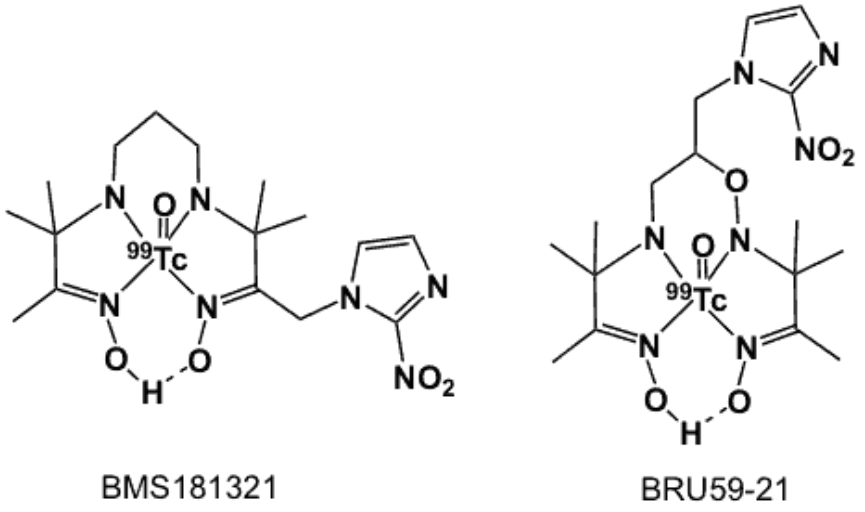

Figure 8: Structures of ^{99m}Tc-labelled SPET hypoxia radiotracers. Adapted from [119, 120]

Unlike PET tracers labelled with positron-emitting radioactive isotopes, the SPECT tracers are labelled by gamma-emitting radioactive isotopes and the radiation is measured directly. In PET, the annihilation of positrons creates two gamma photons leading to a higher resolution than in SPECT. Whereas the advantage of SPECT is the low cost. The first hypoxic SPECT tracer undergone clinical evaluation is [^{123}I]-iodoazomycin arabinoside (IAZA) [117]. However, this tracer has inconsistent uptake into various tumors [117, 118]. The alternative radioisotope, which is more widely available, less expensive, and easily chelated to different compounds, is ^{99m}Tc. Some representative nitroimidazole ^{99m}Tc-labelled compounds for hypoxia study are BMS 181321 and BRU59-21, and complex ligand HL91. Although BMS 181321 selectively accumulates in hypoxic cells, the instability and high background level limit the application of the tracer [119]. The latter generation BRU59-21showed a better stability and higher tumor/ normal tissue contrast [120].

2.2.2. Bioreductive complexes Cu-ATSM – PET tracer

An alternative class of PET markers for hypoxia study is Cu-ATSM [Cu(II)-diacetyl-bis(N 4-methylthiosemicarbazone)]. Cu-ATSM can be labelled with different positron-emitting

radionuclides of copper including ^{60}Cu (t1/2 = 0.39 h), ^{61}Cu (t1/2 = 3.33 h), ^{62}Cu (t1/2 = 0.16 h), and ^{64}Cu (t1/2 = 12.70 h). Thanks to the low molecular weight and lipophilicity characteristic (logP = 1.48), Cu-ATSM presents a high membrane permeability and fast tumor uptake. Together with an efficient washout kinetics, the imaging could be done rapidly after injection (as low as 30 min) [121] with a high hypoxia/ normoxia contrast. Although the hypoxia specificity is believed to be related to the irreversible reduction under low oxygen conditions of Cu(II) to Cu(I) which is trapped within cells, the exact mechanism of Cu-ATSM retention is still not completely understood. The Cu-ATSM uptake seems to be influenced by other factors than hypoxia [122, 123]. Thus, controversial results have been reported in terms of the value of Cu-ATSM as hypoxia marker. Specific Cu-ATSM retention has been observed in H&NC, rectal, cervical cancer, lung cancer as well as gliomas as reviewed by Fleming et al. [101]. Those data support the possibility of using Cu-ATSM as a marker of outcome to radiotherapy. However, an *in vivo* study evidenced that Cu-ATSM accumulation could depend on tumor-type [124]. In addition, *in vitro* data have shown an impact of cell line, time, and redox status on tracer uptake and retention [122]. The study of Hueting et al. has raised the concern whether the hypoxic specificity of Cu-ATSM is related to the behaviour of ionic Cu or to Cu-ATSM itself since the authors have found a similar distribution between ^{64}Cu-ATSM and ^{64}Cu-acetate [125]. Evidences have shown that Cu-ATSM was insensitive to the change in tumor oxygenation [126, 127]. Nonetheless, investigation on the co-localization of Cu-ATSM distribution and pimonidazole immunohistochemistry yielded both positive and negative correlations [128, 129]. In brief, more information is needed to confirm the potential of Cu-ATSM as a specific marker for tumor hypoxia**.**

2.3. Indirect oxygen measurements - Endogenous markers

The method detects tumor hypoxia based on the overexpression or accumulation of molecules under (patho)physiological conditions of low oxygenation. These molecules are called “endogenous” or “intrinsic” hypoxia markers.

The mostly used hypoxia- inducible biomarkers are HIF-1α protein, the main regulator of the hypoxia response, and proteins under the regulation of HIF-1α including erythropoietin (EPO), carbonic anhydrase IX (CA IX), glucose transporter 1 (GLUT1) and vascular endothelial growth factor (VEGF). In a recent review by Vordermark and Horsman, endogenous markers seem to be a promising tool. Numerous clinical results suggest a high expression level of HIF-1-related proteins correlated to a poor outcome of cancer treatment [52]. Positive correlations between hypoxic fractions determined by Eppendorf oxygen electrode and the immunohistochemical expressions of HIF-1α, CA IX and GLUT1 have been reported in cancer patients [130-132]. Of note in these studies, only HIF-1α expression was quantified by the percentage of HIF-1α positive area over the whole tumor, the expression of CA IX and GLUT 1 were evaluated by a range of score from 0 to 3 based on staining intensities. Besides, the spatial resolution between

the Eppendorf histograph and IHC is different. On the one hand, the electrode provides histrograms of averaged oxygenation of hundreds of cells around the probe at each step of its path. On the other hand, IHC provides spatial distribution profile of tumor oxygenation status at the microscopic scale of the whole tumor slide. An important point is that HIF-1α and its target genes are regulated by a complex network. For example, the *in vitro* HIF-1α expression has been found to be common under normoxic conditions in human malignant cells, such as lymphoma and leukemia cells [133] suggesting that this protein expression is cell-type dependent. In addition, level of HIF-1α expression is also influenced by factors unrelated to hypoxia such as mutations in the von Hippel Lindau gene, activation of oncogenes, the effect of growth factors and cytokines [45].

Other class of hypoxic endogenous markers involves plasma markers or circulating markers. They are molecules secreted by hypoxic tumor cells into body fluids and in the plasma of the patient. The measurement of this type of markers allows evaluating both the total tumor burden and their oxygenation level. The best-studied marker is osteopontin (OPN). Evidences supported plasma level of OPN as marker for hypoxia. OPN was correlated with pO_2 measured by Eppendorf electrode in H&NC patients [134]. The OPN level was successfully used to stratify patient for adapted cancer treatment [135]. Likewise, OPN was also evaluated to predict the outcome of patients [52]. However, OPN is not specific for hypoxia since the regulation of the response of the protein is controlled by other factors than oxygenation level (e.g. wound healing [136]).

Another class of tumor hypoxia biomarkers is gene expression signatures [137]. The method determines the change in gene transcriptional response under hypoxic condition using microarray gene expression assay. The hypoxia signature can both derive from cellular (*in vitro*) or from clinical (*ex vivo*) data. Each approach has its own pros and cons. On the one hand, the *in vitro* approach exposes cells to hypoxic and normoxic conditions to determine genes that are significantly up/down-regulated or differing from baseline threshold of normoxic condition. However, the approach may not accurately recapitulate the hypoxia phenotype observed in tumors such as the tumor microenvironment and heterogeneity. On the other hand, the *ex vivo* approach involves the validation of *in vitro*-derived signature genes in clinical samples. In addition, aggregation of additional genes could be further achieved by using computational methods in order to obtain a more representative hypoxic signature for tumor hypoxia phenotype. Yet, the *ex vivo* biopsies are prone to be contaminated by stromal tissue resulting the identification of false-positive signals derived from pathways less relevant for tumors. Steps of development of the hypoxia signatures are summarized in Figure 9. From the review of Harris et al., hypoxia signatures show great variety [137]. The expression level depends not only on the nature of the sample (culture cell or human tumor tissue) but also on the tumor type. The future perspective is to identify a core hypoxia signature, which involves the validation the *in vitro* derived signatures in *ex vivo* setting as well as in new cancer types. Another challenge is to translate hypoxia signatures into clinical message to identify a hypoxic tumor. No common method is

widely accepted to classify tumor hypoxia using gene signatures. In addition, there is a need of a reliable method to measure tumor hypoxia in order to compare the performance of different hypoxic classification approaches. Last but not least, it should be noted that the expression profile of hypoxic signatures could be affected by factors unrelated to hypoxia, e.g. the common renal cell carcinoma mutation VHL. Consequently, patients might be inaccurately stratified.

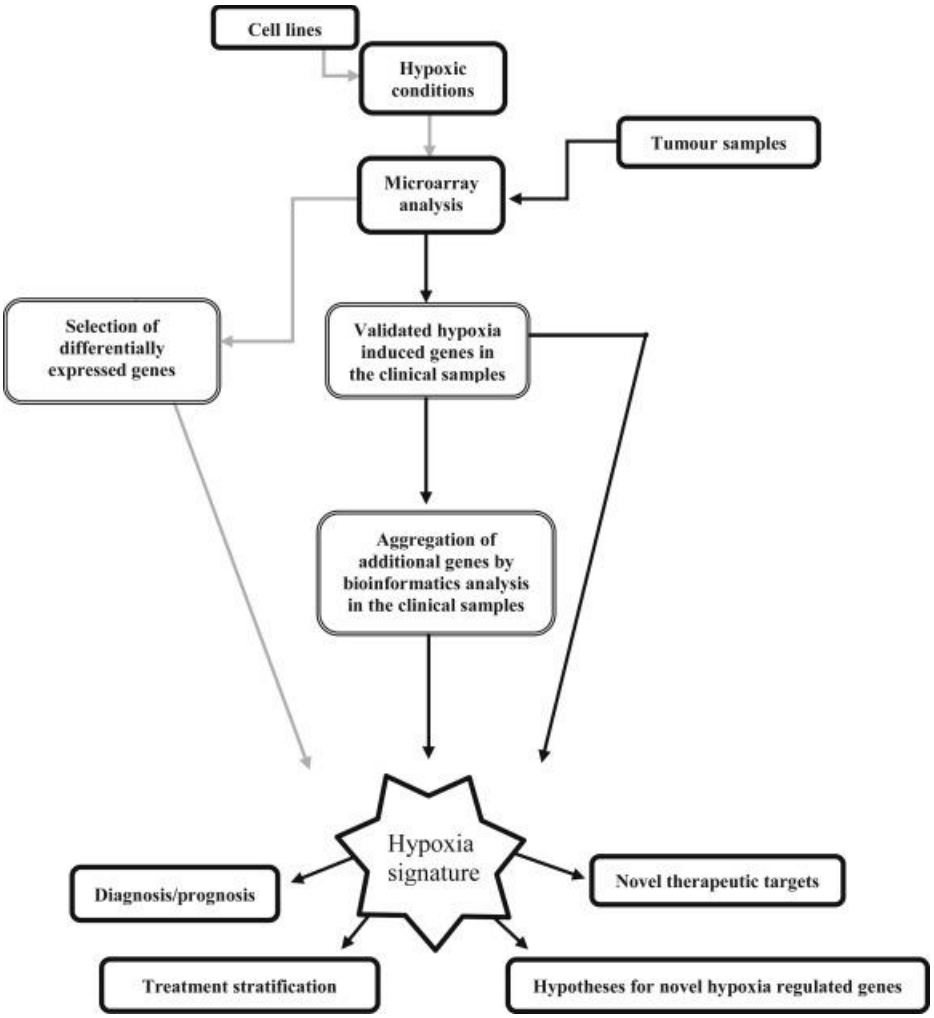

Figure 9: In vitro (grey arrows) and ex vivo (black arrows) approaches to generate hypoxia signature. Reprinted from [137]

2.4. Vascular parameters

2.4.1. Perfusion

Another approach to evaluate the tumor oxygenation is to assess the hemodynamics information of the tumor. Indeed, the main route for oxygen delivery to tissue is via the vascular network. Thus, the perfusion is an indirect indication of hypoxia; e.g., poor perfusion increases chronic hypoxia whereas fluctuation in perfusion may induce acute hypoxia [96].

Dynamic contrast-enhanced magnetic resonance imaging (DCE-MRI) monitors the functionality of tumor vasculature by intravenously injecting a contrast agent then monitoring its distribution in a region of interest. The contrast agents are generally gadolinium-based chelates, which shorten T_1 proportionally to the concentration of the chelates. The contrast agent diffuses through blood vessel walls and distributes into the extracellular space at a rate that is dependent on blood perfusion, vascular density, tissue permeability, and extracellular volume fraction [138]. The quantitative magnetic resonance (MR) parameters are calculated reflecting the vascular flow and permeability, which provide indirect information of O_2 delivery and necrosis. Indeed, necrosis areas have little or no contrast uptake that does not conform to the mathematic kinetics assumption. Thus, these voxels should be excluded from analysis [139].

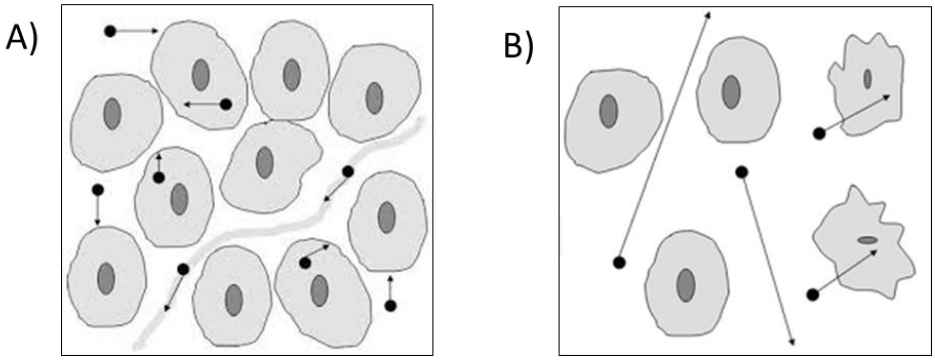

Figure 10: A) Restricted diffusion of water molecules in regions with high degree of cellularity and intact cell membranes. B) Free diffusion of water molecules in regions with low degree of cellularity in and defective cell membranes. Water molecules: dark circles with arrows. Reprinted from [140]

Otherwise, a method that allows direct measurement of tumor necrosis is diffusion weighed MRI (DW-MRI). The principle relies on the exploration of random motion of water molecules in biologic tissue, in particular water molecules in the intracellular, extracellular and intravascular space [140]. Since cell membranes and macromolecules restrain the motion of water molecules, the degree of water diffusion is inversely correlated with the tissue cellularity and the integrity of cell membranes. Thus, the motion of water molecules is less restricted in regions with low cellularity such as necrotic area (Figure 10).

Clinical evidences reported the correlation between parameters obtained from DCE-MRI and oxygen electrode measurements in cervix cancer [138, 141], PIMO in H&NC [142, 143], [^{18}F]-FMISO in glioblastoma [144]. Besides, DCE-MRI is the only MR technique whose measurements have been found to be predictive for the radiotherapy outcome both in preclinical and in clinical settings [52, 145].

[^{15}O]-labelled water is a PET tracer that allows the estimation of tumor perfusion. Nevertheless, the conflicting results obtained from clinical studies in H&NC patients questions the usefulness of the method as a hypoxia marker [146, 147].

Tumor blood flow estimated by **computed tomography (CT) perfusion** is comparable to [^{15}O]-labelled water perfusion [148]. The advantages of CT perfusion is a more widely availability and a less expensive cost than [^{15}O]-labelled water. H&NC patients with reduced perfused tumors assessed by CT presented poorer radiotherapy outcome [149-151]. Yet, the attempt to correlate the CT perfusion and pimonidazole was unsuccessful [142].

Cautions should be taken when using perfusion markers to assess hypoxia since hypoxia is not only determined by oxygen supply. Other factors contribute to the development of hypoxia including the capacity of blood to carry and release O_2 or the OCR. Interestingly, perfusion markers may become a useful tool providing information regarding fluctuating hypoxia. In order to do this, we have to measure the change in perfusion rather than the perfusion per se [96].

2.4.2. Hemoglobin saturation

Blood oxygen level-dependent (BOLD) MRI is a functional MRI method that evaluates indirectly and noninvasively the change in tumor oxygenation by detecting the modification in hemoglobin saturation. The method uses gradient echo sequences that are sensitive to the effective MR transversal relaxation time of protons T_2^* ($R_2^* = 1/T_2^*$). While deoxyhemoglobin (dHb) is paramagnetic, oxyhemoglobin (HbO_2) is not. Thus, dHb creates large magnetic field variations that modify the relaxation properties of the protons of water molecules (especially T_2^*) in blood and in the surrounding tissue resulting the change in MRI signal intensity [12].

It should be noted that BOLD signal is also sensitive to other factors than the change in dHb concentration, such as variations in blood volume, blood flow, hematocrite concentration, pH, glucose level and temperature [22]. The use of multiple echo sequence is intended to assess a BOLD signal that is independent on the inflow effect [152].

Preclinical and clinical evidences have evidenced that the BOLD signal is able to assess the change in tumor oxygenation induced by hyperoxic challenges [139, 145], yet correlation with absolute tumor pO_2 is controversial [153, 154]. Correlations of MR signal with the hypoxic marker pimonidazole produced conflicting results [155, 156]. In a preclinical study using OCR modifiers, insulin and a non-steroidal anti-inflammatory drug, intended to modify tumor oxygenation, a lack of change in BOLD signal was observed [157]. In brief, BOLD-MRI is useful to qualitatively assess the change in oxygenation induced by an increase in oxygen supply as well as the effect of the treatment on radiation therapy [158]. Indeed, the relationship between BOLD signal and pO_2 is curvilinear where the change in MRI signal is more pronounced at pO_2 around 5 to 15 mmHg than at pO_2 around 40 to 50 mmHg [158]. Moreover, BOLD-MRI reports tissue oxygenation via the evolution of dHb concentration but does not measure pO_2 directly. Consequently, the sensitivity of the approach is reduced in regions containing small amount of dHb (e.g. regions of sparse vasculature) or in regions containing too much dHb (e.g. large vessels) [158].

The advantages of BOLD including the noninvasiveness and the real-time detection have been applied to study the fluctuations of hypoxia [11]. Thus, BOLD imaging has the potential to address relevant biological questions that may aid treatment design to overcome hypoxia.

2.5. ^{1}H relaxation imaging

The method is based on the measurement of the longitudinal relaxation time T_1 (longitudinal relaxation rate $R_1 = 1/T_1$) of water protons, which is sensitive to the dissolved O_2 in blood plasma, in interstitial fluid or in intracellular water. Indeed, molecular O_2 is paramagnetic and shortens the T_1 of protons of water molecules containing dissolved oxygen. ^{1}H MRI methods present several advantages that make the technique translatable for clinical detection of hypoxia, including the noninvasive real-time monitoring of tumor pO_2 without the introduction of a reporter probe, its availability in medical imaging centers, better spatial resolution and more reasonable price than PET. Theoretically, the change in relaxation rate is proportional to the change in dissolved O_2 for a given voxel [159]. Evidences have shown an increase in R_1 after a hyperoxic challenge [160 - 162]. It should be noted that R_1 is sensitive to factors that are also unrelated to the change in pO_2, including temperature, water content of tissue of interest, and blood flow.

The frequency of hypoxic regions is an indication of poor clinical prognosis [163]. Despite the importance of hypoxia, most clinical radiology and research studies only measure average parameter values [164]. The group of O'Connor has validated a R_1-based approach, with the so called oxygen-enhanced MRI (OE-MRI), to monitor the change in tumor pO_2 following oxygen breathing to quantify the variations of hypoxia [165, 166]. The voxel wise analyses revealed that the combined information on the oxy-R fraction (fraction lacking a positive R_1 in response to oxygen challenge) and perfusion data was correlated with the hypoxic fraction detected by pimonidazole in two different vascularized tumor models, 786–0-R and SW620 as well as in patients with renal cell carcinoma [165, 166].

One drawback of R_1 is its low sensitivity to the change in tumor oxygenation. To overcome the limitation, a new technique has been proposed by Jordan et al. [167] in 2013. The method with the acronym MOBILE (mapping of oxygen by imaging lipid relaxation enhancement) assesses the signal of R_1 of lipid protons instead of the global R_1 (including the signal of water and lipid protons, mostly dominated by water proton signal), as the solubility of oxygen in lipid is higher than that in water. It was shown in lipid-rich mammary tumors that lipid R_1 was more sensitive to both negative and positive changes in tumor oxygenation than the conventional global R_1 [168]. Besides, the authors also found a positive correlation between R_1 in lipid and pO_2 assessed by EPR oximetry. The method had then been investigated in the clinical setting in stroke and glioma patients [169, 170]. Both R_1 parameters were able to distinguish the unaffected brain tissue from the infarcted area in stroke patients [169] as well as from tumors in glioma patients [170].

3. TARGETING HYPOXIA IN RADIATION THERAPY

Since tumor hypoxia is a main hurdle that impairs the outcome of cancer therapy, we will now describe some therapeutic approaches to overcome hypoxia and their potential impact on the response to radiotherapy.

3.1. Increasing tumor oxygenation

Tumor oxygenation is the result of the balance between tumor oxygen supply and oxygen consumption of cancer cells. Hence, the two possible approaches to increase tumor oxygenation consist in increasing oxygen supply or decreasing oxygen consumption rate.

3.1.1. Increasing oxygen supply

One of the earliest approaches to deal with hypoxia by increasing oxygen supply involved the "hyperbaric oxygen (HBO) therapy". Patients were allowed to inhale high oxygen content gas under hyperbaric (typically 3 atmospheres) condition during radiotherapy [171]. The method increases the oxygen saturation in blood more than

under normobaric conditions. Clinical evidences confirmed the superior outcome of radiotherapy given under HBO than under air breathing condition [172]. Patients with H&NC, uterine cervix carcinoma, or bronchogenic carcinoma, irradiated under HBO showed a significant benefit in local tumor control and subsequent survival. However, the complexity of the method and the patient compliance discontinued the use of HBO in the clinical setting [172].

The use of high oxygen gas breathing under normobaric conditions including 100% oxygen or carbogen (95% oxygen + 5% carbon dioxide) have been proved to radiosensitize tumors [173]. Carbogen (CB) is more advantageous than pure oxygen since the CO_2 component in carbogen is believed to have a vasodilatation effect and to counteract the vasoconstriction effect of breathing high oxygen content gas. Still, clinical evidences have failed to demonstrate any significant therapeutic gain using this approach [174]. The pre-irradiation gas breathing time (PIBT) could be one explanation for the failure since this factor has been shown to be critical for enhancing the irradiation effect [175]. Unfortunately, PIBT varies from tumor to tumor thus, it is impossible to pre-define a common optimal PIBT for a significant outcome improvement. Hence, to enhance the response to irradiation, treatment planning should ideally be decided individually based on the monitoring of tumor oxygenation. Indeed, thanks to the information obtained, oncologists could determine if breathing carbogen can improve the tumor oxygenation as well as the moment of maximal reoxygenation to apply irradiation on an individual basis. Besides, the fact that carbogen is more likely to affect diffusion-limited chronic hypoxia rather than on perfusion-limited acute hypoxia could also contribute to the failure of the method.

Experimental studies have demonstrated that nicotinamide prevents transient fluctuations in tumor blood flow and thus reduces acute hypoxia [176]. Hence, the combination of nicotinamide and treatment targeted at chronic hypoxia is relevant to overcome radioresistance related to chronic and acute hypoxia. The ARCON protocol (Accelerated Radiotherapy with Carbogen and Nicotinamide) combined the two strategies has rooted since 1990s. The protocol has been pre-clinically validated with positive results for the use of ARCON [177]. For clinical studies, phase 1 and 2 trials in various tumors have demonstrated the feasibility and tolerability of ARCON [177]. Especially, H&NC and bladder cancer have showed a higher local-tumor control rate than other studies leading to phase 3 trials of these tumor types [177]. In a phase 3 trial, patients with squamous cell laryngeal cancer were randomly assigned to accelerated radiotherapy (AR) or ARCON [178]. With a median follow-up of 44 months in 345 patients, the local tumor control rate was identical for two treatment arms (78% AR versus 79% ARCON, $p = 0.8$) whereas the regional control was better in patients treated with ARCON (86% AR versus 93% ARCON, $p = 0.04$) [178]. Interestingly, the improved regional control was specifically observed in patients with hypoxic tumors (100%) but not in patients with well-oxygenated tumors (55%) ($p = 0.01$) [178].

Another approach is to improve the oxygen transport capacity of the blood via increasing the hemoglobin level. The role of hemoglobin on the response to radiation therapy has been well described in smoking and non-smoking H&NC patients with a significant better loco-regional control is observed in non-smokers [179]. Indeed, smokers could reduce more than 30% of the oxygen-unloading capacity of the blood, which is responsible for the reduction of oxygen delivery to tumor. In 1986, Hirst proved that an increase in hemoglobin concentration via blood transfusion could increase tumor oxygenation [180]. However, the clinical trials using transfusion in anaemic patients revealed conflicting results, either positive [181] or showing no effect [182] on radiotherapeutic response. The disappointing results coupled with well-known risks of transfusion e.g. infections, acute/ chronic reactions and immunosuppression, limited the application of the method. The reason for the failure could be that (i) the effect of transfusion to increase tumor oxygenation was only transient and (ii) the tumor was able to adapt to this change. Indeed, in Danish head and neck cancer (DANHACA) trials, the patients received transfusion several days prior to irradiation where adaptation of tumor may occur [182]. Thus, the final concentration of hemoglobin might not be as important as the introduction of a transient oxygen enhancement via transfusion during radiation therapy to induce an optimal radio sensitisation [183]. The hemoglobin level could also be increased by using EPO. Unlike blood transfusion, EPO stimulates the production of hemoglobin gradually over time. Although EPO improved hemoglobin level in anaemic patients, those who received EPO treatment presented a poorer outcome to radiotherapy than controlled patients who did not received EPO [184, 185]. Indeed, EPO is a growth factor and consequently triggers the development of tumors, outbalancing the effect of the increase in tumor oxygenation.

An improvement in the tumor oxygen delivery can be obtained via manipulating the oxygen unloading capacity of blood. Allosteric effector of hemoglobin promotes the dissociation of oxygen from hemoglobin by right shifting the oxygen dissociation curve, thus increasing tumor oxygenation. Compounds under clinical investigation such as OXY111A (*myo*-inositol tripyrophosphate, ITPP) [186, 187] and Efaproxiral [188] were well tolerated and induced an increase in partial pressure of oxygen in preclinical models. Efaproxiral has reached phase III in patients with brain metastases from breast cancer. Yet, no significant improvement on overall survival has been observed using the combination of efaproxiral and whole brain radiation therapy [189].

Recently, the use of ultrasound-sensitive oxygen microbubble was assessed in a pre-clinical study. The method involves the injection of surfactant-shelled microbubbles with oxygen core intravenously. Then the microbubbles were triggered by noninvasive ultrasound to locally increase oxygenation. Results revealed that the method significantly increased the tumor pO_2 up to 20 mmHg in a xenograft murine model MDA-MB-231. When combine with radiotherapy, ultrasound-triggered oxygen delivery nearly tripled the radiosensitivity of tumor. In addition, the photoacoustic imaging revealed that

the transport of oxygen microbubbles is independent of hemoglobin transport. Therefore the method can potentially improve oxygenation in avascular regions. [190]

3.1.2. Decreasing oxygen consumption

Although most studies have employed increasing oxygen supply approaches to increase tumor oxygenation [191], decreasing oxygen consumption is however suggested as a more efficient way for this purpose [192]. Indeed, the mathematical simulation of Secomb et al., which is based on *in vivo* data, showed that hypoxia can be abolished only by reducing 30% of tumor consumption rate versus an increase in arterial pO_2 up to 11 times. Thus, modulating OCR becomes an attractive strategy to reduce hypoxia and radiosensitize tumor. Different treatments to decrease OCR have been described in the pre-clinical settings, and have been reviewed by Gallez et al. [193].

a) Drug-based OCR modulators

Cytotoxic drugs

Paclitaxel (PTX), an anti-cancer chemotherapeutic agent, is able to enhance the response of tumors to radiation therapy via multiple mechanisms. Initially, the radiosensitization of PTX has been described as the result of at least two factors: the tumor reoxygenation and the cell cycle arrested at the radiosensitive G2 and M phases [194]. Recently, PTX-loaded micelles (M-PTX) were tested, consisting in a new formulation of PTX that increases the Maximum Tolerated Dose (MTD) of the compound, [195]. The authors described mechanisms that could be responsible for the reoxygenation of the tumors [195]: M-PTX decreases OCR via inducing apoptosis and decreasing mitochondrial respiration. In addition, the decrease in cell number also reduces the compression of blood vessel caused by tumor cells, thereby elevating tumor blood flow and increasing oxygen supply. Consequently, the combined effects of decreasing OCR and increasing O_2 supply enhance the oxygen availability for the tumor.

Arsenic trioxide (As_2O_3) radiosensitizes tumors by decreasing OCR via enhancing intracellular ROS (Reactive Oxygen Species) production mediated by decreased GSH (Glutathione) levels on the mitochondrial respiratory chain [92]. Importantly, the dose of As_2O_3 to modify tumor oxygenation is below the toxic dose. Of note, As_2O_3 induces a decrease in blood flow that could reduce the oxygen delivery to the tumor. However, the overall result obtained is an increase in oxygenation. This observation confirmed the theoretical simulation of Secomb [192] that reducing OCR is more important to alleviate tumor pO_2 than increasing O_2 supply.

Endogenous NO stimulator and exogenous NO donors

The radio-sensitizing effect of insulin relates to its ability to stimulate the endothelial nitric oxide synthase activity in tumors which triggers the production of endogenous nitric oxide (NO). NO reduces tumor hypoxic fraction through a decrease in the tumor OCR by the regulation of mitochondrial respiration. NO also presents intrinsic radiation sensitizing effects. Similarity, exogenous NO donors such as isosorbide dinitrate and S-nitrosocaptopril act with a similar mechanism. Finally, nitrites can be selectively converted to NO under the low extracellular pH of tumor to enhance radiosensitivity of tumor [196].

Glucocorticoids (hydrocortisone, dexamethasone, and prednisolone) and Nonsteroidal anti-inflammatory drugs NSAIDs (piroxicam, indomethacin, diclofenac, and NS-398)

Evidences have been reported that these compounds can inhibit oxygen consumption by affecting the mitochondrial respiratory chain. While NSAIDs are responsible for the uncoupling of oxidative phosphorylation in mitochondria [90], the decrease in OCR induced by glucocorticoids is explained by the inhibition of cytochrome c oxidase (complex IV) of the mitochondrial respiratory chain [91].The effect of glucocorticoids on tumor oxygenation improved the radio efficacy by a factor of 1.7 [91]. The response of anti-inflammatory drug depends on dose and type of NSAIDs [90].

Anti-angiogenic agents and Mitogen Activated Protein Kinase (MAPK) inhibitors

Anti-angiogenic agents were initially believed to destroy tumor vasculature and to cut off the oxygen and nutrition supply for tumors. Other findings suggested that some agents could transiently normalize abnormal structure of tumor vasculature, making them more efficient for oxygen as well as drugs transportation [197]. Some anti-angiogenic agents such as SU5416 [198] and vandenatib [199] as well as the electrotransfer of a plasmid encoding an antiangiogenic factor, the recombinant disintegrin domain of ADAM-15 [200], have been found to decrease OCR and then improve tumor pO_2.

The MAPK inhibitor sorafenib has been described to increase tumor pO_2 and to improve the radiation response in murine FSAII tumors. The sorafenib effect was the combination of a decrease in OCR related to the depletion of mitochondrial function and an increase in tumor perfusion related to the anti-angiogenic effect (vascular normalization) [201]. The epidermal growth factor receptor (EGFR) inhibitor gefitinib was also found to improve tumor oxygenation via a decrease in OCR. The depolarization of mitochondrial membrane might contribute to this effect [202].

Drug repurposing

Drugs used in diseases other than cancer but showing mitochondrial inhibition properties are potential candidates to radiosensitize tumors such as the anti-malarial atovaquone [203], metformin for the treatment of type 2 diabetes [204], the anti-thyroid propylthiouracil [205].

b) Physical-based treatments

Irradiation has a profound effect on tumor oxygenation status. First, irradiation decreases cell number that is increasing the tumor O_2 availability. Second, irradiation triggers the production of endogenous NO that increases both the tumor blood flow and decreases OCR in surviving cell. Hence, the effect could be beneficial to the outcome of fractionated irradiation when an appropriate schedule is applied to match the time point of maximal reoxygenation with the timing of irradiation [206 - 208].

Mild hyperthermia can both radiosensitize tumors via reoxygenation and can kill hypoxic cells, thereby enhancing radiation response [209]. The mechanism of tumor reoxygenation induced by hyperthermia is the combination of the activation of HIF-1, the increase in tumor perfusion and the decrease in oxygen consumption [210]. The incorporation of hyperthermia as hypoxia-targeted treatment for irradiation therapy becomes one of the best approaches to target hypoxia in order to improve the outcome of radiation. The value of hyperthermia has been proved by numerous clinical trials on different tumor sites subjected to chemotherapy or radiotherapy [209, 211]. Nevertheless, the best way to use the technology remains unclear despite the raising number of publications using the approach. Technically, hyperthermia can be administered locoregionally or systemically. The delivery of hyperthermia requires trained personnel and specialised equipment. Risks of hyperthermia e.g. superficial overheating, cardiac dysfunction, coagulation abnormalities, and fall in peripheral arterial resistance limits the application of the method in clinical setting [211]. Although further studies are needed to clarify the mechanisms by which hyperthermia improved clinical outcomes, hyperthermia remains a promising candidate for the future adjunct to conventional oncology treatments as the statement made by Januszewski and Stebbing ‘Scepticism is often justified, but data are increasing and the design of ongoing studies is robust. It is time that this technology is given the attention it deserves.’ [211].

In brief, many strategies have been developed to increase tumor oxygenation to enhance the radiation therapy outcome. In order to screen for a potential candidate for clinical evaluation, efforts should be concentrated to understand the exact mechanism responsible for the improvement of oxygenation. Besides, *in vivo* comparison between different oxygen modulators is substantial for the selection of the best candidate for clinical trials, yet there is a lack of study regarding this subject for the moment. In addition, monitoring the dynamic change of tumor microenvironment (e.g. oxygenation,

OCR, oxygen blood flow, potential cytotoxic effect) is essential to decide when, how and which therapeutic modalities to combine for an optimal treatment outcome.

3.2. Targeting hypoxic cells

3.2.1. Hypoxic cell radiosensitizers

One class of hypoxic radiosensitizers are agents that increase the sensitivity of hypoxic cells to irradiation by mimicking the electron-affinity characteristic of oxygen [212]. The highly electron-affinic nitroimidazoles have been demonstrated *in vitro* to radiosensitize hypoxic cells [213]. The finding has led to a series of clinical trials to evaluate nitroimidazoles as modifiers of hypoxia [214]. Without the patient screening for the presence of hypoxia before enrollment in clinical trial, it is difficult to evaluate the benefit of a hypoxic modification modality. Despite a considerable heterogeneity among individual tumors, the meta-analysis on over 7000 patients enrolled in 50 trials indicated a significant benefit of nitroimidazoles to improve the outcome of irradiation therapy. Unlike oxygen, nitroimidazoles are slowly metabolized by tumor cells and thus reach all the cells in tumors by diffusion. Under hypoxic conditions, the compounds are trapped within the cells and stabilize DNA lesions in the presence of ionizing radiation. Importantly, toxicity of the drugs can constitute a limitation for the success of the trial. Indeed, no benefit can be seen if drug tolerance is below the dose that is required for expected hypoxic modifications. Besides, it should be noted that the most tolerable drugs of this class present the lowest preclinical radiosensitized activity. Consequently, only nimorazole, a less efficient sensitizer but less toxic drug in this class has been incorporated into current standard radiotherapy treatment in H&NC in Denmark [182].

3.2.2. Hypoxia-activated cytotoxic prodrugs

Hypoxia-activated cytotoxic prodrugs also target hypoxic cells. Unlike hypoxic radiosensitizers, the cytotoxic prodrugs kill cells by reduction from non-toxic prodrugs to cytotoxic drugs under hypoxic condition without any external activation. Three basic classes of bioreductive compounds having the potential to be metabolized by enzymatic reduction under hypoxic condition that have been developed for this purpose are quinones, nitroaromatics and N-oxides [215, 216].

The first compound that has been developed is the quinone mitomycin C. This bioreductive alkylating compound was evaluated as adjuvant treatment with irradiation therapy on patients [217]. However, the potential of mitomycin C to improve radiation-induced tumor damage produced conflicting results, with either benefit [218, 219] or lack of benefit [220]. The lack of response could be due to the small ability of mitomycin C to be selective for hypoxic cells [221]. Despite disappointing clinical results, mitomycin C served as the model to develop more efficient quinones with a better selectivity to preferentially kill hypoxic cells. Although the two analogues of mitomycin C, porfiromycin

and EO9, showed promising preclinical data, no real additional benefit has been found clinically [221].

Interestingly, the radioradiosensitizer nitroimidazoles have also been found to be cytotoxic in oxygen deficient cells [222]. The attempt to improve the weak cytotoxicity and the moderate hypoxic cells selectivity [223] has led to the development of new analogues of nitroimidazole, such as RSU1069, PR-104 and TH-302. Among them, TH-302 showed a good selectivity for hypoxic cells in preclinical models [224].

The lead compound of N-oxide is tirapazamine with a hypoxic-aerobic differential of up to 200 in murine cells and 50 in human cell lines [225]. This cytotoxic prodrug has been evaluated clinically in numerous types of cancer including lung, cervical, ovarian, H&N cancers and melanoma [226]. Nevertheless, the additional benefit of tirapazamine in combination with radiation therapy and chemotherapy is conflicting. While a phase II clinical trial in H&NC patients showed a general outcome improvement [227], randomized trials were somewhat disappointing [226]. These inconsistent results might be the consequence of the fact that patients were not screened for hypoxia prior to trial enrolment. Therefore, it has been suggested that the additional benefit of tirapazamine to conventional oncology treatments could be achieved if patient stratification based on hypoxic status is included [183]. Tirapazamine is also suggested to quickly react once activated under hypoxic conditions resulting in little cell killing. Besides, this compound presented a poor tumor penetration property [228]. However, the potential of tirapazamine stimulated interest for the development of related compounds such as chlorambucil N-oxide and banoxantrone [215].

While previous described agents induce DNA damage once activated by enzymatic reduction under hypoxic condition, an emerging strategy involves the design of hypoxia-activated prodrugs in which an inhibitor of DNA damage repair prodrug is masked by a bioreductive group. The proof-of-concept studies provided promising results. The hypoxic conditions release the active inhibitor that induces cellular cytotoxicity (CH-01 [229]) or sensitizes hypoxic radio-resistance cells (BCCA621C [230]).

3.3. Vascular targeting agents

The tumor vasculature is considered as one of the factors responsible for the development of hypoxia and becomes an attractive target for therapy. Two approaches have emerged [231]. The first one prevents angiogenesis from occurring (angiogenesis inhibiting agents; AIAs) while the second one damages the already established vasculature (vascular disrupting agents; VDAs).

Although both vascular targeting agents (VTAs) show antitumor effects, significant improvements in tumor control have only been seen in combination with radiation [231] but not when used alone, even when combined with other VTAs [231, 232].

3.3.1. Angiogenesis inhibiting agents

Experimental evidences suggested that AIAs could normalize the tumor vasculature, resulting in a better functional vasculature for oxygen transport. Consequently, AIAs are described to reduce tumor hypoxia and to improve the radiation response [233]. In contrary to the promising pre-clinical results, many studies showed that AIAs induced a lack of change or even a decrease in tumor oxygenation [231]. The controversial results have raised the question about the role of vessel normalization on the outcome of irradiation therapy. In parallel, it also underlines the importance of synchronizing of the two modalities for an optimal benefit.

3.3.2. Vascular disrupting agents

VDAs damage blood vessels and disrupt blood flow to affected tumor regions resulting local ischemia and hypoxia. These agents preferably kill the hypoxic cells which are already under oxygen and nutrient deprivation [231]. CA4DP, the lead VDA currently under clinical evaluation, has been evaluated for its ability to increase response to radiation therapy. The agent was tested before, during and after irradiation. Although the drug alone does not have any impact on tumor control, the introduction of CA4DP after irradiation significantly improves the local tumor control in rodent C3H mammary carcinomas [183]. The combination of irradiation that kills aerobic cells and VDAs that kill irradiation-resistant cells constitutes a good rationale for this approach. Moreover, the additive tumor response could not be seen when CA4DP was given before radiation therapy suggesting the drugs may kill previously hypoxic cells but also induce hypoxia in aerobic cells. Consequently, these cells become a source of radiation resistance, resulting in a lack of enhancement in radiation response. This observation again outlined the importance of an appropriate timing and sequence for an optimal eradication of tumor cells.

3.4. Targeting hypoxia response pathways

Cells respond to hypoxia by the activation of many genes and subsequent pathways. Among the different pathways activated in response to hypoxia, HIF-1 has been extensively studied and is considered as a tumor-specific target for anticancer treatment [33, 234]. Targeting HIF-1 is considered to improve tumor radiosentization. Based on the regulation mechanism of HIF, there are three distinct approaches to inhibit the HIF-1 pathway: targeting the upstream pathways of HIF-1, targeting HIF-1 directly, or targeting on relevant downstream pathways activated by HIF-1 [235].

BAY-84-7296, an orally bioavailable inhibitor of mitochondrial complex I and hypoxia-induced HIF-1 activity, has been demonstrated to reduce the hypoxic fraction in tumor xenografts and to improve local tumor control in HNSCC after a single dose and fractionated irradiation [236, 237].

YC-1 inhibits the growth and spread of tumors by decreasing HIF-1α accumulation and HIF-1 target gene expression under hypoxic conditions [238, 239]. The combination of YC-1 treatment and irradiation has been reported to significantly delay tumor growth compared to radiation therapy alone [32, 240].

Acriflavine directly binds to HIF-1α that is blocking HIF-1 dimerization and transcriptional activity. The proof of principle showed that the drug can prevent and arrest tumor growth via the inhibition of intratumoral expression of angiogenic cytokines, of mobilization of angiogenic cells into peripheral blood, and of tumor vascularization. Thus, acriflavine becomes a potential molecule to induce radiosensitizing effect [241].

Although hypoxia response pathways provide many options for anticancer treatment, the clinical usefulness of this approach needs to be confirmed in future research. Indeed, the expression of HIF-1 is not limited to hypoxic tumor cells. Evidences have shown that cells possessing mutations of human epidermal growth factor receptor 2 (HER2/neu), RAS or SRC are also able to activate HIF-1 [242]. Thus, concern is raised in terms of the specificity of drugs inhibiting HIF-1 since they could potentially also target aerobic cells in tumors [243]. The evaluation of the approach is not easy since hypoxia response pathways is a complex network. For example, HIF-1 is a well-known response pathway to hypoxia, yet there are probably numerous unknown other molecular pathways that respond to the hypoxic environment and vice versa, HIF-1 is not only be regulated by hypoxic conditions. Hence, continued research is needed for a better understanding of this intricate network which contributes to novel hypoxia-based treatment modalities.

3.5. Fractionated radiation

Fractionated therapy is more advantageous than single dose irradiation since the method can increase therapeutic effect and decrease severe side-effects in normal tissues [244, 245]. The rational of dose fractionation refers to the attribution of positive and negative influences of the four “Rs” of radiotherapy: recovery/repair of radiation-induced damage to the cells, redistribution of cell cycle status, reoxygenation of hypoxic cells, and repopulation of surviving cells. All biological effects occur in the time interval between dose fractions and are characterized by the magnitude of the effects as well as by their kinetics. The sum of the impacts of 4Rs on tumors and normal tissues determines whether a change in dose fractionation will generate a therapeutic improvement.

Repair: Cells exposed to sparse radiation suffer from sublethal damage that can be repaired. While a high irradiation dose intentionally delivered to tumor induces a cell killing effect, normal tissue is also irradiated with unintended sparse irradiation. Fractionated irradiation provides injured normal tissue time to repair and gives normal cells a potential therapeutic advantage over tumor cells.

Repopulation: Although irradiation reduces the total population of clonogenic tumor cells in a tumor, cells surviving from radiation can repopulate the tumor by proliferation and/or reduced cell loss. This parameter determines the irradiation schedule since the efficacy of treatment is reduced if repopulation of clonogenic tumor cells occurs during the course of fractionated radiotherapy.

Redistribution: The radiosensitivity of cells varies with respect to the cell cycles. After irradiation, some cells will lose their reproductive integrity and some will retain this ability. There is a great possibility that the surviving cells are in S phase, the most radioresitant phase. Thus, irradiation synchronies cell cycle of cells that survive irradiation. With increasing time after irradiation, the cell cycle synchronization will be lost and the distribution of the cell cycle in surviving clonogenic cells will return the same as before irradiation.

Reoxygenation: The distribution of oxygen to hypoxic tumor cells is dramatically improved after fractionated radiotherapy as explained in 3.1.2. Since tumor oxygenation plays a substantial role in the radiation therapy outcome, it is important to determine when and how the reoxygenation occurs [206]. The knowledge of the timing of reoxygenation could provide the clinician with crucial information to adequately schedule fractionated irradiation for an optimal eradication of tumor cells while limiting undesirable side-effects in normal tissue.

Several regimes have been proposed that correspond to different situations. The most conventional regimes consist in about 1.8–2.0 Gy per day, 9.0–10 Gy per week, and up to about 60 Gy in total for 6 weeks. Hyperfractionation is proposed for a better control of locally advanced cancers in which smaller doses at a higher frequency are given (1.1–1.2 Gy twice per day with an interval of about 6 hours). Hence, the total irradiation dose is increased with more therapeutic benefit and fewer side-effects. Accelerated fractionation is designed for rapid growing tumors with reduced treatment duration. Indeed, irradiation is given at a relatively high dose (1.5–1.6 Gy) twice a day while total dose is set at the same level as the conventional dose.

3.6. Hypoxia directed radiotherapy (Dose painting)

Hypoxia has been well described to reduce the amount of reactive oxygen species produced by irradiation and thus limiting DNA damage in hypoxic region. In consequence, conventional radiation is only effective in aerobic cells. Since the radiation response depends on the locally delivered radiation dose, an optimal eradication of tumor could be obtained via “dose painting” by boosting the radiation dose in tumor hypoxic regions [246]. The terms “dose painting” describes the heterogeneous distribution of irradiation dose within the tumor volume by targeting radioresistant areas defined by functional imaging. Three evidence-based-causes of radiation therapy failure

in the clinic are the current aims of dose painting: tumor burden, tumor cell proliferation and hypoxia [247]. In this thesis, we only address the dose painting of hypoxia.

In order to adequately design dose painting, number of technological innovations have been developed in radiotherapy, including intensity-modulated radiation therapy (IMRT), volumetric modulated arc therapy, tomotherapy and proton therapy [248-251]. These studies indicated that non-homogenous dose of radiation can be delivered and optimized within a tumor to overcome hypoxia with different techniques. For example, the IMRT technique allows radiation oncologists to control the distribution of radiation doses by the combination of the anatomical/ functional information (obtained by CT, PET or MRI) that precisely determines tumor regions for dose boosting and the development of multileaf collimators that modulate the photon beam intensity during radiation therapy. Besides, the integration of multiple external beams enables a complex three-dimensional planning of dose distribution.

The translation of hypoxic functional imaging to dose prescription is currently based on two methods: dose painting by contours (DPBC) and dose painting by numbers (DPBN).

The dose boosting volume in DPBC is selected based on a threshold value e.g. tumor-to-blood uptake ratio (T/B) ≥ 1.3 for FMISO [252] or standardized uptake value (SUV) ≥1.4 for Cu-ATSM [253]. Most studies so far have used this approach since it is generally simple and easy to implement into conventional clinical routine. However, the trade-off of the simplicity (less steep dose gradients, more uniform dose boost regions) makes the approach more robust to spatial errors [254]. The evaluations of DPBC based on functional image of ^{18}F-FMISO are under clinical trial (reviewed in [255]).

DPBN individually calculates dose for each voxel of a tumor. Based on local biological information from functional imaging, the dose escalation in DPBN schemes is proposed as a linear function of image intensity.

Some authors have suggested “dose redistribution” rather than dose escalation, since any improvement in tumor control probability (TCP) is more likely due to the non-uniform dose plan rather than to an increase in mean dose [254]. In this scheme, the mean dose delivered to the entire target volume is maintained constant while dose is optimized for each compartment to improve TCP. Søvik et al [256] have shown that the dose redistribution strategy improved TCP comparing to conventional uniform dose. Moreover, the TCP could be further enhanced in combination with fractionated irradiation.

A big problem of this approach is to precisely identify the hypoxic regions with current clinically available technologies. Since hypoxic regions can be seen at a sub-millimeter scale, the most precise modern radiotherapy approaches are unable to assess this subregional heterogeneity (the best functional imaging is at millimeter scale) [49]. The

insufficient spatial resolution issue results in an averaging problem. As a consequence, the detected hypoxic voxels could contain both hypoxic and non-hypoxic cells. Meanwhile, in voxels showing a lack of hypoxia, the amount of hypoxia may be not large enough to raise the overall threshold value. Besides, tumor hypoxia is also characterized by temporal heterogeneity, thus hypoxia measured prior to the start of therapy may not be the same as that during therapy. Indeed, studies evaluating the reproducibility of intratumor distribution of [^{18}F] misonidazole in head and neck cancer patients revealed conflicting results [257, 258].

4. IMAGING AND TUMOR HYPOXIA IDENTIFICATION

As discussed above, oxygen plays a substantial role in treatment response. The presence of hypoxia is associated with resistance to therapy and contributes to a worse overall prognosis. Dated from 1980's, evidences of the role of oxygen to the outcome of radiotherapy has been well established in preclinical tumor models [259]. This knowledge has led to the evaluation of dozens of hypoxia-directed therapies with varying degrees of success [260]. Overall, the meta-analysis from over 10,000 patients enrolled in nearly 90 randomized trials over the past 40 years favours the use of hypoxia modification strategies for a better patient prognosis [260]. However, the benefit of these hypoxia modification trials was only marginal. The fact that patients were not screened for the presence of hypoxia prior the enrolment influenced the therapeutic value of these approaches leading to the unstable results of these trials [261]. In other words, if patients have not been selected, we do not know whether the modification is applied on the cohort that can benefit or not. In three trials, the combination of cancer treatment and hypoxic modification modalities resulted in a better response in tumors previously identified as hypoxic at baseline [115, 178, 262]. Despite evidences for a need for hypoxia screening, this step has not been an entry criterion in hypoxia modification trials yet. This fact emphasizes the need for a method able to estimate tumor hypoxia that could be applicable in clinical practice in order to improve clinical protocols testing hypoxia-targeted therapies. Yet, there is no currently available method for measuring hypoxia in routine clinical setting, nor an approved mean for reducing its impact in the management of cancer patients.

The "4D heterogeneity" of hypoxia is a big challenge for hypoxic detection. Regarding the spatial heterogeneity, tumor hypoxia can occur at micron scale with a steep pO_2 gradient between well-oxygenated and hypoxic subvolume (may up to 60 mmHg/mm) [49]. Besides, tumor hypoxia is unstable and changes dynamically over time, which is described as cycling hypoxia. Depending on the nature of hypoxia, the hypoxic cycles could range from minutes to many days. Moreover, the tumor oxygenation varies between tumors. The tumor hypoxic status cannot be accurately determined anatomically since the amount and severity of hypoxia varies among patients with similar histology [259]. Data have shown that the presence of hypoxia is independent of tumor size, stage, grade or histology [9]. These characteristics of tumor hypoxia make imaging

an ideal method for hypoxia detection. Indeed, imaging presents many advantages that fulfill the criteria for hypoxia detection, such as real time monitoring, accessibility with minimal or no invasiveness and can function over wide ranges of time and size scales involved in biological and pathological processes. An ideal method to follow tumor oxygenation should be able to provide real-time measurement, practical for clinical routine, repeatable, relatively non-invasive and having high spatial resolution allowing repeated measurements not only before treatment, but also throughout and after complex therapeutic regimens [263].

Possessing an adequate tool for measuring tumor hypoxia provides the potential to improve the use of existing hypoxia-directed therapies as well as the potential to facilitate the development of new approaches to circumvent hypoxia. The tool will aid oncologists to stratify patients and to deliver the optimized personal treatment regimens for specific individual based on the pretreatment oxygen distributions and the changes in oxygenation during therapy. Number of patients enrolled in trials testing new hypoxia-directed therapies may decrease if screening for pretreatment oxygen levels occurs. Thanks to the patient selection, sample heterogeneity could be reduced meaning that a smaller population is needed to achieve adequate statistical power [22, 261]. Evaluation of the change in tumor oxygenation during a pretreatment intervention to modulate pO_2 may guide oncologist to identify the most beneficial approach for individual patients [264, 265].

Another important issue is to maintain the balance between keeping analyses and data acquisition simple enough for practical reason and having sufficient information for therapy guidance or decision.

5. ASSESSMENT OF TUMOR OXYGENATION TO PREDICT OUTCOME OF RADIATION THERAPY

5.1. Direct oxygen mesurements

5.1.1. Polarographic oxygen electrodes

The development of the Eppendorf histograph marked the revolution that evidenced the impact of hypoxia on therapy outcome, especially on radiation therapy.

In an international multi-center study on 397 patients with advanced head and neck cancer treated with radiation therapy, fraction of pO_2 values less than 2.5 mmHg (HP2.5) measured by Eppendorf was shown to be associated with a poor prognosis [55]. Study on advanced squamous cell carcinoma of the head and neck (SCCHN) patients also suggested that the pretreatment tumor oxygenation was predictive for radiation response when HP2.5 assessed by Eppendorf was used as endpoint [62]. The prognostic value of pre-treatment median tumor pO_2 measured by Eppendorf has also

been demonstrated. SCCHN patients with median tumor oxygenation more than 10 mmHg presented a significantly better disease free survival compared to patients with median tumor pO_2 less than 10 mmHg (78% vs. 22%). In addition, a significantly lower pre-treatment pO_2 was found in relapsing patients [266]. Interestingly, in a study on 134 SCCHN patients treated primarily with radio- or radiochemotherapy, the evaluation of Eppendorf pO_2 histography as a predictive test to select patients for treatment alternatives was failed, although the impact of the tumor oxygenation on the prognosis of patients has been established [54].

The value of pretreatment oxygenation on disease control following irradiation was highlighted by a study in patients with uterine cervical cancer [57]. Tumor oxygenation measured by Eppendorf was assessed before and after radiation therapy along with other biological parameters: vascular density, cell density, frequency of mitosis and apoptosis. The study showed that patients with smaller pre-treatment hypoxic subvolume (volume of tumor with pO_2 less than 5 mm Hg, HSV5) showed a higher control probability after a median follow-up time of 50 months than patients with a larger HSV5. Authors suggested that pretreatment oxygenation was more important for patient outcome than the post-treatment oxygenation or the changes in oxygenation during this time as well as other biological parameters assessed in the study.

The tumor oxygenation status assessed by Eppendorf has also been evaluated for the long-term biochemical outcome after brachytherapy in 57 men with localized prostate cancer [59]. The hypoxic tumor was defined of having the pO_2 of prostate cancer less than 10% the pO_2 of normal muscle tissue. Biochemical failure was based on both the American Society of Therapeutic Radiation Oncology (ASTRO) (three consecutive (prostate-specific antigen) PSA raises) and the current Phoenix (PSA value of ≥ 2 ng/mL above the PSA nadir) definitions. With a median follow-up time of 8 years, the pre-treatment tumor oxygenation status measured by Eppendorf significantly predicted for poor biochemical outcome independently of well-established risk factors, including tumor stage, Gleason score, and PSA and also for age, perineural invasion, serum hemoglobin level, and hormonal therapy use.

5.1.2. ^{19}F-MRI

A preclinical study on Dunning prostate R3327-AT1 tumors has evidenced the usefulness of tumor pO_2 mapping by ^{19}F FREDOM MRI for prediction of irradiation response [76]. While breathing hyperoxic gas did not influence on the hypoxic status of the tumors as well as on the tumor growth delay after irradiation, tumor oxygenation at time of irradiation was observed to be correlated with the therapy outcome, especially when mean pO_2 > 10 torr.

5.1.3. Electron paramagnetic resonance

Currently, the predictive value of the technique for the outcome of radiation therapy has only been assessed in preclinical animal models.

EPR oximetry

In vivo evidences showed that pO_2 assessed by EPR oxymetry was able to predict the tumor response to radiotherapy as well to monitor the efficacy of co-treatments in order to determine the window of reoxygenation for an optimal radiation therapy efficacy [267]. The method was also applied for scheduling fractionated irradiation at times of reoxygenation induced by carbogen breathing or by irradiation [268, 269]. As monitored by EPR oximetry, an increase in tumor oxygenation induced by carbogen breathing significantly improved the tumor growth delay after radiation therapy [268]. Moreover, Hou et al. have evidenced for fractionated irradiation that the better the tumors were reoxygenated after the first irradiation, the stronger the tumor responded to therapy [269]. Thus, the assessment of temporal changes in tumor pO_2 during fractionated radiotherapy can potentially be used to enhance and predict therapeutic response. Besides, thanks to the ability to perform repeated measurement, EPR oximetry can stratify tumor based on whether an increase in oxygenation occurred after irradiation, thereby allowing the design of oxygen guided treatment plans to improve the outcome [269].

EPR imaging (EPRI)

The advantage of EPRI compared to EPR oximetry is that the approach provides spatial information of tumor oxygenation allowing the calculation of tumor hypoxic fraction or the distinction between chronic and cycling hypoxia. Radiation dose and fraction of hypoxic tumor (pO_2 < 10 mmHg) assessed by EPRI have been showed to predict for the curability of FSa fibrosarcomas under both normal (air breathing) and clamped tumor conditions [86]. Also, vascular renormalization in tumor-bearing mice treated with sunitinib, a multi-tyrosine kinase inhibitor, was visualized by longitudinally mapping tumor pO_2 and microvessel density by EPRI and MRI [270]. The longitudinal and noninvasive EPRI monitoring of tumor pO_2 allowed identifying the window of vascular renormalization of the antiangiogenic treatment where the extent of cycling tumor hypoxia was suppressed and the tumor oxygenation was transiently improved. The authors evidenced the efficacy of radiation treatment applied during this therapeutic window period resulted in a synergistic delay in tumor growth [270].

5.2. Indirect oxygen measurements - Exogenous markers

5.2.1. 2-nitroimidazole IHC markers

IHC using 2-nitroimidazole markers is widely considered as reference technique to detect and quantify tumor hypoxia. The most extensively used marker is PIMO. PIMO

binding is prognostic in head and neck carcinomas patients where a better radiation induced local tumor control was observed in those with little or no PIMO binding [271]. However, in a prospective international multi-centre study, the marker was not predictive for loco-regional tumor control or overall survival in uterine cervix patients [272]. Another nitroimidazole marker, EF5 is also found to have a prognostic value for outcomes in H&NC patients with severe hypoxia [273].

5.2.2. PET markers: 2-nitroimidazole and Cu-ATSM

The hypoxic PET markers have been evaluated in both clinical (Table 2) and pre-clinical (Table 3) studies as prognosis factor for outcome after radiotherapy. The most clinically studied tracer is ^{18}F-FMISO with the majority of studies involved head and neck cancer (Table 2). These studies showed a lack of consistency in terms of image acquisition (static or dynamic scan, the delay acquisition) as well as the parameters used to determine hypoxic tumor (different parameters, different threshold). In general, tumors showing a higher tracer uptake, which was consistent with hypoxia, were more likely to present a tendency for poor radiotherapy response [96].

Table 2: Clinical evaluation to correlate the hypoxia estimated by PET tracers with outcome to radiation therapy

Tracer	Tumor type(s)	N	PET-related parameters	Treatments	Results	Ref
^{18}F-MISO	H&N	73	Mean T/B_{max}	(chemo)radiotherapy or surgery +/- RT	Pretherapy FMISO uptake was a strong independent prognostic measure to predict patient survival	274
^{18}F-MISO	H&N	12	SUV_{max} at 2 h and 4 h p.i Hypoxia definition: SUV>1.4	RT	SUVmax showed borderline significance for stratifying the patient group	275
^{18}F-MISO	H&N	15	T/B_{max} Hypoxic volume: T/B>1.2 Pre-, post- and during RT scans	chemoradiotherapy	Disease-free survival correlated negatively with $T/B_{max\text{-}pretreatment}$, $T/B_{max\text{-}during\ treatment}$ and the initial hypoxic volume	276
^{18}F-MISO	H&N	20	2 pretreatment scans and 1 mid-treatment scan Acquisition at 2-3 h p.i	chemoradiotherapy	Neither hypoxia presented or not as detected on the mid-treatment PET scans did not correlate with patient outcome	277
^{18}F-MISO	H&N	17	Median SUV_{max}: 2.3 Median T/M: 1.3 Pretreatment scans at 150 min p.i. Hypoxic volume: uptake ≥ Median	surgery or (chemo)radiotherapy	Hypoxic tumors defined by SUV_{max} or T/M had lower local tumor control rates with RT. Only hypoxic tumors defined by SUV_{max} had lower disease-specific	278

			SUV_{max} or Median T/M		survival rate with RT or surgery.	
^{18}F-MISO	H&N	25	SUV_{max} T/B_{max} Hypoxic volumes at different T/B 1 pretreatment scan and 3 scans during treatment Acquisition at 2 and 4 h p.i	chemoradiotherapy	The local-progression-free-survival endpoint correlated with all FMISO-related parameter at the week 1 and 2 time-points after the treatment started.	279
^{18}F-MISO	H&N	22	Median T/B_{max}: 2 Acquisition at 4 h p.i	chemoradiotherapy	To accuracy predict the treatment outcome, the common pre-defined T/B_{max} should deviate less than 10% from reference conditions (T/Bmax: 2).	280
^{18}F-MISO	Glioblastoma multiforme	22	Pretreatment scan at 2 h p.i Median T/B_{max} Hypoxic volume: T/B>1.2	RT	Hypoxic volume and T/B_{max} before radiotherapy are strongly associated with poorer time to progression and survival.	281
^{18}F-FAZA	Cervical	15	Dynamic and static scans before, during and after therapy. T/M_{max}: 1.2–3.6 at 60 min and 120 min p.i.	RT	Predictive and prognostic value of FAZA remains to be clarified.	107
^{18}F-FAZA	H&N	40	Static pretreatment scan at 2 h p.i Repetitive scan during RT: 13 patients Hypoxic volume: T/M≥1.4	RT	During a median follow up of 19 months, patients with non-hypoxic tumors had a better disease free survival rate compared to those with hypoxic tumors (93% vs 60%).	112
^{60}Cu-ATSM	Cervical	14	Pretherapy scan Recurrence threshold and hypoxic definition: T/M 3.5	RT and chemotherapy	Cu-ATSM uptake was inversely related to progression-free survival and overall survival. With a 14-24 months follow-up evaluation, 6/9 patients with normoxic tumors are free of disease and 5/5 patients with hypoxic tumors have already developed recurrence.	282
^{60}Cu-ATSM	Cervical	38	Pretherapy scan Recurrence threshold and	RT and chemotherapy	Cu-ATSM uptake was inversely related to progression-free survival	283

			hypoxic definition: T/M 3.5		and cause-specific survival. 3-y progression-free survival of patients with normoxic tumors and of patients with hypoxic tumors were 71% and 28%, respectively.	
^{60}Cu-ATSM	Cervical	15	_	RT and chemotherapy	With the mean follow-up of 48 months, the overall survival were 75% for patients with non-hypoxic tumors and 33% for those with hypoxic tumors	284
^{62}Cu-ATSM	H&N	15	Residual/ recurrent threshold: SUV_{max} 5	chemoradiotherapy	The SUV_{max} differed significantly between patients with or without residual/recurrent tumor. 6/10 patients with SUV_{max} >5.00 had residual/recurrent tumor, whereas 5/5 patients with SUV_{max} <5.00 were free of disease	285
^{60}Cu-ATSM	Lung	19	Pretreatment scan Responder: Mean T/M 1.5 Non-responder: Mean T/M 3.4 Response threshold : T/M 3	RT ± chemotherapy or chemotherapy alone	With the follow-up evaluation of 2-46 months, mean T/M was lower in responder than non-responder to therapy.	286
^{60}Cu-ATSM	Rectal	17	Hypoxic and prognosis threshold: Median T/M 2.6	chemoradiotherapy	Both overall and progression-free survivals were worse with hypoxic tumors than with nonhypoxic tumors.	287

Table 3: Pre-clinical evaluation to correlate the hypoxia estimated by PET tracers with outcome to radiation therapy

Tracer	**Tumor type(s)**	**PET-related parameters**	**Treatments**	**Results**	**Ref**
^{18}F-MISO	FaDu human squamous cell carcinoma xenografts	Pretreatment scan from 3.5 to 4 h p.i. SUVmax Hypoxic volume: tracer concentrations $\geqslant$39% of the maximal activity concentration within the tumor.	Single dose irradiation	Hypoxic volume of FMISO had a negative effect on permanent local tumor control. SUVmax was not correlated with local tumor control.	288

^{18}F-FAZA	C3H mammary carcinomas	Hypoxic threshold: Median T/B	Single dose irradiation	Significant lower tumor control was found in more hypoxic tumors.	289
^{18}F-FAZA	9L-glioma	Mean T/B	Single dose irradiation	T/B significantly correlated with tumor growth delay.	290
^{60}Cu-ATSM	Spontaneous sinonasal tumors in canine patients	SUV_{max}, SUV_{mean}	accelerated hypofractionated radiation therapy	Cu-ATSM PET were not predictive for therapy outcome.	291

5.2.3. SPECT markers

The nitroimidazole markers were also labelled with gamma-emitting radioactive isotopes for SPECT detection. Among a number of [^{123}I/^{125}I]-iodoazomycin derivatives developed, only ^{123}I-IAZA has been evaluated clinically. In H&NC, patients presenting positive ^{123}I-IAZA scans had a poorer outcome in response to radiotherapy than those with negative scans [117]. The non-nitro compound HL91 labelled by ^{99m}Tc was found to have a prognostic value for the outcome in response to radiation therapy in non-small-cell lung cancer patients [292].

5.3. Indirect oxygen measurements - endogenous markers

Numerous clinical studies suggested a high level of expression of HIF-1-related proteins is correlated with the poor treatment response [52]. HIF-1α overexpression was associated with reduced overall survival or disease-specific survival following radiotherapy in patients with squamous cell cancer of the oropharynx [293], cervical cancer [294, 295]. The predictive value of CA IX is less consistent than the one of HIF-1α. The marker was predictive for the (chemo)-radiotherapy outcome only in combination with other potential markers, HIF-1α or GLUT-1 [296, 297].

5.4. Vascular parameters

5.4.1. DCE MRI

DCE MRI indirectly identifies low-perfused tumor regions that suffer from an insufficient oxygen supply like hypoxic tumor regions. DCE-MRI is the only MRI marker that has been evaluated both pre-clinically and clinically in terms of the predictivity to radiotherapy outcome.

Regarding preclinical studies, low values of k^{trans} (the volume transfer constant of Gd-DTPA) were found to be associated with extensive hypoxia and radiation resistance in CK-160 and TS-415 cervical carcinoma xenografts and with high incidence of metastases in CK-160 tumors [298]. Another study on R-18 melanoma xenografts

associated low K^{trans} values with the higher probability of resistance to radiation and of developing lymph node metastases [299]. Yet, in a study in TLT mouse fibrosarcomas, no correlation was found in any of the tested DCE parameters and radiotherapy outcome [300].

In a clinical study on locally advanced carcinoma of the cervix, patients with poor amplitude of contrast enhancement (A) tumors had significantly worse disease-specific survival than well-enhancing tumors [301]. The longitudinal changes in DCE MRI signal intensity during RT were found to be correlated with treatment outcome in a study on 98 patients with cervical cancer [302]. On one hand, patients with persistent low perfusion tumors measured before RT, during early RT and during RT had a high risk of treatment failure. On other hand, patients with initially high perfusion tumors or those with initially low perfusion tumors but presenting important perfusion improvement during treatment had more favourable outcome. Besides, in another study on 81 cervical cancer patients treated with chemoradiotherapy, the percentile–time screening assessed by DCE-MRI parameters was predictive for long-term locoregional control after chemoradiotherapy independent of tumor stage, volume, and lymph node [303]. The skewness of k^{trans} was predictive for the progression-free survival and overall survival in head-and-neck squamous cell carcinoma patients with nodal metastases subjected for chemoradiation therapy or surgery [304].

5.4.2. BOLD MRI

Since the BOLD MRI does not directly measure tissue oxygenation, perfused regions showing relative high R_2* compared to surrounding regions are assumed to be hypoxic. Clinical and pre-clinical evidences have described the correlation between BOLD-MRI and the outcome of radiotherapy.

The predictivity of BOLD-MRI has been pre-clinically validated as a prognostic indicator of acute radiotherapeutic response in GH3 prolactinomas and RIF-1 fibrosarcomas. Pre-treatment R_2* and carbogen induced ΔR_2* were measured prior to radiation therapy in both tumor models. The authors found that GH3 tumors exhibiting a relatively fast baseline R_2* and large ΔR_2* showed growth inhibition while RIF-1 tumors exhibiting a relatively slow baseline R_2* and negligible ΔR_2* appeared to progress [305]. Further, in a clinical study, pre-treatment R_2* was found to be inversely correlated with final tumor size in 30 patients with cervical cancer treated with concurrent chemoradiotherapy [306].

5.5. ^{1}H relaxation imaging

Recently, the predictive value of R_1 has been investigated in animal models and results have shown a correlation between the changes of R_1 induced by hyperoxic challenges and the outcome of radiation therapy. Study on Dunning R3327-AT1 rat prostate tumors demonstrated a strong correlation between tumor growth delay following single dose irradiation and the change in tissue oxygen level dependent (TOLD) signal induced by

oxygen [154]. Another study on the same tumor models showed the utility of the change of TOLD induced by oxygen challenge to predict the tumor response to hypofractionation [307]. Nevertheless, these studies are only preliminary and further investigations are needed.

In conclusion, all described methods are able to predict the outcome of radiotherapy. Nevertheless, the results cannot be used to stratify patients that are hypoxic on an individual basis [52]. Since each method reflects one aspect of the tumor microenvironment, combining different approaches is more robust to assess tumor oxygenation. Besides, the majority of studies assessed tumor oxygenation by average value leading to the loss of spatially heterogeneity information. Consequently, analyses of hypoxic heterogeneity may improve the predictivity of the method used and potentially be able to stratify patients on an individual basis.

AIMS OF THESIS

In oncology, hypoxia is associated with poor patient prognosis and can be responsible for resistance to radiation therapy. Yet, despite an increasing number of studies developing approaches to alleviate hypoxia, none of the approach could be translated in routine clinical practice to improve the outcome of cancer treatment yet. This might be due to the fact that screening for the presence of hypoxia has not been the entry criterion prior to hypoxia modification trials. Thus, there is an important need for a technique to identify hypoxic regions in tumors for treatment optimization. Among the different techniques developed to measure oxygenation, we focused on MRI based oxygen sensitive endogenous contrasts including R_1 and R_2*. R_2* is sensitive to the concentration of dHb and reflects vascular oxygenation, whereas R_1 is sensitive to dissolved O_2 concentration and thereby reflects tissue oxygenation. The sensitivity of R_1 to the change in oxygenation has been improved by assessing the signal of R_1 of lipid protons (lipid R_1) [167] instead of water protons. However, the method was only validated in lipid-rich tumor models. In this thesis, in order to expand the application to non-lipid-rich tumors, a biexponential deconvolution method was used to extract R_1 of lipid protons as well as R_1 of water protons (water R_1).

The aim of this thesis was to address the value of combined endogenous MRI biomarkers R_1 and R_2* for the guidance of hypoxia-driven intervention in radiation therapy. Indeed, the combination of these two parameters is expected to assess tumor oxygenation more robustly than the use of an individual method. For this purpose, R_2* along with different R_1 MR-derived parameters, including lipid R_1, water R_1 and global R_1 were evaluated in terms of sensitivity to changes in tumor oxygenation and in terms of predictivity to radiation therapy outcome. To achieve this goal, the thesis was divided in two parts. The first part involved the validation of imaging MRI biomarkers using an hyperoxic carbogen breathing challenge to modify tumor oxygenation. The sensitivity of MRI biomarkers was assessed in three ways. We first cross-validated the combined R_1 and R_2* MR biomarkers with a quantitative oximetry technique, EPR spectroscopy. We then evaluated the ability of biomarkers to predict basal tumor oxygenation and response of tumor to carbogen breathing. Finally, MRI biomarkers were evaluated for their predictive values as biomarkers of radiation therapy outcome.

In the second part, we investigated the ability of combined endogenous MRI biomarkers to assess changes in tumor oxygenation using an allosteric effector of hemoglobin, *myo*-inositol tripyrophosphate (ITPP). The rationale for this choice relies in the different mechanisms of reoxygenation of carbogen and ITPP. While carbogen increases the oxygen supply by saturating the arterial blood with oxygen, ITPP is known to decrease the binding affinity of O_2 for hemoglobin thus enhancing the dissociation of Hb-O_2 towards a higher tissue oxygenation [308]. The purpose of this second part is to improve the knowledge on the predictive value of the oxygen-dependent MR biomarkers R_1 and R_2*, by assessing their behavior in response to an alternative way to modify tumor oxygenation.

RESULTS

1. VALIDATION OF IMAGING MRI BIOMARKERS USING CARBOGEN

Monitoring tumor response to carbogen breathing by oxygen-sensitive magnetic resonance parameters to predict the outcome of radiation therapy: a preclinical study

Thanh-Trang Cao-Pham, Ly-Binh-An Tran, Florence Colliez, Nicolas Joudiou, Sabrina El Bachiri, Vincent Grégoire, Philippe Levêque, Bernard Gallez, and Bénédicte F. Jordan

International Journal of Radiation Oncology Biology Physics. 2016;96(1):149-160.

International Journal of Radiation Oncology biology • physics

www.redjournal.org

Biology Contribution

Monitoring Tumor Response to Carbogen Breathing by Oxygen-Sensitive Magnetic Resonance Parameters to Predict the Outcome of Radiation Therapy: A Preclinical Study

Thanh-Trang Cao-Pham, BSc,* Ly-Binh-An Tran, PhD,* Florence Colliez, PhD,* Nicolas Joudiou, PhD,* Sabrina El Bachiri, PhD,† Vincent Grégoire, PhD,‡ Philippe Levêque, PhD,* Bernard Gallez, PhD,* and Bénédicte F. Jordan, PhD*

**Université Catholique de Louvain, Louvain Drug Research Institute, Biomedical Magnetic Resonance Research Group, Brussels, Belgium; †Université Catholique de Louvain, IMMAQ Technological Platform, Methodology and Statistical Support, Louvain-la-Neuve, Belgium; and ‡Université Catholique de Louvain, Institute of Experimental and Clinical Research, Center for Molecular Imaging, Radiotherapy and Oncology, Brussels, Belgium*

Received Oct 21, 2015, and in revised form Apr 25, 2016. Accepted for publication Apr 30, 2016.

Summary

This study compared R_1-related parameters and R_2* in assessing sensitivity to changes in tumor oxygenation and evaluated their potential as predictive markers for the outcome of radiation therapy (RT) in rat tumor models. At the intratumoral level, all magnetic resonance biomarkers successfully reflected the tumor

Purpose: In an effort to develop noninvasive in vivo methods for mapping tumor oxygenation, magnetic resonance (MR)-derived parameters are being considered, including global R_1, water R_1, lipids R_1, and R_2*. R_1 is sensitive to dissolved molecular oxygen, whereas R_2* is sensitive to blood oxygenation, detecting changes in dHb. This work compares global R_1, water R_1, lipids R_1, and R_2* with pO_2 assessed by electron paramagnetic resonance (EPR) oximetry, as potential markers of the outcome of radiation therapy (RT).
Methods and Materials: R_1, R_2*, and EPR were performed on rhabdomyosarcoma and 9L-glioma tumor models, under air and carbogen breathing conditions (95% O_2, 5% CO_2). Because the models demonstrated different radiosensitivity properties toward carbogen, a growth delay (GD) assay was performed on the rhabdomyosarcoma model and a tumor control dose 50% (TCD50) was performed on the 9L-glioma model.
Results: Magnetic resonance imaging oxygen-sensitive parameters detected the positive changes in oxygenation induced by carbogen within tumors. No consistent correlation

Reprint requests to: Bénédicte F. Jordan, PhD, Biomedical Magnetic Resonance Group (REMA), Louvain Drug Research Institute, Université Catholique de Louvain, Ave Mounier 73 − B1.73.08, B-1200 Brussels, Belgium. Tel: (+32) 2-7647364; E-mail: benedicte.jordan@uclouvain.be

Conflict of interest: none.

Supplementary material for this article can be found at www.redjournal.org.

Acknowledgment—The authors thank Chrystelle Po for development of the magnetic resonance postprocessing routine (R_1 biexponential deconvolution) and assistance with data analysis. TT Cao-Pham and F. Colliez are Televie Research Fellows, B.F. Jordan is Senior F.R.S./fNRS Research Associate.

Int J Radiation Oncol Biol Phys, Vol. 96, No. 1, pp. 149−160, 2016
0360-3016/$ - see front matter
http://dx.doi.org/10.1016/j.ijrobp.2016.04.029

oxygenation changes induced by carbogen. Yet, the R_1 parameters failed to predict the curability of a carbogen-sensitive model in a tumor control dose 50% assay, whereas R_2* was found to be correlated with RT outcome ($P<.05$).

was seen throughout the study between MR parameters and pO_2. Global and lipids R_1 were found to be correlated to pO_2 in the rhabdomyosarcoma model, whereas R_2* was found to be inversely correlated to pO_2 in the 9L-glioma model ($P=.05$ and .03). Carbogen increased the TCD50 of 9L-glioma but did not increase the GD of rhabdomyosarcoma. Only R_2* was predictive ($P<.05$) for the curability of 9L-glioma at 40 Gy, a dose that showed a difference in response to RT between carbogen and air-breathing groups. ^{18}F-FAZA positron emission tomography imaging has been shown to be a predictive marker under the same conditions.

Conclusion: This work illustrates the sensitivity of oxygen-sensitive R_1 and R_2* parameters to changes in tumor oxygenation. However, R_1 parameters showed limitations in terms of predicting the outcome of RT in the tumor models studied, whereas R_2* was found to be correlated with the outcome in the responsive model.

Introduction

Hypoxia is a common feature of solid tumors, which heralds a poor prognosis for cancer treatment, especially irradiation (1). Studies demonstrate that tumor hypoxia is highly individual dependent (2). Additionally, tumor hypoxia modification improves the outcome of cancer therapy and overall survival (2). So, there is a need for a reliable, robust, and easily conducted method for measuring tumor oxygenation that could allow radiotherapists to select an appropriate way to overcome hypoxia. Although many techniques have been investigated, there is still no available array of methods for routine practice (3, 4). Imaging allows repeatable measurements and appears to be an appropriate technique for assessing oxygenation because hypoxia extends spatially and temporally. Magnetic resonance imaging (MRI)-based endogen contrast techniques including R_1 and R_2* appear to be promising because MRI is noninvasive and nonionizing, and it does not require any injection of a reporter probe. R_1 is sensitive to dissolved molecular oxygen (5), whereas R_2* is sensitive to blood oxygenation, detecting changes in deoxyHb (6). Given that each technique assesses tumor hypoxia in different compartments, efforts are being made to combine R_1 and R_2* to better understand tissue oxygenation and to make use of the predictive value of these parameters for tumor response to radiation therapy (RT) (7, 8). Recently, O'Connor et al, as well as, Dewhirst and Birer (9, 10) validated oxygen-enhanced MRI (an R_1-based method) for quantifying the spatial variation of hypoxia with pimonidazole staining in 3 tumor lines with different hypoxic fractions. In 2013, we proposed an innovative noninvasive MRI R_1-based method for measuring tumor oxygenation. The method, with the acronym MOBILE (Mapping of Oxygen By Imaging relaxation Enhancement), is based on the assessment of lipids R_1 instead of global R_1 because oxygen is more soluble in lipids than in water (11). In this context, we expected that lipids R_1 should be more sensitive than global R_1 to the actual change in tumor oxygenation.

Our current work focuses on the assessment of R_2* and R_1 MR-derived parameters, including lipids R_1, water R_1, global R_1, and R_2*, as markers of tumor oxygenation and response to RT. Lipids R_1 and water R_1 were extracted using a biexponential deconvolution method (see Methods and Discussion sections). These MR biomarkers were compared with electron paramagnetic resonance (EPR) oximetry, which was used as a reference measurement of tumor pO_2 in vivo (12). MR acquisition was carried out under normoxic (air) and hyperoxic (carbogen, 95% O_2, 5% CO_2) conditions to evaluate the sensitivity of these MR parameters to changes in oxygenation. In addition, tumors were irradiated with or without hypoxia-driven intervention (carbogen) to evaluate the relation between RT outcome and MR parameters. In a previous study, it was determined by EPR oximetry and PET ^{18}F-FAZA that rhabdomyosarcoma and 9L-glioma had different hypoxic fractions and, importantly, that ^{18}F-FAZA was able to predict the outcome of RT in those models (13). The same protocol was used in this study to assess the predictivity of noninvasive MR parameters with regard to the outcome of RT.

Methods and Materials

Tumor models

Two tumor models were included in the study: rhabdomyosarcoma (n=32) and 9L-glioma (n=63). Fragments from a syngeneic rhabdomyosarcoma (1 mm^3) were grafted subcutaneously in 1 thigh of male adult WAG/Rij rats, according to a model developed by the Laboratory of Experimental Radiobiology, Katholieke Universiteit Leuven, Belgium. 9L-glioma cells were grown in Roswell Park Memorial Institute (RPMI) medium supplemented with 10% fetal calf serum (heat inactivated), 1% of a mixture of antibiotics (penicillin 100 UI/mL, streptomycin 0.1 mg/mL), 1% nonessential amino acids, and 1% sodium pyruvate. Cells were maintained in a balanced wet atmosphere (37°C and CO_2 5%). To establish 9L-glioma tumors in vivo, male adult Fisher F344 rats were inoculated subcutaneously in their thighs with 5.10^6 cells. Tumor implantations were performed with the rats under general

anesthesia with intraperitoneal injection of ketamine and xylazine (80 and 10 mg/kg, respectively) on rats weighing between 200 and 250 g. The animals were introduced into the study when the tumors reached the size of 15 to 20 mm.

Experimental design

The study was approved by the local ethics committee. Studies were undertaken in accordance with the national and local regulations of the ethical committee (agreement number UCL/2010/MD/001).

Rhabdomyosarcoma

Four cohorts were involved. An experiment course of 3 days was designed for the first and second cohorts (Fig. E4A; available online at www.redjournal.org). For the first 2 days, animals of these 2 cohorts underwent the same procedure. Rats were anesthetized with isoflurane 1.5% for all interventions. Gas delivery (medical air or carbogen mixed with isoflurane) was continuous at 2 L/min through a nosepiece. On day 1, animals were subjected to MRI studies for R_1 and R_2* measurements. On day 2, tumor pO_2 was measured by EPR oximetry. All MR measurements were conducted under baseline and hyperoxic condition, which was obtained after 30 minutes of carbogen breathing. On day 3, rats were divided randomly into 2 subgroups for irradiation at 20 Gy under either air or carbogen breathing for growth delay (GD) assay (13). A third nonirradiated non-MRI control cohort was included. The fourth cohort was assigned to verify the repetition of tumor oxygenation over a period of 48 hours (Table E1; available online at www.redjournal.org). The details of the experimental design and the number of animals used in each cohort are presented, respectively, in Figures E4A and E4B (available online at www.redjournal.org).

At least twice a week, tumor size was assessed by a caliper and measured as the average of the longest and the shortest perpendicular diameters until the tumors reached 30 mm. The GD was calculated as the time after irradiation required for a tumor to grow to 1.5 times D_0, the tumor size at the time of treatment or at the beginning of the follow-up period (for control animals).

9L-glioma

There were 2 experimental series. For the first series, animals were randomly divided in 2 groups for baseline and carbogen challenge. Tumor was subjected to R_1 and R_2* acquisition and was then irradiated under the same breathing condition. In each group of breathing conditions, animals were randomly allocated in 5 subgroups, with the irradiation dose ranging from 10 to 60 Gy. For the second series, the same experiment as in the first and second cohorts of rhabdomyosarcoma was applied (Fig. E4A; available online at www.redjournal.org). Animals were irradiated at 40 Gy on the third day.

Details on numbers of animals can be found in Table E2 (available online at www.redjournal.org). Of note in the group irradiated at 40 Gy, data included all tumors of the second series, and those who received 40 Gy of RT in the first series.

Tumors were followed up until their diameters reached 30 mm. Animals were considered to be cured because there was no tumor regrowth at day 120 after irradiation. Responses to RT of 2 series were summed on tumor cure assay, which is known to be the most relevant assay for clinical translation.

MR measurements

Magnetic resonance imaging was performed on a 11.7-Tesla, 16-cm inner diameter bore system (Bruker, Biospec) with a 7-cm birdcage coil for signal emission and a surface coil for signal reception. A warm water blanket was used to maintain the animal's temperature at 37°C, and the temperature was monitored with an MR-compatible rectal probe.

A multislice Rapid Acquisition with Relaxation Enhancement (RARE) sequence was first used to determine the most representative tumor slice for further measurement, with the following parameters: echo time (TE)/Repetition time (TR)/RARE-factor/field of view (FOV)/matrix size/slice thickness = 10.66 ms/2500 ms/6/35 × 35 mm/256 × 256/1 mm. The segmented IR-FISP sequence (SSFP-FID mode) was used for R_1 acquisition with the following parameters: TR/TE/FA/BW/FOV/matrix size/slice thickness = 4 ms/1.35 ms/10°/100 kHz/55 × 30 mm/100 × 85/1 mm, 4 segments, 100 TI from 13 ms to 8329 ms every 84 ms, and a total acquisition time of 20 minutes. Multi-Gradient Echo R_2* images were acquired at TR/FA/slice thickness = 3000 ms/15°/1 mm with a FOV of 35 × 35 mm on a 256 × 256 matrix, 12 echoes from 3.5 ms to 58.5 ms every 5 ms. The total acquisition time was 9 minutes 36 seconds.

The EPR spectroscopy permitted a direct measurement of tumor oxygenation through the conversion of EPR linewidth to pO_2 by using a calibration curve (14). The method of EPR data acquisition has been described elsewhere (12). Briefly, charcoal wood powder (CX0670-1, EM Science, Gibbstown, NJ) was used as an oxygen-sensitive sensor. About 200 μL charcoal suspension (100 mg/mL) was introduced within tumor at a depth of 3 to 6 mm using a 23-gauge needle on day 1, after MRI acquisitions. The EPR experiments were performed 24 hours after probe implantation by using an L-band EPR spectrometer (Magnettech, Berlin, Germany) equipped with a low-frequency microwave bridge operating at 1.2 GHz and a loop-gap resonator. For that purpose, animals were anesthetized for EPR measurement. and tumors were placed at the center of the loop-gap resonator, whose sensitivity extends to 1 cm around the loop. The modulation frequency was 100 kHz,

and the amplitude modulation was less than one-third of the peak-to-peak linewidth to avoid peak distortion. The linewidth of the first derivative EPR spectrum that was the average of 5 scan accumulations was then converted to pO_2 using a calibration curve. After the pO_2 value was recorded under normoxic conditions, the rats were allowed to inhale carbogen for 30 minutes, and the acquisition was then repeated to obtain the value of pO_2 with the rats under hyperoxic conditions.

Irradiation

Tumors received a single dose of irradiation delivered by a ^{137}Cs irradiator IBL-637 (Oris, France). The dose rate was equal to 1 Gy/min. Animals were anesthetized with isoflurane 1.5% and were placed on a lead brick 3-mm thick to protect from whole-body irradiation while the tumors were exposed through a hole 25 mm in diameter. Tumors were turned midway through the exposure time to ensure homogeneity of dose distribution. For the carbogen group, the animals were allowed to inhale carbogen at 2 L/min for 5 minutes before and during irradiation (15).

Data analysis and statistics

Data analysis was performed on an in-house program developed under ImageJ and MATLAB. R_1s and R_2* maps were calculated with an MRI analysis calculator plug-in in ImageJ software. This MRI analysis method is adapted from the original plugin created by Karl Schmidt (http://rsb.info.nih.gov/ij/). The method use a curve fitting method based on the Simplex method described Caceci and Cacheris (16). Lipids R_1 and water R_1 were extracted from the global R_1 map by a biexponential deconvolution method. Regions of interest (ROIs) were drawn manually around the tumor on the selected anatomic slice and were transferred to all R_2* and R_1s maps of the same slice. The subtraction of 2 maps air and carbogen is done pixels par pixels, resulting in maps of delta.

Normality of the data distribution was checked before selection of the appropriate statistics using a normal quantile plot. Statistical significance of changes between MR parameters before and after carbogen challenge was assessed with the Student paired t test (Figs. 1 and 2). Values were expressed as mean ± standard equivalent of the mean or as relative variations.

The linear association between MR parameters and pO_2 measured using EPR (Fig. 3) was tested by correlation analysis. Pearson R coefficient was considered statistically significant for $P<.05$.

Response of the rhabdomyosarcoma to 20-Gy irradiation (GD curves, Fig. 4A) was analyzed with a linear mixed model. Fixed effects included in the model were the group, the time, and the interaction between the group and the time. Random effects included were a random intercept and a random slope. Linear relation between the GD and MR

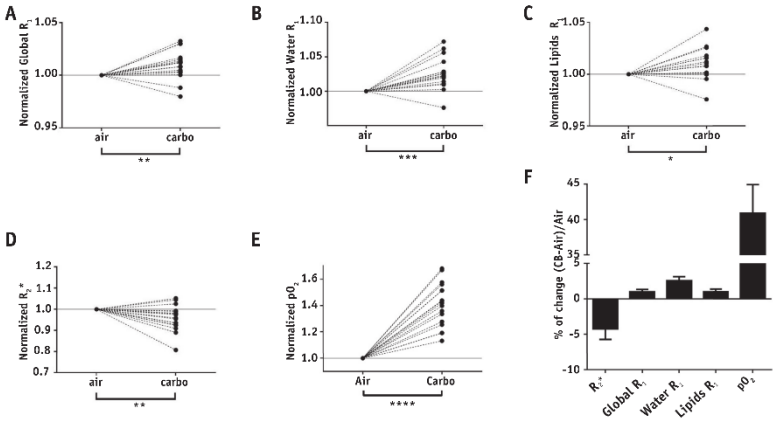

Fig. 1. Changes in magnetic resonance (MR) parameters in second series of 9L-glioma (n=17), baseline and hyperoxic conditions. (A-E) Individual normalized changes after carbogen challenge. (F) Mean relative changes ± standard equivalent of the mean (%). All MR parameters could track the change in tumor oxygenation induced by carbogen. *Abbreviation:* Carbo = carbogen.

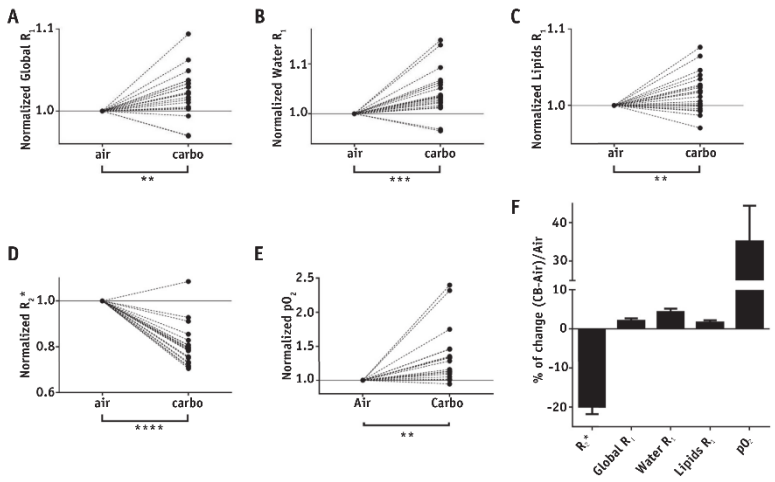

Fig. 2. Changes of magnetic resonance (MR) parameters in rhabdomyosarcoma (n = 19-22) of baseline and hyperoxic condition. (A-E) Individual normalized changes after carbogen challenge. (F) Mean relative changes ± standard equivalent of the mean (%). All MR parameters could track the change in tumor oxygenation induced by carbogen. *Abbreviation:* Carbo = carbogen.

parameters was tested in the rhabdomyosarcoma model by correlation tests (Fig. 4B-F).

With respect to the TCD50 assay in the 9L-glioma model, the predictive value of pretreatment (air vs carbogen) MRI (R_2*, global R_1, water R_1, lipids R_1) parameters on RT (40 Gy) treatment outcome was tested by logistic regression. For MRI parameters, multicollinearity was first checked. Based on the correlation matrix, global R_1 and lipids R_1 were found to be highly correlated. Two different models were built, 1 including global R_1 and 1 including lipids R_1 in the logistic model. The models were validated with the likelihood-ratio χ^2 value (model 1, $P = .0036$; model 2, $P = .0032$) (Table 1).

In the 9L-glioma group irradiated at 40 Gy, the difference of MRI parameters between cured and uncured animals was assessed with the Wilcoxon rank-sum scores because of a nonnormal distribution of the data.

Optimal sample size was computed by use of nQuery 2.0 with an α of 0.05 and a power of 0.8.

Statistical analyses were performed with the GraphPad (Prism) program, JMP Pro 12 (SAS Institute, Cary, NC), and SAS 9.4 for the mixed model.

Results

Representative parametric maps of spatial distribution of carbogen-induced ΔR_2*, water ΔR_1, lipids ΔR_1, global ΔR_1, and EPR spectra taken under air and carbogen breathing conditions in rhabdomyosarcoma and 9L-glioma are presented in Figure E1 (available online at www.redjournal.org). All MRI maps show heterogeneity within tumors in response to carbogen, with a mixture of pixels sensitive to and refractory to carbogen challenge, similar to that in the data shown in a recent study assessing R_1 in response to an oxygen challenge (17). In both models, carbogen generated an increment of pO_2 that broadened the linewidths of EPR spectra.

Figures 1 and 2 present precarbogen and postcarbogen challenge MR data for 9L-glioma and for rhabdomyosarcoma, respectively. The purpose was to study the ability of the breathing treatment to induce changes in oxygenation and to assess the values of the MR parameters reflecting this change. Information on the change in MR intrinsic values for 9L-glioma and rhabdomyosarcoma can be found in Figures E2 and E3 (available online at www.redjournal.org).

A rise in pO_2 resulted in a larger R_1. Global R_1 increased after carbogen from $2.23 \pm 0.04\ s^{-1}$ to $2.25 \pm 0.04\ s^{-1}$ in 9L-glioma ($n = 17$, $P = .008$) (Fig. 1A) and from $2.14 \pm 0.02\ s^{-1}$ to $2.19 \pm 0.02\ s^{-1}$ in rhabdomyosarcoma ($n = 22$, $P = .002$) (Fig. 2A). The response of global R_1 to carbogen breathing was quite similar in both models: 2 9L-glioma tumors (12%) and 3 rhabdomyosarcoma tumors (14%) had a negative global ΔR_1 (Figs. 1A and 2A). Water R_1 and lipids R_1 demonstrated the same trend. In response

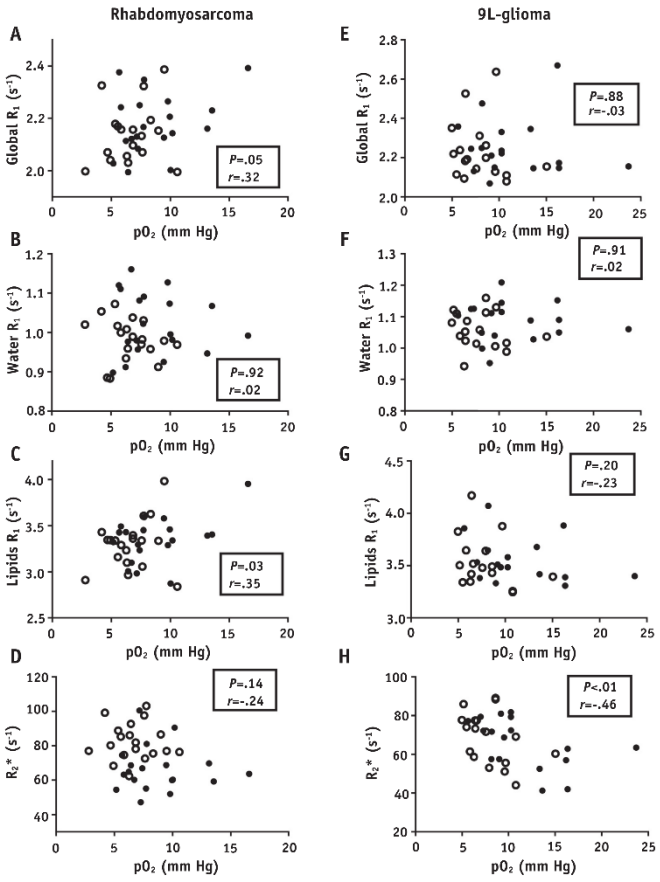

Fig. 3. Correlation between different magnetic resonance parameters with pO_2 assessed by electron paramagnetic resonance oximetry. Left (A-D), Rhabdomyosarcoma. Right (E-H), 9L-glioma. Each point was representative for an individual tumor subjected either to room air (open symbol) or to carbogen (filled symbol).

to carbogen breathing, the water R_1 increased from $1.06 \pm 0.01\ s^{-1}$ to $1.09 \pm 0.02\ s^{-1}$ ($P = .0003$) (Fig. 1B) and from $0.98 \pm 0.01\ s^{-1}$ to $1.03 \pm 0.02\ s^{-1}$ ($P = .0002$) (Fig. 2B) in 9L-glioma and rhabdomyosarcoma, respectively. We observed an even transition of this parameter generated by carbogen, whereas 6% of the 9L-glioma (1 tumor) and 9% of the rhabdomyosarcoma (2 tumors) did not respond to the challenge (Figs. 1B and 2B). The change was less pronounced for lipids R_1. Lipids R_1 was, respectively, $3.54 \pm 0.06\ s^{-1}$ (baseline) and $3.56 \pm 0.05\ s^{-1}$ (hyperoxic) ($P = .0196$) in 9L-glioma (Fig. 1C) and $3.30 \pm 0.05\ s^{-1}$ (baseline), $3.35 \pm 0.05\ s^{-1}$ (hyperoxic) ($P = .0051$) in rhabdomyosarcoma (Fig. 2C). Eighteen percent of the 9L-glioma (3 tumors) and 27% of the rhabdomyosarcoma (6 tumors) did not respond to carbogen breathing (Figs. 1C and 2C).

When blood oxygenation went up, dHb decreased as an effect of the increase of HbO_2; this led to a decrease in R_2*.

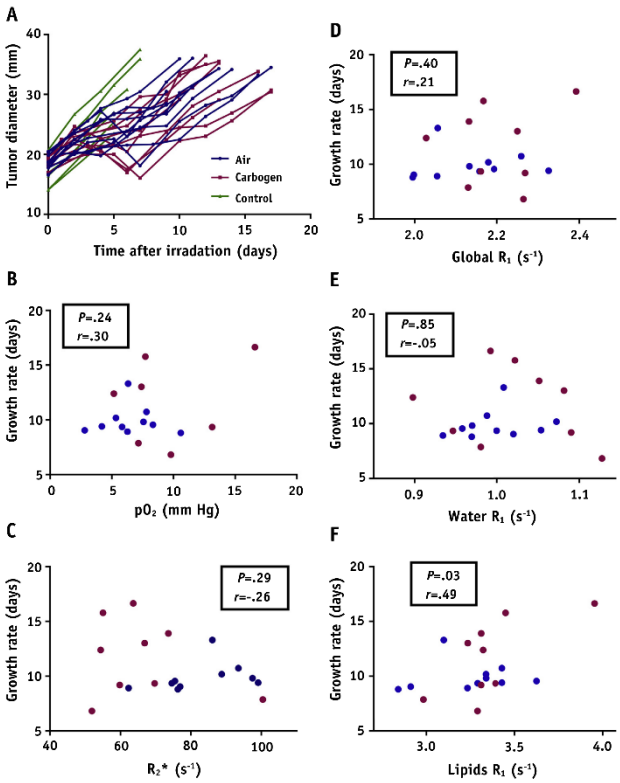

Fig. 4. (A) Response of rhabdomyosarcoma to irradiation of 20 Gy (control n=6, baseline n=10, carbogen n=9). (B-F) Relationship between magnetic resonance parameters and growth delay in rhabdomyosarcoma (n=19, except B n=17). Each point represents a tumor irradiated under baseline (blue symbols) or carbogen breathing condition (red symbols). Note, we expected a negative slope for R_2* and pO_2 correlation and a positive slope for R_1 correlation.

Carbogen reduced R_2* in 9L-glioma (n=17) from 68.72 ± 3.30 s^{-1} to 65.73 ± 3.14 s^{-1} (P=.01) (Fig. 1D) and from 82.79 ± 2.18 s^{-1} to 66.44 ± 2.63 s^{-1} (P<.0001) (Fig. 2D) in rhabdomyosarcoma (n=22). The R_2* alteration showed that both models were responsive to the carbogen challenge (Figs. 1F and 2F). Three glioma did not respond to carbogen in terms of R_2*, versus 1 rhabdomyosarcoma. Interestingly, the tumors that showed a lack of response in terms of R_1 were different from those that showed a lack of response in terms of R_2*.

These MR parameters were compared with the pO_2 obtained by EPR. Carbogen breathing increased pO_2 from 8.0 ± 0.6 mm Hg to 11.4 ± 1.1 mm Hg in 9L-glioma (n=17) (P<.0001) (Fig. 1E) and from 6.7 ± 0.4 mm Hg to 8.7 ± 0.7 mm Hg in rhabdomyosarcoma (n=19) (P=.0008) (Fig. 2E). Whereas the pO_2 of all the 9L-glioma increased on hyperoxic challenge (Fig. 1E), the pO_2 of 1 rhabdomyosarcoma decreased (Fig. 2E). Note that only the pO_2 in 9L-glioma increased beyond 10 mm Hg. Interestingly, changes in R_1s and R_2* induced by a rise in pO_2, observed here by EPR oximetry, matched those seen with use of the OxyLite system (fluorescence-quenching fiberoptic-based method) by O'Connor et al (10), showing that changes in MRI parameters are reproducible across different tumor models and laboratories.

Table 1 Logistic regression and odds ratio

Variable	Coefficient (β)	Standard error	*P* value	Odds ratio	95% Confidence interval
Intercept	43	29	.14	-	-
Air/carbogen	−2.8	1.27	.0006	270	6.5-5.17 10^5
R_2* (s^{-1})	0.26	0.14	.0094	1.29	1.05-1.92
Lipids R_1 (s^{-1})	−9.8	5.9	.021	5.2 10^{-5}	3.8 10^{-12} to 3 10^{-1}
Water R_1 (s^{-1})	−21.6	19.3	.205	4.3 10^{-10}	2.9 10^{-33} to 4.4 10^4
Intercept	34	29	.24	-	-
Air/carbogen	−2.34	1.11	.002	106	4-6.6 10^4
R_2* (s^{-1})	0.22	0.12	.012	1.25	1.04-1.76
Global R_1 (s^{-1})	−15.7	10.5	.019	1.5 10^{-7}	2.6 10^{-21} to 0.14
Water R_1 (s^{-1})	−10.8	16.2	.48	2.0 10^{-5}	8.33 10^{-23} to 1.34 10^8

Above, model includes lipids R_1 as explicative variable but not global R_1. Below, model includes global R_1 but not lipids R_1.

To study the quantitative aspect of MRI biomarkers, we correlated individual MRI parameters and their corresponding pO_2 under distinct breathing conditions (Fig. 3). As discussed above, an increase in pO_2 resulted in a decrease in R_2* and an increase in R_1. Thus, theoretically, we expect a negative slope in pO_2-R_2* correlation and a positive slope in pO_2-R_1 correlation. The correlations were found to be significant in global R_1-pO_2 and in lipids R_1-pO_2 for rhabdomyosarcoma (P=.05 and .03, respectively) (Figs. 3A and 3C) and in R_2*-pO_2 for 9L-glioma (P<.01) (Fig. 3H).

Figure 4 presents the GD assay (Fig. 4A) and the correlations between RT responses with different MR parameters in rhabdomyosarcoma (Fig. 4B-F). The mixed model analysis did not show any difference between groups, meaning that carbogen was not able to significantly radiosensitize this tumor model, and did show an influence of time. As R_1 becomes larger, tumor oxygenation is higher; thus, a longer GD is expected. In that case, the slopes correlating R_1 and GD should theoretically increase (Fig. 4D-F). For R_2* the slope should theoretically decrease because a shorter R_2* corresponds to a higher oxygen level (Fig. 4C). A similar trend should be observed for correlation with pO_2 (Fig. 4B). Here, only the correlation between lipids R_1 and GD was found to be significant (P=.03, R=.49) (Fig. 4F). Note that actual pO_2 values also did not correlate with GD and that this might be due, in part, by the lack of individuals with high pO_2 values.

It should be noted that for rhabdomyosarcoma, 22 rats underwent MRI acquisition. However, the EPR signals of 3 rats were not exploitable. These 22 animals were then irradiated under either air or carbogen breathing; 3 died before the TGD experiment ended. Briefly, 17 had complete MRI, TGD, and EPR information; 2 had MRI and TGD information; 2 had MRI and EPR information; and 1 had only MRI information; this explains the discrepancy in the number of results in this model.

A TCD50 assay was performed on 9L-glioma. Figure 5 shows the radiation dose-response curves for tumor curability 120 days after irradiation. Carbogen decreased the TCD50 from 41.6 Gy in the group irradiated under air breathing conditions (95% confidence interval, 38.5-44.6 Gy) to 32.2 Gy in the group irradiated under carbogen breathing conditions (95% confidence interval, 31.8-32.6 Gy). The dose-modifying factor DMF50 was 1.29, obtained by dividing the TCD50 of the group irradiated under carbogen breathing by that of the radiation-alone group. Inasmuch as the DMF value was greater than 1, we conclude that carbogen enhanced the radioresponse of 9L-glioma tumor.

To evaluate the predictivity of MR biomarkers in RT (40 Gy) outcome, we performed a logistic regression (Table 1).

The first logistic analysis (using lipids R_1, water R_1, R_2*, carbogen/air) showed a significant predictive value for the carbogen pretreatment (P=.0006) and for R_2* (P=.009) and lipids R_1 (P=.02). Water R_1 was not significant (P=.20). In other terms, the carbogen group was 270 times more likely in terms of odds to have a positive RT outcome than was the air-treated group (odds ratio [OR] 270, CI 6-517,155). With regard to MRI parameters, tumors with a lower R_2* were 29% more likely in terms of odds to have a positive RT outcome (OR per unit 1.29; CI 1.05-1.92). The odds ratio for lipids R_1 was 5.25 10^{-5} (CI 3.87 10^{-12}-0.30). The odds probability ratio over the entire range was 830,137 for R_2* compared with 0.000128 for lipids R_1. The predictive value of R_2* is consequently likely to be of greater interest than that of lipids R_1.

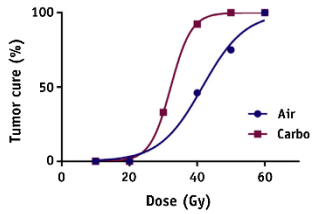

Fig. 5. Tumor cure assay on 9L-glioma 120 days after irradiation. *Abbreviation:* Carbo = carbogen.

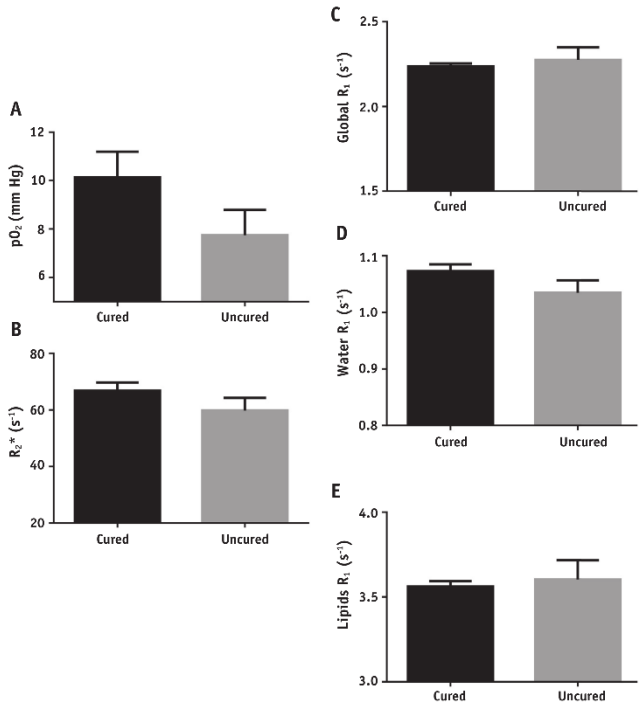

Fig. 6. Comparison of intrinsic magnetic resonance parameters between cured (n=18) and uncured group (n=8) of 9L-glioma tumors irradiated at 40 Gy (n=26), (except A, cured n=12, uncured n=5). No magnetic resonance parameter was predictive for the curability of the 9L-glioma model. A: pO_2 (mmHg) assessed using EPR oximetry; B: R_2* MR parameter; C: Global R_1 MR parameter; D: Water R_1 MR parameter; E: Lipids R_1 MR parameter.

The second logistic model (using global R_1 instead of lipids R_1) showed similar results, confirming the strong correlation between global R_1 and lipids R_1 (OR carbogen/air 106, CI 4-66.448; OR R_2* 1.25, CI 1.04-1.76; global R_1 1.5 10^{-7}, CI 2.6 10^{-21}-0.14). The predictive value of R_2* is consequently likely to be of greater interest than that of global R_1.

We also compared the MR intrinsic values of cured (n=18) and uncured (n=8) groups irradiated at 40 Gy (Fig. 6). The data in Figure 6A refer to tumors in the second series which underwent the EPR measurement (cured n=12, uncured n=5). None of the parameters showed a significant difference between the cured and uncured groups, although the actual pO_2 values assessed by EPR oximetry do show that the cured group presented pO_2 values around 10 mm Hg, which is the theoretical radiosensitivity threshold, unlike the uncured group, which presented values around 8 mm Hg and therefore below this threshold. It should be noted that the statistical test used was nonparametric, inasmuch as the distribution was non-normal. Although robust, this test requires a large sample size to demonstrate a difference. In this particular case, the required size sample would be 31 animals per group at a risk level α of 0.05 and a power of 0.8.

Discussion

This work had 2 goals: (*1*) to assess the sensitivity of oxygen-sensitive MR parameters to changes in tumor oxygenation, including lipids R_1, water R_1, global R_1, and R_2*, in comparison with pO_2 assessed by EPR oximetry;

and (2) to correlate the tumor response to irradiation with these MR parameters to assess the relevance of each parameter as a potential predictive marker of the outcome of RT.

The modulation of tumor oxygenation was achieved by carbogen (5% CO_2 95% O_2) breathing. Because many factors can influence the oxygen modulation capacity of carbogen, tumors do not respond to this gas systematically. Thus, we selected tumor models that have previously been described to respond to carbogen (13). The purposes of using carbogen were: (1) to improve the understanding of different MR oxygen-sensitive parameters; and (2) to interpret these parameters in the context of outcome of RT.

For R_1 parameters, we observed that carbogen generated significant increases in all R_1 MR-derived parameters (global R_1, water R_1, lipids R_1) corresponding to the increases in pO_2 assessed by EPR oximetry (Figs. 1 and 2). Nevertheless, when R_1 parameters were compared, the response of lipids R_1 was less pronounced than that of global or water R_1, contrary to our assumption. The lipids R_1 values obtained in this work seemed less sensitive than those presented in a previous work (11, 18). The discrepancy could be due to different imaging acquisition sequences. The earlier work used 2 distinct sequences for global R_1 and lipids R_1. However, this sequence worked only on tumor models with a high amount of lipids (ie, mammary tumor models). In this study, we used 2 tumor models with a lower lipid content, and therefore we needed to adapt the type of acquisition (1 acquisition for global R_1, biexponential deconvolution of the signal to extract fast and slow components). The fast and slow components are attributed to lipids and water relaxation (19), but we cannot exclude a contribution to the fast component from water linked to macromolecules. In fact, water exists both in blood and tissue, and water R_1 represents the variation of oxygen in both compartments. However, water may be present in tissue under multiple states, ranging from unbound to partially structured or fully bound to macromolecules. Although these bound water protons are in the minority, they do have a significant relaxation effect on R_1. Water that forms a hydration layer around macromolecules has restricted motion. This leads to an increase in R_1 because those water protons are involved in interactions near the Larmor frequency (20, 21). The membrane phospholipids of blood cells barely contribute to the lipids R_1 signal because the substance participates only in oxygen exchange. Consequently, lipids R_1 can probably account only for lipids in tissue. Hence, the results obtained could be explained by the fact that water R_1 reflects the oxygen in blood and tissue, and lipids R_1 focuses mostly on oxygen in tissues. Inasmuch as global R_1 takes account of both fast and slow relaxation rates, its response is intermediate. In fact, 2 approaches could be considered to modulate tumor oxygenation: modification of oxygen consumption or of oxygen supply. Carbogen could increase the oxygen supply through arterial blood saturation, but it does not necessarily produce the same effect on tumor oxygenation. Hence, we assumed that the sensitivity of lipids R_1 depends on the type of modulation of tumor oxygenation. For a better understanding of lipids R_1 behavior, additional studies should be performed with pharmacologic agents able to modulate the oxygen consumption of tumor cells.

With regard to the quantitative aspect of R_1s, correlations of global R_1 and lipids R_1 were significant in the rhabdomyosarcoma model, which is less responsive to carbogen (Figs. 3A and 3C) but not in the more carbogen-responsive 9L-glioma model, where R_2* was found to be significant (Fig. 3H). In healthy mouse brain, Beeman et al (22) showed that R_1 was linearly dependent on pO_2 assessed by optical probe, using 3 breathing conditions: hypoxic gas, 100% O_2, and carbogen. In addition, the ΔR_1 of hypoxic gas and carbogen could discriminate between normal brain, radiation-induced lesions, and tumor lesions. In a report by O'Connor et al (23), a different approach to analyzing R_1 maps was investigated. Comparing R_1 maps for air breathing and 100% O_2 breathing, they hypothesized that tumor fractions that had R_1 refractory to oxygen challenge ($\Delta R_1 < 0$) would be a key biomarker of hypoxia, not ΔR_1 or ΔR_2*. The work provided evidence that the "oxy refractory fraction" along with DCE MRI was able to determine the hypoxia fraction in different models. Furthermore, this parameter was also sensitive to dynamic changes in tumor oxygenation. That study work also emphasizes the potential valued of analyzing intratumor heterogeneity (23).

For R_2*, the paramagnetic dHb generates a field gradient that causes an increase in R_2* not only in the water of blood plasma but also in neighboring tissues. Consequently, R_2* drops if the dHb concentration per unit of tissue volume decreases, either by a reduction of dHb concentration in the blood or by a decrease in blood volume. In this context, carbogen generated a decrease in R_2* in both tumor models. These changes result not only from the decrease of dHb in the blood resulting from the binding of oxygen-hemoglobin but also from the contribution of other factors. Some possible changes induced by carbogen that influence the R_2* signal are modification of tumor blood flow, pH, response of tumor vessels, or tumor blood volume. Although these effects are minor and are normally outweighed by the decrease in dHb while breathing carbogen, they still contribute to the change in R_2* image intensity. Briefly, R_2* represents more than just vessel oxygenation, and ΔR_2* induced by carbogen reflects both the hemodynamic and vasoactive response of the tumor to CO_2 in combination with the real change in blood oxygenation. In this context, R_2* was found to be inversely correlated with pO_2 in 9L-glioma ($P < .01$) (Fig. 3H). In addition, ΔR_2* in rhabdomyosarcoma ($16.34 \pm 1.59\ s^{-1}$) was larger than in 9L-glioma ($2.98 \pm 0.97\ s^{-1}$), whereas ΔpO_2 in 9L-glioma (3.5 ± 0.5 mm Hg) was more intense than in rhabdomyosarcoma (2.1 ± 0.5 mm Hg). Although the R_2* response is individual dependent, it is interesting to note that R_2* is more sensitive when the basal oxygenation level is lower (24) (the baseline pO_2 of rhabdomyosarcoma

and 9L-glioma are 6.7 ± 0.4 mm Hg and 8.0 ± 0.6 mm Hg, respectively).

Obviously, understanding the mechanisms behind the responses of MR parameters to the changes in tumor oxygenation is helpful. But above all, the more fundamental need in clinical practice is to address the question of whether these MR methods can predict the outcome of radiation therapy. In both models, carbogen induced significant changes in all MRI parameters, reflecting an increase in tumor oxygenation. These modifications were confirmed by pO_2 assessed by EPR. However, irradiation under carbogen breathing conditions significantly increased the survival of 9L-glioma but not of rhabdomyosarcoma. This established a paradigmatic situation with 1 responsive and 1 unresponsive model. With respect to the distinct radiosensitive properties of the 2 tumor models, we conducted a GD assay on the rhabdomyosarcoma model and a more clinically relevant TCD50 assay on the 9L-glioma model.

The GD was performed at 20 Gy. Indeed, in a preceding study (13), the RT dose escalation from 15 Gy to 20 Gy significantly increased the response to irradiation in rhabdomyosarcoma. Yet, there was no benefit of carbogen on RT response between animals irradiated under air versus carbogen breathing conditions. Thus, we decided to remain at this dose rate to further correlate the GD and MR parameters. Lipids R_1 was correlated with the GD in rhabdomyosarcoma (Fig. 4F). A lack of correlation between GD and pO_2 was observed, which could be due to the lack of radiosensitive individuals (pO_2 >10 mm Hg) in this correlation (Fig. 4B).

In 9L-glioma, the more clinically relevant TCD50 assay confirmed the radiosensitizing properties of carbogen in this model. We selected the dose of 40 Gy to assess the predictivity of intrinsic MRI parameters because we observed a clear difference in response to irradiation between the 2 groups (carbogen vs air breathing). R_2* alone was likely to be predictive for the curability of 9L-glioma in this assay, whereas all R_1-related parameters failed to predict RT outcome.

Briefly, the R_1s and R_2* could tackle the individual change in tumor oxygenation induced by carbogen breathing. Yet, only R_2* was likely to predict the outcome of RT in 9L-glioma (tumors with a lower R_2* were 29% more likely to have a positive RT outcome), whereas ^{18}F-FAZA was shown earlier to be able to robustly predict the outcome of RT with a similar protocol. A possible explanation is the high heterogeneity between and within individuals (Fig. E1; available online at www.redjournal.org) and the influence of bound water on the long R_1 component. Nonetheless, the combination of R_2* and R_1 parameters should be further characterized in tumor models that are still more responsive to carbogen breathing and with other modulators of tumor oxygenation, including inhibitors of oxygen consumption. Alternative methods to extract R_1 of lipids should also be considered.

With respect to the translational aspect of the techniques, R_2* and R_1 have been applied to multiple patient studies at 1.5 T for R_2* (25, 26) and for R_1 (5), and 3T for R_2* (27) and for R_1 (28), which shows that these techniques can translate across multiple body sites and tumor types. A higher sensitivity of R_1 and a lower sensitivity of R_2* can be expected at lower magnetic fields than the 11.7 T used in the current study, yet more adapted to small animal studies.

In conclusion, this work illustrates the sensitivity of R_1 oxygen-sensitive MR parameters to changes in tumor oxygenation but shows their limitations in terms of predicting the outcome of RT in the tumor models under study, whereas R_2* was found to be partially correlated with the outcome in the carbogen responsive model. In line with the recent comment by Dewhirst and Birer (9) on oxygen-enhanced MRI, additional studies are needed to further validate MRI parameters for future patient stratification for hypoxia modification.

References

1. Harris AL. Hypoxia: A key regulatory factor in tumour growth. *Nat Rev Cancer* 2002;2:38-47.
2. Overgaard J. Hypoxic radiosensitization: Adored and ignored. *J Clin Oncol* 2007;25:4066-4074.
3. Vikram DS, Zweier JL, Kuppusamy P. Methods for noninvasive imaging of tissue hypoxia. *Antioxid Redox Signal* 2007;9:1745-1756.
4. Tatum JL. Hypoxia: Importance in tumor biology, noninvasive measurement by imaging, and value of its measurement in the management of cancer therapy. *Int J Radiat Biol* 2006;82:699-757.
5. O'Connor JP, Naish JH, Parker GJ, et al. Preliminary study of oxygen-enhanced longitudinal relaxation in MRI: A potential novel biomarker of oxygenation changes in solid tumors. *Int J Radiat Oncol Biol Phys* 2009;75:1209-1215.
6. Robinson SP, Rijken PF, Howe FA, et al. Tumor vascular architecture and function evaluated by non-invasive susceptibility MRI methods and immunohistochemistry. *J Magn Reson Imaging* 2003; 17:445-454.
7. Burrell JS, Walker-Samuel S, Baker LC, et al. Exploring ΔR_2* and ΔR_1 as imaging biomarkers of tumor oxygenation. *J Magn Reson Imaging* 2013;38:429-434.
8. Hallac RR, Zhou H, Pidikiti R, et al. Correlations of noninvasive BOLD and TOLD MRI with pO_2 and relevance to tumor radiation response. *Magn Reson Med* 2014;71:1863-1873.
9. Dewhirst MW, Birer SR. Oxygen-enhanced MRI is a major advance in tumor hypoxia imaging. *Cancer Res* 2016;76:769-772.
10. O'Connor JP, Boult JK, Jamin Y, et al. Oxygen-enhanced MRI accurately identifies, quantifies, and maps tumor hypoxia in preclinical cancer models. *Cancer Res* 2016;76:787-795.
11. Jordan BF, Magat J, Colliez F, et al. Mapping of oxygen by imaging lipids relaxation enhancement: A potential sensitive endogenous MRI contrast to map variations in tissue oxygenation. *Magn Reson Med* 2013;70:732-744.
12. Gallez B, Baudelet C, Jordan BF. Assessment of tumor oxygenation by electron paramagnetic resonance: Principles and applications. *NMR Biomed* 2004;17:240-262.
13. Tran LB, Bol A, Labar D, et al. Potential role of hypoxia imaging using ^{18}F-FAZA PET to guide hypoxia-driven interventions (carbogen breathing or dose escalation) in radiation therapy. *Radiother Oncol* 2014;113:204-209.
14. Jordan BF, Baudelet C, Gallez B. Carbon-centered radicals as oxygen sensors for in vivo electron paramagnetic resonance: Screening for an optimal probe among commercially available charcoals. *MAGMA* 1998;7:121-129.

15. Tran LB, Bol A, Labar D, et al. Hypoxia imaging with the nitroimidazole ^{18}F-FAZA PET tracer: A comparison with OxyLite, EPR oximetry and ^{19}F-MRI relaxometry. *Radiother Oncol* 2012;105:29-35.
16. Caceci MS, Cacheris WP. Fitting curves to data: The simplex algorithm is the answer. *Byte* 1984;9:340-362.
17. Dunn TJ, Braun RD, Rhemus WE, et al. The effects of hyperoxic and hypercarbic gases on tumour blood flow. *Br J Cancer* 1999;80:117-126.
18. Colliez F, Neveu MA, Magat J, et al. Qualification of a noninvasive magnetic resonance imaging biomarker to assess tumor oxygenation. *Clin Cancer Res* 2014;20:5403-5411.
19. Renou JP, Kopp J, Valin C. Use of low resolution NMR for determining fat content in meat products. *Int J Food Sci Technol* 1985;20:23-29.
20. Edzes HT, Samulski ET. Cross relaxation and spin diffusion in the proton NMR or hydrated collagen. *Nature* 1977;265:521-523.
21. Zhang L, Wang L, Kao YT, et al. Mapping hydration dynamics around a protein surface. *Proc Natl Acad Sci U S A* 2007;104:18461-18466.
22. Beeman SC, Shui YB, Perez-Torres CJ, et al. O_2-sensitive MRI distinguishes brain tumor versus radiation necrosis in murine models. *Magn Reson Med* 2016;75:2442-2447.
23. O'Connor JP, Rose CJ, Waterton JC, et al. Imaging intratumor heterogeneity: Role in therapy response, resistance, and clinical outcome. *Clin Cancer Res* 2015;21:249-257.
24. Baudelet C, Gallez B. How does blood oxygen level-dependent (BOLD) contrast correlate with oxygen partial pressure (pO_2) inside tumors? *Magn Reson Med* 2002;48:980-986.
25. Rijpkema M, Kaanders JH, Joosten FB, et al. Effects of breathing a hyperoxic hypercapnic gas mixture on blood oxygenation and vascularity of head-and-neck tumors as measured by magnetic resonance imaging. *Int J Radiat Oncol Biol Phys* 2002;53:1185-1191.
26. Griffiths JR, Taylor NJ, Howe FA, et al. The response of human tumors to carbogen breathing, monitored by gradient-recalled echo magnetic resonance imaging. *Int J Radiat Oncol Biol Phys* 1997;39:697-701.
27. Hallac RR, Ding Y, Yuan Q, et al. Oxygenation in cervical cancer and normal uterine cervix assessed using blood oxygenation level-dependent (BOLD) MRI at 3T. *NMR Biomed* 2012;25:1321-1330.
28. Linnik IV, Scott ML, Holliday KF, et al. Noninvasive tumor hypoxia measurement using magnetic resonance imaging in murine U87 glioma xenografts and in patients with glioblastoma. *Magn Reson Med* 2014;71:1854-1862.

Materials and Methods

Tumor models

Two tumor models were included in the study, rhabdomyosarcoma (n=32) and 9L-glioma (n=63). Fragments from a syngeneic rhabdomyosarcoma (1mm^3) were grafted subcutaneously in one thigh of male adult WAG/Rij rats, according to a model developed by the Laboratory of Experimental Radiobiology, Katholieke Universiteit Leuven, Belgium. 9L-glioma cells were grown in RPMI medium supplemented with 10% foetal calf serum (FBS heat inactivated), 1% of a mixture of antibiotics (penicillin 100 UI/ml, streptomycin 0.1 mg/ml), 1% non-essential acid amine and 1% sodium pyruvate. Cells were maintained in a balanced wet atmosphere (37°C and CO_2 5%). To establish 9L-glioma tumors *in vivo*, male adult Fisher F344 rats were inoculated subcutaneously in thighs with 5.10^6 cells. Tumor implantations were performed under general anesthesia using intraperitoneal injection of ketamine and xylazine (80 and 10mg/kg, respectively) on rats weighted between 200g and 250g. Animals were introduced in study when tumors reached the size of 15-20mm.

Experimental design

The study was approved by the local ethics committee. (details removed for blinded review purposes)

Rhabdomyosarcoma

Four cohorts were involved. An experiment course of 3 days was designed for the first and second cohorts (supplementary Fig.4A). For the two first days, animals of these two cohorts underwent the same procedure. Rats were anesthetized with isoflurane 1.5% for all interventions. Gas delivery (medical air or carbogen mixed with isoflurane) was continuous at 2L/min through a nose piece. On day 1, animals were subjected to MRI studies for R_1 and R_2* measurements. On day 2, tumor pO_2 was measured by EPR oximetry. All MR measurements were conducted under baseline and hyperoxic condition which was obtained after 30min of carbogen breathing. On day 3, rats were divided randomly in two subgroups for irradiation at 20Gy either under air or carbogen breathing for GD assay [1]. A third non-irradiated non-MRI control cohort was included.

The 4th cohort was assigned to verify the repetition of tumor oxygenation over a period of 48h (supplementary Table 1). The details of experimental design and the number of animal used in each cohort are presented in supplementary Fig.4A and 4B, respectively.

At least twice a week, tumor size was assessed by a caliper and measured as the average of the longest and the shortest perpendicular diameters until reaching 30mm. GD was calculated as the time post-irradiation required for a tumor to growth to 1.5 times D_0 which is the tumor size at the time of treatment or at the beginning of the follow up (for control animals).

9L-glioma

There were 2 experimental series.

For the first series, animals were randomly divided in two groups for baseline and carbogen challenge. Tumor was subjected to R_1 and R_2* acquisition then was irradiated under the same breathing condition. In each group of breathing condition, animals were randomly allocated in 5 sub-groups with the irradiation dose ranging from 10 to 60Gy.

For the second series, the same experiment as the first and second cohorts of rhabdomyosarcoma was applied (supplementary Fig.4A). Animals were irradiated at 40Gy on the third day.

Details on numbers of animals can be found in supplementary Table 2. Of note in group irradiated at 40Gy, data included all tumors of the 2nd series and those received 40Gy of RT in the 1st series

Tumors were followed until diameter up to 30mm. Animals were considered as cured since there was no tumor regrowth at day 120 post-irradiation. Responses to RT of two series were summed on tumor cure assay which is known as the most relevant assay for clinical translation.

MR measurements

MRI was performed on a 11.7-Tesla, 16cm inner diameter bore system (Bruker , Biospec) with a 7cm birdcage coil for signal emission and a surface coil for signal reception. A warm water blanket was used to maintain the animal temperature at 37°C and temperature was monitored using a MR-compatible rectal probe.

A multi-slice RARE sequence was first used to determine the most representative tumor slice for further measurement with the following parameters TE/TR/RARE-factor/FOV/matrix size/slice thickness = 10.66ms/2500ms/6/35x35mm/256x256/1mm. The segmented IR-FISP sequence (SSFP-FID mode) was used for R_1 acquisition with the following parameters TR/TE/FA/BW/FOV/matrix size/slice thickness = 4ms/1.35ms/10°/100kHz/55x30mm/100x85/1mm, four segments, 100 TI from 13ms to 8329ms every 84ms and a total acquisition time of 20 minutes. MGE R_2* images were acquired at TR/FA/slice thickness = 3000ms/15°/1mm with a FOV of 35x35mm on a 256x256 matrix, 12 echoes from 3.5ms to 58.5ms every 5ms. Total acquisition time was 9min 36s.

EPR spectroscopy permitted a direct measurement of tumor oxygenation through the conversion of EPR linewidth to pO_2 by using a calibration curve [2]. Method for EPR data acquisition was described elsewhere [3]. Briefly, charcoal wood powder (CX0670-1, EM Science, Gibbstown, NJ) was used as oxygen sensitive sensor. About 200µl of charcoal suspension (100mg/ml) was introduced within tumor at a depth of 3–6mm using a 23-gauge needle on day 1, after MRI acquisitions. EPR experiments were performed 24 h after probe implantation by using an L-band EPR spectrometer (Magnettech, Berlin, Germany) equipped with a low-frequency microwave bridge operating at 1.2GHz and a loop-gap resonator. For that purpose, animals were anesthetized for EPR measurement and tumors were placed at the center of loop-gap resonator whose sensitivity extends to 1cm around the loop. The modulation frequency was 100kHz and the amplitude modulation was less than one third of the peak-to-peak linewidth to avoid peak distortion. The linewidth of the first-derivative EPR spectrum that was the average of five scan accumulations was then converted to pO_2 using a calibration curve.

After recording the pO_2 value under normoxic condition, the rats were let inhale carbogen for 30min, the acquisition was then repeated to obtain the value of pO_2 under hyperoxic condition.

Irradiation

Tumors received a single dose of irradiation delivered by a Cs-137 irradiator IBL-637 (Oris, France). The dose rate was equal to 1Gy/min. Animals were anesthetized with isoflurane 1.5% and were placed on a lead brick of 3mm thickness to protect from whole-body irradiation while exposing tumors via a hole of 25mm in diameter. Tumors were turned midways through the exposure time to ensure homogeneity of dose distribution. For the carbogen group, animals were allowed to inhale carbogen at 2L/min for 5 minutes prior and during irradiation [1].

Data analysis and Statistics

Data analysis was performed on an in-house program developed under ImageJ and Matlab. R_1s and R_2* maps were calculated using an MRI analysis calculator plug-in in ImageJ software. This MRI analysis method is adapted from the original plugin created by Karl Schmidt (http://rsb.info.nih.gov/ij/). The method use a curve fitting method based on the Simplex method described in the article by Caceci MS [4]. Lipids R_1 and water R_1 were extracted from global R_1 map using a bi-exponential deconvolution method. Regions of interest (ROIs) were drawn manually around the tumor on the selected anatomical slice. ROI were transferred to all R_2* and R_1s map of the same slice. The subtraction of 2 maps air and carbogen is done pixels par pixels resulting in maps of delta.

Normality of the data distribution was checked prior to selecting the appropriate statistics using normal quantile plot. Statistical significance of changes between MR parameters pre- and post-carbogen challenge was assessed using Student's pair t-test (Fig.1-2). Values were expressed as mean±SEM (Fig.1A-E, Fig.2A-E) or as relative variations (Fig.1F-J, Fig.2F-J).

The linear association between MR parameters and pO_2 measured using RPE (Fig.3) was tested by correlation analysis. Pearson R coefficient was considered statistically significant for $p<0.05$.

Response of the rhabdomyosarcoma to 20Gy irradiation (GD curves, Fig.4A) was analyzed using a Linear Mixed Model. Fixed effects included in the model were the group, the time and the interaction between the group and the time. Random effects included are a random intercept and a random slope. Linear relation between GD and MR parameters was tested in the rhabdomyosarcoma model by correlation tests (Fig.4B-F).

With respect to the TCD50 assay in the 9L-glioma model, the predictive value of pre-treatment (air vs. carbogen), MRI (R_2*, global R_1, water R_1, lipids R_1) parameters on RT (40Gy) treatment outcome was tested using a Logistic regression. For MRI parameters, multicollinearity was first checked. Based on the correlation matrix, global R_1 and lipids R_1 were found highly correlated. Two different models were built, one including global R_1 and one including lipids R_1 in the Logistic model. The models were validated using the likelihood-ratio Chi-square value (model 1, p=0.0036; model 2, p=0.0032) (Fig.5B).

In the 9L-Glioma group irradiated at 40Gy (Fig.6), difference of MRI parameters between cured and uncured animals was assessed with the Wilcoxon rank-sum scores, because of a non-normal distribution of the data.

Optimal sample size was computed using nQuery 2.0 with an alpha of 0.05 and a power of 0.8.

Statistical analyses were performed with the GraphPad (Prism) program, JMP Pro 12 (SAS institute), and SAS 9.4 for the mixed model.

References

1. Tran LBA, Bol A, Labar D, Karroum O, Bol V, Jordan B, Grégoire V, Gallez B. Potential role of hypoxia imaging using ^{18}F-FAZA PET to guide hypoxia-driven interventions (carbogen breathing or dose escalation) in radiation therapy. Radiotherapy and Oncology 2014; 113:204–209.

2. Jordan BF, Baudelet C, Gallez B. Carbon-centered radicals as oxygen sensors for in vivo electron paramagnetic resonance: screening for an optimal probe among commercially available charcoals. MAGMA 1998; 7:121–129.

3. Tran LBA, Bol A, Labar D, Jordan B, Magat J, Mignion L, Grégoire V, Gallez B. Hypoxia imaging with the nitroimidazole ^{18}F-FAZA PET tracer: A comparison with OxyLite, EPR oximetry and ^{19}F-MRI relaxometry. Radiotherapy and Oncology 2012; 105:29–35.

4. Caceci MS, Cacheris WP. Fitting Curves to data: the Simplex algorithm is the answer. Byte May 1984; 340-362.

Supplementary figure and table captions:

Sup Fig.1: Representative parametric maps of global ΔR_1, water ΔR_1, lipids ΔR_1, ΔR_2^* induced by carbogen and EPR spectra of baseline and hyperoxic condition in rhabdomyosarcoma and 9L-glioma

Sup Fig.2: Individual changes of MR parameters in 2nd series in 9L-glioma (n=17) of baseline and hyperoxic condition

Sup Fig.3: Individual changes of MR parameters in rhabdomyosarcoma (n=22, except **(D)** n=19) of baseline and hyperoxic condition.

Sup Fig.4: Rhabdomyosarcoma **(A)** Experimental protocol for the first and second cohorts. **(B)** Number of animals used in this tumor model

Sup Table 1: Evolution of pO_2 in rhabdomyosarcoma 4th cohort over a period of 48h, air breathing condition

Sup Table 2: Number of animals used in 9L-glioma

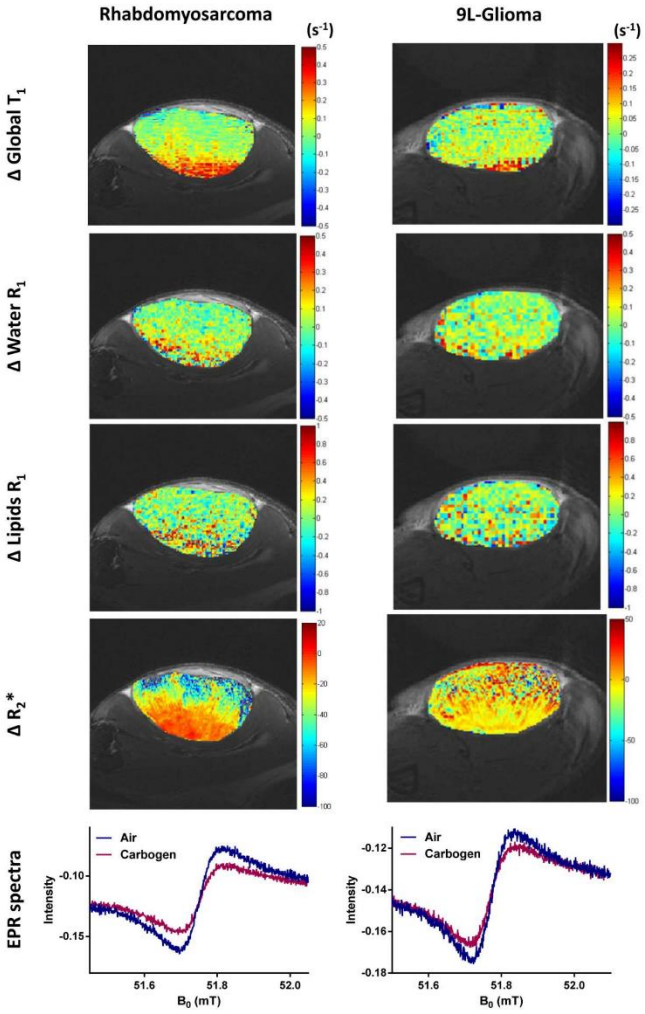
Rhabdomyosarcoma
9L-Glioma
(s-1)
Δ Global T1
Δ Water R1
Δ Lipids R1
Δ R2*
EPR spectra
Air
Carbogen
Intensity
B0 (mT)
51.6
51.8
52.0

SUP FIGURE 1

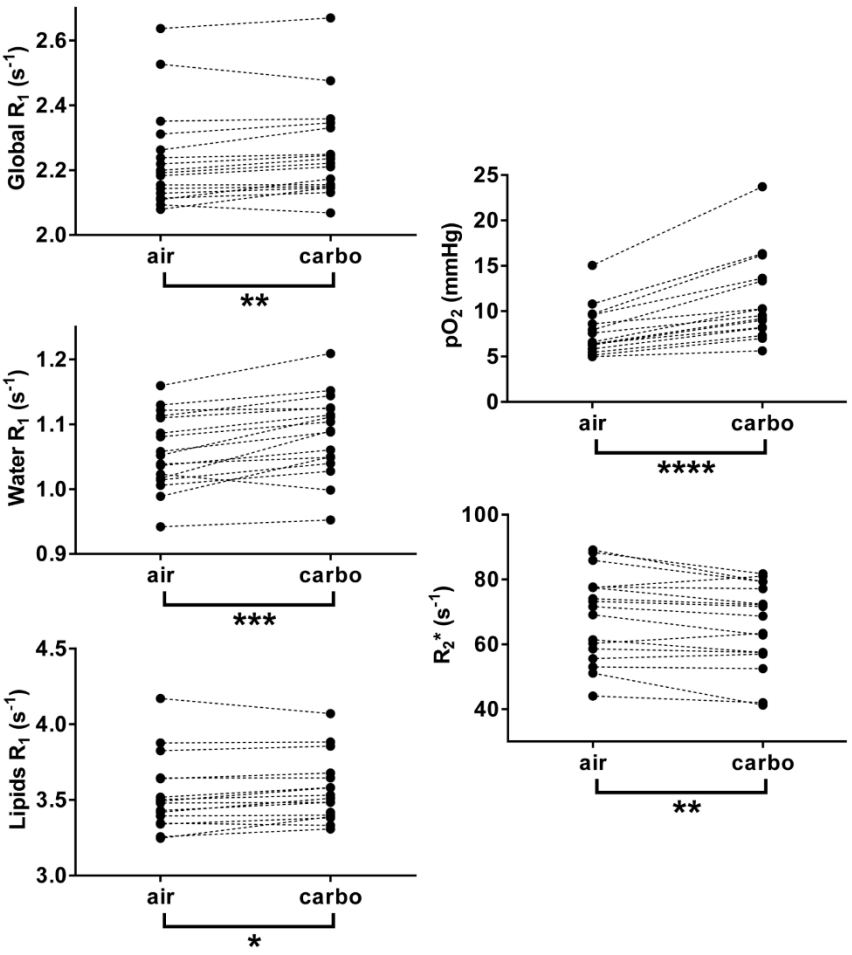
Global R_1 (s^{-1})
2.6
2.4
2.2
2.0
air
carbo
**
Water R_1 (s^{-1})
1.2
1.1
1.0
0.9
air
carbo
***
Lipids R_1 (s^{-1})
4.5
4.0
3.5
3.0
air
carbo
*
pO_2 (mmHg)
25
20
15
10
5
0
air
carbo
****
R_2^* (s^{-1})
100
80
60
40
air
carbo
**

SUP FIGURE 2

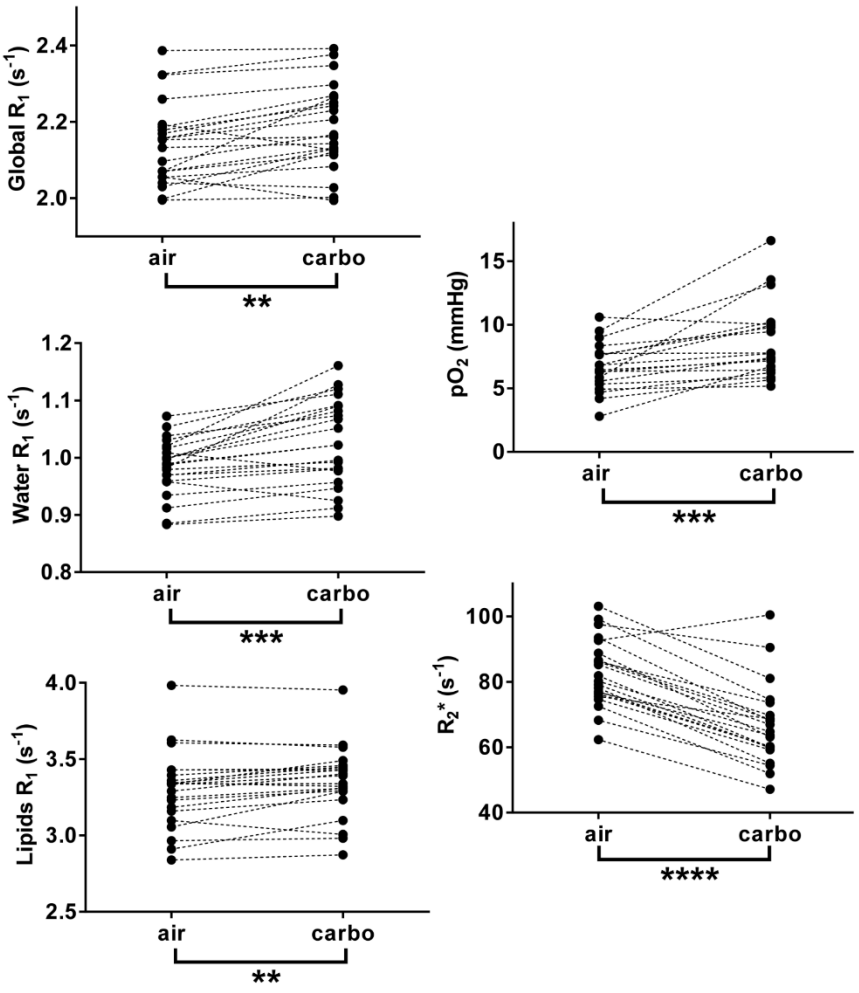
Global R_1 (s^{-1})
2.4
2.2
2.0
air
carbo
**
Water R_1 (s^{-1})
1.2
1.1
1.0
0.9
0.8
air
carbo
***
Lipids R_1 (s^{-1})
4.0
3.5
3.0
2.5
air
carbo
**
pO_2 (mmHg)
15
10
5
0
air
carbo
***
R_2^* (s^{-1})
100
80
60
40
air
carbo
****

SUP FIGURE 3

A. Experiment design

Day 1: MRI acquisition

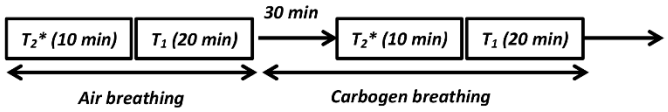

Day 2: EPR spectroscopy

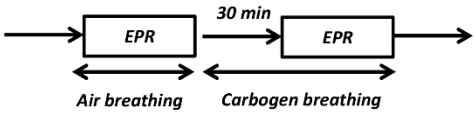

Day 3: Radiation therapy

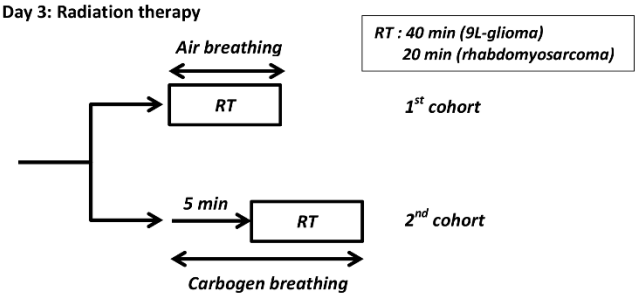

B. Animals used

	rhabdomyosarcoma
RT on air (1st cohort)	12 (2 died before TGD end)
RT on carbogen (2nd cohort)	10 (1 died before TGD end)
Control (3rd cohort)	6
Control (4th cohort)	4
TOTAL	**32**

SUP FIGURE 4

	Day 1	Day 2	Day 3
Rat 1	6.21	6.51	6.41
Rat 2	7.09	6.33	6.22
Rat 3	6.65	6.27	6.05
Rat 4	7.42	7.08	6.43

Paired t-test: Day 1 vs. Day 3: p = 0.13

Day 1 vs. Day 2: p = 0.27

SUP TABLE 1

Dose	Number of animal		Total
	1st series (Air/ Carbogen)	2nd series (Air/ Carbogen)	
10Gy	3/5		**3/5**
20Gy	4/4		**4/4**
30Gy	0/3		**0/3**
40Gy	4/5	9/8	**13/13**
50Gy	4/5		**4/5**
60Gy	5/4		**5/4**
Total	**20/26**	**9/8**	**29/34**

SUP TABLE 2

Combined endogenous MR biomarkers to predict basal tumor oxygenation and response to hyperoxic challenge.

Thanh-Trang Cao-Pham, Nicolas Joudiou, Matthias Van Hul, Caroline Bouzin, Patrice D. Cani, Bernard Gallez, and Bénédicte F. Jordan.

NMR in Biomedicine. 2017;30(12):e3836.

Received: 2 February 2017 | Revised: 18 August 2017 | Accepted: 31 August 2017
DOI: 10.1002/nbm.3836

WILEY NMR IN BIOMEDICINE

RESEARCH ARTICLE

Combined endogenous MR biomarkers to predict basal tumor oxygenation and response to hyperoxic challenge

Thanh-Trang Cao-Pham[1] | Nicolas Joudiou[1] | Matthias Van Hul[2] | Caroline Bouzin[3] | Patrice D. Cani[2] | Bernard Gallez[1] | Bénédicte F. Jordan[1]

[1] Université catholique de Louvain, Louvain Drug Research Institute, Biomedical Magnetic Resonance Research Group, Brussels, Belgium
[2] Université catholique de Louvain, Louvain Drug Research Institute, Metabolism and Nutrition Research Group, Brussels, Belgium
[3] Université catholique de Louvain, IREC Imaging Platform, Brussels, Belgium

Correspondence
B. F. Jordan, Biomedical Magnetic Resonance Group (REMA), Louvain Drug Research Institute, Université catholique de Louvain, Avenue Mounier 73 – B1.73.08, B-1200 Brussels, Belgium.
Email: benedicte.jordan@uclouvain.be

Funding information
Fournier-Majoie Foundation; Belgian National Fund for Scientific Research (FNRS)

Hypoxia is a common feature of solid tumors, which translates into increased angiogenesis, malignant phenotype cell selection, change in gene expression and greater resistance to radiotherapy and chemotherapy. Therefore, there is a need for markers of hypoxia to stratify patients, in order to personalize treatment to improve therapeutic outcome. However, no modality has yet been validated for the screening of hypoxia in routine clinical practice. Magnetic resonance imaging (MRI) R_1 and R_2^* relaxation parameters are sensitive to tissue oxygenation: R_1 is sensitive to dissolved oxygen and R_2^* is sensitive to intravascular deoxyhemoglobin content. Two rat tumor models with distinct levels of hypoxia, 9L–glioma and rhabdomyosarcoma, were imaged for R_1 and R_2^* under air and carbogen (95% O_2 and 5% CO_2) breathing conditions. It was observed that the basal tumor oxygenation level had an impact on the amplitude of response to carbogen in the vascular compartment (R_2^*), but not in the tissue compartment (R_1). In addition, the change in tissue oxygenation estimated by ΔR_1 correlated with the change in vascular oxygenation estimated by ΔR_2^*, which is consistent with an increase in oxygen supply generating an elevated tumor pO_2. At the intra-tumoral level, we identified four types of voxel to which a hypoxic feature was attributed (mild hypoxia, severe hypoxia, normoxia and vascular steal), depending on the carbogen-induced change in R_1 and R_2^* values for each voxel. The results showed that 9L–gliomas present more normoxic fractions, whereas rhabdomyosarcomas present more hypoxic fractions, which is in accordance with a previous study using ^{18}F–fluoroazomycin arabinoside (^{18}F–FAZA) and electron paramagnetic resonance (EPR) oximetry. The response of the combined endogenous MRI contrasts to carbogen challenge could be a useful tool to predict different tumor hypoxic fractions.

KEYWORDS
ΔR_1, ΔR_2^*, carbogen, MRI, tumor hypoxia

1 | INTRODUCTION

Hypoxia is a micro-environmental component of solid tumors and an important prognostic biomarker for tumor aggressiveness and patient outcome. This feature is related to the recurrence of tumors and the failure of cancer treatment. In a systematic review of over 10 000 patients, Overgaard[1] found that the modification of tumor hypoxia improves the efficiency of radiotherapy. Modalities are under evaluation in an effort to counteract the negative effects of hypoxia.[2] Regrettably, screening for the presence of hypoxia is not an entry criterion prior to hypoxia modification in trials.[2] To bridge the gap between the prevalence of tumor hypoxia and clinical routine practice, there is a need to identify

Abbreviations used: BOLD, blood oxygenation level-dependent; BSA, bovine serum albumin; BW, bandwidth; CB, carbogen; DAB, 3,3′-diaminobenzidine; DCE, dynamic contrast-enhanced; dHb, deoxyhemoglobin; EPR, electron paramagnetic resonance; FA, flip angle; ^{18}F–FAZA, ^{18}F–fluoroazomycin arabinoside; FOV, field of view; IR-FISP, inversion-recovery fast imaging with steady state precession; MOBILE, mapping of oxygen by imaging lipids relaxation enhancement; MRI, magnetic resonance imaging; PISTOL, proton imaging of siloxanes to map tissue oxygenation levels; RARE, rapid acquisition with relaxation enhancement; ROI, region of interest; RPMI, Roswell Park Memorial Institute; SEM, standard error of the mean; SSFP-FID, Steady State Free Precession Free Induction Decay; TBS, Tris- Buffered Saline; Tris/EDTA, tris(hydroxymethyl)aminomethane/ethylenediaminetetraacetic acid; α-SMA, α-smooth muscle actin

markers of hypoxia in order to stratify patients who might benefit from oxygen modulation and to tailor therapy to the characteristics of the tumor. Several techniques allow the quantification of tumor oxygenation,[3,4] e.g. ^{19}F–magnetic resonance imaging (^{19}F–MRI) of perfluorocarbon,[5] electron paramagnetic resonance (EPR) oximetry,[6] ^{1}H–MRI of hexamethyldisiloxane PISTOL (proton imaging of siloxanes to map tissue oxygenation levels),[7] polarographic needle electrodes[8] and fiberoptic probes.[9] Nevertheless, these methods are either invasive or require the injection of a reporter probe.

The oxygen-sensitive endogenous MRI contrasts, R_1 and R_2^*, are considered to be potential methods for the evaluation of tumor hypoxia. The effective spin–spin relaxation rate R_2^* is sensitive to the concentration of deoxyhemoglobin (dHb) per volume of tissue. A decrease in [dHb], e.g. an increase in blood saturation, results in a decrease in R_2^*. However, R_2^* is not only sensitive to the change in blood oxygenation through the change in [dHb], but is also sensitive to factors unrelated to the change in oxygenation, such as hematocrit, vascular volume, pH, flow and vessel density,[10] as well as the experimental setting, e.g. voxel size, shimming procedure, TE sampling and quantification method.[11]

The spin–lattice relaxation rate R_1 is sensitive to the oxygen molecules dissolved in plasma and tissue fluid. Nevertheless, the change in relaxivity constant as a function of O_2 depends on the dissolved media.[12] Thus, R_1 is biased by factors independent of the change in O_2 content, such as the water content of tissue or the blood flow.[12] In 2013, Jordan et al.[13] developed a noninvasive R_1-based MRI method to measure tumor oxygenation. The method with the acronym MOBILE (mapping of oxygen by imaging lipids relaxation enhancement) explores the signal of R_1 in lipids instead of the global R_1, as the solubility of oxygen in lipids is higher than that in water. It was shown in lipid-rich mammary tumors that lipid R_1 was more sensitive to the change in tumor oxygenation than the conventional global R_1.[14] Because this method is not applicable in tumors with a low lipid content, we have recently proposed a method in which the global R_1 signal is deconvoluted into fast and slow components attributed to lipid and water relaxation, respectively.[15]

As R_1 and R_2^* reflect different properties of tumor oxygenation, the combination of these two parameters provides complementary information which can aid in the interpretation of MRI data.[16] Previous studies using R_1 and R_2^* have been performed on animals,[17-21] as well as on humans,[16,22] to obtain insights into tissue oxygenation. However, these studies used mean values of R_1 and R_2^*, and did not take into account the tumor heterogeneity and the extent of hypoxia, which are crucial factors for the stratification of patients. In the work of Remmele et al.,[22] the scatter plots of ΔR_1 and ΔR_2^* were employed to investigate the response of different regions of interest to carbogen (CB) breathing. O'Connor et al.[23] demonstrated that the combined information on the oxy-R fraction (fraction lacking a positive ΔR_1 in response to oxygen challenge) and perfusion data, measured by dynamic contrast-enhanced (DCE)-MRI, was correlated with the hypoxic fraction detected by pimonidazole in two different vascularized tumor models, 786-0-R and SW620.

The breathing of hyperoxic gas is a simple method to improve tumor oxygenation. Yet, the response varies between individuals and within tumors. The purpose of this work was to study the role of the basal tissue and vascular tumor oxygenation on the amplitude of response to CB challenge (95% O_2 and 5% CO_2) at the inter-tumoral level, using the combined parameters R_2^* and three types of R_1 (global R_1 or R_{1G}, water R_1 or R_{1W}, lipid R_1 or R_{1L}). The analysis of the intra-tumoral level allowed the categorization of voxels into four types to which a hypoxic feature was attributed (mild hypoxia, severe hypoxia, normoxia, vascular steal). We aimed to compare R_{1G}, R_{1W} and R_{1L} in terms of their sensitivity and predictive power to evaluate the response of a tumor to CB breathing. Two rat tumor models, rhabdomyosarcoma and 9L–glioma, exhibiting distinct basal oxygenation status and different levels of response to CB breathing, were used. The rhabdomyosarcoma model has been described previously to be more hypoxic and less responsive to CB breathing than the 9L–glioma model.[24] Indeed, the mean pO_2 values recorded by EPR oximetry were 9 ± 1 mmHg and 5 ± 1 mmHg at baseline, and increased to 17 ± 2 mmHg and 9 ± 1 mmHg under CB breathing, for 9L–gliomas and rhabdomyosarcomas, respectively.[24] It should be noted that 10 mmHg is often suggested as the radiosensitivity threshold. The 9L–glioma model was therefore more responsive to CB by increasing the pO_2 value above this threshold.

2 | MATERIALS AND METHODS

The study was approved by the local ethics committee. The study was undertaken in accordance with the national and local regulations of the ethical committee (agreement number UCL/2014/MD/026).

2.1 | Tumor models

Two tumor models were included in the study: rhabdomyosarcoma (n = 29) and 9L–glioma (n = 25).

Fragments from a syngeneic rhabdomyosarcoma (1 mm^3) were grafted subcutaneously into the thigh of male adult WAG/Rij rats, according to a model developed by the Laboratory of Experimental Radiobiology, Katholieke Universiteit Leuven, Belgium.

9L–glioma cells were grown in Roswell Park Memorial Institute (RPMI) medium supplemented with 10% fetal calf serum (heat inactivated), 1% of a mixture of antibiotics (penicillin, 100 UI/mL; streptomycin, 0.1 mg/mL), 1% nonessential amino acids and 1% sodium pyruvate. Cells were maintained in a balanced wet atmosphere (37°C and 5% CO_2). To establish 9L–glioma tumors *in vivo*, male adult Fisher F344 rats were inoculated subcutaneously in the thigh with 5 × 10^6 cells.

Tumor implantations were performed under general anesthesia with intraperitoneal injection of ketamine and xylazine (80 and 10 mg/kg, respectively) in rats weighing between 200 and 250 g. The animals were introduced into the study when the tumors reached 15–20 mm.

2.2 | Experimental design

Two cohorts were involved. The MR measurements were performed on the first cohort including 22 rhabdomyosarcomas and 18 9L–gliomas.

The second cohort included seven rhabdomyosarcomas and seven 9L–gliomas. Animals of the second cohort were euthanized using an overdose of pentobarbital when the tumors reached 15–20 mm. Tumors were harvested and cut in half. One half was dedicated to the measurement of the lipid content. Immunohistochemistry was performed on the other half of the tumor to quantify the mature blood vessels.

2.3 | MR measurements

Animals of the first cohort were subjected to R_1 and R_2^* measurements under baseline (air breathing) and hyperoxic (after 30 min of CB inhalation) conditions (Supporting Information Figure S1). Rats were anesthetized with isoflurane 1.5% during MRI experiments. Gas delivery (medical air or CB mixed with isoflurane) was continuous at 2 L/min through a nosepiece.

MRI was performed on an 11.7-T, 16-cm inner-diameter bore system (Bruker, Biospec, Ettlingen, Karlsruhe, Germany) with a 7-cm birdcage coil for signal transmission and a surface coil for signal reception. A warm water blanket was used to maintain the animal's temperature at 37°C, and the temperature was monitored with an MR-compatible rectal probe.

A multi-slice rapid acquisition with relaxation enhancement (RARE) sequence was first used to determine the most representative tumor slice for further measurement, with the following parameters: TE/TR/RARE-factor/field of view (FOV)/matrix size/slice thickness = 10.66 ms/2500 ms/6/35 × 35 mm^2/256 × 256/1 mm. The segmented inversion-recovery fast imaging with steady state precession (IR-FISP) sequence (SSFP-FID or Steady State Free Precession Free Induction Decay mode) was used for R_1 acquisition with the following parameters: TR/TE/flip angle (FA)/bandwidth (BW)/FOV/matrix size/slice thickness = 4 ms/1.35 ms/10°/100 kHz/55 × 30 mm^2/100 × 85/1 mm, four segments, 100 TI from 13 ms to 8329 ms every 84 ms, and a total acquisition time of 20 min. The resonance frequency for excitation of the R_1 sequence was on resonance for water. Multi-gradient echo R_2^* images were acquired at TR/FA/slice thickness = 3000 ms/15°/1 mm, with a FOV of 35 × 35 mm^2 on a 256 × 256 matrix, with 12 echoes from 3.5 ms to 58.5 ms every 5 ms. The total acquisition time was 9 min and 36 s.

2.4 | Dosage of total lipids

The total lipid content of the tumor was measured by gravimetry following the Folch extraction method with slight modifications. We extracted lipids from about 100 mg of tumor tissue. The sample (M) was homogenized with 1 mL of Folch solution (methanol–chloroform, 1: 2) by a TissueLyser (Qiagen, Hilden, Germany) for 8 min at 30 Hz. The homogenate was centrifuged at 1006g for 5 min to separate the solid and liquid phases. The liquid (lipid) phase was collected in the first centrifuge tube. The pellet was then extracted twice with 1 mL of Folch solution each time. The homogenates were collected in the second centrifuge tube and mixed at room temperature for 20 min. A solution of 0.9% NaCl was added to the two centrifuge tubes (0.2 volume of the lipid phase). The mixtures were then vortexed twice for 1 min each time and centrifuged at 931g for 10 min. The lower chloroform phases in the two tubes were transferred into a preweighed vial (W_{pre}). The vial was dried under a continuous nitrogen flow until a constant mass was achieved (W_{post}). The percentage dry mass of lipids (% lipids) was calculated as:

$$\%\ \text{lipids} = \frac{W_{post} - W_{pre}}{M} \times 100$$

2.5 | Histological analysis for pericyte coverage

Tumors were formalin-fixed and paraffin-embedded. α-Smooth muscle actin (α-SMA) staining was performed on 5-µm sections to detect mature blood vessels covered by pericytes. After manual deparaffinization, endogenous peroxidases were inhibited by a 20-min treatment with 3% H_2O_2 in methanol. Sections were then subjected to antigen retrieval in tris(hydroxymethyl)aminomethane/ethylenediaminetetraacetic acid (Tris/EDTA) buffer, pH 9, at 98°C for 45 min, and then at room temperature for 15 min with 540 µL of Triton 20% added. Aspecific antigen-binding sites were blocked with a Tris-Buffered Saline (TBS) solution containing 5% bovine serum albumin (BSA) and 0.05% Triton. Slices were stained with mouse anti-human α-SMA primary antibodies (Dako M0851, Agilent Technologies Belgium, Diegem, Belgium) overnight at 4°C at a 1: 500 dilution, followed by incubation with envision anti-mouse secondary antibodies (Dako K4001) for 30 min at room temperature. This reaction was visualized using 3,3′-diaminobenzidine (DAB) (Dako K3468). After counterstaining with hematoxylin (Dako S3301), slices were dehydrated and coverslipped.

Slides were finally digitalized at 20× magnification with an SCN400 slide scanner (Leica, Wetzlar, Germany). Images were analyzed using Tissue IA software (Leica Biosystems, Dublin, Ireland). Color deconvolution was applied to each pixel using hematoxylin and DAB matrices of the software. On the DAB matrices, a threshold was adjusted for DAB detection according to intensity (gray values from 0 to 255). The results were expressed as α-SMA-positive area percentages and calculated as (α-SMA-stained area/total tissue area) × 100.

2.6 | Data analysis and statistics

Data analysis was performed using an in-house program developed under ImageJ and MATLAB (MATLAB R2013b, The Math Works, Massachusetts, United States). R_1 and R_2^* maps were calculated with an MRI analysis calculator plug-in in ImageJ software. This MRI analysis method is adapted from the original plugin created by Karl Schmidt (http://rsb.info.nih.gov/ij/) using a curve-fitting method based on the Simplex technique. R_{1L} and R_{1W} were extracted from the R_{1G} map by a biexponential deconvolution method. Hence, the term R_{1G} refers to R_1 acquired by MRI and is the sum of the contributions of R_{1W} and R_{1L}. Meanwhile, R_{1L} and R_{1W} indicate the generated data obtained by the deconvolution of R_{1G}. Regions of interest (ROIs) were drawn manually around the tumor on the selected anatomical slice and were transferred to R_{1L}, R_{1W}, R_{1G} and R_2^* maps of the same slice. The subtraction of the two maps acquired under air and CB breathing conditions was performed voxel by voxel, resulting in maps of ΔR_{1L}, ΔR_{1W}, ΔR_{1G} and ΔR_2^*. Co-registration was performed using a homemade script on Matlab. During acquisition, a similar orientation was used for the R_2^* and R_1 maps so that only translation transformations were needed for co-registration.

For the multi-parametric analysis, the spatial resolution of the R_{1L}, R_{1W} and R_{1G} maps was adapted to the size of the voxel of the R_2^* maps. After obtaining the delta maps, we superimposed the two maps of ΔR_{1l} (or ΔR_{1W} or ΔR_{1G}) and ΔR_2^* voxel by voxel by selecting a common point to navigate. We established for each tumor a scatter plot of CB-induced ΔR_2^*, ΔR_1. Each voxel was presented by a point in the scatter plot (ΔR_2^*, ΔR_1). The point was then encoded with a color code, based on the position over the four quadrants of the scatter plot. Blue was dedicated to voxels with $\Delta R_1 > 0$ and $\Delta R_2^* \geq 0$, cyan to voxels with $\Delta R_2^* > 0$ and $\Delta R_1 < 0$, orange to voxels with $\Delta R_1 \leq 0$ and $\Delta R_2^* < 0$, and red to voxels with $\Delta R_1 > 0$ and $\Delta R_2^* < 0$. The number of voxels was calculated and the percentage was generated for each color in a tumor.

It should be noted that there was no significant difference in the number of voxels analyzed between the two models. The numbers of voxels analyzed per tumor were 5435 ± 403 and 5927 ± 322 for 9L–gliomas and rhabdomyosarcomas, respectively ($p = 0.34$, Student's t-test).

For Figures 1-3, we fitted the mean value of the ROI. For Figure 4, tumors were analyzed voxel-wise. The ΔR_1 map was superimposed on the ΔR_2^* map and the percentages of the four types of voxel were obtained for each tumor. Figure 4 features the mean value of each type of voxel of the tumors in the same models.

Statistical analyses were performed with the GraphPad (Prism) program (GraphPad Software, Inc., California, United States). Results were expressed as mean ± standard error of the mean (SEM) (Table 1). To evaluate the differences between groups of data, we used the unpaired t-test (Table 1). The linear associations between R_2^* and ΔR_2^* (Figure 1), between ΔR_2^* and ΔR_{1L}, ΔR_2^* and ΔR_{1W}, and ΔR_2^* and ΔR_{1G} (Figure 2), and

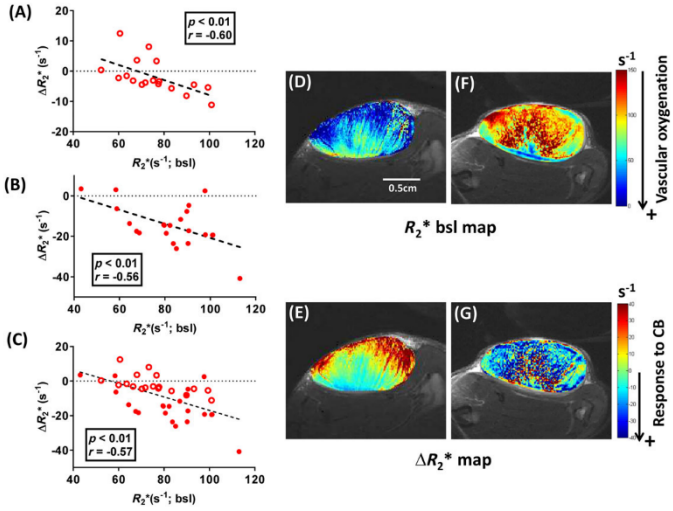

FIGURE 1 (A–C) Correlation between the median values of baseline (bsl) R_2^* and carbogen (CB)-induced ΔR_2^* for 9L-gliomas (A), rhabdomyosarcomas (B) and the pooled data (C). Each point represents one individual tumor. (D) Representative parametric maps showing the R_2^* baseline of a rhabdomyosarcoma. (E) Representative parametric maps showing ΔR_2^* of a rhabdomyosarcoma. (F) Representative parametric maps showing the R_2^* baseline of a 9L–glioma. (G) Representative parametric maps showing ΔR_2^* of a 9L–glioma. ΔR_2^* was obtained by subtracting R_2^* baseline from R_2^* CB. Areas in which $\Delta R_2^* < 0$ are expected to show a decrease in deoxyhemoglobin content [dHb]

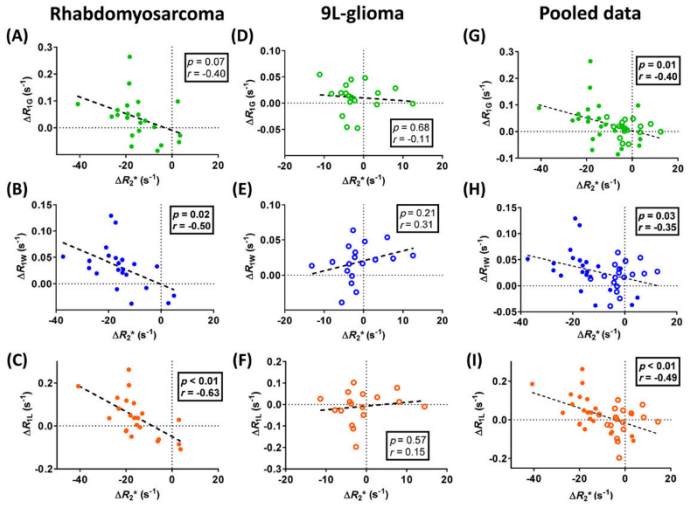

FIGURE 2 Correlations between the median values of ΔR_{1G}, ΔR_{1W}, ΔR_{1L} and ΔR_2^* for rhabdomyosarcomas (A–C), 9L-gliomas (D–F) and the pooled data (G–I). Graphs show correlations between ΔR_2^* and ΔR_{1G} (A, D, G), ΔR_{1W} (B, E, H) and ΔR_{1L} (C, F, I) in response to carbogen (CB) challenge. Each point represents one individual tumor

between R_{1G} and ΔR_{1G}, R_{1L} and ΔR_{1L}, and R_{1W} and ΔR_{1W} (Figure 3) were tested by correlation analysis. For all tests, $p < 0.05$ was considered to be significant.

3 | RESULTS

3.1 | In the vascular compartment, the basal tumor oxygenation influences the amplitude of response to a hyperoxic challenge

As R_2^* is sensitive to the intravascular [dHb], we decided to examine whether the amplitude of change induced by the hyperoxic challenge in the tumor vascular oxygenation was influenced by its basal status.

An increase in vascular oxygenation converts dHb to HbO_2 and thus results in a decrease in R_2^*. It should be noted that the level of hemoglobin saturation at baseline, estimated by the basal R_2^*, can also influence the tumor response to the hyperoxic gas challenge.[21] We observed strong correlations between ΔR_2^* and basal R_2^* (Figure 1A: 9L-glioma, $p < 0.01$ and $r = -0.60$; Figure 1B: rhabdomyosarcoma, $p < 0.01$ and $r = -0.56$; Figure 1C: pooled data, $p < 0.01$ and $r = -0.57$), meaning that tumors that had a better basal vascular oxygenation status (slow basal median R_2^*) were less responsive to CB breathing than tumors that had a lower basal vascular oxygenation status (fast basal median R_2^*). No significant differences were observed between basal R_2^* of 9L-glioma (75.56 ± 3.20 s^{-1}) and basal R_2^* of rhabdomyosarcoma (82.29 ± 3.55 s^{-1}) ($p = 0.18$).

This observation is also true at the intra-tumoral level. Figure 1D–G shows representative maps of R_2^* and CB-induced ΔR_2^* of the two tumor models. In the R_2^* basal map (Figure 1D, F), the tumor periphery (colder color) has a better vascular oxygenation than the tumor core (hotter color). Meanwhile, the ΔR_2^* maps (Figure 1E, G) show that the tumor core, which has a lower basal vascular oxygenation, responds better to CB (colder color), and that the tumor periphery, which has a better basal vascular oxygenation, responds less well to CB (hotter color). Significant correlations between R_2^* and ΔR_2^* of voxels within the two presented tumors were also observed (Supporting Information Figure S2A: $p < 0.01$, $r = -0.62$ for the presented rhabdomyosarcoma; Figure S2B: $p < 0.01$, $r = -0.65$ for the presented 9L-glioma), meaning that voxels that had a better basal vascular oxygenation status (slow basal R_2^*) were less responsive to CB breathing than were voxels that had a lower basal vascular oxygenation status (fast basal R_2^*). It should be noted that a higher R_2^* could be associated with the accumulation of the paramagnetic debris of necrosis. This possibility was excluded as no necrosis was detected by histology at this stage of development (15–20 mm).

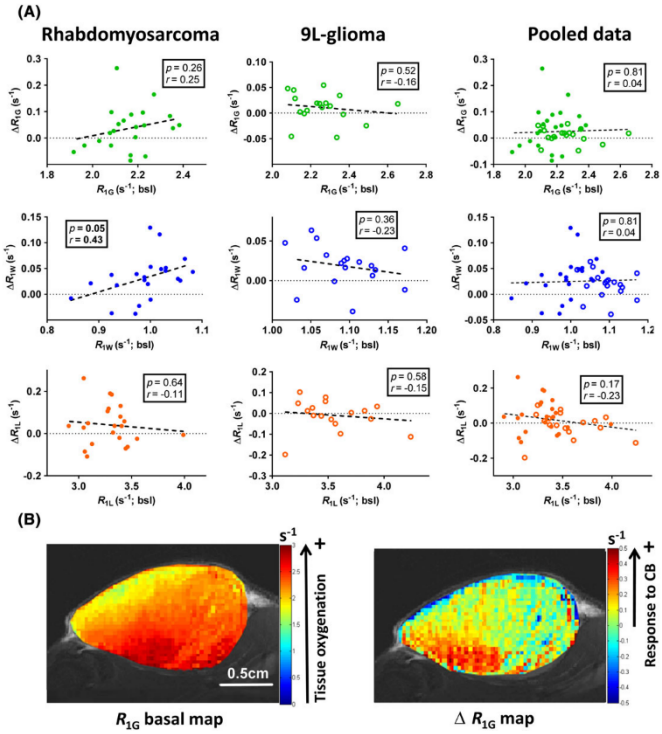

FIGURE 3 (A) Correlations between the median values of ΔR_{1G} and basal R_{1G} (first row), ΔR_{1W} and basal R_{1W} (second row), and ΔR_{1L} and basal R_{1L} (third row) for rhabdomyosarcoma (left column), 9L–glioma (middle column) and the pooled data (right column). Each point represents one individual tumor. (B) Representative parametric maps showing R_{1G} baseline (bsl) (left) and carbogen (CB)-induced ΔR_{1G} (right) of a rhabdomyosarcoma

3.2 | A change in vascular oxygenation results in a change in tissue oxygenation in a model that is responsive to a hyperoxic challenge

We looked for the impact of the change in tumor vascular oxygenation on the tissue oxygenation. For this purpose, we tested correlations between ΔR_2^* and ΔR_{1L}, ΔR_{1W} and ΔR_{1G} of the same tumors.

A more negative ΔR_2^* corresponds to a better reoxygenation of the vascular compartment in response to CB, whereas a more positive ΔR_1 corresponds to a better reoxygenation of the tissue compartment.

In rhabdomyosarcomas, correlations of ΔR_{1W} and ΔR_2^*, and ΔR_{1L} and ΔR_2^*, were significant (Figure 2B: ΔR_{1W} and ΔR_2^*, $p = 0.02$, $r = -0.50$; Figure 2C: ΔR_{1L} and ΔR_2^*, $p < 0.01$, $r = -0.63$). However, the correlation of ΔR_{1G} and ΔR_2^* was not significant, although a trend was present (Figure 2A, $p = 0.07$, $r = -0.40$). In this tumor model, the vascular reoxygenation in response to CB challenge led to a significant change in tissue oxygenation.[24]

However, similar analysis in the 9L–glioma model, which shows a higher basal oxygenation,[24] did not give any significant correlation between vascular and tissue changes in oxygenation (Figure 2D–F).

Interestingly, correlations of the pooled data of the two tumor models were stronger than the correlations of each model separately (Figure 2G: ΔR_{1G} and ΔR_2^*, $p = 0.01$, $r = -0.40$; Figure 2H: ΔR_{1W} and ΔR_2^*, $p = 0.03$, $r = -0.35$; Figure 2I: ΔR_{1L} and ΔR_2^*, $p < 0.01$, $r = -0.49$).

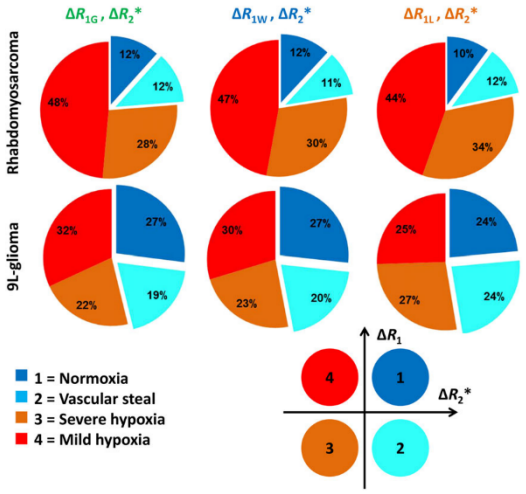

FIGURE 4 Mean fractional carbogen-induced ΔR_1, ΔR_2^* response categories from rhabdomyosarcomas (top row) and 9L–gliomas (bottom row) showing the percentage of total region of interest (ROI) voxels. Each tumor is fractionated based on the response of ΔR_1 and ΔR_2^* to carbogen challenge of each voxel (see graph at the bottom right). From left to right: ΔR_{1G} and ΔR_2^*, ΔR_{1W} and ΔR_2^*, and ΔR_{1L} and ΔR_2^* analyses

TABLE 1 Heterogeneity of response of R_1 and R_2^* to carbogen challenge. Each voxel was encoded by a different color depending on its carbogen-induced ΔR_1 and ΔR_2^*. Blue indicates voxels with $\Delta R_1 > 0$ and $\Delta R_2^* \geq 0$, cyan voxels with $\Delta R_2^* > 0$ and $\Delta R_1 < 0$, orange voxels with $\Delta R_1 \leq 0$ and $\Delta R_2^* < 0$ and red voxels with $\Delta R_1 > 0$ and $\Delta R_2^* < 0$

Response category	% total ROI voxels (ΔR_{1G} and ΔR_2^*)			% total ROI voxels (ΔR_{1W} and ΔR_2^*)			% total ROI voxels (ΔR_{1L} and ΔR_2^*)		
	9L–glioma	Rhabdomyosarcoma	p	9L–glioma	Rhabdomyosarcoma	p	9L–glioma	Rhabdomyosarcoma	p
Blue	27.0 ± 2.8	11.7 ± 2.0	<0.0001	26.7 ± 2.0	11.9 ± 1.4	<0.0001	23.6 ± 2.0	10.1 ± 1.4	<0.0001
Cyan	19.2 ± 2.3	12.1 ± 3.0	*0.0713*	20.3 ± 1.1	10.6 ± 2.3	0.0010	23.8 ± 1.4	11.6 ± 2.6	0.0005
Orange	21.9 ± 2.8	27.7 ± 3.3	*0.1997*	23.3 ± 1.8	30.4 ± 1.7	0.0066	27.2 ± 2.0	33.7 ± 1.9	0.0238
Red	31.9 ± 3.1	48.6 ± 5.2	0.0120	29.7 ± 1.7	47.1 ± 3.4	0.0001	25.5 ± 1.7	44.6 ± 3.6	<0.0001
Orange–red	53.8 ± 2.6	76.2 ± 3.9	<0.0001	53.0 ± 2.6	77.5 ± 3.4	<0.0001	49.8 ± 4.0	78.3 ± 3.8	<0.0001

Values are mean ± standard error of the mean (SEM); unpaired *t*-test. The significance of italic 'p' values marked the $p > 0.05$.

3.3 | In the tissue compartment, the basal tumor oxygenation does not influence the response to a hyperoxic challenge

As rhabdomyosarcoma and 9L–glioma exhibit different basal oxygenation status (rhabdomyosarcoma being more hypoxic than 9L–glioma[24]), we sought a possible impact of the basal oxygenation status on the amplitude of response in tumor tissues to the hyperoxic challenge. Faster median R_1 values correspond to a better tissue oxygenation, and a positive ΔR_1 corresponds to a better reoxygenation of the tissue compartment in response to CB. We tested correlations between R_{1G}, R_{1W} and R_{1L} and their corresponding delta values (R_{1G} and ΔR_{1G}, R_{1W} and ΔR_{1W}, R_{1L} and ΔR_{1L}) in both tumor models.

Except for a weak correlation between R_{1W} and ΔR_{1W} in rhabdomyosarcoma ($p = 0.05$, $r = 0.43$; Figure 3A), the remaining correlations of rhabdomyosarcoma and 9L–glioma were insignificant (Figure 3A). It should be noted that the basal R_1 of 9L–gliomas (2.26 ± 0.03 s^{-1}) is significantly higher than the basal R_1 of rhabdomyosarcomas (2.16 ± 0.03 s^{-1}) ($p = 0.02$). Although correlations of median values of R_{1G} and ΔR_{1G}, R_{1W} and ΔR_{1W}, and R_{1L} and ΔR_{1L} show that a relation between the basal tissue oxygenation and its response to CB does not exist, the representative maps of basal R_{1G} and ΔR_{1G} of a rhabdomyosarcoma (Figure 3B) suggest the contrary. Indeed, the region which is initially better oxygenated (hotter color, R_{1G} basal map) appears to be more responsive to CB challenge (hotter color, ΔR_{1G} map), and vice versa. The correlation between R_{1G} and ΔR_{1G} of voxels within this tumor was significant ($p < 0.01$, $r = 0.16$, Supporting Information Figure S3). This observation underlines the importance of the tumor heterogeneity and suggests that further analysis at the voxel scale should be considered. Therefore, a multi-parametric intra-tumoral analysis was performed.

3.4 | Multi-parametric analysis of tumor heterogeneity of response to a hyperoxic challenge

The multi-parametric analysis was performed by superimposing the two maps of ΔR_{1G} and $\Delta R_2{}^*$, ΔR_{1W} and $\Delta R_2{}^*$, and ΔR_{1L} and $\Delta R_2{}^*$ voxel by voxel. Each voxel was encoded by different colors depending on its CB-induced ΔR_1, $\Delta R_2{}^*$ as shown in Figure 4.

In order to quantify the distribution of the four fractions, the percentage of tumor voxels of each color code was calculated (Figure 4). In the analysis of $\Delta R_2{}^*$ and ΔR_{1G}, $\Delta R_2{}^*$ and ΔR_{1W}, and $\Delta R_2{}^*$ and ΔR_{1L} in the two models, the percentage of 'blue voxels' was significantly higher in 9L–gliomas, whereas the percentage of 'red voxels' was significantly higher in rhabdomyosarcomas (Table 1). In the analysis of $\Delta R_2{}^*$ and ΔR_{1G}, we observed a higher percentage of 'cyan voxels' in 9L–glioma than in rhabdomyosarcoma, but the difference was insignificant ($p = 0.07$). Meanwhile, there was no significant difference between the percentage of 'orange voxels' ($p = 0.20$) between the two models. The same analysis using ΔR_{1W} and ΔR_{1L} with $\Delta R_2{}^*$ showed a significantly higher proportion of 'cyan voxels' in 9L–glioma and a significantly higher proportion of 'orange voxels' in rhabdomyosarcoma. These observations indicate that the multi-parametric analysis of tumor response to hyperoxic breathing challlenge could be useful to characterize the tumor oxygenation heterogeneity.

3.5 | Total lipid content

No significant difference was found between the lipid contents in the two tumor models: 2.1 ± 0.1% and 2.3 ± 0.2% for rhabdomyosarcomas and 9L–gliomas, respectively (mean ± SEM).

3.6 | α-SMA staining

The α-SMA-positive area percentages were 5.7 ± 0.5% and 1.9 ± 0.2% for rhabdomyosarcomas and 9L–gliomas, respectively ($p < 0.01$, unpaired *t*-test).

4 | DISCUSSION

In this study, CB was used to alter tumor oxygenation. This gas increases the oxygen supply to the tumor by saturation of the arterial blood. Other possible impacts of CB are as follows: (1) an increase in the rate of breathing; (2) a decrease in the blood pH, resulting in an increase in O_2 delivery by right shifting of the dissociation curve of hemoglobin and O_2; (3) counteraction of the vasoconstriction effect of O_2 by the CO_2 component.[25] In the two models studied, CB induced a greater effect in tumors that were initially less oxygenated in the vascular compartment (faster basal $R_2{}^*$ values; Figure 1). Indeed, in these tumors, dHb was more abundant at baseline status and these free heme sites of dHb preferentially bind to oxygen under the hyperoxic breathing CB challenge. In contrast, a high proportion of hemoglobin was already saturated at baseline status in tumors with a well-oxygenated vascular compartment. Thus, the hyperoxic challenge barely changed the amount of dHb in these tumors.[21] This observation is in agreement with a previous study which showed that $R_2{}^*$ was more sensitive in a situation of low oxygenation.[26] This observation held true at both the inter- and intra-tumoral levels (Figure 1), as well as between models. It should be noted that CB induced a significantly greater reduction in $R_2{}^*$ in rhabdomyosarcomas than in 9L–gliomas ($p < 0.01$, unpaired Student's *t*-test, Supporting Information Figure S4). Meanwhile, 9L–gliomas have been described to present a better basal oxygenation status than rhabdomyosarcomas.[24] In conclusion, in this context, CB could modulate the vascular oxygenation in the two tumor models studied, and the magnitude of modification was dependent on the basal tumor oxygenation status.

It should be noted that, in the case of 13762NF breast carcinoma,[27] the change in $R_2{}^*$ induced by oxygen challenge was not found to be correlated with the baseline $R_2{}^*$ value in a voxel-by-voxel analysis. This behavior may contradict the results observed in the present study (Figure 1). However, different levels of tumor oxygenation between models could contribute to this observation. Indeed, the 13762NF carcinomas studied in the work of Zhao et al.[27] were better oxygenated than the 9L–gliomas and rhabdomyosarcomas in the current work. Under oxygen breathing, pO_2 of 13762NF increased from 18 to 68 Torr. However, pO_2 increased from 9 to 17 mmHg and 5 to 9 mmHg under CB breathing in 9L–gliomas and rhabdomyosarcomas, respectively.[24] As stated in the work of Baudelet and Gallez,[26] the *in vivo* blood oxygenation level-dependent (BOLD) signal change was more pronounced when passing from 5 to 15 mmHg than the higher range of pO_2, and a plateau was reached at a pO_2 value above 30 mmHg. Thus, the lack of correlation between $R_2{}^*$ and oxygen-induced $\Delta R_2{}^*$ in 13762NF carcinomas could be a result of the lack of $\Delta R_2{}^*$ change because of the abundance of well-oxygenated voxels. Hence, only a slight change in $\Delta R_2{}^*$ occurred when these voxels reached a superior level of oxygenation.

It was expected that tumors which had benefited from vascular reoxygenation induced by CB would also show an increase in oxygenation in the tissue compartment. This behavior was seen in the more hypoxic rhabdomyosarcoma tumor model ($p < 0.05$), but a lack of correlation was found in the 9L–glioma model (Figure 2). Remarkably, the correlations of the pooled data (Figure 2G–I) were stronger than the correlations of each model separately (Figure 2A–C for rhabdomyosarcomas and Figure 2D–F for 9L–gliomas). This observation was consistent with an increase in vascular oxygenation generating an elevated tumor pO_2 and could be explained as follows. First, the mechanism of CB for the modification of tumor oxygenation is to increase the O_2 supply. Second, both 9L–glioma and rhabdomyosarcoma models have been demonstrated previously to be responsive to CB breathing.[24]

Interestingly, the correlation of the R_1 and R_2^* responses to CB challenge of Dunning prostate R3327-HI and R3327-AT1 tumors[20] reveals a remarkably similar behavior to Figure 2. Indeed, in both studies, one model showed a significant correlation between ΔR_1 and ΔR_2^* (HI and rhabdomyosarcomas), whereas the other showed no relation (AT1 and 9L–gliomas). It should be noted that HI tumors are known to be better vascularized and less hypoxic than AT1 tumors. However, rhabdomyosarcomas have been reported to be more hypoxic than 9L–gliomas. Although this seems to be controversial as the correlation was observed in a less hypoxic model (HI compared with AT1) and a more hypoxic model (rhabdomyosarcoma compared with 9L–glioma), we all noted a poor response of R_2^* in AT1 and 9L–gliomas. In brief, whether the small ΔR_2^* originates from the poor vascularization or from saturated dHb, it could be the reason for the lack of correlation between ΔR_1 and ΔR_2^*.

Another scenario was seen in the work of Burrell et al.,[21] where R_1 and R_2^* were measured pre- and post-CB breathing in GH3 and PC3 tumors. The scatter plot showing the relationship between ΔR_1 and ΔR_2^* suggested that a smaller ΔR_2^* was associated with a larger ΔR_1, and vice versa, but no significant relationship was found. GH3 has been reported to be more hypoxic than PC3. The authors theorized that there was a high proportion of dHb in the blood of the hypoxic GH3 model. Hence, the elevated O_2 supplied by CB leads to a decrease in the dHb content of the tumor, and thus a decrease in R_2^*. Meanwhile, in the less hypoxic model PC3, where dHb was already saturated, a boost in O_2 supply did not change the dHb content, but resulted in an increase in dissolved O_2, and thus increased R_1. The hypothesis was supported by a faster R_2^* baseline and a slower R_1 baseline of GH3 than of PC3, which suggested a richer dHb content in GH3 and a higher pO_2 in PC3. Moreover, the CB-induced ΔR_2^* in GH3 was significantly larger than that in PC3, which is consistent with this hypothesis. Although no significant difference between ΔR_1 of GH3 and PC3 was reported, the authors observed a larger change in PC3. In brief, the lack of correlation of ΔR_1 and ΔR_2^* could be a result of the lack of ΔR_1 change in GH3 and the lack of ΔR_2^* change in PC3.

With regard to the translational aspect, Remmele et al.[22] used combined R_1 and R_2^* parameters to study human brain tumors. They established a voxel-wise scatter plot (CB-induced ΔR_1 and ΔR_2^*) of different areas in the brain. The shape and distribution of the cluster provided information on the change in dHb and O_2 content, and thus served as a tool to classify tissue regions.

The magnitude of the response of ΔR_1 to CB could not be correlated with its basal status in the tumor models in this study (Figure 3A, except for a weak correlation of ΔR_{1W}–R_{1W} in rhabdomyosarcoma). The representative maps of R_{1G} and ΔR_{1G} of a rhabdomyosarcoma, however, suggest that there may be a relationship between basal R_1 and its response to CB at the intra-tumoral level. Therefore, an intra-tumoral analysis was performed which revealed four different types of voxel behavior, based on the response to CB in terms of ΔR_1 and ΔR_2^*.

In the so-called 'red voxels', CB induced an increase in R_1 and a decrease in R_2^*, which means an increase in dissolved oxygen and a decrease in [dHb]. Mild hypoxia is a reasonable hypothesis for this type of voxel. Indeed, to obtain this type of response, hemoglobin should not be completely saturated at baseline status. As the hyperoxic challenge is induced, increasing oxygen would bind to the heme sites of the free dHb molecules,

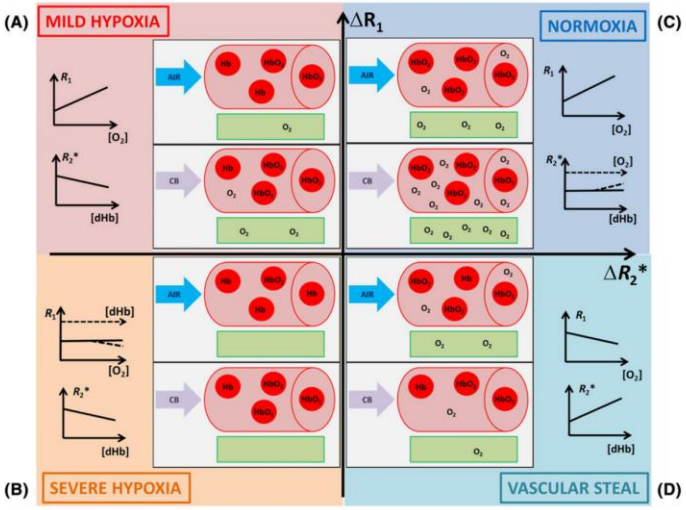

FIGURE 5 Hypothesis corresponding to red (A), orange (B), blue (C) and cyan (D) voxels. The arrows indicate the breathing conditions applied [blue arrow, air; purple arrow, carbogen (CB)]. The red cylinder is the vessel and the green box is the tumor tissue. The red blood cells are represented by red spheres. dHb, deoxyhemoglobin; Hb, hemoglobin

thereby decreasing [dHb], and thus decreasing R_2*. The remaining oxygen re-oxygenates the tissue, which increases the content of dissolved oxygen, thus increasing R_1 (Figure 5A).

In a more severely hypoxic tissue, represented by 'orange voxels' ($\Delta R_1 \leq 0$ and $\Delta R_2^* < 0$, Figure 5B), the majority of hemoglobin should be unsaturated at baseline. The extra oxygen supply brought by the CB challenge is just enough to bind to dHb, but hardly able to increase the amount of dissolved oxygen. Thus, R_2* decreases as the result of a decrease in [dHb]. Interestingly, R_1 does not exclusively depend on the concentration of dissolved oxygen, but also on the paramagnetic [dHb].[28] At a low hemoglobin saturation level, an increase in O_2 supply decreases R_1 as a result of the decrease in [dHb]. The value of R_1 is minimal when all the heme sites are bound to oxygen and dissolved oxygen is minimal.[28] Severe hypoxia could be a possible explanation for the 'orange voxels' in which $\Delta R_1 > 0$ is absent. This theory is in agreement with the work of O'Connor et al.[23]

In the opposite case of the so-called 'blue voxels', where $R_1 > 0$ and $R_2^* \geq 0$, we attribute these voxels to normoxic tissue (Figure 5C). In this tissue type, most of the hemoglobin molecules are already saturated, which hinders further oxygen binding when hyperoxygenation is induced. Thus, the CB challenge increases only the concentration of dissolved oxygen and the dHb/HbO_2 ratio remains almost constant. Consequently, $\Delta R_1 > 0$ is observed. As R_2^* is sensitive to [dHb], it depends on the blood oxygen saturation, hematocrit and the blood volume.[10]

In this context, using CB, a change in hematocrit was not expected. There are therefore two possible schemes for the increase in R_2^*.

1. $\Delta R_2^* > 0$ could be caused by the change in dissolved oxygen in the blood compartment. There are two mechanisms explaining the effect of oxygen on R_2^*.[29] First, the increase in paramagnetic oxygen influences the magnetic susceptibility difference between blood and tissue. Second, $\Delta R_2^* > 0$ is indirectly linked to the oxygen–hemoglobin dissociation curve. In tissues that are normoxic at baseline, most of the oxygen molecules are bound to hemoglobin. During capillary transit, oxygen is extracted from the heme sites. Thus, there is a dramatic decrease in oxygen–hemoglobin. Under a CB challenge, the concentration of bound oxygen remains almost unchanged compared with baseline with a significant increase in dissolved oxygen. The capillary transit extracts preferably the unbound oxygen and leaves the oxygen bound to hemoglobin nearly untouched. Hence, $\Delta R_2^* > 0$ is the result of the increase in [dHb] at baseline.
2. The increase in R_2^* could also be linked to the increase in regional blood volume. The tumor vasculature comprises both mature and unstable, immature blood vessels. Only the mature blood vessels with the pericytes integrated in the wall are believed to be 'responsive' to CB breathing. In other words, the mature blood vessels could be dilated under the effect of the CO_2 component of CB, thereby inducing an increase in blood volume in the neighborhood and a steal effect in other parts of the tumor. The increase in blood volume leads to an increase in [dHb] in an image voxel. It should be noted that the increase in blood volume and the increase in blood oxygenation have inverse effects on R_2^*.[10] A similar response, where hyperoxic challenge increases R_2^*, has been observed in normal tissue.[16]

Interestingly, the surface of pericyte coverage detected by immunohistochemistry was significantly higher in rhabdomyosarcomas than in 9L–gliomas. In other words, the blood volume effect of R_2^* might be more remarkable in rhabdomyosarcomas than in 9L–gliomas (scheme 2). However, the proportion of blue voxels in rhabdomyosarcomas was significantly smaller than that in 9L–gliomas. This observation supports the first scheme (scheme 1) proposing that the increase in R_2^* is predominantly a result of the change in dissolved oxygen in the blood compartment.

The last voxel behavior in response to CB is represented by 'cyan voxels' ($\Delta R_1 < 0$ and $\Delta R_2^* > 0$, Figure 5D). This type of response could be a result of the vascular steal effect. Indeed, the CO_2 component of CB is believed to have a vasodilation effect on mature blood vessels.[30] Meanwhile, the tumor vasculature is heterogeneous, and is composed of mature and immature vessels (which do not respond to CO_2).[30] Hence, under CB challenge, the dilated mature vessels redistribute the blood away from sites of immature vessels. This event leads to further blood desaturation (i.e. increased dHb/HbO_2 ratio) and a decreased oxygen concentration. Thus, a decrease in R_1 and an increase in R_2^* are observed. Previous studies on the steal effect of the whole tumor induced by hydralazine have provided a similar trend of R_1 and R_2^* responses.[23,31]

Briefly, based on the hypothesis of four types of voxel, 9L–gliomas present more normoxic fractions than rhabdomyosarcomas (Table 1, blue voxels). Furthermore, about three-quarters of rhabdomyosarcomas *versus* one-half of 9L–gliomas were found to be hypoxic (both severe hypoxia and mild hypoxia; Table 1, orange and red voxels). This observation is in accordance with that observed in the work of Tran et al.[24] using EPR oximetry and ^{18}F–FAZA positron emission tomography.

In line with the work of O'Connor et al.,[23] we confirm that the median values of ΔR_1 and ΔR_2^* are not robust enough to represent the tumor oxygenation status quantitatively, or the extent of hypoxia, which emphasizes the importance of the intra-tumoral heterogeneity.

In the current work, R_{1L} and R_{1W} values deconvoluted from R_{1G} showed no advantage in terms of the predictive capacity of the basal tumor oxygenation or of the response of tumor to CB breathing, except in the correlations between ΔR_1 and ΔR_2^* in the rhabdomyosarcoma tumor model (Figure 2A–C). Indeed, although ΔR_{1G} and ΔR_2^* correlation was unable to show an impact of vascular reoxygenation on the change in tissue oxygenation ($p = 0.07$, Figure 2A), correlations of ΔR_2^*, ΔR_{1L} and ΔR_2^*, ΔR_{1W} were significant (Figure 2B: ΔR_{1W} and ΔR_2^*, $p = 0.02$; Figure 2C: ΔR_{1L} and ΔR_2^*, $p < 0.01$).

The major contribution of this work is to provide a concept to map tumor oxygenation by combining different endogenous oxygen-sensitive markers. Indeed, this is a noninvasive, easily translatable method to broaden the understanding and assessment of tumor oxygenation, as there is currently no gold standard to measure hypoxia. Moreover, this work addresses tumor heterogeneity by analyzing changes in the relaxation parameters at the voxel scale. Thus, the segmentation of tumor voxels with respect to their type of response to a hyperoxic challenge could be useful to predict tumor hypoxia, and could be translated and evaluated in other tumor models as well as in the clinical setting.

4.1 | Limitations

The use of CB to alter tumor hypoxia could induce some changes that might become potential sources of R_1 and R_2^* fluctuations. CB could induce a vasodilation effect on mature blood vessels. This could create a change in blood flow that influences R_1[12] and/or a change in blood volume that alters [dHb] per tissue volume, thereby influencing R_2^*.[10] In addition, CB could induce blood acidification which, in turn, might shift the O_2–hemoglobin dissociation curve to the right. This effect might increase R_2^*.[10] It should be noted that the right shift of the hemoglobin–O_2 dissociation curve and the blood volume induce a potential increase in R_2^*, whereas blood oxygenation decreases R_2^*.

It should be noted that tumors often show spontaneous fluctuations in O_2. In FSa fibrosarcomas, the spontaneous fluctuations in T_2^* were proven to be associated with the fluctuations in tumor oxygenation linked to acute hypoxia, which occurs both in functional tumor regions and in tumor regions with non-perfused and/or immature vessels.[32,33] It would be ideal to assess the average of several maps pre- and post-challenge or to increase the imaging time, as a longer time could reveal regions exhibiting a longer cycle of hypoxia.[32] The authors discovered that the frequency of the fluctuation cycle ranged from 3 min to 1 h.[32] In the current work, the acquisition times of R_1 and R_2^* were 20 and 10 min, respectively. This acquisition time could cover at least the short fluctuation cycles.

ACKNOWLEDGEMENTS

This study was supported by grants from the Belgian National Fund for Scientific Research (FNRS) and the 'Fournier-Majoie Foundation'.

ORCID

Bernard Gallez http://orcid.org/0000-0002-5708-1302
Bénédicte F. Jordan http://orcid.org/0000-0002-7126-2206

REFERENCES

1. Overgaard J. Hypoxic radiosensitization: adored and ignored. *J Clin Oncol*. 2007;25:4066-4074.
2. Dewhirst MW, Birer SR. Oxygen-enhanced MRI is a major advance in tumor hypoxia imaging. *Cancer Res*. 2016;76:769-772.
3. Krohn KA, Link JM, Mason RP. Molecular imaging of hypoxia. *J Nucl Med*. 2008;49(Suppl. 2):129S-148S.
4. Tatum JL. Hypoxia: importance in tumor biology, noninvasive measurement by imaging, and value of its measurement in the management of cancer therapy. *Int J Radiat Biol*. 2006;82:699-757.
5. Jordan BF, Cron GO, Gallez B. Rapid monitoring of oxygenation by ^{19}F magnetic resonance imaging: simultaneous comparison with fluorescence quenching. *Magn Reson Med*. 2009;61:634-638.
6. Gallez B, Baudelet C, Jordan BF. Assessment of tumor oxygenation by electron paramagnetic resonance: principles and applications. *NMR Biomed*. 2004;17:240-262.
7. Kodibagkar VD, Wang X, Pacheco-Torres J, Gulaka P, Mason RP. Proton imaging of siloxanes to map tissue oxygenation levels (PISTOL): a tool for quantitative tissue oximetry. *NMR Biomed*. 2008;21:899-907.
8. Dewhirst MW, Klitzman B, Braun RD, Brizel DM, Haroon ZA, Secomb TW. Review of methods used to study oxygen transport at the microcirculatory level. *Int J Cancer*. 2000;90:237-255.
9. Gu Y, Bourke VA, Kim JG, Constantinescu A, Mason RP, Liu H. Dynamic response of breast tumor oxygenation to hyperoxic respiratory challenge monitored with three oxygen-sensitive parameters. *Appl Optics*. 2003;42:2960-2967.
10. Baudelet C, Gallez B. Current issues in the utility of blood oxygen level dependent MRI for the assessment of modulations in tumor oxygenation. *Curr Med Imag Rev*. 2005;1:229-243.
11. Mürtz P, Flacke S, Müller A, et al. Changes in the MR relaxation rate R_2^* induced by respiratory challenges at 3.0 T: a comparison of two quantification methods. *NMR Biomed*. 2010;23:1053-1060.
12. O'Connor JPB, Naish JH, Parker GJM, et al. Preliminary study of oxygen-enhanced longitudinal relaxation in MRI: a potential novel biomarker of oxygenation changes in solid tumors. *Int J Radiat Oncol Biol Phys*. 2009;75:1209-1215.
13. Jordan BF, Magat J, Colliez F, et al. Mapping of oxygen by imaging lipids relaxation enhancement: a potential sensitive endogenous MRI contrast to map variations in tissue oxygenation. *Magn Reson Med*. 2013;70:732-744.
14. Colliez F, Neveu MA, Magat J, Cao-Pham TT, Gallez B, Jordan BF. Qualification of a noninvasive magnetic resonance imaging biomarker to assess tumor oxygenation. *Clin Cancer Res*. 2014;20:5403-5411.
15. Cao-Pham T-T, Tran L-B-A, Colliez F, et al. Monitoring tumor response to carbogen breathing by oxygen-sensitive magnetic resonance parameters to predict the outcome of radiation therapy: a preclinical study. *Int J Radiat Oncol Biol Phys*. 2016;96:149-160.
16. O'Connor JPB, Naish JH, Jackson A, et al. Comparison of normal tissue R_1 and R_2^* modulation by oxygen and carbogen. *Magn Reson Med*. 2009;61:75-83.
17. White DA, Zhang Z, Li L, et al. Developing oxygen-enhanced magnetic resonance imaging as a prognostic biomarker of radiation response. *Cancer Lett*. 2016;380:69-77.
18. Winter JD, Akens MK, Cheng H-LM. Quantitative MRI assessment of VX2 tumour oxygenation changes in response to hyperoxia and hypercapnia. *Phys Med Biol*. 2011;56:1225.
19. Hallac RR, Zhou H, Pidikiti R, et al. Correlations of noninvasive BOLD and TOLD MRI with pO2 and relevance to tumor radiation response. *Magn Reson Med*. 2014;71:1863-1873.
20. Zhao D, Pacheco-Torres J, Hallac RR, et al. Dynamic oxygen challenge evaluated by NMR T_1 and T_2^*-insights into tumor oxygenation. *NMR Biomed*. 2015;28:937-947.

21. Burrell JS, Walker-Samuel S, Baker LCJ, et al. Exploring ΔR_2^* and ΔR_1 as imaging biomarkers of tumor oxygenation. *J Magn Reson Imaging*. 2013;38:429-434.
22. Remmele S, Sprinkart AM, Müller A, et al. Dynamic and simultaneous MR measurement of R_1 and R_2^* changes during respiratory challenges for the assessment of blood and tissue oxygenation. *Magn Reson Med*. 2013;70:136-146.
23. O'Connor JPB, Boult JKR, Jamin Y, et al. Oxygen-enhanced MRI accurately identifies, quantifies, and maps tumor hypoxia in preclinical cancer models. *Cancer Res*. 2016;76:787-795.
24. Tran LBA, Bol A, Labar D, et al. Potential role of hypoxia imaging using ^{18}F-FAZA PET to guide hypoxia-driven interventions (carbogen breathing or dose escalation) in radiation therapy. *Radiother Oncol*. 2014;113:204-209.
25. Kaanders JH, Bussink J, van der Kogel AJ. ARCON: a novel biology-based approach in radiotherapy. *Lancet Oncol*. 2002;3:728-737.
26. Baudelet C, Gallez B. How does blood oxygen level-dependent (BOLD) contrast correlate with oxygen partial pressure (pO_2) inside tumors? *Magn Reson Med*. 2002;48:980-986.
27. Zhao D, Jiang L, Hahn EW, Mason RP. Comparison of ^{1}H blood oxygen level-dependent (BOLD) and ^{19}F MRI to investigate tumor oxygenation. *Magn Reson Med*. 2009;62:357-364.
28. Blockley NP, Jiang L, Gardener AG, Ludman CN, Francis ST, Gowland PA. Field strength dependence of R_1 and R_2^* relaxivities of human whole blood to prohance, vasovist, and deoxyhemoglobin. *Magn Reson Med*. 2008;60:1313-1320.
29. Schwarzbauer C, Deichmann R. Vascular component analysis of hyperoxic and hypercapnic BOLD contrast. *Neuroimage*. 2012;59:2401-2412.
30. Robinson SP, Rijken PFJW, Howe FA, et al. Tumor vascular architecture and function evaluated by non-invasive susceptibility MRI methods and immunohistochemistry. *J Magn Reson Imaging*. 2003;17:445-454.
31. Howe FA, Robinson SP, McIntyre DJO, Stubbs M, Griffiths JR. Issues in flow and oxygenation dependent contrast (FLOOD) imaging of tumours. *NMR Biomed*. 2001;14:497-506.
32. Baudelet C, Ansiaux R, Jordan BF, Havaux X, Macq B, Gallez B. Physiological noise in murine solid tumours using T_2^*-weighted gradient-echo imaging: a marker of tumour acute hypoxia? *Phys Med Biol*. 2004;49:3389-3411.
33. Baudelet C, Cron GO, Ansiaux R, et al. The role of vessel maturation and vessel functionality in spontaneous fluctuations of T_2^*-weighted GRE signal within tumors. *NMR Biomed*. 2006;19:69-76.

SUPPORTING INFORMATION

Additional Supporting Information may be found online in the supporting information tab for this article.

How to cite this article: Cao-Pham T-T, Joudiou N, Van Hul M, et al. Combined endogenous MR biomarkers to predict basal tumor oxygenation and response to hyperoxic challenge. *NMR in Biomedicine*. 2017;30:e3836. https://doi.org/10.1002/nbm.3836

SUPPLEMENTARY MATERIALS

Figure S1: MRI acquisition protocol

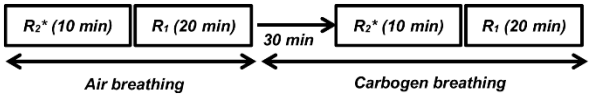

Figure S2. Spatial correlation between R_2^* and ΔR_2^*.

Graphs are shown for the representative rhabdomyosarcoma tumor (Fig. S2A) and for the representative 9L-glioma tumor (Fig. S2B) in Figure 1. Significant correlations between R2* and ΔR2* of voxels within tumors were observed (Fig. S2A: $p<0.01$, $r=-0.62$ for rhabdomyosarcoma tumor. Fig. S2B: $p<0.01$, $r=-0.65$ for 9L-glioma tumor).

A)

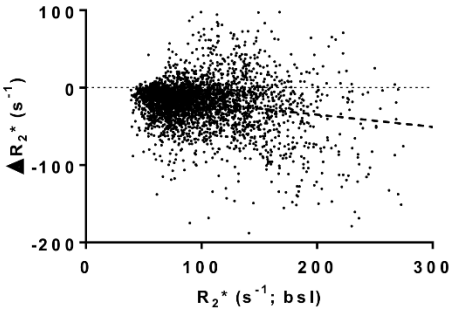

B)

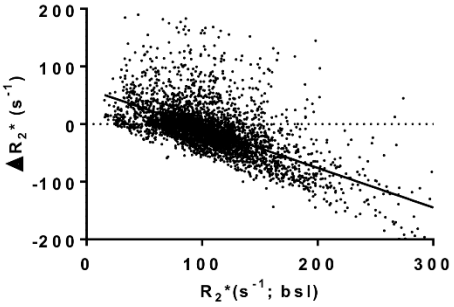

Figure S3. Spatial correlation between R_1 and ΔR_1.

Graph is shown for the representative rhabdomyosarcoma tumor in Figure 3. A significant correlation between R_1 and ΔR_1 of voxels within this tumor was observed ($p<0.01$, $r=-0.16$).

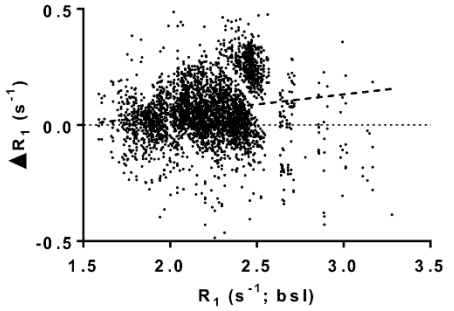

Figure S4: Summary of carbogen induced ΔR_2^* determined from 9L-gliomas and rhabdomyosarcomas. Data are presented as mean ± SEM. ****P < 0.0001, Student's two tailed t-test.

The ΔR_2^* are -1.3 ± 1.4 s^{-1} and -14.6 ± 2.2 s^{-1} for 9L-gliomas and rhabdomyosarcomas, respectively. *Abbreviation: rhabdo = rhabdomyosarcoma*

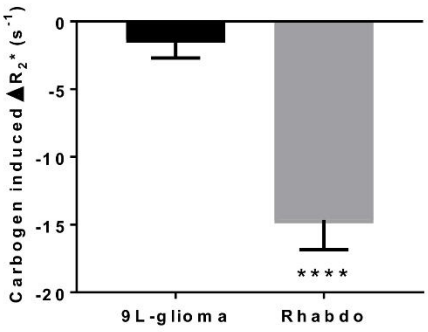

2. APPLICATION OF IMAGING MRI BIOMARKERS TO ASSESS CHANGES IN TUMOR OXYGENATION INDUCED BY ITPP

Combined endogenous MR biomarkers to assess changes in tumor oxygenation induced by an allosteric effector of hemoglobin

Thanh-Trang Cao-Pham, An Tran-Ly-Binh, Arne Heyerick, Catherine Fillée, Nicolas Joudiou, Bernard Gallez, Bénédicte F. Jordan

Summiting for NMR in Biomedecine

Combined endogenous MR biomarkers to assess changes in tumor oxygenation induced by an allosteric effector of haemoglobin

Thanh-Trang Cao-Pham [1], An Tran-Ly-Binh [1], Arne Heyerick [2], Catherine Fillée [3], Nicolas Joudiou [1], Bernard Gallez [1], Bénédicte F. Jordan [1]

[1] Université catholique de Louvain, Louvain Drug Research Institute, Biomedical Magnetic Resonance Research Group, Brussels, Belgium
[2] Normoxys Inc., Boston, MA 02135, USA
[3] Université catholique de Louvain, Clinique University Saint-Luc, Department of Clinique Laboratories, Belgium

Corresponding author:

Bénédicte F. Jordan
Biomedical Magnetic Resonance Group (REMA)
Louvain Drug Research Institute
Université catholique de Louvain
Avenue Mounier 73 – B1.73.08
B-1200 Brussels, Belgium
Phone: +32 2 7647364
Fax: +32 2 7647390
Email: benedicte.jordan@uclouvain.be

Number of words: (graphical abstract: 80/80, abstract 297/300, text 3988, table and figure legends 308)

Number of pages: 34

Number of tables: 0

Number of figures: 7

Keywords: MRI; ITPP; tumor hypoxia; ΔR_2^*; ΔR_1

GRAPHICAL ABSTRACT (80/80)

The combined endogenous MR biomarkers, R_1 and R_2*, reflecting tissue and vascular oxygenation respectively are promising tools to assess tumor hypoxia. In the current work, R_1 and R_2* successfully tracked the increase in tumor oxygenation induced by an allosteric effector of hemoglobin, ITPP. The effect of ITPP is the combination of a decrease in the binding affinity of Hb-O_2, in blood pH and in oxygen consumption rate of tumor cells, which translated into a significant increase in R_1 and R_2*.

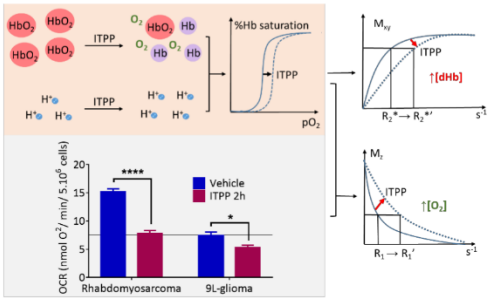

ABSTRACT (300/300)

Hypoxia is a crucial factor in cancer therapy determining prognosis and effectiveness of treatment. Although efforts are being made to develop methods to assess tumor hypoxia, no markers of hypoxia are currently being applied in routine clinical practice.

Recently, we showed that the combined endogenous MR biomarkers, R_1 and R_2*, reflecting tissue and vascular oxygenation respectively, were able to detect changes in tumor oxygenation induced by a hyperoxic breathing challenge.

In the current work, we further validated the ability of the combined MR biomarkers to predict the change in tumor oxygenation induced by an allosteric effector of hemoglobin, *myo*-inositol tripyrophosphate (ITPP) on two hypoxic rat tumor models, rhabdomyosarcoma and 9L-glioma.

An increase in tumor pO_2 was observed using L-band EPR oximetry. Besides, ITPP induced an increase in both R_1 and R_2* parameters. The increase in R_1 indicated an increase in [O_2] whereas, the increase in R_2* resulted from an increase in O_2 release from blood inducing an increase in [dHb]. The impact of ITPP was then evaluated on factors that are able to influence tumor oxygenation, including tumor perfusion, saturation rate of hemoglobin, blood pH and oxygen consumption rate (OCR). ITPP decreased [HbO_2] in blood of healthy animals. Besides, ITPP significantly increased the blood acidity, which is also a factor that right shifts the oxygen dissociation curve. A lack of change in tumor perfusion was observed after ITPP treatment. Interestingly, ITPP decreased the OCR in both tumor cell lines.

In conclusion, ITPP increased tumor pO_2 via a combined mechanism involving a decrease in OCR and an allosteric effect on hemoglobin that was further enhanced by a decrease in blood pH. MR biomarkers could assess the change in tumor oxygenation induced by ITPP. At the intra-tumoral level, a majority of tumor voxels were responsive to ITPP treatment in both models studied.

INTRODUCTION (620)

Hypoxia is a common situation occurring in solid tumors. The deprivation of tumor oxygenation is the result of the insufficient oxygen supply and the increasing oxygen

demand of metabolically active tumor cells. Hypoxia is known to be a factor that can contribute to the failure of cancer treatment as well as to tumor recurrence [1]. One attractive strategy to improve the effectiveness of radiation therapy is to decrease hypoxia at the time of irradiation. The meta-analysis on over 10.000 patients from 86 randomized trials showed that the modification of tumor hypoxia improved the outcome of patients treated with radiation therapy with an odds ratio of 0.77 [2]. However, such intervention only had modest benefit since screening for the presence of hypoxia has not been the entry criterion prior to hypoxia modification in those trials. A better treatment response was observed in trials in which identification of hypoxic tumor has been performed prior to irradiation [3]. Thus, a raising demand is to detect hypoxic tumors and patients who could benefit from hypoxia modification modalities. Various techniques have been developed to quantify tumor oxygenation including ^{19}F-MRI of perfluorocarbon [4], EPR oximetry [5], ^{1}H-MRI of hexamethyldisiloxane PISTOL [6], PET imaging of nitroimidazoles [7], polarographic needle electrodes [8], and fibre optic probes [9]. Nevertheless, no standard method is available for routine clinical practice up to date since they cannot address all practical challenges such as non-invasiveness, tumor accessibility or spatial and temporal resolutions.

Among the different oximetric techniques, imaging is considered as an appropriate method for hypoxia detection because it suits two remarkable features of hypoxia: spatial and temporal variations in oxygenation [3]. In order to be adopted in routine oncology practice, some requirements should be considered like non-invasiveness, possibility for repeated measurements, high spatial and temporal resolution, cost-effectiveness, robustness, and easy translation to human trials [3]. One potential method

to evaluate tumor hypoxia consists in the assessment of the oxygen-sensitive endogenous MR contrast parameters R_1 and R_2*, since they fulfill most of these criteria. Both MR biomarkers are sensitive to the change in pO_2 but reflect distinct features. The dissolved paramagnetic molecular oxygen in tissue fluid and in blood plasma increases the spin lattice relaxation rate R_1 via dipolar interaction. Meanwhile, the effective spin-spin relaxation rate R_2* is accelerated by an increase in paramagnetic deoxyhemoglobin. R_1 is therefore mostly reflecting tissue oxygenation while R_2* is more sensitive to changes in vascular oxygenation [10-14].

One drawback of R_1 is its low sensitivity. Starting from the fact that the solubility of oxygen is better in lipids than in water, our group previously assessed the signal of R_1 of lipid protons (R_{1L}) instead of the global R_1 (R_{1G}) (that mostly reflects the signal of water protons (R_{1W})), expecting that it should be more sensitive to the changes in pO_2 [15, 16].

It should be noted that a change in tumor pO_2 is the additive result of multi-factorial processes within the tumor. Each technique can only provide information about one or some facets of the whole change in the tumor microenvironment. Thus, there is an interest in combining multiple parameters to expand the understanding and assessment of the tumor hemodynamics, which are essential for personalized treatment. In a previous study, we combined R_1 and R_2* to evaluate the changes in tumor pO_2 induced by an hyperoxic gas breathing challenge [14].

The purpose of the current study was to further validate the combined endogenous MRI contrasts R_1 (including R_{1G}, R_{1W}, R_{1L}) and R_2* parameters to predict the change in tumor oxygenation induced by a pharmacological oxygen-modifier agent, *myo*-inositol tripyrophosphate (ITPP). ITPP is an allosteric effector of haemoglobin (Hb) which

decreases the binding affinity of O_2 for hemoglobin, and enhances the dissociation of Hb-O_2 towards a higher oxygenation [17-19].

MATERIALS AND METHODS (1428)

The study was approved by the local ethics committee. Studies were undertaken in accordance with the national and local regulations of the ethical committee (agreement number UCL/2014/MD/026).

Tumor models

Two tumor models were included in the study: rhabdomyosarcoma and 9L-glioma.

Rhabdomyosarcoma cells were grown in Roswell Park Memorial Institute (RPMI) medium supplemented with 10 % foetal calf serum (heat inactivated), 1 % of a mixture of antibiotics (penicillin 100 UI/mL, streptomycin 0.1 mg/mL) for *in vitro* experiment. For *in vivo* study, fragments from a syngeneic rhabdomyosarcoma ($1mm^3$) were grafted subcutaneously in one thigh of male adult WAG/Rij rats. The model was developed by the Laboratory of Experimental Radiobiology, Katholieke Universiteit Leuven, Belgium.

9L-glioma cells were grown in RPMI medium supplemented with 10 % foetal calf serum (heat inactivated), 1 % of a mixture of antibiotics (penicillin 100 UI/mL, streptomycin 0.1 mg/mL), 1 % nonessential amino acids, and 1 % sodium pyruvate. To establish 9L-glioma tumors *in vivo*, male adult Fisher F344 rats were inoculated subcutaneously in their thighs with 5.10^6 cells.

Tumor implantations were performed with the rats under general anaesthesia with intraperitoneal injection of ketamine and xylazine (80 and 10 mg/kg, respectively) on rats

weighing between 200 and 250 g. The animals were introduced into the study when the tumors reached the size of 15 to 20 mm.

ITPP treatment

ITPP was gratefully provided by NormOxys Inc. (Boston, MA). For *in vivo* study, ITPP was prepared at a concentration of 200 mg/mL in saline for IP injection at dose of 2 g/kg. For *in vitro* studies, adherent cells were treated with medium containing 10 mM ITPP. The effect of ITPP was studied after 2 h of treatment.

***In vivo* experimental design**

Four cohorts were involved. The blood gas test for the measurement of the saturation of hemoglobin and of blood pH was done in the first cohort. The tumor pO_2 was measured on the second cohort. The MRI measurements were done on the third cohort. The forth cohort was dedicated for the measurement of the perfused area by Patent blue staining method.

Blood gas test

Venous blood sample of animals of the first cohort was taken at two time points, before and 2h after ITPP administration. Rats were anesthetized with isoflurane 1.5% during blood sampling. Gas delivery (medical air mixed with isoflurane) was continuous at 2L/min through a nosepiece. About 1mL of blood was drawn from the lateral tail vein to a syringe specialized for blood test (safePICO Aspirator, Radiometer Medical, Denmark). The gas bubble was removed and the blood was kept intact with the external air thank to a special cap. The sample was mixed with heparin presented in syringe to reduce the

risk of clots. Blood samples were analysed by ABL901 analyser (Radiometer, Denmark) within 1h after the sampling.

L-band EPR oximetry

L-band EPR spectroscopy allowed a direct measurement of tumor oxygenation through the conversion of EPR linewidth to pO_2 by using a calibration curve [20]. Briefly, charcoal wood powder (CX0670-1, EM Science, Gibbstown, NJ) was used as oxygen sensitive sensor. About 200 µL of charcoal suspension (100 mg/mL) was introduced within tumor at a depth of 3–6 mm using a 23 gauge needle. EPR experiments were performed 24 h after probe implantation by using an L-band EPR spectrometer (Magnettech, Berlin, Germany) equipped with a low-frequency microwave bridge operating at 1.2 GHz and a loop-gap resonator. For that purpose, animals were anesthetized (isoflurane 1.5 %, 2 L/min) for EPR measurement and tumors were placed at the center of loop-gap resonator whose sensitivity extends to 1 cm around the loop. The modulation frequency was 100 kHz and the amplitude modulation was less than one third of the peak-to-peak linewidth to avoid peak distortion. The linewidth of the first-derivative EPR spectrum that was the average of five scan accumulations was then converted to pO_2 using a calibration curve. After recording the pO_2 value, animals of the second cohort were treated with ITPP and the acquisition was then repeated after 2 h of administration.

MRI study

Animals of the third cohort were subjected to R_1 and R_2* measurements before and 2 h after ITPP administration. Rats were anesthetized with isoflurane 1.5 % (2 L/min) during MRI experiments.

MRI was performed on an 11.7-Tesla, 16-cm inner diameter bore system (Bruker, Biospec) with a 7-cm birdcage coil for signal transmission and a surface coil for signal reception. A warm water blanket was used to maintain the animal's temperature at 37 °C, and the temperature was monitored with an MR-compatible rectal probe.

A multi-slice Rapid Acquisition with Relaxation Enhancement (RARE) sequence was first used to determine the most representative tumor slice for further measurement, with the following parameters: TE/ TR/ RARE-factor/ FOV/ matrix size/ slice thickness = 10.66 ms/ 2500 ms/ 6/ 35x35 mm/ 256x256/ 1 mm. The segmented IR-FISP sequence (SSFP-FID mode) was used for R_1 acquisition with the following parameters: TR/ TE/ FA/ BW/ FOV/ matrix size/ slice thickness = 4 ms/ 1.35 ms/ 10°/ 100 kHz/ 55x30 mm/ 100x85/ 1 mm, 4 segments, 100 TI from 13 ms to 8329 ms every 84 ms, and a total acquisition time of 20 minutes. The resonant frequency for excitation of R_1 sequence was on resonance for water. Multi-Gradient Echo R_2* images were acquired at TR/FA/slice thickness = 3000 ms/ 15°/ 1 mm with a FOV of 35x35 mm on a 256x256 matrix, 12 echoes from 3.5 ms to 58.5 ms every 5 ms. The total acquisition time was 9 minutes 36 seconds.

Data analysis was performed on an in-house program developed under ImageJ and MATLAB (MATLAB R2013b, The Math Works). R_1 and R_2* maps were calculated with an MRI analysis calculator plug-in in ImageJ software. This MRI analysis method is adapted from the original plugin created by Karl Schmidt (http://rsb.info.nih.gov/ij/) using a curve fitting method based on the Simplex method. R_{1L} and R_{1W} were extracted from the R_{1G} map by a bi-exponential deconvolution method. Hence, the term R_{1G} refers to the R_1 acquired by MRI and is the sum of the contributors of R_{1W} and R_{1L}. Meanwhile,

R_{1L} and R_{1W} indicate the generated data obtained by the deconvolution of R_{1G}. Regions of interest (ROIs) were drawn manually around the tumor on the selected anatomic slice and were transferred to R_{1L}, R_{1W}, R_{1G} and R_2* maps of the same slice. The subtraction of the two maps acquired before and after ITPP treatment was done voxels per voxels, resulting in maps of ΔR_{1L}, ΔR_{1W}, ΔR_{1G} and ΔR_2*. Co-registration has been made using a homemade script on Matlab. During acquisition, similar orientation was used for R_2* map and R_1 map so that only translation transformations were needed for co-registration.

Perfusion study – Patent blue staining

In order to obtain a rough estimate of tumor perfusion fraction, we used the Patent blue method. The method has been validated by comparison with DCE-MRI [21, 22]. Animals of the forth cohort were treated with vehicle, 1 mL NaCl 0.9 % (10 rhabdomyosarcomas and 6 9L-gliomas) or ITPP (10 rhabdomyosarcomas and 8 9L-gliomas). Two hours after treatment, Patent blue was injected through the tail vein (Sigma-Aldrich, 1 mL of Patent blue solution 1.25 %). The animals were sacrificed by an overdose of pentobarbital exactly one minute after the administration of Patent blue. Tumors were rapidly excised, cut into two size-matched halves. Tumor perfusion fraction was estimated by the percentage of stained area of the whole cross section analysing on ImageJ.

Oxygen consumption rate

The oxygen consumption rate (OCR) was measured using a Bruker EMXplus EPR spectrometer operating at 9.5 GHz. Briefly, adherent cells were trypsinized and resuspended in fresh medium (10^7 cells/mL). A mix of 100 µL of cell suspension, 100 µL of 20 % dextran was sealed in a glass capillary tube in the presence of 0.2 mM of a nitroxide proble acting as an oxygen sensor (^{15}N 4-oxo-2,2,6,6-tetramethylpiperidine-d_{16}-

^{15}N-1-oxyl, CDN isotopes, Pointe-Claire, Quebec, Canada). The sample was placed in a quartz ESR tube and maintained at 37 °C by heated nitrogen during the acquisition of the spectra. EPR linewidth was measured every minute and reported on a calibration curve to obtain the oxygen concentration [23]. OCR was determined by the absolute value of the slope of the decrease in oxygen concentration in the closed capillary tube over time.

Statistical analysis

Statistical analyses were performed with the GraphPad (Prism) program. Results were expressed as mean ± SEM (standard error of the mean). To evaluate the differences between groups of data, we used the two-tailed t-test. For all test, $p < 0.05$ was considered as significant (*$p < 0.05$; **$p < 0.01$; ***$p < 0.001$; ****$p < 0.0001$)

RESULTS (882)

In a preliminary work, we found that a single dose of ITPP induced an increase in tumor pO_2 that was maximal at 2 h post-administration [24]. In this study, we selected this time point to evaluate the impact of ITPP treatment on tumor pO_2 and oxygen-dependent MR parameters of two rat tumor models

The change in *in vivo* tumor pO_2 was assessed by L-band EPR oximetry (Fig. 1). In both models studied, we observed significant increase in tumor pO_2 after ITPP administration. pO_2 increased from 5.7 ± 0.3 mmHg to 8.4 ± 0.2 mmHg ($p < 0.01$) and from 7.9 ± 0.5 mmHg to 14.4 ± 1.0 mmHg ($p < 0.01$) in rhabdomyosarcomas and in 9L-gliomas, respectively. Interestingly, the effect of ITPP on 9L-gliomas was more important (80 % change) than on rhabdomyosarcomas (50 % change).

Figure 2 and 3 present pre- and post-ITPP treatment MRI data for rhabdomyosarcomas and for 9L-gliomas, respectively. The data were normalized to the vehicle values.

A change in R_2* can be due to a change in [dHb] per volume of tissue which eventually relates to the change in O_2 released from blood. ITPP significantly increased R_2* from 83.8 ± 6.4 s^{-1} to 98.6 ± 8.7 s^{-1} in rhabdomyosarcomas ($p < 0.01$, Fig. 2A) and from 83.1 ± 4.3 s^{-1} to 89.6 ± 4.4 s^{-1} in 9L-gliomas ($p = 0.02$, Fig. 3A). R_2* of all tumors in both models studied (n = 8-9/model) increased after ITPP administration, except one 9L-glioma tumor that showed a decrease in R_2* (Fig. 3A).

A change in R_1 could be the result of a change in dissolved O_2. A significant faster relaxation rate was the general observation for all R_1 parameters (R_{1G}, R_{1W}, R_{1L}) in both models after ITPP administration ($p < 0.05$) (Fig. 2 and 3 B, C, D). R_{1G} increased from 2.11 ± 0.03 s^{-1} to 2.19 ± 0.04 s^{-1} in rhabdomyosarcomas ($p < 0.01$, Fig. 2B) and from 2.12 ± 0.05 s^{-1} to 2.25 ± 0.05 s^{-1} in 9L-gliomas ($p = 0.05$, Fig. 3B). R_{1W} was, respectively, 1.01 ± 0.01 s^{-1} (vehicle) and 1.08 ± 0.02 s^{-1} (ITPP) ($p < 0.01$) in rhabdomyosarcomas (Fig. 2C) and 1.05 ± 0.01 s^{-1} (vehicle) and 1.13 ± 0.02 s^{-1} (ITPP) ($p < 0.01$) in 9L-gliomas (Fig. 3C). R_{1G} increased after ITPP treatment in both tumor models (Fig. 2B and 3B). However, for the R_{1W} parameter, there was one tumor in each model presenting an opposite trend in response to ITPP treatment. In response to ITPP, R_{1L} increased from 3.24 ± 0.08 s^{-1} to 3.36 ± 0.09 s^{-1} ($p = 0.04$) (Fig. 2D) and from 3.45 ± 0.06 s^{-1} to 3.57 ± 0.07 s^{-1} ($p < 0.01$) (Fig. 3D) in rhabdomyosarcomas and in 9L-gliomas, respectively. Two rhabdomyosarcomas and one 9L-glioma showed a decrease in R_{1L} after ITPP treatment. R_{1L} was not shown to be more sensitive to changes in tumor oxygenation than R_{1G} or R_{1W} in those models.

Figure 4 shows the heterogeneity in R_1 and R_2* response to ITPP challenge in rhabdomyosarcomas and in 9L-gliomas at the inter-tumoral level. In both models, ITPP induced increases in R_1 and R_2* in most (> 50 %) of the voxels in each tumor.

Since R_2* is sensitive to the change in [dHb], we assessed the impact of ITPP on HbO_2 saturation in the blood (Fig. 5). ITPP significantly decreased the saturation of hemoglobin from 91.6 ± 1.1 % to 67.9 ± 4.4 % ($p < 0.01$) (Fig. 5A). Interestingly, we also found a slight but significant decrease in blood pH. Indeed, the pH values were 7.46 ± 0.01 and 7.40 ± 0.01 for vehicle and ITPP treated samples, respectively ($p < 0.01$, paired t-test) (Fig. 5B). Both factors contribute to a right shift of the oxygen dissociation curve (ODC).

We further tested the impact of ITPP on the perfusion of tumors to verify whether the change in R_2* was not due to a change in tumor perfusion. The Patent blue staining method provides a rough estimation of tumor-perfused fraction [21, 22]. The experiment showed a lack of difference in percentage of colored area between tumors of vehicle group and tumors treated with ITPP in both models (Fig. 6). The colored area percentages were 82.5 ± 2.7 % (vehicle, n = 10) and 77.2 ± 2.1 % (ITPP, n = 10) ($p = 0.14$) for rhabdomyosarcomas and 56.7 ± 2.5 % (vehicle, n = 6) and 44.0 ± 4.9 % (ITPP, n = 8) ($p = 0.06$) for 9L-gliomas. We excluded a potential role of an increase in R_2* related to a change in perfusion. It should be noted that rhabdomyosarcomas were better perfused than 9L-gliomas ($p < 0.01$, unpaired t-test).

Two factors determine the tumor pO_2, O_2 supply and O_2 consumption of tumor cells. An increase in tumor pO_2 can be induced by increasing the O_2 supply or / and decreasing the O_2 consumption. The *in vitro* OCR of both cell lines was assessed by X-band EPR

oximetry and results are presented in figure 7. ITPP treatment significantly decreased OCR in both cell lines. OCR decreased from 15.21 ± 0.5 to 7.85 ± 0.51 nmol O_2/ min/ 5.10^6 cells ($p < 0.01$) and from 7.47 ± 0.61 to 5.3 ± 0.43 nmol O_2/ min/ 5.10^6 cells ($p = 0.02$) for rhabdomyosarcoma and 9L-glioma cells, respectively.

DISCUSSION (1058)

In previous studies, we highlighted the added value of combining R_1 and R_2* MRI biomarkers to map changes in tumor oxygenation induced by an hyperoxic breathing challenge [14]. In this work, we further validated the predictive value of the combined R_1 and R_2* MR oxygen-dependent parameters to assess changes in tumor oxygenation induced by a pharmacological oxygen modifier agent, ITPP. ITPP is described to right shift the dissociation curve of Hb-O_2 towards higher pO_2 values [25].

All oxygen-sensitive MR parameters (R_{1G}, R_{1W}, R_{1L} and R_2*) increased after ITPP administration (Fig. 2 and 3). The result at the inter-tumoral level (Fig. 2 and 3) was confirmed at the intra-tumoral level (Fig.4). Indeed, the majority of tumors in both models presented a higher proportion of voxel with ITPP-induced $\Delta R_1>0$ or $\Delta R_2*>0$. We also found that R_{1L} and R_{1W} did not show any superiority compared with R_{1G} in terms of sensitivity to the change in tumor oxygenation induced by ITPP. The observation was consistent with what we obtained in previous studies using carbogen [14, 15].

Since R_1 is sensitive to the oxygen molecules dissolved in plasma and tissue fluid, the increase in R_1 corresponds to an increase in dissolved oxygen in tumor tissue. With respect to changes in oxygenation, two mechanisms can be involved in the modification

of the tumor oxygenation: an increase in the O_2 supply and a decrease in the OCR of tumor cells. While an increase in O_2 supply by right shifting the ODC of ITPP was previously shown [17-19], we evidenced that ITPP was also able to induce a significant reduction of OCR *in vitro*, in both tumor cell lines studied.

An increase in R_2* is the result of an increase in the paramagnetic Hb concentration per tissue volume. It should be noted that R_2* can be influenced by other factors than the total Hb content, unrelated to the change in tumor pO_2 , such as haematocrit, vascular volume, pH, flow, vessel density [26] as well as experimental setting (e.g. voxel size, shimming procedure, TE sampling, quantification method) [27]. The ability of ITPP to change the Hb saturation was assessed *in vivo* on venous blood in healthy rats. Besides, ITPP also slightly but significantly increased blood acidity. Both factors therefore contributed to a right shift of ODC towards a higher O_2 release from the blood and an increase in the total dHb content according to the Bohr Effect. We also compared the perfusion in treated and untreated tumors to evaluate whether ITPP could induce an acute effect on tumor perfusion, which in turn could modify the tumor blood volume and dHb content. Our study did not show any significant change in tumor perfusion after ITPP administration. Of note, Kieda *et al.* found that long-term ITPP treatment was able to normalize tumor vessel in melanoma and in breast cancer syngeneic models [28]. However, this effect is not expected to happen early after ITPP administration (2h) in our study. Finally, with respect to R_2* measurement, we used a low flip angle (10°) to minimize any potential “in-flow” effect [29]. Indeed, the signal created by water of blood flowing into the imaging slice is much stronger than the static water at high flip angles (30° - 90°) because the spin of the static water is partially saturated by previous pulses.

While R_2* is generally assumed to decrease in response an hyperoxic challenge, because the breathing of high oxygen content gas (carbogen or 100% oxygen) increases the hemoglobin saturation of blood and therefore decreases R_2* signal, we show here that the direction of change in R_2* depends on the mechanism of action of the oxygen modifier under study. Indeed, while using a pharmacological agent that is able to modify Hb saturation and oxygen consumption, an increase in R_2* is being observed. This is similar to observations made using inhibitors of oxygen consumption [30]. Moreover, in a previous study, we showed that the change in R_2* is not only influenced by tumor pO_2 but also by the degree of Hb saturation at baseline [14]. This has also been proved at the intratumoral level in a work from the group of O'Connor [31].

However, two studies using another allosteric effector of Hb, RSR13, did not observe similar changes in R_2*. Indeed, RSR13 induced an increase in BOLD signal intensity (meaning a decrease in R_2*) in NCI-H460 human lung carcinoma xenograft [32]. Whereas, in the work of Hou et al., RSR13 almost did not influence the R_2* signal in RIF-1 tumors [33]. It should be noted that both ITPP and RSR13 significantly enhanced tumor pO_2 in the models under study [28, 33]. Consequently, the equilibrium of pO_2 after treatment is likely to depend on many factors such as tumor type, the impact of drug on metabolic rate or on oxygen consumption rate of tumor cells.

Indeed, the mechanism of OCR modulators can be complex and usually includes the change in tumor perfusion or in tumor metabolic activity [30, 34]. These factors are unrelated to the real change in tumor pO_2 and can modify R_2* signal, hindering the interpretation of the results. In brief, caution should be made while interpreting R_2* since the marker reflects the concentration of dHb per volume but not the oxygenation per se.

Recently, R_1 has gained more and more attention as a tool to estimate tumor oxygenation since R_1 is sensitive directly to dissolved O_2 concentration. An increase in R_1 is generally observed in tumors under hyperoxic challenge [13, 15, 35, 36]. The group of O'Connor has validated the mapping of spatial variation of hypoxia based on different response of R_1 to oxygen breathing [12].

In conclusion, ITPP was able to increase tumor pO_2 in the two models under study, rhabdomyosarcoma and 9L-glioma. The combined endogenous MRI biomarkers R_1 and R_2* were sensitive to these changes. Since R_1 and R_2* can be biased by multiple factors, unrelated to changes in pO_2, data interpretation needs to take this into account. In this study, we identified that the acute effect of ITPP on tumor pO_2 was the result of a combination of right shifting of ODC, decrease in pH and decrease in OCR. Considering the fact that R_1 and R_2* measurements are already applied in many clinical trials in different tumor types [37-41], we believe that the combined endogenous MRI biomarkers could be a helpful tool in clinical setting for personalized treatment.

ABBREVIATIONS

ODC: oxygen dissociation curve

dHb: deoxy-hemoglobin

OCR: oxygen consumption rate

MRI: magnetic resonance imaging

ITPP: *Myo*-inositol tripyrophosphate

ROI: region of interest

DCE-MRI: dynamic contrast enhanced MRI

FUNDING

This study was supported by grants from the Belgian National Fund for Scientific Research (FNRS) and the “Fournier-Majoie Foundation”. BFJ is Senior Research Associate of the FNRS.

REFERENCES

1. Vaupel P, Mayer A. Tumor Hypoxia: Causative Mechanisms, Microregional Heterogeneities, and the Role of Tissue-Based Hypoxia Markers. In: Luo Q, Li LZ, Harrison DK, Shi H, Bruley DF, eds. Oxygen Transport to Tissue XXXVIII. Vol 923. Cham: Springer International Publishing; 2016:77-86.
2. Overgaard J. Hypoxic Radiosensitization: Adored and Ignored. JCO. 2007;25(26):4066-4074.
3. Dewhirst MW, Birer SR. Oxygen-Enhanced MRI Is a Major Advance in Tumor Hypoxia Imaging. Cancer Res. 2016;76(4):769-772.
4. Jordan BF, Cron GO, Gallez B. Rapid monitoring of oxygenation by 19F magnetic resonance imaging: Simultaneous comparison with fluorescence quenching. Magn Reson Med. 2009;61(3):634-638.
5. Gallez B, Baudelet C, Jordan BF. Assessment of tumor oxygenation by electron paramagnetic resonance: principles and applications. NMR Biomed. 2004;17(5):240-262.
6. Kodibagkar VD, Wang X, Pacheco-Torres J, Gulaka P, Mason RP. Proton imaging of siloxanes to map tissue oxygenation levels (PISTOL): a tool for quantitative tissue oximetry. NMR Biomed. 2008;21(8):899-907.
7. Tran L-B-A, Bol A, Labar D, et al. Hypoxia imaging with the nitroimidazole ^{18}F-FAZA PET tracer: A comparison with OxyLite, EPR oximetry and ^{19}F-MRI relaxometry. Radiotherapy and Oncology. 2012;105(1):29-35.

8. Dewhirst MW, Klitzman B, Braun RD, Brizel DM, Haroon ZA, Secomb TW. Review of methods used to study oxygen transport at the microcirculatory level. Int J Cancer. 2000;90(5):237-255.
9. Gu Y, Bourke VA, Kim JG, Constantinescu A, Mason RP, Liu H. Dynamic response of breast tumor oxygenation to hyperoxic respiratory challenge monitored with three oxygen-sensitive parameters. Appl Opt. 2003;42(16):2960-2967.
10. O'Connor JPB, Naish JH, Jackson A, et al. Comparison of normal tissue R_1 and R_2* modulation by oxygen and carbogen. Magn Reson Med. 2009;61(1):75-83.
11. Burrell JS, Walker-Samuel S, Baker LCJ, et al. Exploring ΔR_2* and ΔR_1 as imaging biomarkers of tumor oxygenation. J Magn Reson Imaging. 2013;38(2):429-434.
12. O'Connor JPB, Boult JKR, Jamin Y, et al. Oxygen-Enhanced MRI Accurately Identifies, Quantifies, and Maps Tumor Hypoxia in Preclinical Cancer Models. Cancer Res. 2016;76(4):787-795.
13. Hallac RR, Zhou H, Pidikiti R, et al. Correlations of noninvasive BOLD and TOLD MRI with pO2 and relevance to tumor radiation response. Magn Reson Med. 2014;71(5):1863-1873.
14. Cao-Pham T-T, Joudiou N, Van Hul M, et al. Combined endogenous MR biomarkers to predict basal tumor oxygenation and response to hyperoxic challenge. NMR Biomed. October 2017.
15. Cao-Pham T-T, Tran L-B-A, Colliez F, et al. Monitoring Tumor Response to Carbogen Breathing by Oxygen-Sensitive Magnetic Resonance Parameters to

Predict the Outcome of Radiation Therapy: A Preclinical Study. Int J Radiat Oncol Biol Phys. 2016;96(1):149-160.

16. Jordan BF, Magat J, Colliez F, et al. Mapping of oxygen by imaging lipids relaxation enhancement: A potential sensitive endogenous MRI contrast to map variations in tissue oxygenation. Magn Reson Med. 2013;70(3):732-744.
17. Limani P, Linecker M, Kron P, et al. Development of OXY111A, a novel hypoxia-modifier as a potential antitumor agent in patients with hepato-pancreato-biliary neoplasms - Protocol of a first Ib/IIa clinical trial. BMC Cancer. 2016;16:812.
18. Fylaktakidou KC, Lehn J-M, Greferath R, Nicolau C. Inositol tripyrophosphate: a new membrane permeant allosteric effector of haemoglobin. Bioorganic & Medicinal Chemistry Letters. 2005;15(6):1605-1608.
19. Duarte CD, Greferath R, Nicolau C, Lehn J-M. myo-Inositol Trispyrophosphate: A Novel Allosteric Effector of Hemoglobin with High Permeation Selectivity across the Red Blood Cell Plasma Membrane. ChemBioChem. 2010;11(18):2543-2548.
20. Jordan BF, Baudelet C, Gallez B. Carbon-centered radicals as oxygen sensors for in vivo electron paramagnetic resonance: screening for an optimal probe among commercially available charcoals. MAGMA. 1998;7(2):121-129.
21. Crokart N, Jordan BF, Baudelet C, et al. Glucocorticoids Modulate Tumor Radiation Response through a Decrease in Tumor Oxygen Consumption. Clinical Cancer Research. 2007;13(2):630-635.
22. Ansiaux R, Baudelet C, Jordan BF, et al. Mechanism of Reoxygenation after Antiangiogenic Therapy Using SU5416 and Its Importance for Guiding Combined Antitumor Therapy. Cancer Research. 2006;66(19):9698-9704.

23. Jordan BF, Grégoire V, Demeure RJ, et al. Insulin increases the sensitivity of tumors to irradiation: involvement of an increase in tumor oxygenation mediated by a nitric oxide-dependent decrease of the tumor cells oxygen consumption. Cancer Res. 2002;62(12):3555-3561.
24. Tran LBA, Cao-Pham TT, Jordan BF, Deschoemaeker S, Heyerick A, Gallez B. Impact of *myo*-inositol trispyrophosphate on tumor oxygenation and response to irradiation in rodent tumor models. J. Cell. Mol. Med. In press DOI:10.1111/jcmm.14092
25. FöRnvik K, Zolfaghari S, Salford LG, Redebrandt HN. ITPP Treatment of RG2 Glioblastoma in a Rat Model. Anticancer Research. 2016;36(11):5751-5756.
26. Baudelet C, Gallez B. Current Issues in the Utility of Blood Oxygen Level Dependent MRI for the Assessment of Modulations in Tumor Oxygenation. Current Medical Imaging Reviews. 2005;1(3):229-243.
27. Mürtz P, Flacke S, Müller A, et al. Changes in the MR relaxation rate R2* induced by respiratory challenges at 3.0 T: a comparison of two quantification methods. NMR Biomed. 2010;23(9):1053-1060.
28. Kieda C, Hafny-Rahbi BE, Collet G, et al. Stable tumor vessel normalization with pO2 increase and endothelial PTEN activation by inositol trispyrophosphate brings novel tumor treatment. J Mol Med. 2013;91(7):883-899.
29. Howe FA, Robinson SP, Rodrigues LM, Griffiths JR. Flow and oxygenation dependent (FLOOD) contrast MR imaging to monitor the response of rat tumors to carbogen breathing. Magnetic Resonance Imaging. 1999;17(9):1307-1318.
30. Jordan BF, Crokart N, Baudelet C, Cron GO, Ansiaux R, Gallez B. Complex relationship between changes in oxygenation status and changes inR*2: The case

of insulin and NS-398, two inhibitors of oxygen consumption. Magnetic Resonance in Medicine. 2006;56(3):637-643.

31. Little RA, Jamin Y, Boult JKR, et al. Mapping Hypoxia in Renal Carcinoma with Oxygen-enhanced MRI: Comparison with Intrinsic Susceptibility MRI and Pathology. Radiology. 2018;288(3):739-747.
32. Amorino GP, Lee H, Holburn GE, et al. Enhancement of tumor oxygenation and radiation response by the allosteric effector of hemoglobin, RSR13. Radiat Res. 2001;156(3):294-300.
33. Hou H, Khan N, O'Hara JA, et al. Effect of RSR13, an allosteric hemoglobin modifier, on oxygenation in murine tumors: an in vivo electron paramagnetic resonance oximetry and bold MRI study. International Journal of Radiation Oncology*Biology*Physics. 2004;59(3):834-843.
34. Jordan BF, Misson P, Demeure R, Baudelet C, Beghein N, Gallez B. Changes in tumor oxygenation/perfusion induced by the no donor, isosorbide dinitrate, in comparison with carbogen: monitoring by EPR and MRI. Int J Radiat Oncol Biol Phys. 2000;48(2):565-570.
35. Burrell JS, Walker-Samuel S, Baker LCJ, et al. Exploring ΔR_2^* and ΔR_1 as imaging biomarkers of tumor oxygenation. J Magn Reson Imaging. 2013;38(2):429-434.
36. Zhao D, Pacheco-Torres J, Hallac RR, et al. Dynamic oxygen challenge evaluated by NMR T1 and T2*--insights into tumor oxygenation. NMR Biomed. 2015;28(8):937-947.
37. O'Connor JPB, Naish JH, Parker GJM, et al. Preliminary Study of Oxygen-Enhanced Longitudinal Relaxation in MRI: A Potential Novel Biomarker of

Oxygenation Changes in Solid Tumors. International Journal of Radiation Oncology*Biology*Physics. 2009;75(4):1209-1215.

38. Rijpkema M, Kaanders JHAM, Joosten FBM, van der Kogel AJ, Heerschap A. Effects of breathing a hyperoxic hypercapnic gas mixture on blood oxygenation and vascularity of head-and-neck tumors as measured by magnetic resonance imaging. International Journal of Radiation Oncology*Biology*Physics. 2002;53(5):1185-1191.
39. Griffiths JR, Taylor NJ, Howe FA, et al. The response of human tumors to carbogen breathing, monitored by Gradient-Recalled Echo Magnetic Resonance Imaging. Int J Radiat Oncol Biol Phys. 1997;39(3):697-701.
40. Hallac RR, Ding Y, Yuan Q, et al. Oxygenation in cervical cancer and normal uterine cervix assessed using blood oxygenation level-dependent (BOLD) MRI at 3T. NMR Biomed. 2012;25(12):1321-1330.
41. Linnik IV, Scott MLJ, Holliday KF, et al. Noninvasive tumor hypoxia measurement using magnetic resonance imaging in murine U87 glioma xenografts and in patients with glioblastoma. Magn Reson Med. 2014;71(5):1854-1862.

TABLE AND FIGURE LEGENDS (308)

Figure 1. Tumor oxygenation of rhabdomyosarcomas (N = 3) and 9L-gliomas (N = 6) obtained by L-band EPR oximetry before and 2h after ITPP administration (Mean ± SEM). Both tumor models were responsive to ITPP with significant increase in tumor pO_2.

Figure 2. Individual normalized changes in MRI parameters in rhabdomyosarcomas (N = 8) before and after 2h of ITPP administration. All MRI parameters increased under the effect of ITPP.

Figure 3. Individual normalized changes in MRI parameters in 9L-gliomas (N = 9) before and after 2h of ITPP administration. All MRI parameters increased under the effect of ITPP.

Figure 4. Mean fractional ITPP-induced $\Delta R_1>0$ and $\Delta R_2^*>0$ from rhabdomyosarcomas (open square) and 9L-gliomas (filled circle) (Mean ± SEM). Each symbol presents the data of a tumor. At intra-tumor level, a majority of voxel in most of the tumors presented $\Delta R_1>0$ and $\Delta R_2^*>0$.

Figure 5. A) Change in haemoglobin saturation before and 2h after ITPP administration in healthy venous rat blood sample (N = 5). ITPP significantly decrease the rate of hemoglobin saturation (Mean ± SEM). **B)** Change in venous blood pH before and after 2h of ITPP administration in healthy venous rat blood sample (N = 5). ITPP slightly but significantly decrease the blood pH (Mean ± SEM).

Figure 6. Mean value ± SEM of Patent blue perfused area in rhabdomyosarcomas (vehicle N = 10; ITPP N = 10) and in 9L-gliomas (vehicle N = 6; ITPP N = 8). No significant different was observed between vehicle group and group treated with ITPP in both models.

Figure 7. Impact of ITPP on *in vitro* OCR in rhabdomyosarcoma cell line (vehicle N = 6; ITPP N = 6) and in 9L-glioma cell line (vehicle N = 8; ITPP N = 6) obtained by X-band

EPR oximetry. ITPP significantly decreased the OCR in both tumor cell lines (Mean ± SEM

FIGURE 1

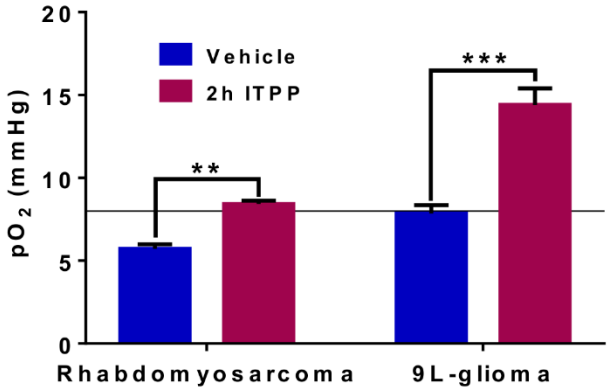

FIGURE 2

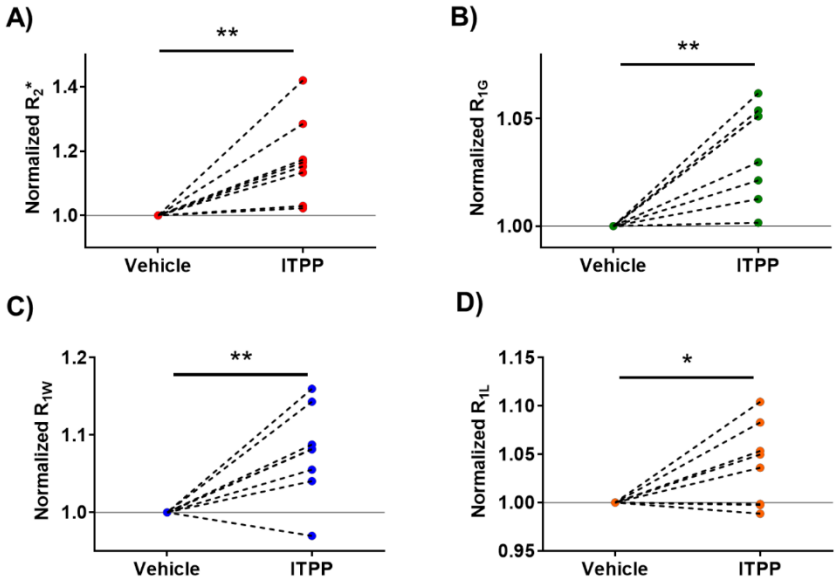

FIGURE 3

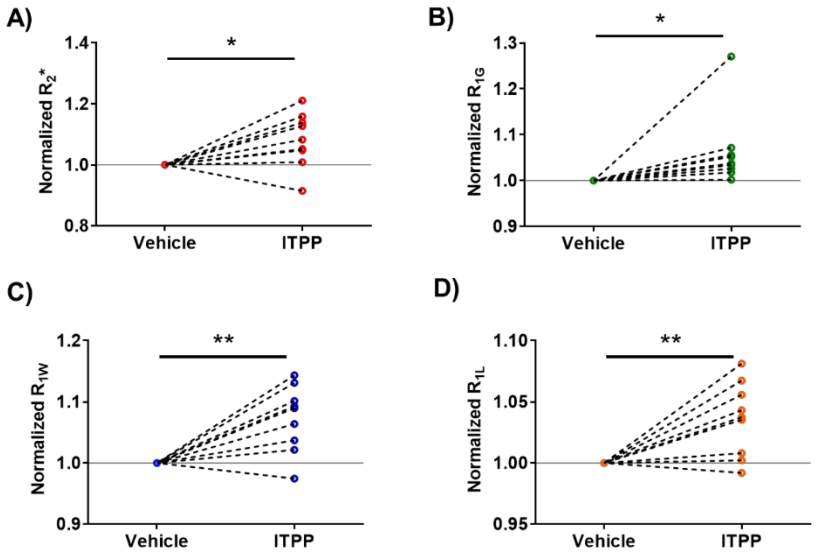

FIGURE 4

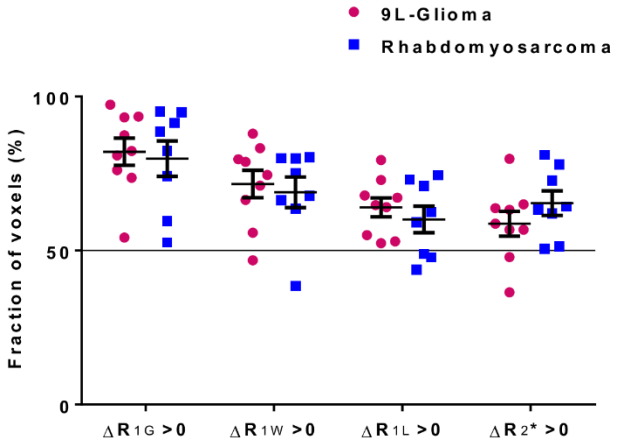

FIGURE 5

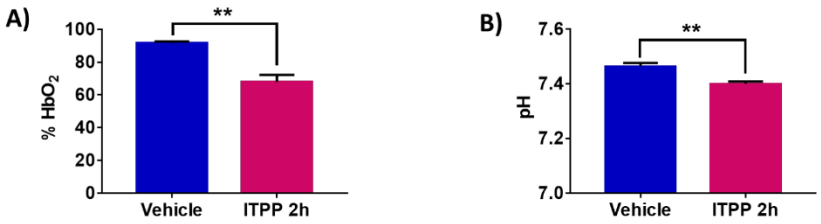

FIGURE 6

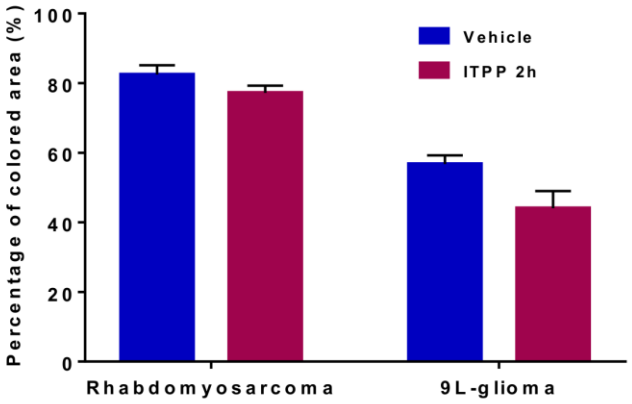

FIGURE 7

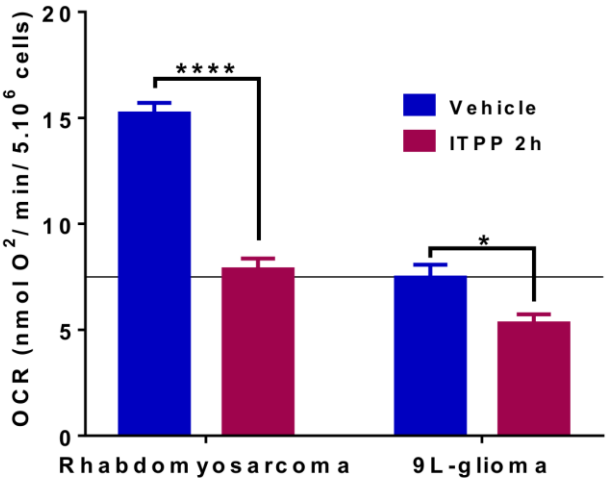
OCR (nmol O2/ min/ 5.10^6 cells)
20
15
10
5
0
****
*
Vehicle
ITPP 2h
Rhabdomyosarcoma
9L-glioma

DISCUSSION

1. MAJOR FINDING OF THE THESIS

The overall aim of the thesis was to validate MRI biomarkers that could be further assessed as tools to stratify patient on an individual basis for personalized therapy. For this purpose, we assessed the predictivity of different MRI biomarkers in terms of response to hypoxia-driven intervention and of outcome to radiation therapy in two rat tumor models (rhabdomyosarcoma and 9L-glioma). The predictivity of the R_1 global (R_{1G}) tissue oxygenation parameter, and of the two derived-parameters, R_1 lipid (R_{1L}) and R_1 water (R_{1W}), was evaluated individually and in combination with R_2*, assessing vascular oxygenation. In this thesis, the fast and slow components of R_{1G} were deconvoluted and attributed to lipid (R_{1L}) and water (R_{1W}) relaxation rates, respectively. For reference, MRI biomarkers were cross-validated with the quantitative EPR oximetry method.

1.1. Validation of MRI biomarkers

The hypoxia-driven intervention used in the first part of the thesis is carbogen. The experiments were conducted under air and carbogen breathing conditions to broaden the range of pO_2 as well as to identify tumors benefiting from the challenge.

1.1.1. Sensitivity of MRI biomarkers to changes in tumor oxygenation

In both tumor models studied, carbogen generated a significant increase in tumor oxygenation as measured by EPR oximetry. We observed a decrease in R_2* corresponding to a decrease in [dHb] relating to the saturation of hemoglobin and an increase in all MR-derived R_1 parameters corresponding to an increase in dissolved O_2. The changes in MRI biomarkers were consistent with the EPR results. Yet, no correlation between pO_2 assessed by EPR oximetry and any of the MRI biomarkers was obtained. In conclusion, R_1 and R_2* were not evaluated as quantitative but as qualitative to monitor tumor oxygenation.

1.1.2. Sensitivity of MRI biomarkers to predict the basal tumor pO_2 and response to CB

In the next step, we investigated the influence of the basal oxygenation on the amplitude of response to carbogen. In the vascular compartment, we observed strong correlations between basal R_2* and carbogen-induced change in R_2* (ΔR_2*) which means well-oxygenated vasculature tumors responded less to carbogen and vice versa. Moreover, the observation was also true at the intratumoral level. Besides, an increase in the O_2 supply in the vascular compartment (ΔR_2*) was found to induce an elevated tumor oxygenation in the tissular compartment (ΔR_{1G}, ΔR_{1W}, ΔR_{1L}), which is consistent with the mechanism of action of carbogen. Despite the negative correlation between the change in tissular oxygenation (ΔR_{1G}, ΔR_{1W}, ΔR_{1L}) and the basal R_1 (including R_{1G}, R_{1W}, R_{1L}), R_1 and ΔR_1 maps suggested a possible relation of R_1 and ΔR_1, suggesting that well

oxygenated regions responded better to CB and vice versa. The observation questioned the robustness of the median value of R_1 and R_2* to assess tumor pO_2. Indeed, the averaged values of MRI biomarkers mask the tumor heterogeneity, which is an important feature of hypoxia. We therefore decided to apply a multi-parametric analysis to explore the response of tumor to carbogen breathing at the voxel scale. Tumors were analysed voxel-wised based on the response of R_1s and R_2* to the carbogen challenge. Each voxel was then categorized to one of four hypoxic features (mild hypoxia, severe hypoxia, normoxia and vascular steal). The results showed that 9L–gliomas presented more normoxic fractions, whereas rhabdomyosarcomas presented more hypoxic fractions, which was in accordance with a previous study using ^{18}F–FAZA and EPR oximetry [290].

In conclusion, basal R_2* was shown to be predictive for the magnitude of response to the carbogen challenge in the vascular compartment (ΔR_2*). In addition, an increase in O_2 supply (ΔR_2*) resulted in an elevated tumor oxygenation (ΔR_1). Yet, we also found that median R_1 and R_2* were not robust enough to represent the tumor pO_2, or the extent of hypoxia. The voxel-wise heterogeneity analysis using the response to carbogen of combined R_1 and R_2* was able to stratify tumors based on their hypoxic status.

1.1.3. MRI parameters as predictive markers of response to the outcome of radiation therapy

For this purpose, tumors subjected for MRI and EPR were then irradiated either under air as vehicle group or under carbogen breathing as hypoxia driven-intervention. The radiation therapy responses were then individually correlated with each biomarker.

In the rhabdomyosarcoma model, carbogen breathing was not able to radiosensitize tumors, as illustrated by the lack of difference in tumor growth delay between the cohort irradiated under air breathing condition and the one irradiated under carbogen breathing condition. Therefore, there was a lack of oxygenated tumors in the correlation. Indeed, although carbogen significantly increased tumor pO_2 in this group, most of the tumors showed pO_2 remaining below 10 mmHg.

In the 9L-glioma model, a tumor control dose 50 (TCD50) assay was conducted. This assay is described to be more clinically relevant than the standard growth delay assay. Carbogen decreased the TCD50 from 41.6 Gy in the group irradiated under air breathing conditions to 32.2 Gy in the group irradiated under carbogen breathing conditions. A dose-modifying factor DMF50 greater than one ($DMF50 = TCD50_{air} / TCD50_{CB} = 1.29$) confirmed the radiosensitizing properties of carbogen in this tumor model. The predictivity of MR parameters was then assessed at 40 Gy, the dose rate that showed a maximum difference in response to irradiation between CB and air breathing groups. Logistic regression analysis showed that only R_2* was likely to be predictive for the

curability of 9L-glioma whereas all R_1-related parameters failed to predict the radiotherapy outcome.

In conclusion, despite the fact that carbogen significantly increased tumor pO_2 in both tumor models, the intervention only radiosensitized 9L-glioma but not rhabdomyosarcoma creating a typical situation with one responsive and one unresponsive model. In this context, only R_2* was predictive for the radiotherapy outcome in the responsive model.

1.2. Application of combined endogenous MR biomarkers to assess changes in tumor oxygenation induced by an allosteric effector of hemoglobin

In this part, the predictive value of the combined MRI biomarkers was further validated to assess changes in tumor oxygenation induced by an allosteric effector of hemoglobin, ITPP, in the same tumor models as the ones used in the first part.

The ability of ITPP to increase tumor oxygenation in the tumor models under study was confirmed by EPR oximetry. We observed that all oxygen-sensitive MR parameters (R_{1G}, R_{1W}, R_{1L} and R_2*) increased after ITPP administration. While an increase in all MR-derived R_1 parameters corresponds to an increase in dissolved O_2, an increase in R_2* corresponds to an increase in [dHb]. The changes in MRI biomarkers were consistent with the mechanism of an allosteric effector of Hb where ITPP reduces the affinity of O_2 to hemoglobin thus increases the O_2 release from Hb and increases [dHb]. The result at the inter-tumoral level was confirmed at the intra-tumoral level where the majority of tumors in both models presented a higher proportion of voxels with ITPP-induced $\Delta R_1>0$ or $\Delta R_2*>0$.

Besides the known mechanism of ITPP, we evidenced that ITPP was also able to induce a significant reduction of oxygen consumption rate *in vitro* in both tumor cell lines studied. This effect likely participates to the increase in tumor oxygenation observed *in vivo*.

Alternative factors potentially influencing R_2* in this context were also evaluated, including tumor perfusion, saturation rate of hemoglobin, and blood pH. The right shift of the oxygen dissociation curve (ODC) induced by ITPP was confirmed by a decrease in saturation rate of Hb. The effect was enhanced by a decrease in blood pH. ITPP treatment did not modify the tumor perfusion, excluding the impact of this factor on the increase in R_2*.

In conclusion, ITPP was able to increase tumor pO_2 in both models under study by a combined effect of right shift of ODC, decrease in pH and decrease in OCR. The combined MRI biomarkers R_1 and R_2* were sensitive to these changes at both inter-tumoral and intra-tumoral level.

2. GENERAL CONCLUSION

2.1. Change in R_1 and R_2* in response to hypoxia-driven intervention

In our thesis, two interventions with distinct mechanisms were used to modify tumor oxygenation: a hyperoxic challenge and an allosteric effector of hemoglobin. These oxygen modifiers are not supposed to alter tumor perfusion nor blood volume, thus the change in R_1 and R_2* were assumed to directly relate to the change in dissolved oxygen and in [dHb], respectively.

*2.1.1. R_2**

In this thesis, CB breathing challenge significantly decreases R_2*. Indeed, the decrease in R_2* is not solely due to the increase in arterial blood oxygen content (that decreases the dHb content). Potential factors that may influence R_2* signal under carbogen breathing challenge are the changes in blood flow, blood volume or blood pH. The 5% CO_2 component of carbogen gas is known to counteract the vasoconstriction effect of high-oxygen content gas breathing and induces the vasodilation effect in mature blood vessels. Thus, breathing CB may cause the change in tumor blood flow and in tumor blood volume. Since no evidence was shown that CB is able to change the tumor OCR, we suppose that the oxygen uptake of tumor cells remains constant over the course of CB breathing. Hence, an increase in blood flow decreases venous dHb content because the fraction of the oxygen extracted from the blood is reduced. In addition, an increase in blood flow may create the inflow effect. The effect is explained since water in blood flowing into imaging slice produces a stronger signal than the static water molecules already excited in the imaged slice. Images obtained with MRI sequences with a short repetition time and high flip angles (30°-90°) are sensitive to the inflow effect [158]. In this thesis, we used a low flip angle (10°) to minimize the in-flow effect. A method that allows the quantification of blood flow without the use of contrast agents is arterial spin labelling (ASL) [309]. The technique involves the use of arterial blood water as tracer by magnetically labeling. The water signal of a slice outside of the tumor volume is inverted by a saturation pulse. Then, a reduction in signal is observed using MRI as the labeled blood water is delivered to targeted tissues.

While the increase in blood flow enhances the decrease in R_2*, CB could also induce effects that changes R_2* in the opposite direction. First, the steal effect occurs in regions where blood vessels are immature and lack smooth muscle receptors. While CB causes vasodilation in mature vessels, immature vessels fail to respond. Consequently, blood is redistributed from regions of immature vessels that further enhance the hypoxic situation. Second, CO_2 may induce a decrease in blood pH that right shifts the ODC of hemoglobin according to Bohr effect. This would increase dHb content that increases R_2*. In addition, the vasodilation effect of carbogen may increase blood volume in affected region that increase the local [dHb]. Last but not least, the increase in

paramagnetic dissolved oxygen in well oxygenated region could also lead to an increase in R_2*.

In breft, the R_2* signal obtained is the result of the combination of several effects. That may explain the presence of both positive and negative ΔR_2* voxels in response to CB breathing observed in our study. It may be complicated to distinguish the contribution of each factor on the obtained R_2* as well as to determine which one rules over the change of R_2*. In order to have a better understand on R_2* behaviour, a possible solution is to combine R_2* with other biomarker, for example R_1, as we have done in this thesis.

Despite both interventions induced significant increase in tumor oxygenation, the change in R_2* was not similar. Indeed, a decrease in R_2* under carbogen breathing is related to the saturation of arterial blood that decreases [dHb] and a possible increase in blood flow as explained above. Whereas, an increase in R_2* under the effect of ITPP means an increase in [dHb]. Interestingly, two other studies found out that allosteric effector of hemoglobin may increase or may not change R_2* regardless significant increases in tumor pO_2 [310, 311]. Figure 11 may explain the different R_2* signal changes (increase/ decrease/ lack of change). If the allosteric effector does not induce any change in tumor blood flow or blood volume, but only induces change in the ODC, the saturation of hemoglobin should be determined by the new corresponding pO_2 value (Figure 11) at the new ODC. The three situations A, B and C illustrated in Figure 11 may be illustrative of the change in R_2*, which is determined by the degree of Hb saturation. Of note, the equilibrium of pO_2 after treatment depends on many factors including tumor type and the impact of drug on metabolic rate or on oxygen consumption rate of tumor cells. In addition, the use of R_2* to assess the effect of oxygen consumption modulator has shown limitations [193]. Indeed, the mechanism of these agents is usually complex and relates to the change in tumor perfusion and in cell metabolism. Thus, the change in R_2* induced by an oxygen consumption modulator may not reflect the real change in tumor pO_2. In brief, R_2* is more suitable to monitor change in tumor oxygenation during hyperoxic challenge. Nevertheless, caution should be made when assimilating the change in R_2* and the change in tumor pO_2 since we have evidenced the positive or negative change in R_2* induced by carbogen is related to the hypoxic status of the tumor region.

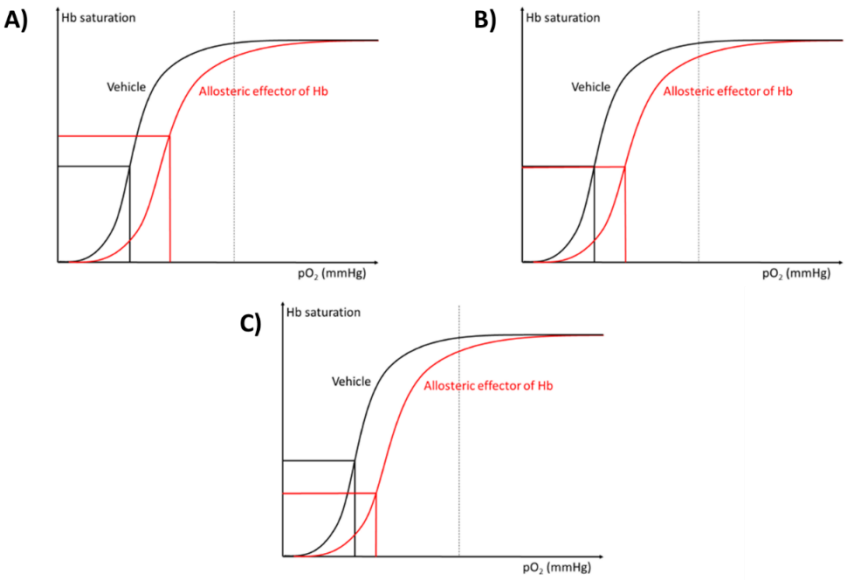

Figure 11: The complexity of R_2 under the effect of allosteric effector of hemoglobin. Of note, if there is no change in the blood flow or blood volume, an increase in the degree of hemoglobin saturation which means a decrease in the proportion of dHb leads to a decrease in R_2* and vice versa. A, B, C illustrated three possibilities of R_2* if the allosteric effector induces a shift in ODC and an enhancement in tumor pO_2. The change of R_2* depends on the degree of Hb saturation but not on the real tumor pO_2.*

2.1.2. R_1

In contrary to R_2*, both carbogen and ITPP induced a significant increase in R_1 which is consistent with the change in tumor oxygenation assessed by EPR oximetry. Efforts have been made to improve the sensitivity of R_1 such as OE-MRI [263] or R_1 of lipid [167]. Besides, R_1 also successfully monitored the negative change in tumor pO_2 induced by CA4 [168] or hydralazine [165]. In brief, R_1 could seem to be suitable to monitor changes in tumor oxygenation. However, this parameter was neither quantitatively correlated with actual pO_2 values, nor shown to be correlated with radiation therapy outcome in our studies.

2.1.3. Combined MRI endogenous biomarkers and heterogeneity analysis

R_1 and R_2* are complementary in essence since one reflects tissular oxygenation and the other reflects vascular oxygenation, respectively. We evidenced the utility of combining R_1 and R_2* in assessing the intratumoral heterogeneity of the response to a hyperoxic challenge by a multi-parametric analysis. The approach could be useful to stratify patients for carbogen breathing and to characterize the basal tumor oxygenation status. Besides, the combined analysis could have the potential to guide dose-painting studies.

The voxel-wise heterogeneity analysis was also useful to predict the response of tumors to ITPP treatment with the majority of voxels presented an increased in R_1 and R_2*. Yet, the analyses were based on one MR parameter, R_1 or R_2*. We did not perform a multi-parametric analysis using combined MRI endogenous biomarkers because the mechanism of action of ITPP is complex. Indeed, the changes in R_1 and R_2* were the results of the combination of multiple effects. Hence, in the context of our study, we still lacked of proof to associate the changes in R_1 and R_2* induced by ITPP and the real change in tumor pO_2 to perform the multi-parametric analysis.

Figure 12 and Figure 13 summarize the changes in R_1 and R_2* induced by the carbogen breathing and allosteric effector of hemoglobin, respectively. The expected changes in MRI biomarkers induced by oxygen modifiers as well as their real changes observed in two studied tumor models were described in Table 4 (CB challenge) and Table 5 (ITPP administration).

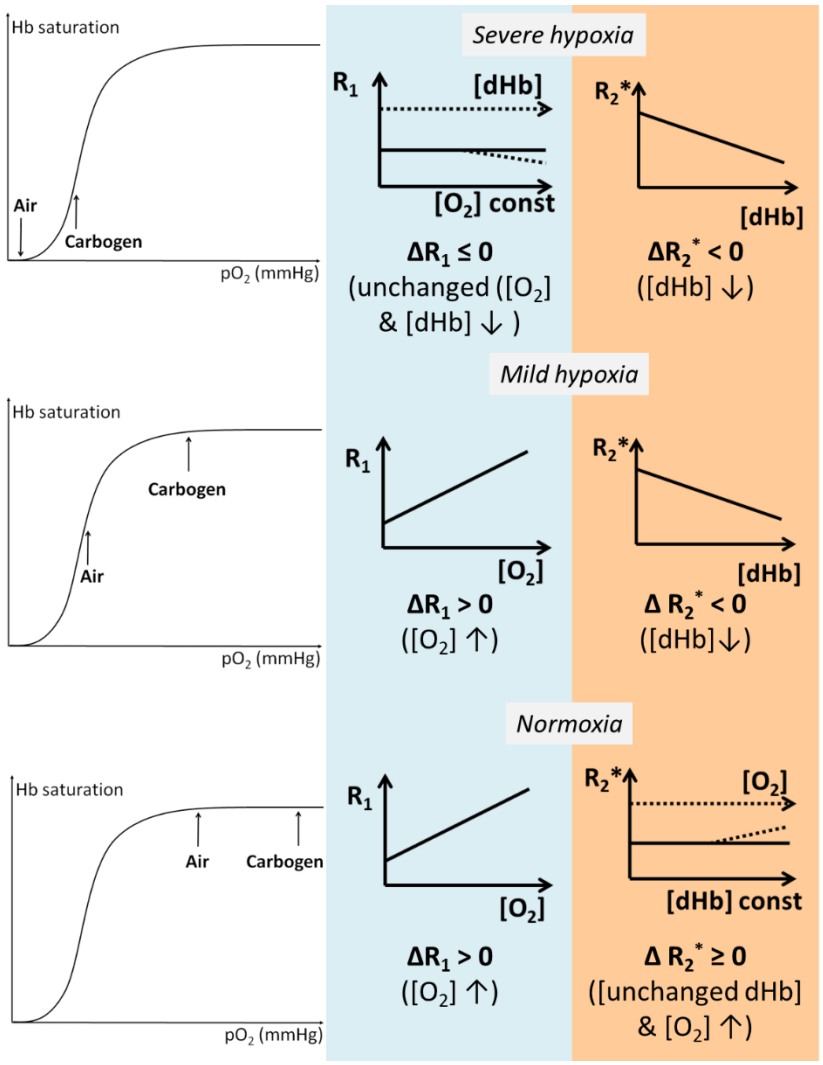

Figure 12: Summary of changes in R_1 and R_2 induced by carbogen breathing*

Table 4: Summary of the changes in R_1 and R_2 induced by carbogen challenge, expected effects created by potential modulators and the results observed*

	Potential modulators	**Change in R_1**	**Change in R_2***
Expected changes in MRI biomarkers	Vasodilation effect of 5% CO_2		
	• ↑ blood volume	↑ R_1	↑ R_2*
	• ↑ blood flow (↓ fraction of O_2 extracted)	↑ R_1	↓ R_2*
	• Induce in-flow effect	/	↓ R_2* or not depend on flip angle
	• Induce steal effect	↓ R_1	↑ R_2*
	5% CO_2 induces ↓ pH (right shift ODC)	↑ R_1	↓ R_2* or ↑ R_2* or does not change R_2*
	95% O_2 saturates arterial blood	↑ R_1	↓ R_2*
Observed changes in MRI biomarkers (c.f. Figure 12)	• Severe hypoxic regions	↓ R_1 (↓ [dHb], $[O_2]$ const)	↓R_2*
	• Mild hypoxic regions	↑ R_1	↓ R_2*
	• Normoxic regions	↑ R_1	↑ R_2* (↑$[O_2]$, [dHb] const)
	• Vascular steal regions	↓ R_1	↑R_2*
	Overall changes	↑ R_1	↓ R_2*

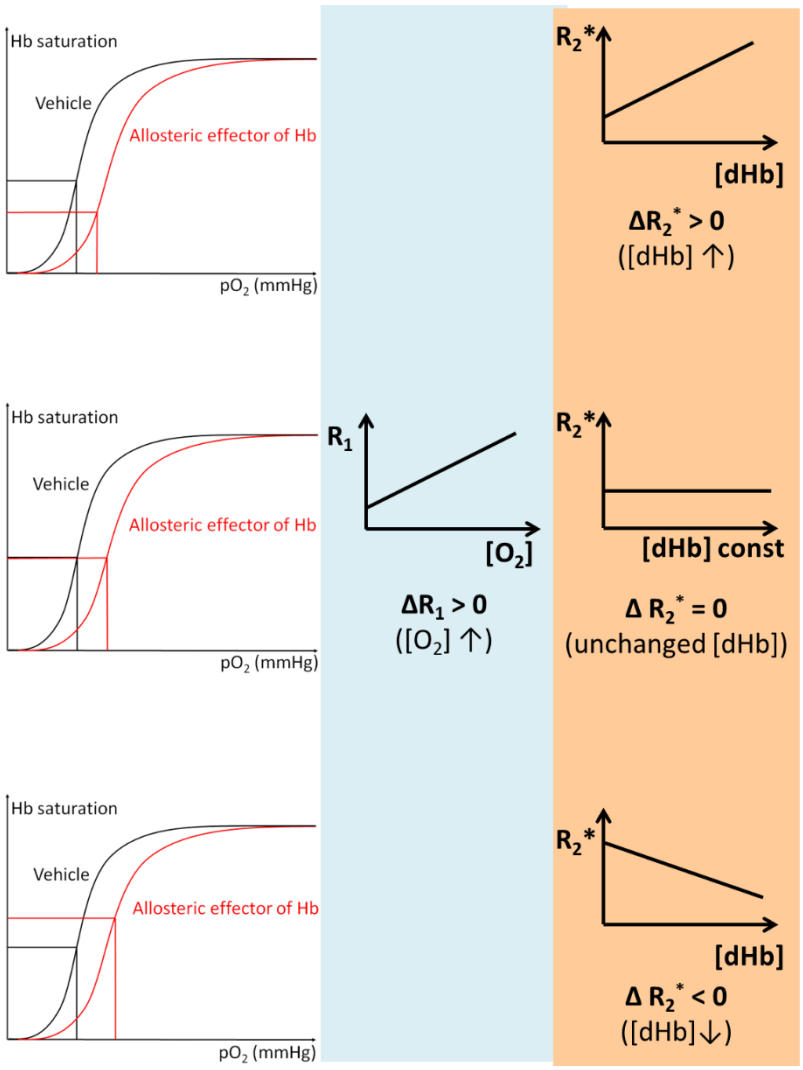

Figure 13: Summary of changes in R_1 and R_2 induced by allosteric effector of haemoglobin*

Table 5: Summary of the changes in R_1 and R_2 induced by ITPP administration, expected effects created by potential modulators and the results observed*

	Potential modulators	**Change in R_1**	**Change in R_2***
Expected changes in MRI biomarkers	Allosteric effector of Hb and ↓ pH (right shift ODC)	↑ R_1	↓ R_2* or ↑ R_2* or does not change R_2*
	↓ Oxygen consumption rate	↑ R_1	/
Observed changes in MRI biomarkers	Overall changes	↑ R_1	↑ R_2*

2.2. Qualitative and quantitative aspects of MRI biomarkers

Studies have been investigated the relationship between tumor oxygenation and BOLD MRI. In a preclinical study used carbogen to induce increase in tumor pO_2, result showed a significant correlation between the average tumor pO_2 assessed by Eppendorf oximetry and the average signal change in BOLD contrast (r = 0.92 at a 95% confidence level) [312]. Yet, the heterogeneity spatial distribution of tumor hypoxia was not integrated in the analysis [312]. The technique was further validated by co-registered the pO_2 assessed by fiber-optic microprobe and BOLD signals in fibrosarcoma xenografts during multiple cycles of different hyperoxic gases [153]. However, no spatial correlation of absolute pO_2 and the magnitude of BOLD signal change was observed that questioned the quantitative aspect of R_2* [153]. Efforts have been made to calibrate the R_2* response to estimate the tumor pO_2 by correcting on effects potentially influencing R_2* other than dHb concentration and blood flow. In a preclinical study on orthotopic rat gliomas, T_2* was assessed together with the transverse relaxation parameter (T_2), macroscopic field inhomogeneities (ΔB_0), and blood volume fraction (BVf) [313]. A simulation mathematical model was developed based on the imaging results to estimate the absolute blood oxygen saturation (SO_2) in the brain tumor model. Although the calculated SO_2 was comparable to literature values, no difference has been observed between SO_2 in normal brain tissue and in tumor [313]. Indeed, the calibration of R_2* to tumor pO_2 is not straightforward because the BOLD signal and dHb content are also affected by factors unrelated to the change in tissue pO_2 [64]. In addition, the curvilinear relationship of R_2* and pO_2 might contribute to the lack of sensitivity of R_2* to oxygenation [158]. Although the method has not been approved for quantitative estimation of tumor hypoxia, R_2* has been successfully monitored the change in tumor pO_2 induced by hyperoxic challenge. Based on R_2* basal and carbogen induced-ΔR_2*, Burrell et al. have characterized two hypoxic tumor models [314]. One tumor model was more hypoxic with fast R_2* at baseline representing for an abundant dHb concentration. This tumor model responded better to carbogen breathing with highly negative ΔR_2*. The other tumor model was less hypoxic with slower R_2* at baseline representing for a poor dHb concentration. Carbogen induced almost no change in R_2* in this tumor model. The result was further pre-clinically and clinically confirmed in renal carcinomas at the intra-tumoral level by the study of Little et al. [166]. The perfused normoxic voxels presented a slower R_2* baseline and responded less to hyperoxic breathing than hypoxic voxels.

The results of our study are in agreement with the observations of Burell et al. [314] and of Little et al. [166]. In addition, multi-parametric analysis suggested the increase in R_2* induced by carbogen breathing challenge was related to the increase in the paramagnetic dissolved O_2 or to the decrease in dHb concentration because of the steal effect. These results suggested that R_2* could be a useful tool to qualitatively monitor the change in tumor pO_2 induced by a hyperoxic breathing challenge. In the contrary, we evidenced that the method may not be suitable to follow change in tumor pO_2 induced by an allosteric effector of hemoglobin.

Regarding R_1, it is possible to establish a correlation between pO_2 and R_1. Yet, the calibration is not easy to obtain since R_1 suffers from the low sensitivity to oxygenation change and is influenced by temperature, tissue water content, blood flow, basal blood oxygen saturation. Thus, R_1 is usually considered as qualitative method to monitor tumor oxygenation.

Colliez. et al successfully correlated pO_2 assessed by EPR oximetry and R_{1L} on mammary lipid-rich tumor models, MDA-MB-231 and NT2. The lipid content in MDA-MB-231 and NT2 tumor tissue was 7% and 9%, respectively [315]. Authors also showed that R_{1L} acquired by a water spoiler sequence was more sensitive than R_{1G} in assessing the change in tumor oxygenation [168]. In this thesis, the sensitivity of R_{1L} in general was not superior to that of R_{1W} and of R_{1G}. The reason may due to the bi-exponential method used in this study to extract R_{1L} in non-rich-lipid tumor models, 9L-glioma and rhabdomyosarcoma. The lipid content of these two models is about 2%. Indeed, R_{1L} was attributed to the fast component of R_{1G} where lipid fast relaxation rate may be contaminated by the fast relaxation of water linked to macromolecules. Although bi-exponential de-convolution method might not be as robust as the water spoiler sequence to assess R_1 signal of lipid protons, we supposed that the amplitude of the contamination of fast relaxation rate by linked macromolecules might be weaker compared to the contribution of lipid to fast relaxation at least in rhabdomyosarcomas. Indeed, we observed R_{1L} was more sensitive to the change in tumor oxygenation than R_{1G} in this tumor model. The amplitude of water contamination to R_{1L} in 9L-gliomas might be clarified by combining with the pO_2 information at the voxel level. A method that allows the mapping of tumor oxygenation is ^{19}F-MRI.

Another issue related to the correlation of MRI biomarkers and pO_2 is the temporal variation of tumor hypoxia. Since the EPR measurements were done one day after the MRI acquisitions, the tumor oxygenation status may not be the same between two measurements. Ideally, the reference method should be co-registered at the same moment of acquisition of the validated method.

3. PERSPECTIVES

3.1. Preclinical research

The combined endogenous MRI biomarkers analysis should undergo further investigations. The mapping of tumor heterogeneity based on the multi-parametric analysis should be validated by other hypoxic imaging modalities to confirm the robustness of the approach. A potential method is ^{18}F-FAZA PET imaging since the tracers selectively accumulate in hypoxic regions.

In our study, the irradiation regime applied in our study was a single dose regime although the recommended regime in practice is fractionated irradiation. If a single dose protocol is sufficient for proof-of-concept experiments, fractionated schemes should be considered in further studies. Another perspective for translational purpose is to use combined MRI biomarkers to follow the dynamics of tumor hypoxia by monitoring tumor oxygenation during treatment. The reason is two folds: to assess cycling hypoxia and to determine individually the moment of maximal reoxygenation to apply irradiation. The information on the window of reoxygenation is helpful for the timing of fractionated irradiation as well as for the combination of hypoxia-driven intervention and radiation therapy. Furthermore, the dynamic monitoring of tumor hypoxia allows the identification of persistent hypoxia (resistant zones) during therapy. Hence, the treatment planning could be individually adapted. Also, it should be noted that during the course of the thesis, we selected one representative slice for each tumor based on anatomic image to analyse the information of MR oxygen sensitive biomarkers. The process is common in the proof-of-concept experiments to evaluate a new approach. In the next step, to increase the robustness of R_1 and R_2*, the analysis should be done on the whole tumor volume. The development of an automatic routine that effectively analyses and integrates the R_1 and R_2* data whould be useful for the combined analysis, that could be implemented for treatment guidance. Indeed, since tumor hypoxia is not stable over time, a treatment guidance tool should provide rapidly and precisely the tumor functional spatial information in order to locally adapt irradiation dose (e.g. dose painting). In addition, it would be worthwhile to investigate whether the 3D distribution of hypoxic regions estimated by combined R_1 and R_2* is relevant to prescribe a radiation boost or an adapted therapy.

Our study could not demonstrate a superior sensitivity of R_{1L} compared with R_{1G} and R_{1W}, the idea of assessing the longitudinal relaxation of lipid protons was therefore only valid in lipid-rich tumor models.

Another important point would be to correlate the fraction of hypoxia determined by combined MRI markers with indirect endogenous markers (e.g. HIF1-α, GLUT1, VEGF). The approach is appealing to establish a relationship between imaging biomarkers and proteins expressed under hypoxic conditions. These studies may aid for the research of

molecular signaling pathways and of cellular responses triggered by or modulated by moderate and severe hypoxia.

3.2. Clinical translation

Considering translational aspects of this work, an advantage is that hyperoxic gas breathing interventions and R_1 and R_2* MRI techniques have already been used in the clinical setting, which is an advantage for translational research of the approach. On the one hand, clinical evidences clearly showed that the decrease of R_2* in response to hyperoxic challenge could estimate tumor hypoxia in prostate, cervical, and H&NC cancers [316-319]. Regarding R_1, a study on patients with advanced cancer of the abdomen showed that oxygen breathing increased R_1 in 8/10 patients. The results were in agreement with the tumor perfusion assessed by DCE MRI [139]. In addition, Remmele et al. used the scatter plots of changes in R_1 and R_2* induced by carbogen breathing observed in both normal volunteers and brain tumor patients to investigate the response of different regions of interest [320]. T_1-weighted oxygen-enhanced MRI using oxygen breathing was found to successfully map tumor hypoxia in combined with DCE-MRI in renal carcinoma patients [166]. On the other hand, R_1 and R_2* baselines have also been investigated as markers of tumor hypoxia. In a study on 25 patients with brain neuroepithelial tumors, both global R_1 and lipid R_1 measured in tumors were significantly slower than the values obtained from normal appearing white matter of the same patient and from the normal brain parenchyma of healthy volunteers [170]. The results suggested the presence of hypoxia in tumors [170]. Yet, the value of baseline R_2* to predict hypoxia appears uncertain. In a study on 20 patients with prostate cancer, a positive correlation between R_2* and pimodazole staining was observed with a high sensitivity (88%) and specificity (36%) [155]. In another study, no difference in R_2* was found between brain neuroepithelial tumors and normal appearing white matter or healthy brain [170].

An important point should be noted when translating the approach from preclinical to clinical evaluation is to adapt to technical and practical differences between two settings. The imaging sequences in clinical settings should cover a larger region of interest within a more restricted timing than in pre-clinical settings. Obviously, the field of view (FOV) in clinical study can be as much as 100 times larger than the FOV in preclinical study [166]. If the resolution in clinical practice had been the same as in preclinical study, the acquisition time would have been increased. Due to a larger FOV and a limited acquisition time, the voxel size in clinical studies is usually much larger than one obtained in preclinical studies. The increase in voxel size in clinical setting results in partial volume averaging effects which reduce the accuracy of the approach. That may lead to the lack of predictivity of the markers, especially in regions presenting steep gradient of pO_2 between normoxia and hypoxia. Perspectives lay on the development of actual method towards fast acquisition scheme to improve the acquisition time while keeping the small voxel size to reduce the averaging effects [322, 323].

To reduce the patient discomfort as little as possible, the acquisition time should be reasonably short. The movement of patient decides the successful of the study, which depends not only on the patient cooperation but also on the localization of tumors. The longer the acquisition time is, the higher the risk of study failure resulting from the patient movement, resulting in the impossibility to acquire robust ΔR_1 and ΔR_2* maps. The risk underlines the importance to maintain the patient immobile throughout the measurement. The adoption of contention system using for radiation therapy may be a direct solution to achieve the optimal patient immobility. Yet, replication of the fabrication of contention system should be foreseen if the dynamic monitor of tumor oxygenation during therapy is adapted. Indeed, the reduction in tumor volume and/or in patient morphology, particularly due to weight loss is usually observed during the treatment.

Another challenge that we have to face in clinical study is physiological movements related to breathing and swallowing that hampers the correct application of the approach on the upper part of the body (e.g. H&NC). Little et al have successfully used OE-MRI in renal carcinoma in patients [166]. This study evidenced the feasibility to map tumor hypoxia using multiple MRI techniques with a hyperoxic breathing challenge in tumors located in the lower part of body.

Evidences have shown the impact of hypoxia on treatment outcome. Yet, an approach to assess the efficacy of agents able to circumvent hypoxia is still unavailable for routine clinical practice despite extensive studies dedicated to this subject. The disposition of an imaging biomarker to stratify patients and evaluate the response to treatments is crucial to determine the translatable properties of a promising hypoxia-driven intervention into the clinic. The hypoxic intervention that was extensively studied in the course of this thesis is carbogen breathing. The approach has also been investigated in clinical trial in ARCON protocol. Of note, results from the Phase III ARCON clinical trial in H&NC was disappointing since patients received ARCON protocol did not show significant improved overall survival compared to control patients who received a standard treatment [178]. Also in the study, authors identified that only patients with hypoxic tumors (using pimonidazole) benefited from ARCON intervention [178]. The finding underlines the need to have a tool to identify patients who would benefit from hypoxia modification intervention for radiation therapy. Another factor is the ability to identify on the individual basis the effectiveness of the treatment on patient, the dynamics of the effect, the fraction of tumor that is responsive and the fraction that is resistant to the treatment. Herein, we have evidenced the use of combined endogenous MRI biomarkers under carbogen breathing could address these two factors. Thus, the approach may serve as a powerful tool for reoxygention challenge protocol. The pre-breathing time protocol of carbogen could be improved and personalized by using repeated measurements to follow the dynamics of the effect.

Dose painting that delivers non-uniform dose to the tumor is attractive since hypoxic tumor regions could receive a boost of irradiation. Yet, the translation to clinical arena

confronts hurdles. Indeed, at the moment, dose painting has been selected based on PET imaging. Of note, as the hypoxic region can be presented at micron scale, the millimeter resolution of PET scan causes the average problem as presented above. Moreover, PET tracers identifying hypoxic regions are FMISO, Cu-ATSM and FAZA. Among them, the hypoxic specificity of Cu-ATSM remains unclear. Another problem is to define the maximal tolerated dose to lower the side effects. For example, in a study applied DPBN based on ^{18}F-FDG, patients were treated with two doses 80.9 Gy and 85.9 Gy [324]. During the latency period of 4 to 10 months, 36 % of patients irradiated with 85.9 Gy developed mucosal ulcers versus 14 % of patients irradiated with 80.9 Gy. In addition, the biological interpretation of images is not straightforward. Evidence suggested that the uptake of FMISO differs between cell types and the extent of necrosis may influence the analysis of the images [325]. The constraints are also imposed by the techniques for dose delivery such as defying the maximum dose gradient or the accuracy of patient position [254]. Since it is still unclear how to effectively use dose painting for the best patient benefit, many studies are needed to apply MRI functional imaging based dose painting.

The concept of guiding irradiation by an imaging tool is ideal and crucial for dose painting because of the dynamics of tumor hypoxia. Yet, it may not be directly applicable in clinical setting since imaging and irradiation facilities are still apart. Consequently, the approach of hypoxia imaging-directed for irradiation planning at the same day would create a big burden for imaging and therapy planning.

REFERENCES

1. Pacheco-Torres J, López-Larrubia P, Ballesteros P, Cerdán S. Imaging tumor hypoxia by magnetic resonance methods. NMR Biomed. 2011;24(1):1-16.
2. Moeller BJ, Cao Y, Vujaskovic Z, Li CY, Haroon ZA, Dewhirst MW. The relationship between hypoxia and angiogenesis. Seminars in Radiation Oncology. 2004;14(3):215-221.
3. Vaupel P. Oxygenation status of malignant tumors: Pathogenesis of hypoxia and significance for tumor therapy. Seminars in Oncology 2001;28:29–35.
4. Corbet C, Feron O. Tumour acidosis: from the passenger to the driver's seat. Nature Reviews Cancer 2017;17:577–593.
5. Mirabello V, Cortezon-Tamarit F, Pascu SI. Oxygen Sensing, Hypoxia Tracing and *in vivo* Imaging with Functional Metalloprobes for the Early Detection of Non-communicable Diseases. Frontiers in Chemistry 2018; 6.
6. Thomlinson RH and Gray LH. The histological structure of some human lung cancers and the possible implications for radiotherapy. Br J Cancer 1955;9:539–549.
7. Brown JM. Evidence for acutely hypoxic cells in mouse tumours, and a possible mechanism of reoxygenation. The British Journal of Radiology 1979;52:650–656.
8. Chaplin DJ, Durand RE, Olive PL. Acute hypoxia in tumors: implications for modifiers of radiation effects. Int. J. Radiat. Oncol. Biol. Phys. 1986;12:1279–1282.
9. Bayer C, Shi K, Astner ST, Maftei C-A, Vaupel P. Acute Versus Chronic Hypoxia: Why a Simplified Classification is Simply Not Enough. International Journal of Radiation Oncology*Biology*Physics 2011;80:965–968.
10. Vaupel P, Mayer A. Hypoxia in Tumors: Pathogenesis-Related Classification, Characterization of Hypoxia Subtypes, and Associated Biological and Clinical Implications. In: Swartz HM, Harrison DK, Bruley DF, eds. Oxygen Transport to Tissue XXXVI. Vol 812. New York, NY: Springer New York; 2014:19-24.
11. Baudelet C, Ansiaux R, Jordan BF, Havaux X, Macq B, Gallez B. Physiological noise in murine solid tumours using T2*-weighted gradient-echo imaging: a marker of tumour acute hypoxia? Phys Med Biol. 2004; 49(15):3389–411
12. Gallez B, Baudelet C, Jordan BF. Assessment of tumor oxygenation by electron paramagnetic resonance: principles and applications. NMR Biomed 2004;17:240–262.
13. Harris AL. Hypoxia—a key regulatory factor in tumour growth. Nat Rev Cancer 2002;2(1):38–47.
14. Semenza GL. Hypoxia-inducible factor 1: oxygen homeostasis and disease pathophysiology. Trends Mol Med 2001;7(8):345–50.
15. Walsh JC, Lebedev A, Aten E, Madsen K, Marciano L, Kolb HC. The Clinical Importance of Assessing Tumor Hypoxia: Relationship of Tumor Hypoxia to

Prognosis and Therapeutic Opportunities Antioxidants & Redox Signaling 2014; 21:1516–1554
16. Wang GL, Jiang BH, Rue EA, Semenza GL. Hypoxia-inducible factor 1 is a basic-helix-loop-helix-PAS heterodimer regulated by cellular O2 tension. Proc Natl Acad Sci USA 1995;92(12):5510–4.
17. Gustafsson MV, Zheng X, Pereira T, et al. Hypoxia requires notch signaling to maintain the undifferentiated cell state. Dev Cell 2005;9(5):617–28.
18. Patel NS, Li JL, Generali D, Poulsom R, Cranston DW, Harris AL. Upregulation of delta like 4 ligand in human tumor vasculature and the role of basal expression in endothelial cell function. Cancer Res 2005;65(19):8690–7.
19. Vogelstein B, Kinzler KW. Cancer genes and the pathways they control. Nat Med 2004;10(8):789–99.
20. Clottes E. Hypoxia-inducible factor 1: regulation, involvement in carcinogenesis and target for anticancer therapy. Bull. Cancer, 2005;92(2):119–127.
21. Liao D, Corle C, Seagroves TN, Johnson RS. Hypoxia-inducible factor-1alpha is a key regulator of metastasis in a transgenic modelof cancer initiation and progression. Cancer Res. 2007;67(2):563–572.
22. Tatum JL, Kelloff GJ, Gillies RJ, et al. Hypoxia: importance in tumor biology, noninvasive measurement by imaging, and value of its measurement in the management of cancer therapy. Int J Radiat Biol. 2006;82(10):699-757.
23. Vaupel P, Kelleher DK, Hockel M. Oxygen status of malignant tumors: pathogenesis of hypoxia and significance for tumor therapy. Semin Oncol. 2001;28(2 Suppl 8):29–35.
24. Das B, Tsuchida R, Malkin D, Koren G, Baruchel S, Yeger H. Hypoxia enhances tumor stemness by increasing the invasive and tumorigenic side population fraction. Stem Cells. 2008;26(7):1818–1830.
25. Graeber TG, Osmanian C, Jacks T, et al. Hypoxia-mediated selection of cells with diminished apoptotic potential in solid tumours. Nature 1996;379:88–91
26. Song CW, Griffin R, Park HJ. Influence of Tumor pH on Therapeutic Response. In: Teicher BA, ed. Cancer Drug Resistance. Totowa, NJ: Humana Press; 2006:21-42.
27. Abraham J, Salama NN, Azab AK. The role of P-glycoprotein in drug resistance in multiple myeloma. Leuk Lymphoma. 2015;56(1):26–33.
28. Cosse JP, Michiels C. Tumour hypoxia affects the responsiveness of cancer cells to chemotherapy and promotes cancer progression. Anticancer Agents Med Chem. 2008;8(7):790–797.
29. Pawlik TM, Keyomarsi K. Role of cell cycle in mediating sensitivity to radiotherapy. International Journal of Radiation Oncology*Biology*Physics. 2004;59(4):928–942.
30. Horsman MR, Wouters BG, Joiner MC, Overgaard J. The oxygen effect and fractionated radiotherapy. In: Joiner M, Van der Kongel A, editors. Basic clinical Radiobiology, 4th edition. London: Edward Arnold 2009;207-216.

31. Rockwell S. Manual de Radiotherapia Oncologia. Yale University; New Haven CT: 1989. Principios de radiobiologia.
32. Moeller BJ, Cao Y, Li CY, Dewhirst MW. Radiation activates HIF-1 to regulate vascular radiosensitivity in tumors: role of reoxygenation, free radicals, and stress granules. Cancer Cell. 2004;5(5):429-441.
33. Semenza GL. Targeting HIF-1 for cancer therapy. Nature Reviews Cancer. 2003;3(10):721-732.
34. Hockel M, Schlenger K, Aral B, Mitze M, Schaffer U, Vaupel P. Association between tumor hypoxia and malignant progression in advanced cancer of the uterine cervix. Cancer Res. 1996;56:4509–4515
35. Sullivan R, Graham CH. Hypoxia-driven selection of the metastatic phenotype. Cancer and Metastasis Reviews. 2007;26(2):319-331.
36. Lu X, Kang Y. Hypoxia and hypoxia-inducible factors: master regulators of metastasis. Clin Cancer Res 2010;16:5928–5935
37. Jin F, Brockmeier U, Otterbach F, Metzen E. New insight into the SDF-1/CXCR4 axis in a breast carcinoma model: hypoxia-induced endothelial SDF-1 and tumor cell CXCR4 are required for tumor cell intravasation. Mol Cancer Res 2012;10:1021–1031
38. Vaupel P, Höckel M, Mayer A. Detection and characterization of tumor hypoxia using pO2 histography. Antioxid Redox Signal. 2007;9:1221–35
39. McKeown SR. Defining normoxia, physoxia and hypoxia in tumours—implications for treatment response. The British Journal of Radiology. 2014;87(1035):20130676.
40. Rankin EB, Giaccia AJ. The role of hypoxia-inducible factors in tumorigenesis. Cell Death Differ. 2008;15:678–85
41. Hockel M, Vaupel P. Tumor Hypoxia: Definitions and Current Clinical, Biologic, and Molecular Aspects. Journal of the National Cancer Institute. 2001;93:266–276
42. Vaupel P, Mayer A. Hypoxia in cancer: Significance and impact on clinical outcome. Cancer Metastasis Rev. 2007;26:225-239
43. Vaupel P. Hypoxia and Aggressive Tumor Phenotype: Implications for Therapy and Prognosis. The Oncologist. 2008;13:21–26
44. Vaupel P. The Role of Hypoxia-Induced Factors in Tumor Progression. The Oncologist. 2004;9:10–17
45. Vaupel P, Mayer A. Tumor Hypoxia: Causative Mechanisms, Microregional Heterogeneities, and the Role of Tissue-Based Hypoxia Markers. In: Luo Q, Li LZ, Harrison DK, Shi H, Bruley DF, eds. Oxygen Transport to Tissue XXXVIII. Vol 923. Cham: Springer International Publishing; 2016:77-86.
46. Lanzen J, Braun RD, Klitzman B, Brizel D, Secomb TW, Dewhirst MW. Direct demonstration of instabilities in oxygen concentrations within the extravascular compartment of an experimental tumor. Cancer Res. 2006;66:2219–23

47. Olive PL, Vikse C, Trotter MJ. Measurement of oxygen diffusion distance in tumor cubes using a fluorescent hypoxia probe. International Journal of Radiation Oncology*Biology*Physics. 1992;22:397–402
48. Torres-Filho IP, Leunig M, Yuan F, Intaglietta M, Jain RK. Noninvasive measurement of microvascular and interstitial oxygen profiles in a human tumor in SCID mice. Proc Natl Acad Sci USA. 1994;91:2081–5
49. Vaupel P, Mayer A. Tumor Oxygenation Status: Facts and Fallacies. In: Halpern HJ, LaManna JC, Harrison DK, Epel B, eds. Oxygen Transport to Tissue XXXIX. Vol 977. Cham: Springer International Publishing; 2017:91-99
50. Vaupel P, Schlenger K, Knoop C, et al. Oxygenation of human tumors: evaluation of tissue oxygen distribution in breast cancers by computerized O2 tension measurements. Cancer Res. 1991;51(12):3316–3322
51. Grosu AL, Souvatzoglou M, Röper B, et al. Hypoxia imaging with FAZA-PET and theoretical considerations with regard to dose painting for individualization of radiotherapy in patients with head and neck cancer. International Journal of Radiation Oncology*Biology*Physics. 2007;69(2):541–551
52. Vordermark D, Horsman MR. Hypoxia as a Biomarker and for Personalized Radiation Oncology, in: Baumann, M, Krause, M, Cordes, N (Eds), Molecular Radio-Oncology Springer Berlin Heidelberg, Berlin, Heidelberg, 2016:123–142
53. Stone HB, Brown JM, Phillips TL, Sutherland RM .Oxygen in human tumors: correlations between methods of measurement and response to therapy Summary of a workshop held November 19–20, 1992, at the National Cancer Institute, Bethesda, Maryland. Radiat Res. 1993;136:422–434
54. Rudat V, Stadler P, Becker A, et al. Predictive value of the tumor oxygenation by means of pO2 histography in patients with advanced head and neck cancer. Strahlenther Onkol. 2001;177:462–468
55. Nordsmark M, Bentzen SM, Rudat V, et al. Prognostic value of tumor oxygenation in 397 head and neck tumors after primary radiation therapy An international multi-center study. Radiother Oncol. 2005;77:18–24
56. Fyles A, Milosevic M, Pintilie M, et al. Long-term performance of interstitial fluid pressure and hypoxia as prognostic factors in cervix cancer. Radiother Oncol. 2006;80:132–137
57. Lyng H, Sundfør K, Tropé C, Rofstad EK. Disease control of uterine cervical cancer: relationships to tumor oxygen tension, vascular density, cell density, and frequency of mitosis and apoptosis measured before treatment and during radiotherapy. Clin Cancer Res. 2000;6:1104–1112
58. Nordsmark M, Alsner J, Keller J, et al. Hypoxia in human soft tissue sarcomas: adverse impact on survival and no association with p53 mutations. Br J Cancer. 2001;84:1070–1075
59. Turaka A, Buyyounouski MK, Hanlon AL, Horwitz EM, Greenberg RE, Movsas B. Hypoxic prostate/muscle Po2 ratio predicts for outcome in patients with localized prostate cancer: long-term results. International Journal of Radiation Oncology*Biology*Physics. 2011;82:e433–e439

60. Sundfør K, Lyng H, Rofstad EK. Tumour hypoxia and vascular density as predictors of metastasis in squamous cell carcinoma of the uterine cervix. Br J Cancer. 1998;78:822–827
61. Gaertner FC, Souvatzoglou M, Brix G, Beer AJ. Imaging of hypoxia using PET and MRI. Curr Pharm Biotechnol. 2012;13:552–570
62. Nordsmark M, Overgaard M, Overgaard J. Pretreatment oxygenation predicts radiation response in advanced squamous cell carcinoma of the head and neck. Radiother Oncol. 1996;41:31–39
63. Griffiths JR, Robinson SP. The OxyLite: a fibre-optic oxygen sensor. The British Journal of Radiology. 1999; 72: 627–630.
64. Vikram DS, Zweier JL, Kuppusamy P. Methods for noninvasive imaging of tissue hypoxia. Antioxid Redox Signal. 2007;9:1745–1756
65. Wilson DF, Cerniglia GJ. Localization of tumors and evaluation of their state of oxygenation by phosphorescence imaging. Cancer Res. 1992;52:3988–3993
66. Fukumura D, Xu L, Chen Y, Gohongi T, Seed B, Jain RK. Hypoxia and acidosis independently up-regulate vascular endothelial growth factor transcription in brain tumors *in vivo*. Cancer Res. 2001;61:6020–6024
67. Zhao D, Jiang L, Hahn EW, Mason RP. Tumor physiologic response to combretastatin A4 phosphate assessed by MRI. International Journal of Radiation Oncology*Biology*Physics. 2005;62:872–880
68. Kodibagkar VD, Wang X, Mason RP. Physical principles of quantitative nuclear magnetic resonance oximetry. Front Biosci. 2008;13:1371–1384
69. Zhang W, Ito Y, Berlin E, Roberts R, Berkowitz BA. Role of hypoxia during normal retinal vessel development and in experimental retinopathy of prematurity. Invest Ophthalmol Vis Sci. 2003;44(7):3119–3123
70. Mason RP, Rodbumrung W, Antich PP. Hexafluorobenzene: a sensitive 19F NMR indicator of tumor oxygenation. NMR Biomed. 1996;9(3):125–134
71. Zhao D, Ran S, Constantinescu A, Hahn EW, Mason RP. Tumor oxygen dynamics: correlation of *in vivo* MRI with histological findings. Neoplasia. 2003;5(4):308–318
72. Mason RP, Constantinescu A, Hunjan S, et al. Regional tumor oxygenation and measurement of dynamic changes. Radiat Res. 1999;152(3):239–249
73. Xia M, Kodibagkar V, Liu H, Mason RP. Tumour oxygen dynamics measured simultaneously by near-infrared spectroscopy and 19F magnetic resonance imaging in rats. Phys Med Biol. 2006;51(1):45–60
74. Hunjan S, Zhao D, Constantinescu A, Hahn EW, Antich PP, Mason RP. Tumor oximetry: demonstration of an enhanced dynamic mapping procedure using fluorine-19 echo planar magnetic resonance imaging in the Dunning prostate R3327-AT1 rat tumor. International Journal of Radiation Oncology*Biology*Physics. 2001;49(4):1097–1108
75. Jordan BF, Cron GO, Gallez B. Rapid monitoring of oxygenation by 19F magnetic resonance imaging: Simultaneous comparison with fluorescence quenching. Magn Reson Med. 2009;61(3):634–638

76. Bourke VA, Zhao D, Gilio J, et al. Correlation of radiation response with tumor oxygenation in the Dunning prostate R3327-AT1 tumor. International Journal of Radiation Oncology*Biology*Physics. 2007;67(4):1179–1186
77. Magat J, Jordan BF, Cron GO, Gallez B. Noninvasive mapping of spontaneous fluctuations in tumor oxygenation using 19F. MRI Med Phys. 2010; 37(10):5434–41
78. Mason RP, Antich PP, Babcock EE, Gerberich JL, Nunnally RL. Perfluorocarbon imaging *in vivo*: a 19F MRI study in tumor-bearing mice. Magnetic Resonance Imaging. 1989;7:475 – 485
79. Zhao D, Jiang L, Mason RP. Measuring changes in tumor oxygenation. Methods Enzymol. 2004;386:378–418.
80. Krishna MC, Subramanian S, Kuppusamy P, Mitchell JB. Magnetic resonance imaging for *in vivo* assessment of tissue oxygenation concentration. Semin Radiat Oncol. 2001;11:58–69
81. Lurie DJ. Free radical imaging. Br J Radiol. 2001;74:782–784
82. Yasui H, Matsumoto S, Devasahayam N, et al. Low-field magnetic resonance imaging to visualize chronic and cycling hypoxia in tumor-bearing mice. Cancer Res. 2010;70(16):6427–36
83. Krishna MC, Matsumoto S, Yasui H, et al. Electron paramagnetic resonance imaging of tumor pO(2). Radiat Res. 2012;177(4):376–86
84. Samouilov A, Caia GL, Kesselring E, Petryakov S, Wasowicz T, Zweier JL. Development of a hybrid EPR/NMR coimaging system. Magn Reson Med. 2007;58: 56–166
85. Matsumoto S, Hyodo F, Subramanian S, et al. Low-field paramagnetic resonance imaging of tumor oxygenation and glycolytic activity in mice. J Clin Invest. 2008;118:1965–1973
86. Elas M, Bell R, Hleihel D, et al. Electron paramagnetic resonance oxygen image hypoxic fraction plus radiation dose strongly correlates with tumor cure in FSa fibrosarcomas. International Journal of Radiation Oncology*Biology*Physics. 2008;71:542–549
87. Gallez B, Jordan BF, Baudelet C, Misson PD. Pharmacological modifications of the partial pressure of oxygen in murine tumors: evaluation using *in vivo* EPR oximetry. Magn Reson Med. 1999;42(4):627–30
88. Ansiaux R, Baudelet C, Jordan BF, et al. Thalidomide radiosensitizes tumors through early changes in the tumor microenvironment. Clin Cancer Res. 2005;11(2 Pt 1):743–50
89. Segers J, Crokart N, Danhier P, Gregoire V, Jordan BF, Gallez B. Use of xanthinol nicotinate as a co-treatment for radio- and chemo-therapy in experimental tumors. Int J Cancer. 2010;126(2):583–8
90. Crokart N, Radermacher K, Jordan BF, et al. Tumor radiosensitization by antiinflammatory drugs: evidence for a new mechanism involving the oxygen effect. Cancer Res. 2005; 65(17):7911–6

91. Crokart N, Jordan BF, Baudelet C, et al. Glucocorticoids modulate tumor radiation response through a decrease in tumor oxygen consumption. Clin Cancer Res. 2007;13(2 Pt 1):630–5
92. Diepart C, Karroum O, Magat J, et al. Arsenic trioxide treatment decreases the oxygen consumption rate of tumor cells and radiosensitizes solid tumors. Cancer Res. 2012;72(2):482–90
93. De Preter G, Deriemaeker C, Danhier P, et al. A fast hydrogen sulfide-releasing donor increases the tumor response to radiotherapy. Mol Cancer Ther. 2016;15(1):154–61
94. Jarvis LA, Williams BB, Schaner PE, et al. Phase 1 Clinical Trial of OxyChip, an Implantable Absolute pO2 Sensor for Tumor Oximetry. International Journal of Radiation Oncology*Biology*Physics. 2016;96(2):S109-S110.
95. Williams BB, Khan N, Zaki B, Hartford A, Ernstoff MS, and Swartz HM. Clinical electron paramagnetic resonance (EPR) oximetry using India ink. Adv Exp Med Biol. 2010;662:149–156
96. Horsman MR, Mortensen LS, Petersen JB, Busk M, Overgaard J. Imaging hypoxia to improve radiotherapy outcome. Nature Reviews Clinical Oncology. 2012;9:674-687
97. Chapman JD, Coia LR, Stobbe CC, Engelhardt EL, Fenning MC, Schneider RF. Prediction of tumour hypoxia and radioresistance with nuclear medicine markers. Br J Cancer Suppl. 1996;27:S204-208
98. Varia MA, Calkins-Adams DP, Rinker LH, et al. Pimonidazole: A Novel Hypoxia Marker for Complementary Study of Tumor Hypoxia and Cell Proliferation in Cervical Carcinoma. Gynecologic Oncology. 1998;71:270–277
99. Evans SM, Hahn S, Pook DR, et al. Detection of hypoxia in human squamous cell carcinoma by EF5 binding. Cancer Res. 2000;60:2018–2024
100. Raleigh JA, Chou SC, Arteel GE, Horsman MR. Comparisons among pimonidazole binding, oxygen electrode measurements, and radiation response in C3H mouse tumors. Radiat Res. 1999;151:580–589
101. Fleming IN, Manavaki R, Blower PJ, et al. Imaging tumour hypoxia with positron emission tomography. Br J Cancer. 2015;112(2):238–50
102. Rasey JS, Nelson NJ, Chin L, Evans ML, Grunbaum Z. Characteristics of the binding of labeled fluoromisonidazole in cells *in vitro*. Radiat Res. 1990;122:301–308
103. Bruehlmeier M, Roelcke U, Schubiger PA, Ametamey SM. Assessment of hypoxia and perfusion in human brain tumors using PET with 18F-fluoromisonidazole and 15O-H2O. J Nucl Med. 2004;45:1851–1859
104. Gagel B, Reinartz P, Dimartino E, et al. pO2 Polarography versus positron emission tomography ([(18)F] fluoromisonidazole, [(18)F]-2-fluoro-2′-deoxyglucose) An appraisal of radiotherapeutically relevant hypoxia. Strahlenther Onkol. 2004;180:616–622
105. Zimny M, Gagel B, DiMartino E, et al. FDG—a marker of tumour hypoxia? A comparison with [18F]fluoromisonidazole and pO2-polarography in

metastatic head and neck cancer. Eur J Nucl Med Mol Imaging. 2006;33:1426–1431
106. Mortensen LS, Buus S, Nordsmark M, et al. Identifying hypoxia in human tumors: a correlation study between 18F-FMISO PET and the Eppendorf oxygen-sensitive electrode. Acta Oncol. 2010;49(7):934–40
107. Schuetz M, Schmid MP, Pötter R, et al. Evaluating repetitive 18F-fluoroazomycin-arabinoside (18FAZA) PET in the setting of MRI guided adaptive radiotherapy in cervical cancer. Acta Oncol. 2010;49:941–947
108. Van Loon J, Janssen MHM, Öllers M, et al. PET imaging of hypoxia using [18F] HX4: a phase I trial. Eur J Nucl Med Mol Imaging. 2010;37:1663–1668
109. Kumar P, Stypinski D, Xia H, McEwan AJB, Machulla H-J, Wiebe LI. Fluoroazomycin arabinoside (FAZA): synthesis, 2H and 3H-labelling and preliminary biological evaluation of a novel 2-nitroimidazole marker of tissue hypoxia. J Label Compd Radiopharm. 1999;42:3–16
110. Busk M, Horsman MR, Jakobsen S, et al. Imaging hypoxia in xenografted and murine tumors with 18F-fluoroazomycin arabinoside: a comparative study involving microPET, autoradiography, PO2-polarography, and fluorescence microscopy. International Journal of Radiation Oncology*Biology*Physics. 2008;70:1202–1212
111. Tran L-B-A, Bol A, Labar D, et al. Hypoxia imaging with the nitroimidazole 18F-FAZA PET tracer: a comparison with OxyLite, EPR oximetry and 19F-MRI relaxometry. Radiother Oncol. 2012;105:29–35
112. Mortensen LS, Johansen J, Kallehauge J, et al. FAZA PET/CT hypoxia imaging in patients with squamous cell carcinoma of the head and neck treated with radiotherapy: results from the DAHANCA 24 trial. Radiother Oncol. 2012;105:14–20
113. Chen L, Zhang Z, Kolb HC, Walsh JC, Zhang J, Guan Y. 18F–HX4 hypoxia imaging with PET/CT in head and neck cancer: A comparison with 18F–FMISO. Nucl Med Commun. 2012;33(10):1096–1102
114. Zegers CML, Van Elmpt W, Wierts R, et al. Hypoxia imaging with [18F]HX4 PET in NSCLC patients: Defining optimal imaging parameters. Radiother Oncol. 2013;109: 58–64
115. Rischin D, Hicks RJ, Fischer R, et al. Prognostic significance of [18F]-misonidazole positron emission tomography-detected tumor hypoxia in patients with advanced head and neck cancer randomly assigned to chemoradiation with or without tirapazamine: a substudy of Trans-Tasman Radiation Oncology Group study 9802. J Clin Oncol. 2006;24:2098–2104
116. Reischl G, Dorow DS, Cullinane C, et al. Imaging of tumor hypoxia with [124I]IAZA in comparison with [18F]FMISO and [18F]FAZA–first small animal PET results. J Pharm Pharm Sci. 2007;10:203–211

117. Urtasun RC, Parliament MB, McEwan AJ, et al. Measurement of hypoxia in human tumours by non-invasive spect imaging of iodoazomycin arabinoside. Br J Cancer. 1996;74(Suppl):S209–S212
118. Parliament MB, Chapman JD, Urtasun RC, et al. Non-invasive assessment of human tumour hypoxia with 123I-iodoazomycin arabinoside: preliminary report of a clinical study. Br J Cancer. 1992;65:90–95
119. Ballinger JR, Kee JW, Rauth AM. *In vitro* and *in vivo* evaluation of a technetium-99m-labeled 2-nitroimidazole (BMS181321) as a marker of tumor hypoxia. J Nucl Med. 1996;37:1023–1031
120. Melo T, Duncan J, Ballinger JR, Rauth AM. BRU59-21, a second-generation 99mTc-labeled 2-nitroimidazole for imaging hypoxia in tumors. J Nucl Med. 2000;41:169–176
121. Holland JP, Lewis JS, Dehdashti F. Assessing tumor hypoxia by positron emission tomography with Cu-ATSM. Q J Nucl Med Mol Imaging. 2009;53:193–200
122. Burgman P, O'Donoghue JA, Lewis JS, Welch MJ, Humm JL, Ling CC. Cell line-dependent differences in uptake and retention of the hypoxia-selective nuclear imaging agent Cu-ATSM. Nucl Med Biol. 2005;32(6):623–30
123. Yoshii Y, Yoneda M, Ikawa M, et al. Radiolabeled Cu-ATSM as a novel indicator of overreduced intracellular state due to mitochondrial dysfunction: studies with mitochondrial DNA-less ρ0 cells and cybrids carrying MELAS mitochondrial DNA mutation. Nucl Med Biol. 2012;39:177–185
124. O'Donoghue JA, Zanzonico P, Pugachev A, et al. Assessment of regional tumor hypoxia using 18F-fluoromisonidazole and 64Cu(II)-diacetyl-bis(N4- methylthiosemicarbazone) positron emission tomography: comparative study featuring microPET imaging, pO2 probe measurement, autoradiography, and fluorescent microscopy in the R3327–AT and FaDu rat tumor models. International Journal of Radiation Oncology*Biology*Physics. 2005;61(5):1493–1502
125. Hueting R, Kersemans V, Cornelissen B, et al. A comparison of the behavior of (64)Cu-acetate and (64)Cu-ATSM *in vitro* and *in vivo*. J Nucl Med. 2014;55(1):128–34
126. Yuan H, Schroeder T, Bowsher JE, Hedlund LW, Wong T, Dewhirst MW Intertumoral differences in hypoxia selectivity of the PET imaging agent 64Cu(II)-diacetyl-bis(N4-methylthiosemicarbazone). J Nucl Med. 2006;47(6):989–98
127. Matsumoto K, Szajek L, Krishna MC, et al. The influence of tumor oxygenation on hypoxia imaging in murine squamous cell carcinoma using [64Cu]Cu-ATSM or [18F]Fluoromisonidazole positron emission tomography. Int J Oncol. 2007;30(4):873–81
128. Hansen AE, Kristensen AT, Jørgensen JT, et al. 64Cu-ATSM and 18FDG PET uptake and 64Cu-ATSM autoradiography in spontaneous canine

tumors: comparison with pimonidazole hypoxia immunohistochemistry. Radiation Oncology. 2012;7(1):89.
129. Carlin S, Zhang H, Reese M, Ramos NN, Chen Q, Ricketts S-A. A comparison of the imaging characteristics and microregional distribution of 4 hypoxia PET tracers. J Nucl Med. 2014;55(3):515-521.
130. 1. Haugland HK, Vukovic V, Pintilie M, et al. Expression of hypoxia-inducible factor-1alpha in cervical carcinomas: correlation with tumor oxygenation. Int J Radiat Oncol Biol Phys. 2002;53(4):854-861.
131. 1. Loncaster JA, Harris AL, Davidson SE, et al. Carbonic anhydrase (CA IX) expression, a potential new intrinsic marker of hypoxia: correlations with tumor oxygen measurements and prognosis in locally advanced carcinoma of the cervix. Cancer Res. 2001;61(17):6394-6399.
132. 1. Airley R, Loncaster J, Davidson S, et al. Glucose transporter glut-1 expression correlates with tumor hypoxia and predicts metastasis-free survival in advanced carcinoma of the cervix. Clin Cancer Res. 2001;7(4):928-934.
133. Zhong H, Mabjeesh N, Willard M, Simons J. Nuclear expression of hypoxia-inducible factor 1alpha protein is heterogeneous in human malignant cells under normoxic conditions. Cancer Lett. 2002;181(2):233-238.
134. Le QT, Sutphin PD, Raychaudhuri S, et al. Identification of osteopontin as a prognostic plasma marker for head and neck squamous cell carcinomas. Clin Cancer Res. 2003;9:59–67
135. Overgaard J, Eriksen JG, Nordsmark M, et al. Plasma osteopontin, hypoxia, and response to the hypoxia sensitiser nimorazole in radiotherapy of head and neck cancer: results from the DAHANCA 5 randomised double-blind placebo-controlled trial. Lancet Oncol. 2005;6:757–764
136. Güttler A, Giebler M, Cuno P, et al. Osteopontin and splice variant expression level in human malignant glioma: radiobiologic effects and prognosis after radiotherapy. Radiother Oncol. 2013;108:535–540
137. Harris BHL, Barberis A, West CML, Buffa FM. Gene Expression Signatures as Biomarkers of Tumour Hypoxia. Clinical Oncology. 2015;27(10):547-560.
138. Lyng H, Vorren AO, Sundfor K, et al. Assessment of tumor oxygenation in human cervical carcinoma by use of dynamic Gd-DTPA-enhanced MR imaging. J Magn Reson Imaging. 2001;14:750–756
139. Price JM, Robinson SP, Koh DM. Imaging hypoxia in tumours with advanced MRI. Q J Nucl Med Mol Imaging. 2013;57:257–270
140. Koh D-M, Collins DJ. Diffusion-Weighted MRI in the Body: Applications and Challenges in Oncology. American Journal of Roentgenology. 2007;188(6):1622-1635.
141. Cooper RA, Carrington BM, Loncaster JA, et al. Tumour oxygenation levels correlate with dynamic contrast-enhanced magnetic resonance imaging parameters in carcinoma of the cervix. Radiother Oncol. 2000;57:53–59

142. Newbold K, Castellano I, Charles-Edwards E, et al. An exploratory study into the role of dynamic contrast-enhanced magnetic resonance imaging or perfusion computed tomography for detection of intratumoral hypoxia in head-and-neck cancer. International Journal of Radiation Oncology*Biology*Physics. 2009;74:29–37
143. Donaldson SB, Betts G, Bonington SC, et al. Perfusion estimated with rapid dynamic contrast-enhanced magnetic resonance imaging correlates inversely with vascular endothelial growth factor expression and pimonidazole staining in head-and-neck cancer: a pilot study. International Journal of Radiation Oncology*Biology*Physics. 2011;81:1176–1183
144. Swanson KR, Chakraborty G, Wang CH, et al. Complementary but distinct roles for MRI and 18F-fluoromisonidazole PET in the assessment of human glioblastomas. J Nucl Med. 2009;50:36–44
145. Colliez F, Gallez B, Jordan BF. Assessing Tumor Oxygenation for Predicting Outcome in Radiation Oncology: A Review of Studies Correlating Tumor Hypoxic Status and Outcome in the Preclinical and Clinical Settings. Frontiers in Oncology. 2017;7:10
146. Komar G, Seppänen M, Eskola O, et al. 18F-EF5: a new PET tracer for imaging hypoxia in head and neck cancer. J Nucl Med. 2008;49:1944–1951
147. Lehtio K, Eskola O, Vijanen T, et al. Imaging perfusion and hypoxia with PET to predict radiotherapy response in head-and-neck cancer. International Journal of Radiation Oncology*Biology*Physics. 2004;59:971–982
148. Ng CS, Kodama Y, Mullani NA, et al. Tumor Blood Flow Measured by Perfusion Computed Tomography and 15O-Labeled Water Positron Emission Tomography: A Comparison Study. Journal of Computer Assisted Tomography. 2009;33(3):460‑5.
149. Hermans R, Lambin P, Van der Goten A, et al. Tumoural perfusion as measured by dynamic computed tomography in head and neck carcinoma. Radiother Oncol. 1999;53(2):105-111.
150. Bisdas S, Nguyen SA, Anand SK, Glavina G, Day T, Rumboldt Z. Outcome Prediction After Surgery and Chemoradiation of Squamous Cell Carcinoma in the Oral Cavity, Oropharynx, and Hypopharynx: Use of Baseline Perfusion CT Microcirculatory Parameters vs. Tumor Volume. International Journal of Radiation Oncology*Biology*Physics. 2009;73(5):1313-1318.
151. Truong MT, Saito N, Ozonoff A, et al. Prediction of Locoregional Control in Head and Neck Squamous Cell Carcinoma with Serial CT Perfusion during Radiotherapy. American Journal of Neuroradiology. 2011;32(7):1195-1201.
152. Lebon V, Carlier PG, Brillault-Salvat C, Leroy-Willig A. Simultaneous measurement of perfusion and oxygenation changes using a multiple gradient-echo sequence: application to human muscle study. Magnetic Resonance Imaging. 1998;16:721–729

153. Baudelet C, Gallez B. How does blood oxygen level-dependent (BOLD) contrast correlate with oxygen partial pressure (pO2) inside tumors? Magn Reson Med. 2002; 48(6):980–6
154. Hallac RR, Zhou H, Pidikiti R, et al. Correlations of noninvasive BOLD and TOLD MRI with pO2 and relevance to tumor radiation response. Magn Reson Med. 2014;71:1863–1873.
155. Hoskin PJ, Carnell DM, Taylor NJ, et al Hypoxia in prostate cancer: correlation of BOLD-MRI with pimonidazole immunohistochemistry-initial observations. International Journal of Radiation Oncology*Biology*Physics. 2007;68(4):1065–71
156. McPhail LD, Robinson SP. Intrinsic susceptibility MR imaging of chemically induced rat mammary tumors: relationship to histologic assessment of hypoxia and fibrosis. Radiology. 2010;254(1):110–8
157. Jordan BF, Crokart N, Baudelet C, Cron GO, Ansiaux R, Gallez B. Complex relationship between changes in oxygenation status and changes in R*2: The case of insulin and NS-398, two inhibitors of oxygen consumption. Magnetic Resonance in Medicine. 2006;56:637–643
158. Baudelet C, Gallez B. Current Issues in the Utility of Blood Oxygen Level Dependent MRI for the Assessment of Modulations in Tumor Oxygenation. Current Medical Imaging Reviews. 2005;1(3):229–43.
159. Young IR, Clarke GJ, Bailes DR, Pennock JM, Doyle FH, Bydder GM. Enhancement of relaxation rate with paramagnetic contrast agents in NMR imaging. J Comput Tomogr. 1981;5:543–547
160. Uematsu H, Takahashi M, Hatabu H, et al. Changes in T1 and T2 observed in brain magnetic resonance imaging with delivery of high concentrations of oxygen. J Comput Assist Tomogr . 2007;31(5):662–5
161. Jones RA, Ries M, Moonen CT, Grenier N. Imaging the changes in renal T1 induced by the inhalation of pure oxygen: a feasibility study. Magn Reson Med. 2002;47(4):728–735
162. O'Connor JP, Jackson A, Buonaccorsi GA, et al. Organ-specific effects of oxygen and carbogen gas inhalation on tissue longitudinal relaxation times. Magn Reson Med. 2007;58(3):490–496
163. Shipitsin M, Campbell LL, Argani P, et al. Molecular definition of breast tumor heterogeneity Cancer Cell 2007;11:259–73
164. O'Connor JP, Jackson A, Asselin MC, Buckley DL, Parker GJ, Jayson GC. Quantitative imaging biomarkers in the clinical development of targeted therapeutics: current and future perspectives Lancet Oncol 2008;9:766–76
165. O'Connor JPB, Boult JKR, Jamin Y, et al. Oxygen-enhanced MRI accurately identifies, quantifies, and maps tumor hypoxia in preclinical cancer models. Cancer Res. 2016;76:787-795
166. Little R, Jamin Y, Boult JKR, et al. Mapping Hypoxia in Renal Carcinoma with Oxygen-enhanced MRI: Comparison with Intrinsic Susceptibility MRI and Pathology .Radiology. 2018

167. Jordan BF, Magat J, Colliez F, et al. Mapping of oxygen by imaging lipids relaxation enhancement: a potential sensitive endogenous MRI contrast to map variations in tissue oxygenation. Magn Reson Med. 2013;70:732-744
168. Colliez F, Neveu MA, Magat J, Cao-PhamTT, Gallez B, Jordan BF. Qualification of a noninvasive magnetic resonance imaging biomarker to assess tumor oxygenation. Clin Cancer Res. 2014;20:5403-5411
169. Colliez F, Safronova MM, Magat J, et al. Oxygen mapping within healthy and acutely infarcted brain tissue in humans using the NMR relaxation of lipids: a proof-of-concept translational study. PLoS One. 2015
170. Safronova MM, Colliez F, Magat J, et al. Mapping of global R1 and R2* values versus lipids R1 values as potential markers of hypoxia in human glial tumors: a feasibility study. Magn Reson Imaging. 2016;34(2):105–13
171. Churchill-Davidson I. The oxygen effect in radiotherapy – historical review. Frontiers Radiat Ther Oncol. 1968;1:1–15
172. Overgaard J. Sensitization of hypoxic tumour cells – clinical experience. Int J Radiat Biol. 1989;56:801–11
173. Suit HD, Marshall N, Woerner D. Oxygen, oxygen plus carbon dioxide, and radiation therapy of a mouse mammary carcinoma. Cancer. 1972;30:1154–8
174. Horsman MR, Lindegaard JC, Grau C, Nordsmark M, Overgaard J. Dose–response modifiers in radiation therapy. In: Gunderson LL, Tepper JE (eds) Clinical radiation oncology, 2nd edition Philadelphia: Churchill Livingstone, 2007;59–73
175. Siemann DW, Hill RP, Bush RS. The importance of the pre-irradiation breathing times of oxygen and carbogen (5% CO2; 95% O2) on the *in vivo* radiation response of a murine sarcoma. International Journal of Radiation Oncology*Biology*Physics. 1977;2:903–11
176. Horsman MR. Nicotinamide and other benzamide analogs as agents for overcoming hypoxic cell radiation resistance in tumours. Acta Oncol. 1995;34:571–87
177. Kaanders JH, Bussink J, van der Kogel AJ. ARCON: a novel biology-based approach in radiotherapy. The Lancet Oncology. 2002;3(12):728-737.
178. Janssens GO, Rademakers SE, Terhaard CH, et al. Accelerated radiotherapy with carbogen and nicotinamide for laryngeal cancer: results of a phase III randomized trial. J Clin Oncol. 2012;30:1777–83
179. Grau C, Overgaard J. Significance of hemoglobin concentration for treatment outcome. In: Molls M, Vaupel P (eds) Medical radiology: blood perfusion and microenvironment of human tumours Heidelberg: Springer-Verlag, 1997;101–12
180. Hirst DG. Anemia: a problem or an opportunity in radiotherapy? International Journal of Radiation Oncology*Biology*Physics. 1986;12:2009–17

181. Grogan M, Thomas GM, Melamed I, et al. The importance of hemoglobin levels during radiotherapy for carcinoma of the cervix. Cancer. 1999;86:1528–36
182. Overgaard J, Sand Hansen H, Overgaard M, et al. A randomised double-blind phase III study of nimorazole as a hypoxic radiosensitizer of primary radiotherapy in supraglottic larynx and pharynx carcinoma Results of the Danish head and neck cancer study (DAHANCA) protocol 5–85. Radiother Oncol. 1998;46:135–46
183. Horsman MR, Van der Kongel AJ. Therapeutic approaches to tumour hypoxia In: Joiner M, Van der Kongel A, editors. Basic clinical Radiobiology, 4th edition. London: Edward Arnold 2009; 233-245
184. Henke M, Laszig R, Rube C, et al. Erythropoietin to treat head and neck cancer patients with anaemia undergoing radiotherapy: randomized double blind, placebo-controlled trial. Lancet. 2003;362:1255–60
185. Machtay M, Pajak TF, Suntharalingam M, et al. Radiotherapy with or without erythropoietin for anemic patients with head and neck cancer: a randomized trial of the Radiation Therapy Oncology Group (RTOG 99–03). International Journal of Radiation Oncology*Biology*Physics. 2007;69:1008–17
186. Raykov Z, Grekova SP, Bour G, et al. Myo-inositol trispyrophosphate-mediated hypoxia reversion controls pancreatic cancer in rodents and enhances gemcitabine efficacy. Int J Cancer. 2014;134:2572–82
187. Kieda C, El Hafny-Rahbi B, Collet G, et al. Stable tumor vessel normalization with pO_2 increase and endothelial PTEN activation by inositol trispyrophosphate brings novel tumor treatment. J Mol Med. 2013;91:883–99
188. Suh JH. Efaproxiral: a novel radiation sensitizer. Expert Opinion on Investigational Drugs. 2004; 13:543–550
189. Suh JH, Stea B, Tankel K, et al. Results of the Phase III ENRICH (RT-016) Study of Efaproxiral Administered Concurrent with Whole Brain Radiation Therapy (WBRT) in Women with Brain Metastases from Breast Cancer. International Journal of Radiation Oncology*Biology*Physics. 2008;72:S50–S51
190. Eisenbrey JR, Shraim R, Liu J-B, et al. Sensitization of Hypoxic Tumors to Radiation Therapy Using Ultrasound-Sensitive Oxygen Microbubbles. International Journal of Radiation Oncology*Biology*Physics. 2018;101:88–96
191. Dewhirst MW, Navia IC, Brizel DM, Willett C, Secomb TW. Multiple Etiologies of Tumor Hypoxia Require Multifaceted Solutions. Clinical Cancer Research. 2007;13:375–377
192. Secomb TW, Hsu R, Ong ET, Gross JF, Dewhirst MW. Analysis of the effects of oxygen supply and demand on hypoxic fraction in tumors. Acta Oncol. 1995;34(3):313-316.
193. Gallez B, Neveu M-A, Danhier P, Jordan BF. Manipulation of tumor oxygenation and radiosensitivity through modification of cell respiration A critical review of approaches and imaging biomarkers for therapeutic guidance. Biochimica et Biophysica Acta (BBA) – Bioenergetics. 2017;1858:700–711

194. Milas L, Hunter NR, Mason KA, et al. Role of reoxygenation in induction of enhancement of tumor radioresponse by paclitaxel. Cancer Res. 1995;55:3564–68
195. Danhier F, Danhier P, Magotteaux N, et al. Electron Paramagnetic Resonance Highlights That the Oxygen Effect Contributes to the Radiosensitizing Effect of Paclitaxel. PLoS ONE. 2012;7:e40772
196. Jordan BF, Sonveaux P. Targeting Tumor Perfusion and Oxygenation to Improve the Outcome of Anticancer Therapy. Front Pharmacol. 2012; 3
197. Jain RK. Normalization of Tumor Vasculature: An Emerging Concept in Antiangiogenic Therapy. Science. 2005;307:58–62
198. Ansiaux R, Baudelet C, Jordan BF, et al. Mechanism of Reoxygenation after Antiangiogenic Therapy Using SU5416 and Its Importance for Guiding Combined Antitumor Therapy. Cancer Research. 2006;66:9698–9704
199. Ansiaux R, Dewever J, Grégoire V, Feron O, Jordan BF, Gallez B. Decrease in Tumor Cell Oxygen Consumption after Treatment with Vandetanib (ZACTIMA™; ZD6474; and its Effect on Response to Radiotherapy. Radiation Research. 2009;172:584–591
200. Crokart N, Danhier F, Daugimont L, et al. Potentiation of radiotherapy by a localized antiangiogenic gene therapy. Radiotherapy and Oncology. 2013;107:252–258
201. Karroum O, Kengen J, Danhier P, et al. Tumor reoxygenation following administration of Mitogen-Activated Protein Kinase inhibitors: A rationale for combination with radiation therapy. Radiotherapy and Oncology. 2012;105:64–71
202. Karroum O, Kengen J, Grégoire V, Gallez B, Jordan BF. Tumor Reoxygenation Following Administration of the EGFR Inhibitor, Gefitinib, in Experimental Tumors. In: Van Huffel S, Naulaers G, Caicedo A, Bruley DF, Harrison DK, eds. Oxygen Transport to Tissue XXXV. Vol 789. New York, NY: Springer New York; 2013:265-271.
203. Ashton TM, Fokas E, Kunz-Schughart LA, et al. The anti-malarial atovaquone increases radiosensitivity by alleviating tumour hypoxia. Nature Communications. 2016;7:12308
204. Zannella VE, Dal Pra A, Muaddi H, McKee TD, Stapleton S, Sykes J, Glicksman R, Chaib S, Zamiara P, Milosevic M, Wouters BG, Bristow RG, Koritzinsky M et al. Reprogramming Metabolism with Metformin Improves Tumor Oxygenation and Radiotherapy Response. Clinical Cancer Research. 2013;19:6741–6750
205. Jordan BF, Christian N, Crokart N, Grégoire V, Feron O, Gallez B. Thyroid Status is a Key Modulator of Tumor Oxygenation: Implication for Radiation Therapy. Radiation Research. 2007;168:428–432
206. Crokart N, Jordan BF, Baudelet C, et al. Early reoxygenation in tumors after irradiation: Determining factors and consequences for radiotherapy

regimens using daily multiple fractions. International Journal of Radiation Oncology*Biology*Physics. 2005;63(3):901-910.
207. Olive PL. Radiation-induced reoxygenation in the SCCVII murine tumour: evidence for a decrease in oxygen consumption and an increase in tumour perfusion. Radiother Oncol. 1994;32(1):37-46.
208. Sonveaux P, Dessy C, Brouet A, et al. Modulation of the tumor vasculature functionality by ionizing radiation accounts for tumor radiosensitization and promotes gene delivery. The FASEB Journal. 2002;16(14):1979-1981.
209. Horsman MR, Overgaard J. Hyperthermia: a potent enhancer of radiotherapy. Clin Oncol. 2007;19:418–26
210. Moon EJ, Sonveaux P, Porporato PE, et al. NADPH oxidase-mediated reactive oxygen species production activates hypoxia-inducible factor-1 (HIF-1) via the ERK pathway after hyperthermia treatment. Proceedings of the National Academy of Sciences. 2010;107(47):20477-20482.
211. Januszewski A, Stebbing J. Hyperthermia in cancer: is it coming of age? The Lancet Oncology. 2014 May;15(6):565–6.
212. Adams GE, Cooke MS. Electron–affinic sensitization I A structural basis for chemical radiosensitizers in bacteria. Int J Radiat Biol. 1969;15:457–71
213. Adams GE, Flockhart IR, Smithen CE, et al. Electron–affinic sensitization VII A correlation between structures, one-electron reduction potentials and efficiencies of some nitroimidazoles as hypoxic cell radiosensitizers. Radiat Res. 1976;67:9–20
214. Overgaard J. Clinical evaluation of nitroimidazoles as modifiers of hypoxia in solid tumors. Oncol Res. 1994;6:509–18
215. McKeown SR, Cowen RL, Williams KJ. Bioreductive drugs: from concept to clinic. Clin Oncol. 2007;19:427–42
216. Wilson WR, Hay MP. Targeting hypoxia in cancer therapy. Nat Rev Cancer. 2011;11:393–410
217. Harrison LB. Impact of Tumor Hypoxia and Anemia on Radiation Therapy Outcomes. The Oncologist. 2002;7:492–508
218. Weissberg JB, Son YH, Papac RJ, et al. Randomized clinical trial of mitomycin C as an adjunct to radiotherapy in head and neck cancer. International Journal of Radiation Oncology*Biology*Physics. 1989;17(1):3-9.
219. Haffty BG, Son YH, Sasaki CT, et al. Mitomycin C as an adjunct to postoperative radiation therapy in squamous cell carcinoma of the head and neck: results from two randomized clinical trials. International Journal of Radiation Oncology*Biology*Physics. 1993;27(2):241-250.
220. Grau C, Prakash Agarwal J, Jabeen K, et al. Radiotherapy with or without mitomycin c in the treatment of locally advanced head and neck cancer: results of the IAEA multicentre randomised trial. Radiother Oncol. 2003;67(1):17-26.

221. Horsman MR, Overgaard J. The impact of hypoxia and its modification of the outcome of radiotherapy. J Radiat Res. 2016;57 Suppl 1: i90–i98
222. Rauth AM, McClelland RA, Michaels HB, et al. The oxygen dependence of the reduction of nitroimidazoles in a radiolytic model system. International Journal of Radiation Oncology*Biology*Physics. 1984;10:1323–6
223. Sutherland RM, Keng P, Conroy PJ, et al. *In vitro* hypoxic cytotoxicity of nitroimidazoles: uptake and cell cycle phase specificity. International Journal of Radiation Oncology*Biology*Physics. 1982;8:745–8
224. Meng F, Evans JW, Bhupathi D, et al. Molecular and cellular pharmacology of the hypoxia-activated prodrug TH-302. Mol Cancer Ther. 2012;11:740–51
225. Zeman EM, Brown JM, Lemmon MJ, et al. SR-4233: a new bioreductive agent with high selective toxicity for human mammalian cells. International Journal of Radiation Oncology*Biology*Physics. 1986;12:1239–42
226. Reddy SB, Williamson SK. Tirapazamine: a novel agent targeting hypoxic tumor cells. Expert Opin Investig Drugs. 2009;18:77–87
227. Rischin D, Peters L, Fisher R, et al. Tirapazamine, Cisplatin, and Radiation Versus Fluorouracil, Cisplatin, and Radiation in Patients With Locally Advanced Head and Neck Cancer: A Randomized Phase II Trial of the Trans-Tasman Radiation Oncology Group (TROG 98.02). Journal of Clinical Oncology. 2005;23(1):79-87.
228. Huxham LA, Kyle AH, Baker JHE, McNicol KL, Minchinton AI. Exploring vascular dysfunction caused by tirapazamine. Microvasc Res. 2008;75:247–255
229. Cazares-Körner C, Pires IM, Swallow ID, et al. CH-01 is a Hypoxia-Activated Prodrug That Sensitizes Cells to Hypoxia/Reoxygenation Through Inhibition of Chk1 and Aurora A. ACS Chemical Biology. 2013;8:1451–1459
230. Lindquist KE, Cran JD, Kordic K, et al. Selective radiosensitization of hypoxic cells using BCCA621C: a novel hypoxia activated prodrug targeting DNA-dependent protein kinase. Tumor Microenvironment and Therapy. 2013;1
231. Horsman MR, Siemann DW. Pathophysiological effects of vascular targeting agents and the implications for combination therapies. Cancer Res. 2006;66:11520–39
232. Siemann DW, Horsman MR. Vascular targeted therapies in oncology. Cell Tissue Res. 2009;335:241–8
233. Jain RK. Normalizing tumor vasculature with anti-angiogenic therapy: a new paradigm for combination therapy. Nat Med. 2001;7:987–9
234. Wouters BG, Weppler SA, Koritzinsky M, et al. Hypoxia as a target for combined modality treatments. Eur J Cancer. 2002;38(2):240-257.
235. Wouters BG, van den Beucken T, Magagnin MG, Lambin P, Koumenis C. Targeting hypoxia tolerance in cancer. Drug Resist Updat. 2004;7(1):25-40.
236. Helbig L, Koi L, Bruchner K, Gurtner K, Hess-Stumpp H, Unterschemmann K, Baumann M, Zips D, Yaromina A. BAY 87-2243, a novel inhibitor of hypoxia-induced gene activation, improves local tumor control after

fractionated irradiation in a schedule-dependent manner in head and neck human xenografts. Radiat Oncol. 2014;9:207
237. Helbig L, Koi L, Bruchner K, et al Hypoxia-inducible factor pathway inhibition resolves tumor hypoxia and improves local tumor control after single-dose irradiation. International Journal of Radiation Oncology*Biology*Physics. 2014;88(1):159–166
238. Shin DH, Kim J-H, Jung Y-J, et al. Preclinical evaluation of YC-1, a HIF inhibitor, for the prevention of tumor spreading. Cancer Letters. 2007;255(1):107-116.
239. Yeo E-J, Chun Y-S, Cho Y-S, et al. YC-1: A Potential Anticancer Drug Targeting Hypoxia-Inducible Factor 1. JNCI Journal of the National Cancer Institute. 2003;95(7):516-525.
240. Harada H, Itasaka S, Zhu Y, et al. Treatment regimen determines whether an HIF-1 inhibitor enhances or inhibits the effect of radiation therapy. British Journal of Cancer. 2009;100(5):747-757.
241. Lee K, Zhang H, Qian DZ, Rey S, Liu JO, Semenza GL. Acriflavine inhibits HIF-1 dimerization, tumor growth, and vascularization. Proceedings of the National Academy of Sciences. 2009;106(42):17910-17915.
242. Giaccia A, Siim BG, Johnson RS. HIF-1 as a target for drug development. Nature Reviews Drug Discovery. 2003;2(10):803–11.
243. Brown JM, Wilson WR. Exploiting tumour hypoxia in cancer treatment. Nature Reviews Cancer. 2004;4(6):437–47.
244. Trott KR. Experimental results and clinical implications of the four R's in fractionated radiotherapy. Radiat Environ Biophys. 1982;20:159–170
245. Egeland TAM, Gaustad J-V, Vestvik IK, Benjaminsen IC, Mathiesen B, Rofstad EK. Assessment of fraction of radiobiologically hypoxic cells in human melanoma xenografts by dynamic contrast-enhanced MRI. Magnetic Resonance in Medicine. 2006;55(4):874-882.
246. Ling CC, Humm J, Larson S, et al. Towards multidimensional radiotherapy (MD-CRT) biological imaging and biological conformality. International Journal of Radiation Oncology*Biology*Physics. 2000;47:551–60
247. Bentzen SM, Gregoire V. Molecular imaging-based dose painting: a novel paradigm for radiation therapy prescription. Semin Radiat Oncol. 2011;21(2):101-110.
248. Flynn RT, Bowen SR, Bentzen SM, Rockwell Mackie T, Jeraj R. Intensity-modulated X-ray (IMXT) versus proton (IMPT) therapy for theragnostic hypoxia-based dose painting. Phys Med Biol. 2008;53:4153
249. Hakansson K, Specht L, Aznar MC, Rasmussen JH, Bentzen SM, Vogelius IR. Prescribing and evaluating target dose in dose-painting treatment plans. Acta Oncol. 2014;53:1251–6
250. Korreman SS, Ulrich S, Bowen S, Deveau M, Bentzen SM, Jeraj R. Feasibility of dose painting using volumetric modulated arc optimization and delivery. Acta Oncol. 2010;49:964–71

251. Thorwarth D, Soukup M, Alber M. Dose painting with IMPT, helical tomotherapy and IMXT: a dosimetric comparison. Radiother Oncol. 2008;86:30–4
252. Lee NY, Mechalakos JG, Nehmeh S, et al. Fluorine-18-Labeled Fluoromisonidazole Positron Emission and Computed Tomography-Guided Intensity-Modulated Radiotherapy for Head and Neck Cancer: A Feasibility Study. International Journal of Radiation Oncology*Biology*Physics. 2008;70(1):2-13.
253. Clausen MM, Hansen AE, Lundemann M, et al. Dose painting based on tumor uptake of Cu-ATSM and FDG: a comparative study. Radiation Oncology. 2014;9(1).
254. Grimes DR, Warren DR, Warren S. Hypoxia imaging and radiotherapy: bridging the resolution gap. The British Journal of Radiology. 2017;90(1076):20160939.
255. Troost EGC, Koi L, Yaromina A, Krause M. Therapeutic options to overcome tumor hypoxia in radiation oncology. Clinical and Translational Imaging. 2017; 5: 455–464
256. Søvik A , Malinen E, Bruland ØS, Bentzen SM, Olsen DR. Optimization of tumour control probability in hypoxic tumours by radiation dose redistribution: a modeling study. Phys Med Biol. 2006;52:499–513
257. Nehmeh SA, Lee NY, Schröder H, et al. Reproducibility of intratumor distribution of 18F-Fluoromisonidazole in head and neck cancer. International Journal of Radiation Oncology*Biology*Physics. 2008;70:235–42
258. Okamoto S, Shiga T, Yasuda K et al. High reproducibility of tumor hypoxia evaluated by 18F-fluoromisonidazole PET in head and neck cancer. J Nucl Med. 2013;54:201–7
259. Rockwell S, Dobrucki IT, Kim EY, Marrison ST, Vu VT. Hypoxia and radiation therapy: past history, ongoing research, and future promise. Curr Mol Med. 2009;9:442–458
260. Overgaard J, Horsman MR. Modification of hypoxia-induced radioresistance in tumors by the use of oxygen and sensitizers. Semin Radiat Oncol. 1996;6:10–21
261. Overgaard J. Hypoxic Radiosensitization: Adored and Ignored. JCO. 2007;25:4066–4074
262. Metwally MA H, Ali R, Kuddu M, et al. IAEA-HypoX A randomized multicenter study of the hypoxic radiosensitizer nimorazole concomitant with accelerated radiotherapy in head and neck squamous cell carcinoma. Radiother Oncol. 2015;116:15–20
263. Dewhirst MW, Birer SR. Oxygen-Enhanced MRI Is a Major Advance in Tumor Hypoxia Imaging. Cancer Research. 2016;76:769–772
264. Ljungkvist ASE, Bussink J, Kaanders JHAM, van der Kogel AJ. Dynamics of tumor hypoxia measured with bioreductive hypoxic cell markers. Radiat Res. 2007;167:127–145

265. Aquino-Parsons C, Lim P, Green A, Minchinton AI. Carbogen inhalation in cervical cancer: assessment of oxygenation change. Gynecol Oncol. 1999;74:259–264
266. Brizel DM, Sibley GS, Prosnitz LR, Scher RL, Dewhirst MW. Tumor hypoxia adversely affects the prognosis of carcinoma of the head and neck. Int J Radiat Oncol Biol Phys. 1997;38(2):285-289.
267. Jordan BF, Gallez B. Surrogate MR markers of response to chemo- or radiotherapy in association with co-treatments: a retrospective analysis of multi-modal studies. Contrast Media Mol Imaging. 2010;5(6):323–32.
268. Khan N, Mupparaju S, Hekmatyar SK, et al. Effect of hyperoxygenation on tissue pO2 and its effect on radiotherapeutic efficacy of orthotopic F98 gliomas. International Journal of Radiation Oncology*Biology*Physics. 2010;78(4):1193–200.
269. Hou H, Mupparaju SP, Lariviere JP, et al. Assessment of the changes in 9L and C6 glioma pO2 by EPR oximetry as a prognostic indicator of differential response to radiotherapy. Radiat Res. 2013;179(3):343–51.
270. Matsumoto S, Batra S, Saito K, et al. Antiangiogenic agent sunitinib transiently increases tumor oxygenation and suppresses cycling hypoxia. Cancer Res. 2011;71(20):6350–9.
271. Kaanders JH, Wijffels KI, Marres HA, et al. Pimonidazole binding and tumor vascularity predict for treatment outcome in head and neck cancer. Cancer Res. 2002;62:7066–7074
272. Nordsmark M, Loncaster J, Aquino-Parsons C, et al. The prognostic value of pimonidazole and tumour pO2 in human cervix carcinomas after radiation therapy: a prospective international multi-center study. Radiother Oncol. 2006;80(2):123‑31.
273. Evans SM, Du KL, Chalian AA, et al. Patterns and levels of hypoxia in head and neck squamous cell carcinomas and their relationship to patient outcome. International Journal of Radiation Oncology*Biology*Physics. 2007;69:1024–1031
274. Rajendran JG, Schwartz DL, O'Sullivan J, et al. Tumor hypoxia imaging with [F-18] fluoromisonidazole positron emission tomography in head and neck cancer. Clin Cancer Res. 2006;12(18):5435–41.
275. Thorwarth D, Eschmann S-M, Holzner F, Paulsen F, Alber M. Combined uptake of [18F]FDG and [18F]FMISO correlates with radiation therapy outcome in head-and-neck cancer patients. Radiother Oncol. 2006;80(2):151–6.
276. Dirix P, Vandecaveye V, De Keyzer F, Stroobants S, Hermans R, Nuyts S. Dose painting in radiotherapy for head and neck squamous cell carcinoma: value of repeated functional imaging with (18)F-FDG PET, (18)F-fluoromisonidazole PET, diffusion-weighted MRI, and dynamic contrast-enhanced MRI. J Nucl Med. 2009;50(7):1020–7.
277. Lee N, Nehmeh S, Schöder H, et al. Prospective trial incorporating pre-/mid-treatment [18F]-misonidazole positron emission tomography for head-and-

neck cancer patients undergoing concurrent chemoradiotherapy. International Journal of Radiation Oncology*Biology*Physics. 2009;75(1):101–8.
278. Kikuchi M, Yamane T, Shinohara S, et al. 18F-fluoromisonidazole positron emission tomography before treatment is a predictor of radiotherapy outcome and survival prognosis in patients with head and neck squamous cell carcinoma. Ann Nucl Med. 2011;25(9):625–33.
279. Zips D, Zöphel K, Abolmaali N, et al. Exploratory prospective trial of hypoxia-specific PET imaging during radiochemotherapy in patients with locally advanced head-and-neck cancer. Radiotherapy and Oncology. 2012;105(1):21–8.
280. Mönnich D, Welz S, Thorwarth D, et al. Robustness of quantitative hypoxia PET image analysis for predicting local tumor control. Acta Oncol. 2015;54(9):1364–9.
281. Spence AM, Muzi M, Swanson KR, et al. Regional Hypoxia in Glioblastoma Multiforme Quantified with [18F]Fluoromisonidazole Positron Emission Tomography before Radiotherapy: Correlation with Time to Progression and Survival. Clinical Cancer Research. 2008;14(9):2623–30.
282. Dehdashti F, Grigsby PW, Mintun MA, Lewis JS, Siegel BA, Welch MJ. Assessing tumor hypoxia in cervical cancer by positron emission tomography with 60Cu-ATSM: relationship to therapeutic response-a preliminary report. International Journal of Radiation Oncology*Biology*Physics. 2003;55(5):1233–8.
283. Dehdashti F, Grigsby PW, Lewis JS, Laforest R, Siegel BA, Welch MJ. Assessing Tumor Hypoxia in Cervical Cancer by PET with 60Cu-Labeled Diacetyl-Bis(N4-Methylthiosemicarbazone). Journal of Nuclear Medicine. 2008 Feb 1;49(2):201–5.
284. Grigsby PW, Malyapa RS, Higashikubo R, et al. Comparison of Molecular Markers of Hypoxia and Imaging with 60Cu-ATSM in Cancer of the Uterine Cervix. Molecular Imaging and Biology. 2007;9(5):278–83.
285. Minagawa Y, Shizukuishi K, Koike I, et al. Assessment of tumor hypoxia by 62Cu-ATSM PET/CT as a predictor of response in head and neck cancer: a pilot study. Annals of Nuclear Medicine. 2011;25(5):339–45.
286. Dehdashti F, Mintun MA, Lewis JS, et al. *In vivo* assessment of tumor hypoxia in lung cancer with 60Cu-ATSM. European Journal of Nuclear Medicine and Molecular Imaging. 2003;30(6):844–50.
287. Dietz DW, Dehdashti F, Grigsby PW, et al. Tumor Hypoxia Detected by Positron Emission Tomography with 60Cu-ATSM as a Predictor of Response and Survival in Patients Undergoing Neoadjuvant Chemoradiotherapy for Rectal Carcinoma: A Pilot Study: Diseases of the Colon & Rectum. 2008;51(11):1641–8.
288. Schütze C, Bergmann R, Brüchner K, et al. Effect of [18F]FMISO stratified dose-escalation on local control in FaDu hSCC in nude mice. Radiotherapy and Oncology. 2014;111(1):81–7.

289. Mortensen LS, Busk M, Nordsmark M, et al. Accessing radiation response using hypoxia PET imaging and oxygen sensitive electrodes: A preclinical study. Radiotherapy and Oncology. 2011;99(3):418–23.
290. Tran L-B-A, Bol A, Labar D, et al. Potential role of hypoxia imaging using 18F-FAZA PET to guide hypoxia-driven interventions (carbogen breathing or dose escalation) in radiation therapy. Radiotherapy and Oncology. 2014;113(2):204–9.
291. Bradshaw TJ, Bowen SR, Deveau MA, et al. Molecular Imaging Biomarkers of Resistance to Radiation Therapy for Spontaneous Nasal Tumors in Canines. International Journal of Radiation Oncology*Biology*Physics. 2015;91(4):787–95.
292. Li L, Yu J, Xing L, et al. Serial hypoxia imaging with 99mTc-HL91 SPECT to predict radiotherapy response in non small cell lung cancer. Amer J Clin Oncol. 2006;29:628–633
293. Aebersold DM, Burri P, Beer KT, et al. Expression of hypoxia-inducible factor-1alpha: a novel predictive and prognostic parameter in the radiotherapy of oropharyngeal cancer. Cancer Res. 2001;61(7):2911–6.
294. Bachtiary B, Schindl M, Pötter R, et al. Overexpression of hypoxia-inducible factor 1alpha indicates diminished response to radiotherapy and unfavorable prognosis in patients receiving radical radiotherapy for cervical cancer. Clin Cancer Res. 2003;9(6):2234–40.
295. Burri P, Djonov V, Aebersold DM, et al. Significant correlation of hypoxia-inducible factor-1alpha with treatment outcome in cervical cancer treated with radical radiotherapy. International Journal of Radiation Oncology*Biology*Physics. 2003;56(2):494–501.
296. Hui EP, Chan ATC, Pezzella F, et al. Coexpression of hypoxia-inducible factors 1alpha and 2alpha, carbonic anhydrase IX, and vascular endothelial growth factor in nasopharyngeal carcinoma and relationship to survival. Clin Cancer Res. 2002;8(8):2595–604.
297. De Schutter H, Landuyt W, Verbeken E, Goethals L, Hermans R, Nuyts S. The prognostic value of the hypoxia markers CA IX and GLUT 1 and the cytokines VEGF and IL 6 in head and neck squamous cell carcinoma treated by radiotherapy ± chemotherapy. BMC Cancer [Internet]. 2005;5(1).
298. Ellingsen C, Hompland T, Galappathi K, Mathiesen B, Rofstad EK. DCE-MRI of the hypoxic fraction, radioresponsiveness, and metastatic propensity of cervical carcinoma xenografts. Radiotherapy and Oncology. 2014;110(2):335–41.
299. Øvrebø KM, Gulliksrud K, Mathiesen B, Rofstad EK. Assessment of Tumor Radioresponsiveness and Metastatic Potential by Dynamic Contrast-Enhanced Magnetic Resonance Imaging. International Journal of Radiation Oncology*Biology*Physics. 2011;81(1):255–61.

300. Jordan BF, Peeterbroeck J, Karroum O, et al. Captopril and S-nitrosocaptopril as potent radiosensitizers: Comparative study and underlying mechanisms. Cancer Letters. 2010;293(2):213–9.
301. Loncaster JA, Carrington BM, Sykes JR, et al. Prediction of radiotherapy outcome using dynamic contrast enhanced MRI of carcinoma of the cervix. International Journal of Radiation Oncology*Biology*Physics. 2002;54(3):759–67.
302. Mayr NA, Wang JZ, Zhang D, et al. Longitudinal Changes in Tumor Perfusion Pattern during the Radiation Therapy Course and its Clinical Impact in Cervical Cancer. International Journal of Radiation Oncology*Biology*Physics. 2010;77(2):502–8.
303. Andersen EKF, Hole KH, Lund KV, et al. Dynamic Contrast-Enhanced MRI of Cervical Cancers: Temporal Percentile Screening of Contrast Enhancement Identifies Parameters for Prediction of Chemoradioresistance. International Journal of Radiation Oncology*Biology*Physics. 2012;82(3):e485–92.
304. Shukla-Dave A, Lee NY, Jansen JFA, et al. Dynamic Contrast-Enhanced Magnetic Resonance Imaging as a Predictor of Outcome in Head-and-Neck Squamous Cell Carcinoma Patients With Nodal Metastases. International Journal of Radiation Oncology*Biology*Physics. 2012;82(5):1837–44.
305. Rodrigues LM, Howe FA, Griffiths JR, Robinson SP. Tumor R2* is a prognostic indicator of acute radiotherapeutic response in rodent tumors J Magn Reson Imaging. 2004;19(4):482–8
306. Kim CK, Park SY, Park BK, Park W, Huh SJ. Blood oxygenation level-dependent MR imaging as a predictor of therapeutic response to concurrent chemoradiotherapy in cervical cancer: a preliminary experience. Eur Radiol. 2014; 24(7):1514–20
307. White DA, Zhang Z, Li L, et al. Developing oxygen-enhanced magnetic resonance imaging as a prognostic biomarker of radiation response. Cancer Lett. 2016;380:69-77
308. Limani P, Linecker M, Kron P, et al. Development of OXY111A a novel hypoxia-modifier as a potential antitumor agent in patients with hepato-pancreato-biliary neoplasms - Protocol of a first Ib/IIa clinical trial. BMC Cancer. 2016;16:812
309. Wong EC. An introduction to ASL labeling techniques. J Magn Reson Imaging. 2014;40(1):1-10.
310. Amorino GP, Lee H, Holburn GE, et al. Enhancement of tumor oxygenation and radiation response by the allosteric effector of hemoglobin, RSR13. Radiat. Res. 2001;156:294–300.
311. Hou H, Khan N, O'Hara JA, et al. Effect of RSR13, an allosteric hemoglobin modifier, on oxygenation in murine tumors: an *in vivo* electron

paramagnetic resonance oximetry and bold MRI study. International Journal of Radiation Oncology*Biology*Physics. 2004;59:834–843.
312. Alhallaq H, River J, Zamora M, Oikawa H, Karczmar G. Correlation of Magnetic Resonance and Oxygen Microelectrode Measurements of Carbogen-Induced Changes in Tumor Oxygenation. International Journal of Radiation OncologyBiologyPhysics. 1998;41(1):151-159.
313. Christen T, Lemasson B, Pannetier N, et al. Is T2* Enough to Assess Oxygenation? Quantitative Blood Oxygen Level–Dependent Analysis in Brain Tumor. Radiology. 2012;262(2):495-502.
314. Burrell JS, Walker-Samuel S, Baker LCJ, et al. Exploring ΔR2* and ΔR1 as imaging biomarkers of tumor oxygenation. J Magn Reson Imaging. 2013;38(2):429-434.
315. Colliez F, Fruytier A-C, Magat J, et al. Monitoring Combretastatin A4-induced tumor hypoxia and hemodynamic changes using endogenous MR contrast and DCE-MRI: Monitoring CA4-Induced Tumor Hemodynamic Changes. Magnetic Resonance in Medicine. 2016;75(2):866-872.
316. Alonzi R, Padhani AR, Maxwell RJ, et al. Carbogen breathing increases prostate cancer oxygenation: a translational MRI study in murine xenografts and humans. Br J Cancer. 2009;100(4):644-648.
317. Hallac RR, Ding Y, Yuan Q, et al. Oxygenation in cervical cancer and normal uterine cervix assessed using blood oxygenation level-dependent (BOLD) MRI at 3T. NMR Biomed. 2012;25(12):1321-1330.
318. Kotas M, Schmitt P, Jakob PM, Flentje M. Monitoring of Tumor Oxygenation Changes in Head-and-Neck Carcinoma Patients Breathing a Hyperoxic Hypercapnic Gas Mixture with a Noninvasive MRI Technique. Strahlentherapie und Onkologie. 2009;185(1):19-26.
319. Rijpkema M, Kaanders JHAM, Joosten FBM, van der Kogel AJ, Heerschap A. Effects of breathing a hyperoxic hypercapnic gas mixture on blood oxygenation and vascularity of head-and-neck tumors as measured by magnetic resonance imaging. International Journal of Radiation Oncology*Biology*Physics. 2002;53(5):1185-1191.
320. Remmele S, Sprinkart AM, Müller A, et al. Dynamic and simultaneous MR measurement of R1 and R2* changes during respiratory challenges for the assessment of blood and tissue oxygenation. Magn Reson Med. 2013;70(1):136-146.
321. Hoskin PJ, Carnell DM, Taylor NJ, et al. Hypoxia in Prostate Cancer: Correlation of BOLD-MRI With Pimonidazole Immunohistochemistry—Initial Observations. International Journal of Radiation Oncology*Biology*Physics. 2007;68(4):1065-1071.
322. Jiang K, Zhu Y, Jia S, Wu Y, Liu X, Chung Y-C. Fast T1 mapping of the brain at high field using Look-Locker and fast imaging. Magnetic Resonance Imaging. 2017;36:49-55.

323. Ma D, Jiang Y, Chen Y, et al. Fast 3D magnetic resonance fingerprinting for a whole-brain coverage: 3D MRF. Magnetic Resonance in Medicine. 2018;79(4):2190-2197.
324. Madani I, Duprez F, Boterberg T, et al. Maximum tolerated dose in a phase I trial on adaptive dose painting by numbers for head and neck cancer. Radiotherapy and Oncology. 2011;101(3):351-355.
325. Warren DR, Partridge M. The role of necrosis, acute hypoxia and chronic hypoxia in 18 F-FMISO PET image contrast: a computational modelling study. Physics in Medicine and Biology. 2016;61(24):8596-8624.